water

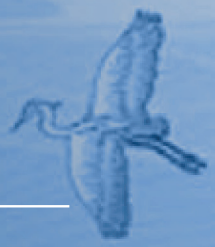

Special Issue Reprint

Yellow River Basin Management under Pressure

Present State, Restoration and Protection III

Edited by
Qiting Zuo, Xiangyi Ding, Guotao Cui and Wei Zhang

mdpi.com/journal/water

MDPI

Yellow River Basin Management under Pressure: Present State, Restoration and Protection III

Yellow River Basin Management under Pressure: Present State, Restoration and Protection III

Guest Editors

Qiting Zuo
Xiangyi Ding
Guotao Cui
Wei Zhang

MDPI

Basel • Beijing • Wuhan • Barcelona • Belgrade • Novi Sad • Cluj • Manchester

Guest Editors

Qiting Zuo
School of Water Conservancy and Transportation
Zhengzhou University
Zhengzhou
China

Xiangyi Ding
Department of Water Resources
China Institute of Water Resources and Hydropower Research
Beijing
China

Guotao Cui
School of Geography and Planning
Sun Yat-Sen University
Guangzhou
China

Wei Zhang
School of Ecology and Environment
Zhengzhou University
Zhengzhou
China

Editorial Office

MDPI AG
Grosspeteranlage 5
4052 Basel, Switzerland

This is a reprint of the Special Issue, published open access by the journal *Water* (ISSN 2073-4441), freely accessible at: https://www.mdpi.com/journal/water/special_issues/22X722R5E0.

For citation purposes, cite each article independently as indicated on the article page online and as indicated below:

Lastname, A.A.; Lastname, B.B. Article Title. *Journal Name* **Year**, *Volume Number*, Page Range.

ISBN 978-3-7258-5989-4 (Hbk)
ISBN 978-3-7258-5990-0 (PDF)
https://doi.org/10.3390/books978-3-7258-5990-0

Cover image courtesy of Wei Zhang

Contents

About the Editors . . . . . **vii**

Qiting Zuo, Xiangyi Ding, Guotao Cui and Wei Zhang
Yellow River Basin Management Under Pressure: Present State, Restoration and Protection III: Lessons from a Special Issue
Reprinted from: *Water* **2025**, *17*, 2907, https://doi.org/10.3390/w17192907 . . . . . **1**

Zhiqiang Zhang, Xinyu Guo, Lianhai Cao, Xizhi Lv, Xiuyu Zhang, Li Yang, et al.
Multi-Scale Variation in Surface Water Area in the Yellow River Basin (1991–2023) Based on Suspended Particulate Matter Concentration and Water Indexes
Reprinted from: *Water* **2024**, *16*, 2704, https://doi.org/10.3390/w16182704 . . . . . **10**

Heying Li, Huiling Ma, Jianchen Zhang, Xueye Chen and Xuefei Hong
Surface Water Resource Accessibility Assessment of Rural Settlements in the Yellow River Basin
Reprinted from: *Water* **2024**, *16*, 708, https://doi.org/10.3390/w16050708 . . . . . **34**

Yujun Wang, Changsai Han and Xiping Zhao
Optimization Study on Sequential Emptying and Dredging for Water Diversity Reservoir Group
Reprinted from: *Water* **2024**, *16*, 2482, https://doi.org/10.3390/w16172482 . . . . . **47**

Bingxuan Li, Jinxin Wang, Yan Zhang and Yongkang Sun
Innovative Adaptive Multiscale 3D Simulation Platform for the Yellow River Using Sphere Geodesic Octree Grid Techniques
Reprinted from: *Water* **2024**, *16*, 1791, https://doi.org/10.3390/w16131791 . . . . . **70**

Zhiqiang Zhang, Weiwei Wang, Xiuyu Zhang, Hui Zhang, Li Yang, Xizhi Lv and Xu Xi
A Harmony-Based Approach for the Evaluation and Regulation of Water Security in the Yellow River Water-Receiving Area of Henan Province
Reprinted from: *Water* **2024**, *16*, 2497, https://doi.org/10.3390/w16172497 . . . . . **90**

Lu Liu, Liuyue He and Qiting Zuo
Evaluating the Human–Water Relationship over the Past Two Decades Using the SMI-P Method across Nine Provinces along the Yellow River, China
Reprinted from: *Water* **2024**, *16*, 916, https://doi.org/10.3390/w16070916 . . . . . **109**

Zhenzhen Yu, Xiaojuan Sun, Li Yan, Shengde Yu, Yong Li and Huijiao Jin
Analysis of the Water Quality Status and Its Historical Evolution Trend in the Mainstream and Major Tributaries of the Yellow River Basin
Reprinted from: *Water* **2024**, *16*, 2413, https://doi.org/10.3390/w16172413 . . . . . **122**

Zhenzhen Yu, Xiaojuan Sun, Li Yan, Yong Li, Huijiao Jin and Shengde Yu
Spatiotemporal Changes in the Quantity and Quality of Water in the Xiao Bei Mainstream of the Yellow River and Characteristics of Pollutant Fluxes
Reprinted from: *Water* **2024**, *16*, 2616, https://doi.org/10.3390/w16182616 . . . . . **139**

Jun Hou, Jianwei Wang, Xiaofeng Chen, Yong Hu and Guoqiang Dong
Soil Erosion Dynamics and Driving Force Identification in the Yiluo River Basin Under Multiple Future Scenarios
Reprinted from: *Water* **2025**, *17*, 2157, https://doi.org/10.3390/w17142157 . . . . . **157**

Daiwei Zhang, Ming Jing, Buhui Chang, Weiwei Chen, Ziming Li, Shuai Zhang and Ting Li
Coordination Analysis and Driving Factors of "Water-Land-Energy-Carbon" Coupling in Nine Provinces of the Yellow River Basin
Reprinted from: *Water* **2025**, *17*, 1138, https://doi.org/10.3390/w17081138 . . . . . **174**

About the Editors

Qiting Zuo

Qiting Zuo is a Professor and Doctoral Supervisor at the School of Water Conservancy and Transportation, Zhengzhou University. He serves as the Dean of the Yellow River Ecological Protection and Regional Coordinated Development Institute, Director of the Water Science Research Center, and Director of the Henan International Joint Laboratory for Water Cycle Simulation and Water Environmental Protection, all at Zhengzhou University. He also holds academic positions including Vice President of the Chinese Society of Natural Resources, Vice Chairman of the Chinese Committee of the International Water Resources Association, and Co-Chairman of the UK–China Association for Resources and Environment (UK-CARE). The team he leads has been recognized by the Ministry of Education as a "National Huang Danian-Style Teacher Team in Higher Education." His research focuses on water resources and the water environment. He has received 12 provincial and ministerial-level science and technology awards, published 21 academic monographs, and authored over 560 academic papers. He has been recognized for having one of China's 100 Most Influential Domestic Academic Papers and is the founder of the discipline of Human–Water Relationship Science. His research findings have been applied to address major national needs including ecological civilization construction, national water network construction, water conservancy modernization, water-saving measures for society, strict water resource management systems, water disaster prevention and control, smart water conservancy, dual carbon goals, high-quality development, and new quality productive forces.

Ding Xiangyi

Ding Xiangyi is an Associate Chief Engineer and Senior Engineer at the Research Institute of Water Resources, China Institute of Water Resources and Hydropower Research, and also serves as the Deputy Director of the Professional Committee on Water Resources of the Chinese Society of Natural Resources. His research primarily focuses on water cycle simulation and regulation, efficient water resource utilization, and water security assurance. He has led over 20 significant national and provincial/ministerial-level research projects, including sub-projects of the National Key R&D Program, research tasks for major National Natural Science Foundation of China projects, special topics for the Chinese Academy of Engineering consulting initiatives, and specific studies for the National Basic Research Program (973 Program) and the development of Beijing's sub-center. His work spans 72 published papers (38 of which are indexed in SCI/EI), 6 authored monographs, 36 granted invention patents, and contributions to 2 national standards, 2 industry standards, and 1 local standard. He has been recognized with prestigious awards, including one special prize, two first prizes, and one second prize at the provincial/ministerial level, as well as the Young Scientist Award from the Chinese Society of Natural Resources.

Guotao Cui

Guotao Cui is an Associate Professor at the School of Geography and Planning, Sun Yat-sen University. His research focuses on water resources and ecohydrology. He has led research projects funded by the National Natural Science Foundation of China and a sub-project of the National Key R&D Program. He serves as a member of the Water Resources Management and Conservation Committee of the Chinese Committee of the International Water Resources Association, and a member of the Water Resources Professional Committee of the Chinese Society of Natural Resources. He also

serves as a Youth Editorial Board Member for the journals *Pearl River* and the *Journal of North China University of Water Resources and Electric Power* (Natural Science Edition). His research findings have been published in journals such as *Remote Sensing of Environment*, *Water Resources Research*, *Journal of Hydrology*, and *Acta Geographica Sinica*.

Wei Zhang

Wei Zhang is a Professor and Doctoral Supervisor. He is recognized as a Henan Higher Education Science and Technology Innovation Talent, an Academic Leader of the Henan Provincial Department of Education, a Youth Talent of the CAST Science and Technology Think Tank, an Elsevier "China Golden Open Access Highly Downloaded Paper Scholar," a recipient of the RIE Excellent Young Scientist Award, a Henan Youth Talent Support Program recipient, a Provincial Higher Education Young Backbone Teacher, and one of the Top Ten Young Teachers at his university. He serves as the Executive Deputy Director of the Henan International Joint Laboratory for Water Cycle Simulation and Water Environmental Protection, Deputy Secretary-General of the 4th Water Resources Professional Committee of the Chinese Society of Natural Resources, and a member of the Youth Workers Committee of the China Association of Urban Water Supply and Drainage. He is also an Editorial Board Member for four journals, including *South-to-North Water Diversion and Water Conservancy Science and Technology* (Chinese and English), and a Youth Editorial Board Member for several journals, including the *Journal of Ecology and Environmental Sciences*. He has led more than 20 research projects, including projects funded by the National Natural Science Foundation of China (General Program/Youth Program) and a National Key R&D Program sub-project. He has received a first prize for Science and Technology Progress in Shaanxi Province and has published more than 70 SCI papers as the first author or corresponding author in top environmental journals such as *Environment International*.

water

MDPI

Editorial

Yellow River Basin Management Under Pressure: Present State, Restoration and Protection III: Lessons from a Special Issue

Qiting Zuo [1,2], Xiangyi Ding [3], Guotao Cui [4] and Wei Zhang [2,5,*]

[1] School of Water Conservancy and Transportation, Zhengzhou University, Zhengzhou 450001, China; zuoqt@zzu.edu.cn
[2] Yellow River Institute for Ecological Protection & Regional Coordinated Development, Zhengzhou University, Zhengzhou 450001, China
[3] Department of Water Resources, China Institute of Water Resources and Hydropower Research, Beijing 100038, China
[4] School of Geography and Planning, Sun Yat-sen University, Guangzhou 510006, China
[5] School of Ecology and Environment, Zhengzhou University, Zhengzhou 450001, China
* Correspondence: zhangwei88@zzu.edu.cn

1. Introduction

This Special Issue is the third edition following the publication of the first issue of "Yellow River Basin Management under Pressure: Present State, Restoration and Protection" in 2022 and the second issue in 2023. Currently, issues such as the coordination of human–water relationships, water security, water resource allocation, ecological environment restoration, water pollutant treatment, and the coexistence of new pollutants continue to constrain the high-quality development of the Yellow River Basin. Thus, this Special Issue focuses on the current state, challenges, and solutions relating to Yellow River basin management and sustainable development under pressure, aiming to help improve ecological protection and achieve high-quality development. The topics included the following:

(1) The current status and constraining factors of the ecological environment and high-quality development in the Yellow River Basin;
(2) Opportunities and strategies for management;
(3) Harmonious regulation of human–water relationships;
(4) Emerging pollutants issues;
(5) The impact of environmental changes on water security and water resource allocation;
(6) Ecological restoration and protection.

This Special Issue has aroused widespread interest among scholars, with a total of 10 related academic papers published online recently.

2. Overview of This Special Issue

This Special Issue includes ten original contributions focused on Yellow River basin management under pressure. Considering the unique regional characteristics of the Yellow River in China, the contributions mainly result from research conducted by universities and R & D institutions in China. The ten articles in this Special Issue can be divided into five categories: category A: "Resource Endowment and Basic Characteristics"; category B: "Opportunities and Strategies for Management"; category C: "Harmonious Regulation of Human–water Relationships"; category D: "Environmental Pollution and Governance"; category E: "Ecological Restoration and Protection".

In category A "Resource Endowment and Basic Characteristics", Zhiqiang Zhang et al. (contribution 1) have analyzed the applicability of nine water indexes in the Yellow River Basin by using the Landsat series images (Landsat 5, 7, 8) and then examined the correlation between the accuracy of the water indexes and suspended particulate matter (SPM) concentrations. They proposed a surface water extraction method considering the SPM concentrations. The study by Heying Li et al. (contribution 2) has developed a quantitative evaluation model of surface water resource accessibility based on three key dimensions: topography, distance, and surface water resources, with rural settlements serving as the research unit.

In category B "Opportunities and Strategies for Management", Yujun Wang et al. (contribution 3) have used compensation reservoirs to replace the emptied reservoir in undertaking water supply tasks as a constraint, established Single-objective optimization models for single reservoirs and multi-objective optimization models for reservoir groups, to optimize the emptying and dredging for water diversity reservoir group. In the study by Bingxuan Li et al. (contribution 4), an adaptive multiscale true 3D crust simulation platform using the Sphere Geodesic Octree Grid was proposed to offer reliable support for constructing basin simulation platforms and provided new technological and scientific insights for the Yellow River Basin's ecological protection and development.

For the category C "Harmonious Regulation of Human–water relationships", Zhiqiang Zhang et al. (contribution 5) selected the Yellow River water-receiving area of Henan Province as the research area, quantified the water security degree of 14 cities from 2010 to 2021, and identified the key obstacle indexes that restrict the improvement of water security. In the study by Lu Liu et al. (contribution 6), 29 evaluation indicators were selected and the single index quantification, multiple index synthesis, and poly-criteria integration method were applied to quantify the spatial–temporal variation in the human–water harmony degree in nine provinces of the Yellow River Basin from 2002 to 2021.

In category D "Environmental Pollution and Governance", Zhenzhen Yu et al. (contribution 7) analyzed the water quality evolution in the Yellow River basin over nearly 40 years, focusing on primary pollutants like chemical oxygen demand (COD), ammonia nitrogen (NH_3-N), and permanganate index (COD_{Mn}). The findings underscored the effectiveness of sustained pollution control and the need for continuous, adaptive management strategies to improve and maintain water quality. The study by Zhenzhen Yu et al. (contribution 8) also conducted field monitoring at 11 locations along the investigated reach of Xiao Bei, assessing eight water quality parameters (temperature, pH, dissolved oxygen (DO), COD, NH_3-N, total phosphorus (TP), COD_{Mn}, and five-day biochemical oxygen demand (BOD5)).

In the category E "Ecological Restoration and Protection", Jun Hou et al. (contribution 9) analyzed historical soil erosion trends (2000–2020), projected future soil erosion risks under multiple Shared Socioeconomic Pathways, and quantified the interactive effects of key driving factors by integrating the Universal Soil Loss Equation, future land use and vegetation cover simulation methods, and the Geodetector model. The study by Daiwei Zhang et al. (contribution 10) analyzed the coupled and coordinated development of the water–soil–energy–carbon system in the provinces of the Yellow River Basin from 2002 to 2022, and systematically explored the interaction relationships among the various factors through water–soil–energy–carbon bond index assessment, factor identification, and driving factor exploration.

3. Advances in Researching Core Scientific Challenges Within the Yellow River Basin

3.1. Synergistic Human–Water Relationship in the Yellow River Basin: Development and Future Vision

The Yellow River is widely recognized as one of the most difficult rivers to manage in the world. The spatial differences in geographical, climatic, and humanistic characteristics across the Yellow River Basin are significant, making it extremely challenging to balance the relationship between human and water [1]. Scholars have conducted extensive scientific research on the human–water relationship in the Yellow River Basin, with diverse and complex research objectives, scopes, directions, and scales [2,3]. Existing achievements hold substantial scientific value and practical significance for the protection and development of the Yellow River Basin [4,5]. However, regarding the complex, dynamic, and interconnected human–water relationship and based on the human–water system involving multi-element participation, multi-dimensional coupling, and multi-level feedback, in-depth exploration is still needed to achieve a harmonious human–water relationship. The key issues in the research on the human–water relationship in the Yellow River Basin mainly include four aspects: insufficient understanding of action mechanisms and evolution processes, inadequate research on theoretical foundations and the theory of harmonious coexistence, the need to deepen research on monitoring-assessment-simulation-regulation, and the need to expand multi-level paths toward harmonious coexistence. To coordinate the human–water relationship in the Yellow River Basin and achieve harmonious coexistence [6], future key research areas include but are not limited to the exploration of river ethics theory and system construction, the research and development as well as application of intelligent perception equipment for human–water system, the analysis of the formation mechanism and variation mechanism of water balance, the evaluation of the status of human–water relationship and paths for improvement, the adaptive adjustment of thresholds for water resources development and utilization, the integration and demonstration of key technologies for the "Defining the scales based on water", the construction of distributed human–water relationship simulators, the construction of multi-level water networks and risk-benefit assessment, the optimization of water conservancy project layout and integrated operation management, and the exploration of new development paths under the rigid constraints of water resources.

3.2. AI-Driven Water Disaster Prediction for the Yellow River Basin

The Yellow River Basin faces numerous challenges in water disaster prediction research due to a combination of complex water-sediment dynamics, unique topographical features, variable climatic conditions, and intense human activity interventions [7,8]. These factors have historically resulted in low prediction accuracy, poor timeliness, and insufficient capacity for integrating multi-source information [9]. In recent years, with the breakthrough development of artificial intelligence technologies, research on water disaster prediction based on machine learning, deep learning, and big data analytics has gradually advanced in the Yellow River Basin [10]. Researchers have constructed multimodal data fusion frameworks that integrate heterogeneous data from meteorological satellite remote sensing, hydrological station observations, geological radar, and socio-economic sources. Algorithms such as Long Short-term Memory, Convolutional Neural Networks, and Random Forests were employed in hydrological process simulation [11], drought and flood monitoring [12], runoff prediction [13], and sediment management [14], and made significant progress. However, current research still faces several bottlenecks, including inconsistent data quality, weak interpretability of model physical mechanisms, and insufficient uncertainty quantification under complex underlying surface conditions. Future

efforts should focus on strengthening interdisciplinary integration and developing simulation models that combine hydrological physical processes with data-driven approaches to enhance predictive capabilities for basin-level water disasters. Overall, the key challenges currently facing water disaster prediction research in the Yellow River Basin include the following: (1) elucidating the complex water-sediment coupling mechanisms in the Yellow River Basin and enhancing the generalization capabilities of AI models for extreme events in data-scarce contexts; (2) dynamic simulation of the Yellow River Basin under the coupled effects of intense human activities and climate change; (3) collaborative application of integrated "space, ground, and water" data in the Yellow River Basin; (4) constructing an intelligent decision-making system that encompasses the entire forecasting-warning-response chain. Moving forward, it is essential to deepen the construction of models that integrate physical mechanisms and data-driven approaches, develop intelligent supercomputing and digital twin platforms at the basin scale, establish intelligent predictive theories and methods for extreme flood events with small and zero samples, and construct adaptive learning and dynamic optimization intelligent early warning systems. Additionally, promoting interdisciplinary and interdepartmental collaboration in intelligent flood prevention and disaster reduction applications will provide robust technological support for ensuring the safety and resilience of the Yellow River.

3.3. Challenges and Strategies for Water Resource Efficiency and Intensive Management in the Yellow River Basin

The Yellow River Basin is characterized by weak natural endowments of water resources and pronounced spatiotemporal unevenness. With a water resources development and utilization rate as high as 80%, the basin has long faced the contradiction between increasing water demand and limited supply capacity. Achieving efficient and intensive utilization of water resources has therefore become the major challenge for ecological protection and high-quality development in the Yellow River Basin [15]. In recent years, scholars have conducted extensive discussions on the issues of efficient utilization and intensive management of water resources in the Yellow River Basin, covering a wide range of topics such as multi-sectoral water efficiency assessment [16], water resources optimal allocation of irrigation region [17], basin-scale regulation of water resources intensive utilization [18], and sustainable management strategies for basin water resources [19]. These research achievements provide valuable reference schemes and data support for integrated management and policy design of water resources in the Yellow River Basin. However, how to effectively integrate multiple dimensions including water resources, socioeconomic systems, and ecological environments under complex and changing conditions, and systematically plan strategies for efficient and intensive water resource utilization in the basin [20], still requires further exploration. In light of the realities of the Yellow River Basin, several key issues remain to be addressed: understanding the evolutionary mechanisms of water resource efficiency and driving forces of supply–demand imbalance; developing comprehensive measurement systems and integrated methodological frameworks for water resource efficiency; constructing dynamic regulation models for basin-scale water resource systems; innovating institutional frameworks and expanding management pathways for intensive water utilization. Consequently, future research priorities under this theme should include, but are not limited to: analysis of basin water system evolutionary mechanisms; integration and optimization of water resource efficiency measurement frameworks; development and coupled simulation of basin water resource regulation models; construction of efficient and intensive management models for basin water resources; simulation of synergistic policies for water resource efficiency and carbon emission reduction; and the design of coordinated development pathways for multi-dimensional systems under the rigid constraints of water resources.

3.4. Ecological Environment Protection and Intelligent Forecasting in the Yellow River Basin

With the increasing improvement of the Yellow River at the national strategic level, the relevant government regulatory authorities have also put forward more stringent requirements for ecological protection along the river basin. Compared with other large rivers in China, such as the Yangtze River and the Huaihe River, the Yellow River has a very high sediment concentration, which gives it relatively complex and changeable hydrological conditions [21]. In addition, suspended sediment plays a dual role in transmission carrier and reaction surface, which is of vital importance in the environmental behavior of contaminants [22]. Against this backdrop, growing scholarly attention has shifted toward integrated studies of hydrological prediction, coupled contaminant-sediment dynamics, and basin-wide ecological risk assessment. Over the past decades, the integration of satellite remote sensing, unmanned aerial vehicles, and in situ sensor arrays revolutionized data acquisition, yielding extensive, high-resolution records of hydrological and ecological processes [23,24]. These datasets, though abundant and of considerable potential value, have long remained underexploited due to technical limitations. The rapid emergence of artificial intelligence now provides new opportunities to unlock its utility. Graph neural networks, long short-term memory architectures, and physics-informed models have proven capable of capturing hydrodynamic complexity while adhering to conservation laws, thereby improving the precision of predictions for contaminant transport and transformation [25,26]. At finer scales, machine-learning frameworks grounded in chemical reaction networks, when coupled with semi-targeted chemical screening, can reveal transient intermediates that are often overlooked by conventional monitoring. Complementary tools such as quantitative structure–activity relationship models and Bayesian inference further extend this analysis, enabling early prediction of toxicological impacts [27,28]. Embedding these tools into basin-scale platforms would allow regulators to identify ecological risk in real time and strategically allocate limited resources to areas of greatest need. Although the vision is encouraging, there are still some obstacles in the current development. For example, the migration and transformation mechanism of contaminants on the sediment interface has not been well verified, which limits the interpretation basis of the prediction work. During extreme seasons, sediment dynamics will deviate from steady-state conditions, resulting in a decrease in prediction accuracy. In addition, there is insufficient integration between hydrology, ecology and computational science. Looking ahead, the coupling of machine learning with mechanism insight and high-resolution analysis technology can improve the accuracy and interpretability of prediction at the same time, which is helpful to change the management mode of the basin from passive restoration to predictive prevention.

3.5. High-Quality Development Path and Strategies

Research on the high-quality development of the Yellow River Basin has gradually established a multi-level and multi-dimensional theoretical framework, achieving notable progress in resource management, ecological restoration, and regional economic coordination [29,30]. Current studies mainly focus on the synergistic mechanisms between ecological conservation and economic growth, the innovative application of green technologies, and differentiated regional governance strategies [31–33], thereby providing essential scientific evidence and strategic guidance for the sustainable development. Achieving high-quality development of the Yellow River Basin, ensuring the effective implementation of strategic pathways and policies, and realizing the harmonious coexistence of the human–water relationship remain pressing issues requiring further in-depth investigation. At present, research in this field faces four critical challenges: (1) uncertainties in pathway selection hinder the implementation of development strategies; (2) the complexity of regionally differentiated governance prevents the establishment of unified management measures;

(3) the mechanisms for coordinated development of the human–water system remain underdeveloped; (4) the application of emerging technologies in water resource management is still constrained. To explore feasible pathways and strategies for high-quality development of the Yellow River Basin and to achieve coordinated development of the human–water system [34], future research priorities should encompass, but are not limited to, the following areas: improve the theory and application of harmonious coexistence of "Defining the scales based on water"; intelligent water resource management and the application of big data; constructing a multi-system collaborative development mechanism for water resources, economy, society, and the ecological environment; optimizing the "supply-use" regulation pattern across multiple water sources, processes, and sectors in the basin; universal application of green technologies and digital management techniques; constructing intelligent water resource scheduling and multi-level management systems; improving the legal framework and policy safeguards for the Yellow River; water resource risk-benefit assessment and emergency management mechanisms; scientifically coordinating the relationship between water and development under the rigid constraints of water resources.

3.6. Construction and Efficient Management of Yellow River Water Conservancy Projects in the New Era

The Yellow River water conservancy projects, as the core infrastructure ensuring flood control safety, water resource supply, and ecological stability in the Yellow River Basin [35], face severe challenges in the new era from climate change, accelerated urbanization processes, and high-quality development demands [36]. Scholars have conducted a large amount of scientific research on the construction and management of Yellow River water conservancy projects, covering aspects such as project planning, construction technology, risk assessment, operation scheduling, and benefit evaluation [37,38]. The existing results have significant scientific value and practical significance in enhancing project resilience, optimizing water resource allocation, and promoting sustainable development [39,40]. However, focusing on the complex and changing engineering systems in the context of the new era, how to achieve green, intelligent, and efficient construction and management of water conservancy projects still requires further deepening. The key issues in the research on Yellow River water conservancy project construction and efficient management include four aspects: insufficient understanding of the establishment of technological innovation and adaptability mechanisms, lack of research on green development theory and integrated operation and management systems, the need to strengthen digital twin simulation technology, and the need to expand multi-level risk prevention and control and benefit enhancement paths. To achieve high-quality development of Yellow River water conservancy projects in the new era, future key research areas include but are not limited to the following aspects: exploration and practical application of green low-carbon water conservancy project theories, analysis of resilience formation mechanisms and climate change adaptation for water conservancy projects, innovation in integrated operation and management modes for water conservancy projects under digital transformation, exploration of sustainable utilization of water conservancy project materials and green development modes, simulation and quantification of multi-disaster coupled risks caused by water conservancy project construction, integrated technology for "monitoring-evaluation-assessment" coupling of water conservancy project construction effectiveness, construction of integrated platforms for intelligent supervision and early warning of water conservancy projects, research and development of health diagnosis technology for water conservancy projects under multi-source data fusion, and research on linkage regulation mechanisms for cross-basin water conservancy projects.

Author Contributions: Methodology, Q.Z.; investigation, X.D. and G.C.; writing—original draft preparation, W.Z.; writing—review and editing, Q.Z.; supervision, Q.Z. All authors have read and agreed to the published version of the manuscript.

Acknowledgments: The authors acknowledge the contributions of all authors of the ten papers in this Special Issue.

Conflicts of Interest: The author declares no conflicts of interest.

List of Contributions:

1. Zhang, Z.; Guo, X.; Cao, L.; Lv, X.; Zhang, X.; Yang, L.; Zhang, H.; Xi, X.; Fang, Y. Multi-Scale Variation in Surface Water Area in the Yellow River Basin (1991–2023) Based on Suspended Particulate Matter Concentration and Water Indexes. *Water* **2024**, *16*, 2704. https://doi.org/10.3390/w16182704.
2. Li, H.; Ma, H.; Zhang, J.; Chen, X.; Hong, X. Surface Water Resource Accessibility Assessment of Rural Settlements in the Yellow River Basin. *Water* **2024**, *16*, 708. https://doi.org/10.3390/w16050708.
3. Wang, Y.; Han, C.; Zhao, X. Optimization Study on Sequential Emptying and Dredging for Water Diversity Reservoir Group. *Water* **2024**, *16*, 2482. https://doi.org/10.3390/w16172482.
4. Li, B.; Wang, J.; Zhang, Y.; Sun, Y. Innovative Adaptive Multiscale 3D Simulation Platform for the Yellow River Using Sphere Geodesic Octree Grid Techniques. *Water* **2024**, *16*, 1791. https://doi.org/10.3390/w16131791.
5. Zhang, Z.; Wang, W.; Zhang, X.; Zhang, H.; Yang, L.; Lv, X.; Xi, X. A Harmony-Based Approach for the Evaluation and Regulation of Water Security in the Yellow River Water-Receiving Area of Henan Province. *Water* **2024**, *16*, 2497. https://doi.org/10.3390/w16172497.
6. Liu, L.; He, L.; Zuo, Q. Evaluating the Human–Water Relationship over the Past Two Decades Using the SMI-P Method across Nine Provinces along the Yellow River, China. *Water* **2024**, *16*, 916. https://doi.org/10.3390/w16070916.
7. Yu, Z.; Sun, X.; Yan, L.; Yu, S.; Li, Y.; Jin, H. Analysis of the Water Quality Status and Its Historical Evolution Trend in the Mainstream and Major Tributaries of the Yellow River Basin. *Water* **2024**, *16*, 2413. https://doi.org/10.3390/w16172413.
8. Yu, Z.; Sun, X.; Yan, L.; Li, Y.; Jin, H.; Yu, S. Spatiotemporal Changes in the Quantity and Quality of Water in the Xiao Bei Mainstream of the Yellow River and Characteristics of Pollutant Fluxes. *Water* **2024**, *16*, 2616. https://doi.org/10.3390/w16182616.
9. Hou, J.; Wang, J.; Chen, X.; Hu, Y.; Dong, G. Soil Erosion Dynamics and Driving Force Identification in the Yiluo River Basin Under Multiple Future Scenarios. *Water* **2025**, *17*, 2157. https://doi.org/10.3390/w17142157.
10. Zhang, D.; Jing, M.; Chang, B.; Chen, W.; Li, Z.; Zhang, S.; Li, T. Coordination Analysis and Driving Factors of "Water-Land-Energy-Carbon" Coupling in Nine Provinces of the Yellow River Basin. *Water* **2025**, *17*, 1138. https://doi.org/10.3390/w17081138.

References

1. Wu, X.; Feng, X.; Fu, B. Climate aridification and intensified human interference undermined water storage in the Lower Yellow River region. *Geogr. Sustain.* **2025**, *6*, 100303. [CrossRef]
2. Zeng, R.; Zhang, Z.; Zhao, S.; Su, R.; Wei, Z.; Wang, X.; Long, Z.; Ma, J.; Chen, G.; Meng, X. Effects of human and tectonic activities on groundwater in the upper Yellow River terraces of the loess Plateau. *J. Hydrol.* **2024**, *645*, 132279. [CrossRef]
3. Sang, S.; Li, Y.; Zong, S.; Yu, L.; Wang, S.; Liu, Y.; Wu, X.; Song, S.; Wang, X.; Fu, B. The modeling framework of the coupled human and natural systems in the Yellow River Basin. *Geogr. Sustain.* **2025**, *6*, 100294. [CrossRef]
4. Man, Y.; Yang, M.; Gou, X.; Wan, G.; Li, Y.; Wang, X. The characteristics and changes of the natural social binary water cycle in the Upper Yellow River Basin under the influence of climate change and human activities: A review. *J. Hydrol.-Reg. Stud.* **2024**, *56*, 102079. [CrossRef]
5. Xie, L.; Gao, R.; Wang, X.; Duan, L.; Fang, L.; Tong, H.; Yue, C.; Liu, T. Spatiotemporal evolution of surface water quality and driving factors across varying levels of human interference in a major subbasin of the Yellow River Basin, China. *J. Hydrol.-Reg. Stud.* **2025**, *59*, 102327. [CrossRef]

6. Gu, X.; Jin, H.; Luo, J. The associated ecological risks identification and optimal management of basin "water-energy-food-ecology" nexus: A case study of the yellow river basin. *J. Clean. Prod.* **2025**, *520*, 146129. [CrossRef]
7. Wang, S.; Yang, Y.; Tang, Z.; Wang, C.; Wang, F. Evolution of urban network patterns in the Yellow River Basin based on human mobility over 1,300 years. *Appl. Geogr.* **2025**, *178*, 103587. [CrossRef]
8. Yu, D.; Zhu, Q.; Zhang, J.; Wang, L.; Wu, X.; Jiang, S.; Fang, X.; Jin, J.; Wang, Y.; Ren, L. Patterns of blue and green water in the Yellow River Basin from 1998 to 2020: Influence of climate change and human activity. *J. Hydrol.-Reg. Stud.* **2025**, *59*, 102367. [CrossRef]
9. Zhang, Y.; Ci, H.; Yang, H.; Wang, R.; Yan, Z. Rainfall-Induced Geological Hazard Susceptibility Assessment in the Henan Section of the Yellow River Basin: Multi-Model Approaches Supporting Disaster Mitigation and Sustainable Development. *Sustainability* **2025**, *17*, 4348. [CrossRef]
10. Ju, Q.; Wu, J.; Shen, T.; Wang, Y.; Cai, H.; Jin, J.; Jiang, P.; Chen, X.; Du, Y. Enhancing climate projections via machine learning: Multi-model ensemble of precipitation and temperature in the source region of the Yellow River. *J. Hydrol.* **2025**, *662*, 133945. [CrossRef]
11. Meng, X.; Lin, C.; Ding, J.; Wang, G.; Zhang, J.; Wang, H.; Chu, C. Spatiotemporal evolution of droughts and floods in the Yellow River Basin: A novel approach combining CMADS-L evaluation, hydroclimatic zonation and CNN-LSTM prediction. *J. Hydrol.-Reg. Stud.* **2025**, *58*, 102250.
12. Ye, P.; Zhang, Q.; Wang, J.; Liu, X.; Wei, D.; Liu, W.; Li, Y.; Huang, X.; Gan, Z. Interdecadal shifts and associated atmospheric circulation anomalies of heavy precipitation during the warm-season in the Upper Yellow River Basin over the past 40 years. *Atmos. Res.* **2025**, *314*, 107801.
13. Wang, J.; Li, X.; Wu, R.; Mu, X.; Baiyinbaoligao; Wei, J.; Gao, J.; Yin, D.; Tao, X.; Xu, K. A runoff prediction approach based on machine learning, ensemble forecasting and error correction: A case study of source area of Yellow River. *J. Hydrol.* **2025**, *658*, 133190. [CrossRef]
14. Ho, L.; Goethals, P. Machine learning applications in river research: Trends, opportunities and challenges. *Methods Ecol. Evol.* **2022**, *13*, 2603–2621. [CrossRef]
15. Wei, J.; Lei, Y.; Yao, H.; Ge, J.; Wu, S.; Liu, L. Estimation and influencing factors of agricultural water efficiency in the Yellow River basin, China. *J. Clean. Prod.* **2021**, *308*, 127249. [CrossRef]
16. Zhang, X.; Guo, P.; Zhang, F.; Liu, X.; Yue, Q.; Wang, Y. Optimal irrigation water allocation in Hetao Irrigation District considering decision makers' preference under uncertainties. *Agr. Water Manag.* **2021**, *246*, 106670. [CrossRef]
17. Niu, C.; Chang, J.; Wang, Y.; Shi, X.; Wang, X.; Guo, A.; Jin, W.; Zhou, S. A Water Resource Equilibrium Regulation Model Under Water Resource Utilization Conflict: A Case Study in the Yellow River Basin. *Water Resour. Res.* **2022**, *58*, e2021WR030779. [CrossRef]
18. Zhang, W.; Liang, W.; Gao, X.; Li, J.; Zhao, X. Trajectory in water scarcity and potential water savings benefits in the Yellow River basin. *J. Hydrol.* **2024**, *633*, 130998. [CrossRef]
19. Zhang, Y.; Yang, P.; Liu, J.; Zhang, X.; Zhao, Y.; Zhang, Q.; Li, L. Sustainable agricultural water management in the Yellow River Basin, China. *Agr. Water Manag.* **2023**, *288*, 108473. [CrossRef]
20. Guo, L.; Zhu, W.; Wei, J.; Wang, L. Water demand forecasting and countermeasures across the Yellow River basin: Analysis from the perspective of water resources carrying capacity. *J. Hydrol.-Reg. Stud.* **2022**, *42*, 101148. [CrossRef]
21. Yin, S.; Gao, G.; Ran, L.; Li, D.; Lu, X.; Fu, B. Extreme streamflow and sediment load changes in the Yellow River Basin: Impacts of climate change and human activities. *J. Hydrol.* **2023**, *619*, 129372. [CrossRef]
22. Liu, R.; Liu, L.; Liu, Y.; Wang, L. Comprehensive evaluation of antibiotic pollution in a typical tributary of the Yellow River, China: Source-specific partitioning and fate analysis. *J. Hazard. Mater.* **2025**, *488*, 137294. [CrossRef]
23. Liu, Q.; Chen, Y.; Brêda, J.P.L.F.; Cui, H.; Duan, H.; Huang, C. Higher-density river discharge observation through integration of multiple satellite data: Midstream Yellow River, China. *Int. J. Appl. Earth Obs.* **2025**, *137*, 104433. [CrossRef]
24. Qiu, Z.; Liu, D.; Duan, M.; Chen, P.; Yang, C.; Li, K.; Duan, H. Four-decades of sediment transport variations in the Yellow River on the Loess Plateau using Landsat imagery. *Remote Sens. Environ.* **2024**, *306*, 114147.
25. Mu, T.; Duan, F.; Ning, B.; Zhou, B.; Liu, J.; Huang, M. ST-GPINN: A spatio-temporal graph physics-informed neural network for enhanced water quality prediction in water distribution systems. *Npj Clean. Water* **2025**, *8*, 74.
26. Wan, H.; Xiang, L.; Cai, Y.; Xie, Y.; Xu, R. Temporal and spatial feature extraction using graph neural networks for multi-point water quality prediction in river network areas. *Water Res.* **2025**, *281*, 123561. [CrossRef]
27. Du, Y.; Tang, T.; Song, D.; Wang, R.; Liu, H.; Du, X.; Dang, Z.; Lu, G. Prediction of chlorination degradation rate of emerging contaminants based on machine learning models. *Environ. Pollut.* **2025**, *372*, 125976. [CrossRef] [PubMed]
28. Huizenga, J.M.; Semprini, L.; Garcia-Jaramillo, M. Identification of Potentially Toxic Transformation Products Produced in Polycyclic Aromatic Hydrocarbon Bioremediation Using Suspect and Non-Target Screening Approaches. *Environ. Sci. Technol.* **2025**, *59*, 7561–7573. [CrossRef]

29. Zhao, X.; Li, X.; Deng, G.; Xi, Y. Decoupling Relationship between Resource Environment and High-Quality Economic Development in the Yellow River Basin. *Sustainability* **2023**, *15*, 9385. [CrossRef]
30. Chen, L.; Yu, W.; Zhang, X. Spatio-temporal patterns of High-Quality urbanization development under water resource constraints and their key Drivers: A case study in the Yellow River Basin, China. *Ecol. Indic.* **2024**, *166*, 112441.
31. Li, X.; Liu, G.; Zhao, Y.; Sun, Y.; Guo, J. Regional Green Development and Corporate Financialization: A Quasi-Natural Experiment on the Ecological Conservation and High-Quality Development of the Yellow River Basin. *Sustainability* **2024**, *16*, 4662.
32. Chen, Y.; Zhu, M.; Lu, J.; Zhou, Q.; Ma, W. Evaluation of ecological city and analysis of obstacle factors under the background of high-quality development: Taking cities in the Yellow River Basin as examples. *Ecol. Indic.* **2020**, *118*, 106771. [CrossRef]
33. Huang, X.; Shen, J.; Sun, F.; Wang, L.; Zhang, P.; Wan, Y. Study on the Spatial and Temporal Distribution of the High–Quality Development of Urbanization and Water Resource Coupling in the Yellow River Basin. *Sustainability* **2023**, *15*, 12270. [CrossRef]
34. An, S.; Zhang, S.; Hou, H.; Zhang, Y.; Xu, H.; Liang, J. Coupling Coordination Analysis of the Ecology and Economy in the Yellow River Basin under the Background of High-Quality Development. *Land* **2022**, *11*, 1235. [CrossRef]
35. Kong, D.; Miao, C.; Duan, Q.; Li, J.; Zheng, H.; Gou, J. Xiaolangdi Dam: A valve for streamflow extremes on the lower Yellow River. *J. Hydrol.* **2022**, *606*, 127426. [CrossRef]
36. Jian, Z.; Yicheng, F.; Jinyong, Z.; Haixue, L.; Na, L. An emergy-based indicator framework for assessing regional ecosystem health and ecological service value: Impacts of water conservancy projects. *Ecol. Indic.* **2025**, *178*, 113954. [CrossRef]
37. Li, F.; Du, X.; Huang, X.; Li, H.; Fei, X. Social stability risk analysis caused by land acquisition and migration for water conservancy project construction. *Sci. Rep.* **2025**, *15*, 18672. [CrossRef] [PubMed]
38. Sun, B.; Hu, S.; Wang, J.; Guo, J.; Wu, S.; Wang, P. Regional slope stability and slope failure mechanics under strong seismic events in the upper reaches of Yellow River cascade reservoir dams via the SEM–FDEM–SPH coupling approach. *Comput. Geotech.* **2025**, *186*, 107334.
39. Liu, Y.; Xia, J.; Zhou, M.; Cheng, Y.; Deng, S.; Miao, C. Response of braiding intensity in a braided reach of the Lower Yellow River to upstream damming. *Glob. Planet. Change* **2025**, *253*, 104911.
40. Shen, Y.; Zheng, S.; Qin, C.; Li, J.; Ma, Z.; Wu, B.; Xu, M.; Xue, Y. Equilibrium tendency of river channel adjustment in response to upstream damming: A case study of the Lower Yellow River. *J. Hydrol.* **2025**, *650*, 132494.

water

MDPI

Article

Multi-Scale Variation in Surface Water Area in the Yellow River Basin (1991–2023) Based on Suspended Particulate Matter Concentration and Water Indexes

Zhiqiang Zhang [1,2], Xinyu Guo [1], Lianhai Cao [1,*], Xizhi Lv [3], Xiuyu Zhang [4], Li Yang [1], Hui Zhang [1], Xu Xi [5,*] and Yichen Fang [1]

[1] College of Surveying and Geo-Informatics, North China University of Water Resources and Electric Power, Zhengzhou 450001, China; zhangzhiqiang@ncwu.edu.cn (Z.Z.); 201904419@stu.ncwu.edu.cn (X.G.); zhyl@ncwu.edu.cn (L.Y.); huihui945726@163.com (H.Z.); fangyichenncwu@163.com (Y.F.)
[2] Key Laboratory of Geospatial Technology for Middle and Lower Yellow River Regions (Henan University), Ministry of Education, Kaifeng 475000, China
[3] Yellow River Institute of Hydraulic Research, Zhengzhou 450003, China; nihulvxizhi@163.com
[4] College of Water Resources, North China University of Water Resources and Electric Power, Zhengzhou 450001, China; zhangxiuyu@ncwu.edu.cn
[5] School of Geography Science and Geomatics Engineering, Suzhou University of Science and Technology, Suzhou 215009, China
* Correspondence: caolianhai1970@163.com (L.C.); xixu@mail.usts.edu.cn (X.X.)

Abstract: Surface water is a crucial part of terrestrial ecosystems and is crucial to maintaining ecosystem health, ensuring social stability, and promoting high-quality regional economic development. The surface water in the Yellow River Basin (YRB) has a high sediment content and spatially heterogeneous sediment distribution, presenting a significant challenge for surface water extraction. In this study, we first analyze the applicability of nine water indexes in the YRB by using the Landsat series images (Landsat 5, 7, 8) and then examine the correlation between the accuracy of the water indexes and suspended particulate matter (SPM) concentrations. On this basis, we propose a surface water extraction method considering the SPM concentrations (SWE-CSPM). Finally, we examine the dynamic variations in the surface water in the YRB at four scales: the global scale, the secondary water resource zoning scale, the provincial scale, and the typical water scale. The results indicate that (1) among the nine water indexes, the MBWI has the highest water extraction accuracy, followed by the AWEInsh and WI2021, while the NDWI has the lowest. (2) Compared with the nine water indexes and the multi-index water extraction rule method (MIWER), the SWE-CSPM can effectively reduce the commission errors of surface water extraction, and the water extraction accuracy is the highest (overall accuracy 95.44%, kappa coefficient 90.62%). (3) At the global scale, the maximum water area of the YRB shows a decreasing trend, but the change amount is small. The permanent water area shows an uptrend, whereas the seasonal water area shows a downtrend year by year. The reason may be that the increase in surface runoff and the construction of reservoir projects have led to the transformation of some seasonal water into permanent water. (4) At the secondary water resource zoning scale, the permanent water area of other secondary water resource zonings shows an increasing trend in different degrees, except for the Interior Drainage Area. (5) At the provincial scale, the permanent water area of all provinces shows an uptrend, while the seasonal water areas show a fluctuating downtrend. The maximum water area of Shandong, Inner Mongolia Autonomous Region, and Qinghai increases slowly, while the other provinces show a decreasing trend. (6) At the typical water scale, there are significant differences in the water area variation process in Zhaling Lake, Eling Lake, Wuliangsuhai, Hongjiannao, and Dongping Lake, but the permanent water area and maximum water area of these waters have increased over the past decade. This study offers significant technical support for the dynamic monitoring of surface water and helps to deeply understand the spatiotemporal variations in surface water in the YRB.

Keywords: surface water extraction; surface water spatiotemporal variation; Yellow River Basin; suspended particulate matter

1. Introduction

Surface water serves as a critical component of terrestrial ecosystems, which is essential for maintaining ecosystem health, ensuring social stability, and promoting high-quality regional economic development. The spatial pattern of global surface water has undergone significant changes primarily due to climate change and human activities' impact [1]. Previous studies have indicated that the global permanent water area has decreased by 90,000 km^2 over the past few decades, with over 70% of this loss concentrated in the Middle East and Asia [2]. Due to dam construction and water conservation policies, China's surface water area has increased by 9110 km^2 from 2000 to 2015 [3–5]. This indicates that although global water areas are generally decreasing, different regions exhibit varying trends. Extreme changes in surface water area often lead to severe water resource issues (such as floods, droughts, etc.), constrain regional economic development, and endanger people's lives and property safety [6]. Therefore, regional monitoring of surface water area changes is essential to mitigate the risks posed by extreme water issues.

Multi-spectral satellite remote sensing images have the advantages of large scale, low cost, and repeated observation, providing valuable data sources for the dynamic monitoring of surface water [7,8]. Compared to traditional site monitoring, remote sensing technology is more conducive to continuous surface water monitoring from a spatial perspective [6]. The water index method is widely used in surface water extraction based on remote sensing images [9]. The method is based on the principle that with the increase in the wavelength, water reflectance gradually decreases, with a higher reflectance observed in the blue-green band and lower reflectance in the infrared band. The Normalized Difference Water Index (NDWI) serves as the first water index leveraging the normalized difference between the green and near-infrared bands [10]. Numerous studies indicate that the NDWI has a good effect on water extraction in areas with high vegetation coverage but performs poorly in complex urban scenes [11]. To address the challenges, Xu [12] modified the NDWI by replacing the near-infrared band with the mid-infrared band. Water exhibits a lower reflectance in the mid-infrared and shortwave infrared bands, which is more effective than using the near-infrared band and shortwave infrared bands in the area covered with urban scenes. Previous studies have explored the applicability of the MNDWI in non-urban scenarios, and the results show that the MNDWI can easily misidentify snow, ice, and mountain shadows as surface water. Yan et al. [13] introduce a water–background linear mixed simulation based on the MNDWI for arid areas with sand, bare soil, and vegetated inland river. They propose the enhanced water index (EWI) to solve the problem of water extraction in arid river areas. To tackle shadow interference, Feyisa et al. [14] propose the Automated Water Extraction Index (AWEI), consisting of two forms: the AWEInsh and AWEIsh. The AWEIsh can effectively distinguish between water and shadow. Fisher et al. [11] construct the WI2015 by the linear discriminant analysis of surface reflectance data. Although this water index has a high extraction accuracy for Australia, its accuracy for other regions is still unknown. Wang et al. [15] constructed the MBWI, which significantly improves the water extraction accuracy in mountainous regions by mitigating mountain shadows. Hu et al. [16] explore the spectral characteristics of water with different sediment contents, and construct the WI2021. This method extracts water by enhancing water signals and suppressing reflectance differences in other ground objects based on the low-reflectance characteristics of water in the blue, green, red, near-infrared, and shortwave infrared bands. Wu et al. [17] construct the ratio water index (RWI), which can eliminate the influence of mixed pixels to a certain extent and make the water–land boundary more obvious.

Although a large number of water indexes have been proposed, each water body index has its own advantages and disadvantages, and no one water index can be applied to all scenarios with perfect performance. Many studies have integrated multiple water indexes to construct water extraction schemes, giving full play to the advantages of multiple water indexes and suppressing the disadvantages of each water index [18,19]. The most commonly used water extraction scheme in mid-latitude regions is the multi-index water extraction rule (MIWER) from Zou et al. [20]. This scheme combines a vegetation index

and water index according to a logical relationship. It limits the impact of vegetation on water through rules, greatly improves the accuracy of water, and has a better extraction effect on areas dominated by vegetation.

Machine learning classification methods, including supervised classification (such as K-Nearest Neighbors [21], Support Vector Machines [22–24], and Decision Trees/Random Forests [7,24–26]), and unsupervised classification (such as K-Means [27], Iterative Self-Organizing Data Analysis Technique [28], Density-Based Clustering [29], and Hierarchical Dynamic Clustering [30,31]), are another widely used approach for surface water extraction. Compared to unsupervised classification methods, supervised classification methods achieve higher water extraction accuracy. However, they rely on training samples, and their accuracy is highly dependent on the quality of these samples [32]. Therefore, how to quickly obtain high-quality training samples has become an important research direction for supervised classification-based surface water extraction. Recent studies frequently incorporate auxiliary data sources, such as OpenStreetMap (OSM) and surface water data products, to expedite the acquisition of training samples. For example, Zhang et al. [33] established an automatic water sample collection model based on OSM, which can automatically obtain high-precision water samples. With the rapid development of image recognition and classification methods, deep learning methods (such as convolutional neural networks [34,35], fully convolutional networks [36–38], U-Net [35,39], DeepLab [40,41], generative adversarial networks [24,42], and self-organizing maps [43]) are increasingly used in surface water extraction. These methods demonstrate strong recognition capabilities and high accuracy in water extraction. However, they require massive training samples and are complex and difficult to understand [44,45].

Overall, both water index methods and machine learning classification techniques have their respective advantages and limitations in water extraction. The water index can effectively extract water bodies through simple and easy band calculations. Therefore, its universality is deeply restricted by the mechanism. Additionally, determining the global optimal threshold is often challenging for large-scale surface water extraction due to the complexity of water spectral characteristics [46]. Machine learning classification methods have high water extraction accuracy, but these methods require researchers to have prior knowledge and collect training samples in advance. Therefore, for simpler scenes, it is advisable to use the water index method. However, the most appropriate water index should be carefully selected beforehand. In complex scenarios with significant heterogeneity in water spectral features, it is advisable to employ machine learning classification methods. In addition, we can also first transform the complex scenario into multiple simple scenarios and then extract surface water with an appropriate water index for each scenario.

Suspended particulate matter (SPM) in water refers to substances that are insoluble in water such as sediments, organic matter, and microorganisms, which can directly affect the water environment and water ecology. Compared with clean surface water, the spectral reflectance of water with a high SPM concentration shows a parabolic shape, with a trend of first increasing and then decreasing. And with the increase in the suspended particulate matter concentration, the reflectance peak shifts towards longer wavelengths, and the reflectance peak increases. According to the water index construction mechanism, the sensitivities to the SPM concentrations of different water indexes are different. Therefore, for areas with large spatial heterogeneity and a high SPM concentration, the water should first be classified according to the SPM concentration, and then the appropriate water index should be selected for each water type. Many studies have constructed SPM inversion methods and verified them with measured data. At present, the optical image inversion method mainly uses the red band reflectance value and the green band reflectance ratio or the near-red band reflectance value and the green band reflectance ratio. For example, the method used by Liu et al. [47] to invert the Yellow River Estuary achieved high accuracy.

The Yellow River is the fifth-longest river in the world, flowing through the Qinghai–Tibet Plateau, the Loess Plateau, and the North China Plain. The Yellow River accounts for only 2% of China's river runoff, but it needs to supply 12% of China's population with

water for production and domestic use and 15% of agricultural water for arable land [48]. Therefore, there is a severe contradiction between water supply and demand in the Yellow River Basin (YRB). Scientifically understanding the dynamic variations in surface water can provide available information for water resource management, agricultural water planning, and water resource optimization, significantly alleviating the supply–demand contradiction [49]. The characteristics of a large sediment content and spectral heterogeneity of surface water in the YRB pose significant challenges to surface water extraction [50]. Previous studies have established multi-index water extraction rules to achieve long-term water dynamic monitoring in the YRB, providing available information to understand the dynamic variation in surface water [3,19,51,52]. However, these methods typically rely on global segmentation thresholds and water extraction rules and have not considered the unique turbid surface water conditions of the YRB, resulting in numerous errors in surface water extraction. Additionally, the existing surface water dynamic monitoring research in the YRB lacks multi-scale comparative analysis.

Given this, this study fully considers the unique surface water characteristics of the YRB and establishes a surface water extraction method considering the suspended particulate matter concentration (SWE-CSPM) based on the concept of classification and grading. In addition, this study clarifies the surface water dynamic variation (1991–2023) in the YRB from four scales: the global scale, the secondary water resource zoning scale, the provincial scale, and the typical water bodies scale. The primary goals of this study are as follows: (1) verify the applicability of nine water indexes in the YRB. (2) Reveal the relationship between the SPM concentration and the water extraction accuracy of each water index and establish a surface water extraction method that accounts for the SPM concentration. (3) Describe the multi-scale surface water area changes in the YRB. This study provides an effective method for surface water extraction from multi-sediment rivers, and an important decision support for water resources management in the YRB.

2. Materials and Methods

2.1. Study Area

The Yellow River originates in the Bayan Har Mountains on the Qinghai–Tibet Plateau and flows eastward through Qinghai, Sichuan, Gansu, Ningxia Hui Autonomous Region, Inner Mongolia Autonomous Region, Shaanxi, Shanxi, Henan, and Shandong provinces, ultimately emptying into the Bohai Sea. The YRB spans approximately 5464 km and provides sufficient irrigation, revered as the cradle of Chinese civilization. It has 220 tributaries covering an area of 795,000 km^2. The mainstream is divided into upper, middle, and lower reaches according to the locations of Hekou Town and Taohuayu. The western source region is on the Qinghai–Tibet Plateau, with relatively high terrain covered with mountainous ice and snow landscapes. The central region lies on the Loess Plateau, with elevations between 1000 and 2000 m. It is prone to severe soil erosion, contributing to the main source of sediment in the Yellow River. The eastern region is part of the North China Plain, with an average elevation below 100 m. The YRB is divided into eight secondary water resource zonings based on topography and climate: Above Longyangxia, Longyangxia to Lanzhou City, Lanzhou City to Hekou Town, Hekou Town to Longmen County, Longmen County to Sanmenxia, Sanmenxia to Huayuankou, Below Huayuankou, and Interior Drainage Area (Figure 1). The YRB is one of the most severely eroded areas globally, with soil erosion affecting approximately 454,000 km^2, of which wind erosion affects about 117,000 km^2 and water erosion about 337,000 km^2. According to hydrological statistics from the Tongguan hydrological station, the annual average sediment transport from 1987 to 2020 was 466 million tons, with a sediment concentration of 18.1 kg/m^3. Serious soil erosion has transformed the Yellow River into a world-famous river with heavy sediment [53].

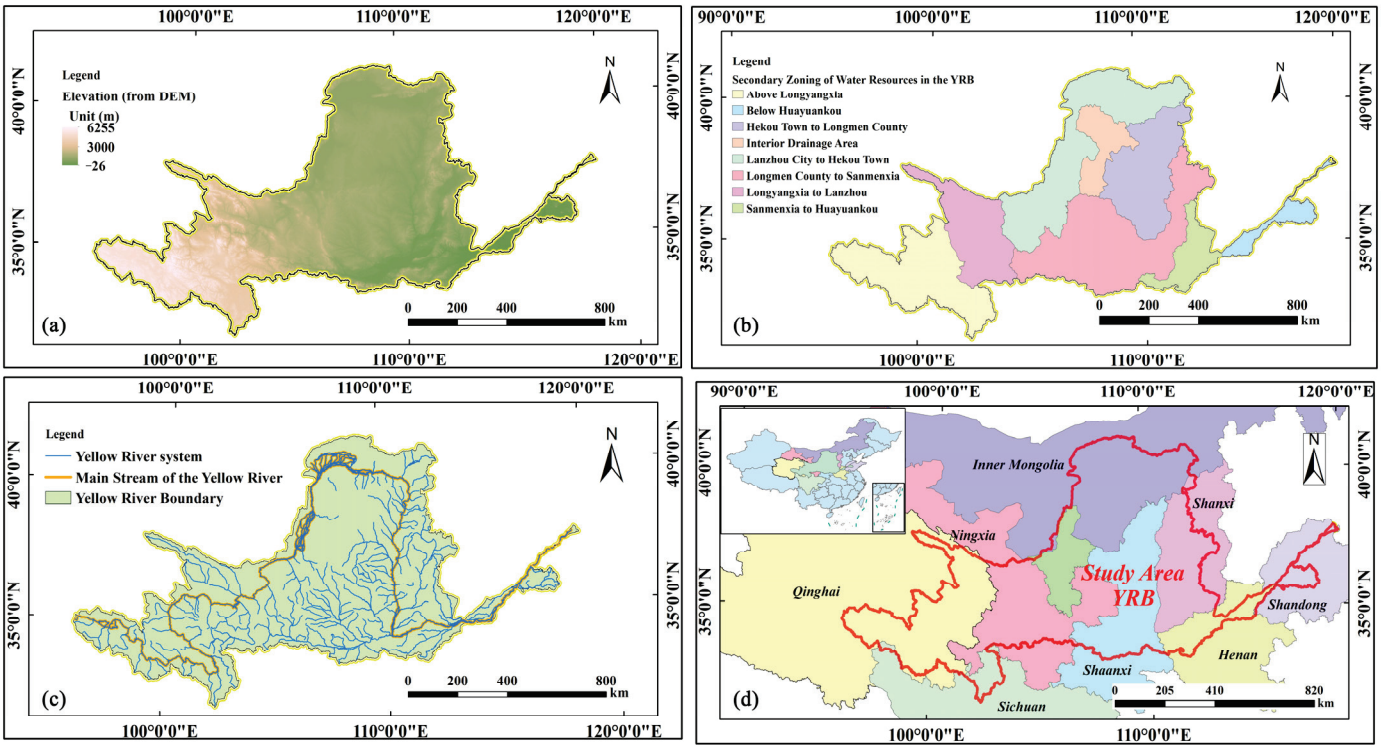

Figure 1. Study area in the YRB. (**a**) is the DEM of the Yellow River Basin, (**b**) is the secondary zoning map of the Yellow River Basin water resources, (**c**) is a schematic diagram of the Yellow River mainstream of the Yellow River Basin, and (**d**) is a provincial map of the Yellow River Basin.

2.2. Data

2.2.1. Remote Sensing Imagery

The Google Earth Engine (GEE) platform is used for data analysis and algorithm implementation. The Landsat series Tier 1 image collections are selected covering the YRB from 1991 to 2023 (a total of 70,642 scenes from Landsat 5, Landsat 7, and Landsat 8). In these images, the F-mask algorithm is used to eliminate invalid observation pixels, while the LEDAPS algorithm and LaSRC algorithm are used for atmospheric correction and geometric correction. In this study, auxiliary data (the Digital Elevation Model, DEM, and Sentinel 2) are chosen for further identification. The spatial resolution of the DEM is 30 m to eliminate the impact on mountain shadows. The JRC Dataset and Sentinel 2 image assist in sample collection and the evaluation of water extraction accuracy.

Figure 2 shows the spatial distribution of valid observations at the pixel scale for the YRB from 1991 to 2023. The northern part of the YRB has significantly more valid observations than the southern part, especially in the overlapping satellite areas. This is primarily due to the high latitude and mountainous terrain of the source region, which is more susceptible to cloud cover. Figure 3 displays the area proportion of valid observation counts for each year. Before 2000, the number of valid observations in most areas of the YRB is between 5 and 20. After 2000, this number is between 11 and 40, except for 2012.

2.2.2. Sample Point Selection

Following a stratified random sampling principle, more than 2900 samples (Figure 4) are visually interpreted and supplemented with Sentinel-2 MSI imagery and JRC data. These samples combine with 12 land cover types, including high-reflectance buildings, low-reflectance buildings, lakes/reservoirs, water in the upper reaches of the YRB, water in the middle reaches of the YRB, water in the lower reaches of the YRB, clouds, snow, building shadows, bare land, other shadows, and vegetation. For buildings, when selecting sample points, white, red, and bright blue buildings in the image are regarded as high-

reflective building elements. Dark gray and gray buildings in the image are regarded as low-reflective building elements.

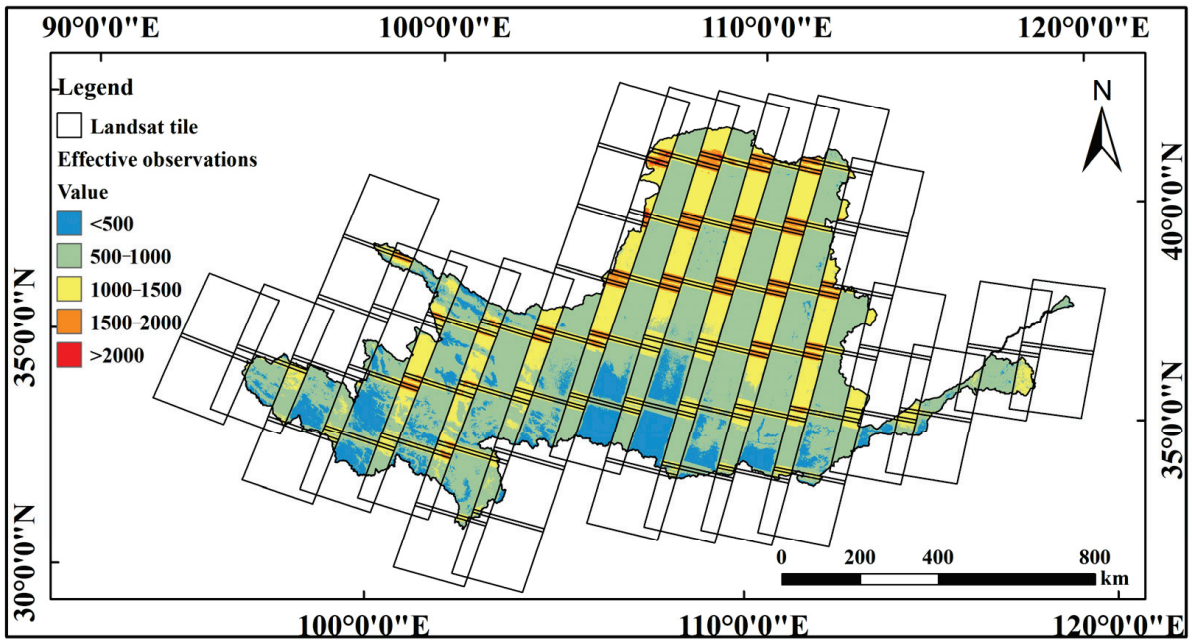

Figure 2. Spatial distribution of valid observations at the pixel scale in the YRB from 1991 to 2023.

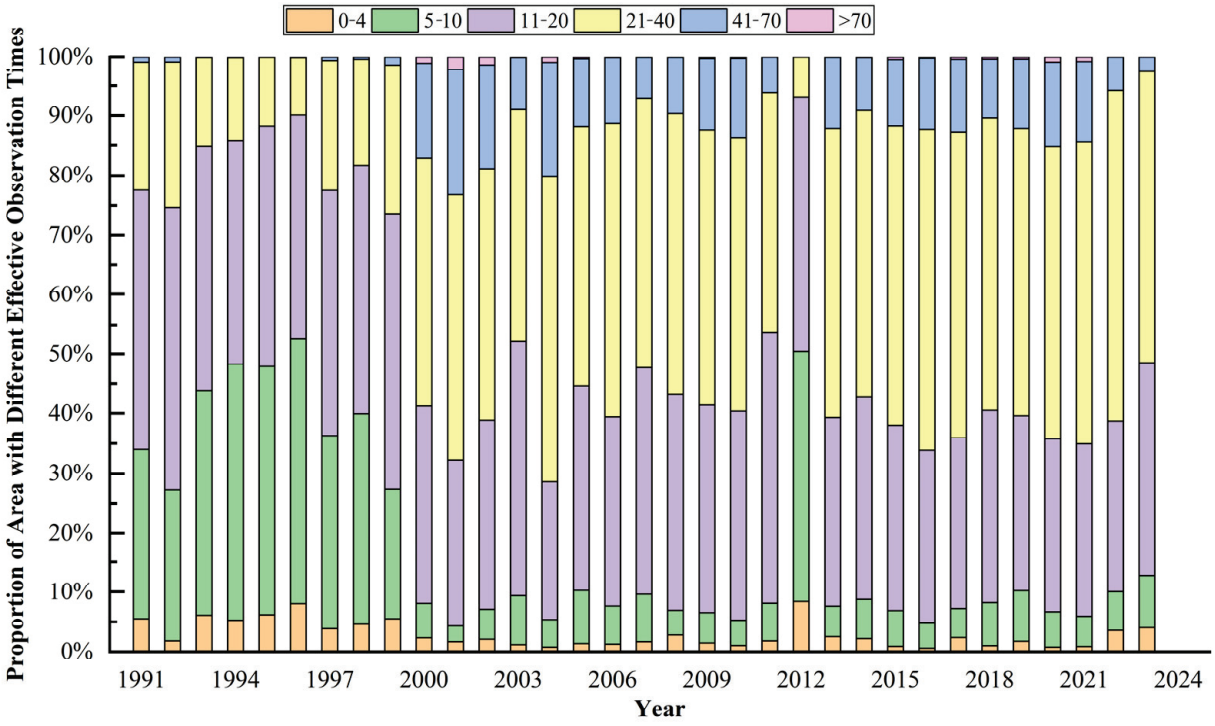

Figure 3. The percentage of pixels with effective observation in each segment. "0–4", "5–10", "11–20", "21–40", "41–70", and ">70" mean that the number of valid observations of a pixel in a year is between 0 and 4, 5 and 10, 11 and 20, 21 and 40, 41 and 70, and more than 70. This study further explores the proportion of the total number of pixels in each segment to the total number of pixels in the YRB.

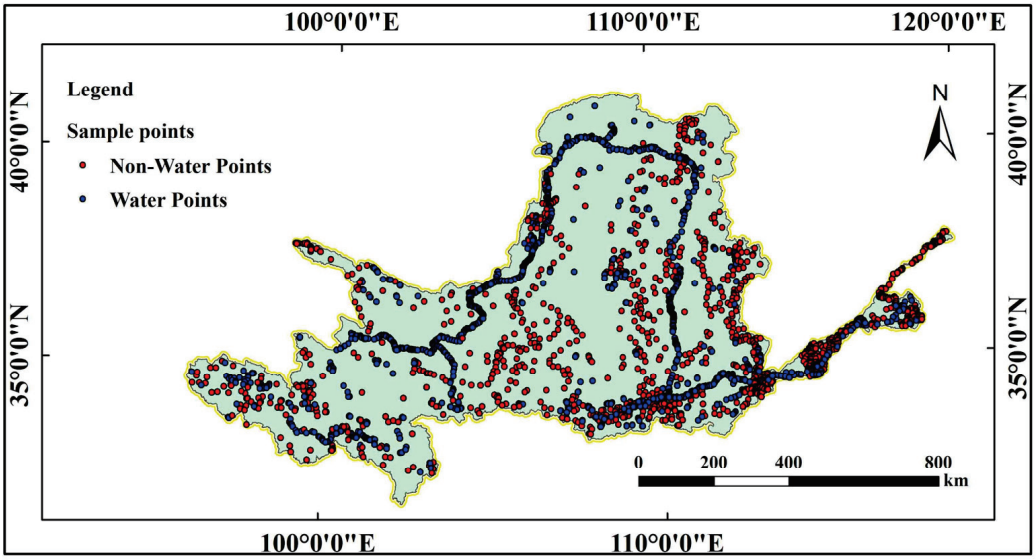

Figure 4. Spatial distribution of samples. For the subsequent accuracy evaluation, the study adopts a binary classification system (water and non-water).

Figure 5 shows the spectral characteristics of different land cover types. The water reflectance of the lower reaches is slightly higher than that of the upper reaches, middle reaches, and lake water. The reflectance peak of the lower reaches water is in the near-infrared band (Figure 5c), whereas the peaks for the upper reaches (Figure 5a) and middle reaches (Figure 5b) are in the red band, and for lakes and reservoirs (Figure 5d), in the green band. It can be inferred that the spectral reflectance of water increases with a higher sediment content, and the wavelength corresponding to the peak reflectance also increases. Shadows (Figure 5e,f) share similar spectral characteristics with water but exhibit a slightly lower reflectance. The spectral reflectance of vegetation (Figure 5g), bare land (Figure 5h), high-reflectance buildings (Figure 5l), low-reflectance buildings (Figure 5i), clouds (Figure 5j), and snow (Figure 5k) is significantly higher than that of water.

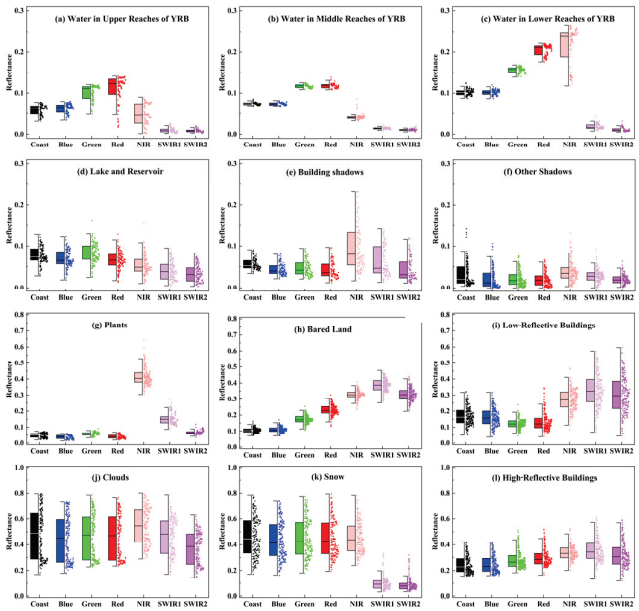

Figure 5. Spectral characteristics of different land cover types. Coast, Blue, Green, Red, NIR, SWIR1, and SWIR2 are the names of Band1-Coast aerosol, Band2-Blue, Band3-Green, Band4-Red, Band5-Near Infrared (NIR), Band6-Shortwave Infrared (SWIR)1, and Band7-Shortwave Infrared (SWIR)2 in Landsat 8 images, respectively.

3. Methods

Figure 6 presents the technical framework of this study, which consists of three parts: (1) analyze the relationship between the water index extraction accuracy and SPM concentration. Nine typical water indexes are selected for comparative analysis of their applicability in the YRB, and the correlation between the extraction accuracy of these indexes and SPM concentration is examined. (2) Establish a water extraction method considering the SPM concentration (SWE-CSPM). The SWE-CSPM is constructed according to the principle of classification and grading. Spectral characteristics and terrain slope are used for post-processing. (3) Multi-scale dynamic monitoring of surface water in the YRB. The surface water dataset of the YRB from 1991 to 2023 is made using the SWE-CSPM, and the water inundation frequency (WIF) model serves as an indicator to divide permanent, seasonal, and maximum water year by year. The dynamic changing characteristics of the surface water are analyzed from the global scale, the secondary water resource zoning scale, the provincial scale, and the typical water scale.

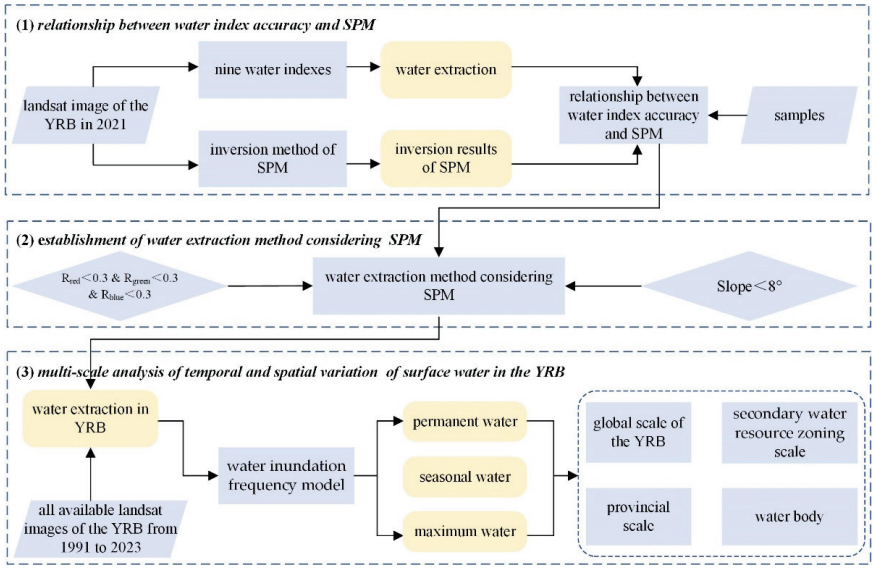

Figure 6. A flowchart of this study.

3.1. Water Indexes

Nine water indexes (NDWI, MNDWI, AWEInsh, AWEIsh, MBWI, WI2015, WI2021, RWI, and EWI) are selected to explore their applicability in the YRB. The details of the calculation for each water index are presented in Table 1.

Table 1. The nine water indexes selected in this study and their originations.

Water Index	Eq Id	Reference
$NDWI = \frac{\rho_{Green}-\rho_{NIR}}{\rho_{Green}+\rho_{NIR}}$	(1)	McFeeters et al. (1996) [10]
$MNDWI = \frac{\rho_{Green}-\rho_{MIR}}{\rho_{Green}+\rho_{MIR}}$	(2)	Xu (2005) [12]
$AWEI_{sh} = 4 \times (\rho_{Green} - \rho_{SWIR1}) - 0.25 \times \rho_{NIR} - 2.75 \times \rho_{SWIR2}$	(3)	Feyisa et al. (2014) [14]
$AWEI_{nsh} = \rho_{Blue} + 2.5 \times \rho_{Green} - 1.5 \times (\rho_{NIR} + \rho_{SWIR1}) - 0.25 \times \rho_{SWIR2}$	(4)	
$MBWI = 2 \times \rho_{Green} - \rho_{Red} - \rho_{NIR} - \rho_{SWIR1} - \rho_{SWIR2}$	(5)	Wang et al. (2018) [15]
$WI_{2021} = \frac{\rho_{Blue}+\rho_{Green}+\rho_{Red}-\rho_{NIR}-\rho_{SWIR1}-\rho_{SWIR2}}{\rho_{Blue}+\rho_{Green}+\rho_{Red}+\rho_{NIR}+\rho_{SWIR1}+\rho_{SWIR2}}$	(6)	Hu et al. (2022) [16]
$WI_{2015} = 1.7204 + 171 \times \rho_{Green} + 3 \times \rho_{Red} - 70 \times \rho_{NIR} - 45 \times \rho_{SWIR1} - 71 \times \rho_{SWIR2}$	(7)	Fisher et al. (2016) [11]
$RWI = \frac{\rho_{Green}+\rho_{Red}-2\times\rho_{NIR}-\rho_{SWIR2}}{\rho_{Green}+\rho_{Red}+2\times\rho_{NIR}+\rho_{SWIR2}}$	(8)	Wu et al. (2022) [17]
$EWI = \frac{\rho_{Green}-\rho_{SWIR1}+0.1}{\rho_{Green}+\rho_{SWIR1}} \times \left(\frac{\rho_{NIR}-\rho_{Red}}{\rho_{NIR}+\rho_{Red}} + 0.5\right)$	(9)	Wang et al. (2007) [13]

Notes: The labels of "ρ_{Blue}", "ρ_{Green} ", "ρ_{Red}", "ρ_{NIR}", "ρ_{MIR}", and "ρ_{SWIR}" represent the reflectance of blue, green, red, near-infrared, middle infrared, and short-wavelength infrared bands in Landsat series images.

3.2. SPM Concentration Retrieval

The SPM concentration is a crucial water quality parameter that is closely related to the spectral characteristics of water bodies. The SPM in the YRB is mainly suspended sediment. The SPM concentration inversion algorithm proposed by Liu et al. [47] is adopted in this study. The algorithm has been successfully applied to the inversion of SPM in the Yellow River Estuary [54]. The calculation model is as follows:

$$SPM = 10^{0.5897 \times \frac{\rho_{Red}}{\rho_{Green}} + 0.9864 \times \frac{\rho_{NIR}}{\rho_{Green}} + 1.3166} \quad (10)$$

where SPM represents the suspended particulate matter concentration, while ρ_{Green}, ρ_{Red}, ρ_{NIR} represent the surface reflectance of Band3-Green, Band4-Red, Band5-Near Infrared (NIR) in the Landsat 8 images, respectively.

Figure 7 shows the spatial distribution of the SPM concentration in the surface water of the YRB in 2021. Statistical analysis indicates that the water in the lower reaches has the highest SPM concentration (average 970 mg/L), followed by that in the middle reaches (average 700 mg/L), and the water in the upper reaches has the lowest concentration (average 630 mg/L).

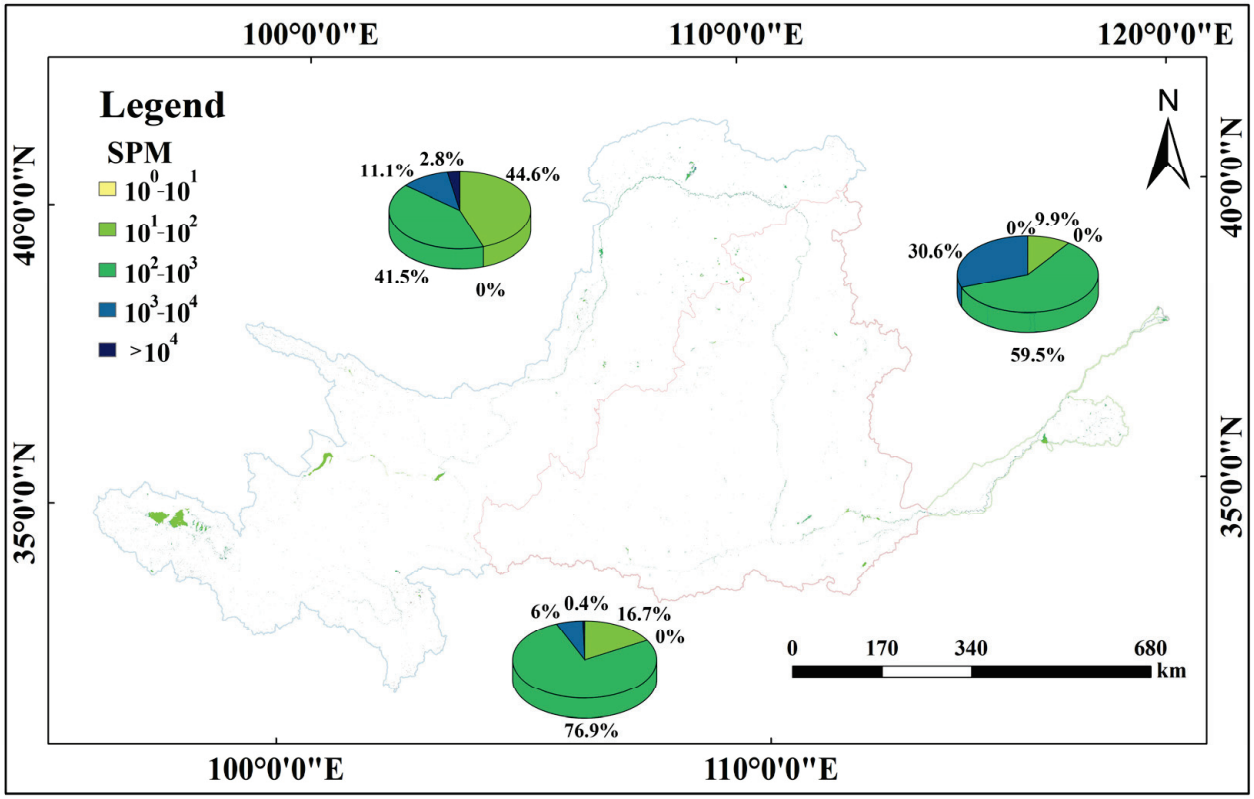

Figure 7. The spatial distribution of SPM concentration in surface water in 2021. The SPM concentration ranges from 0 to 10,000 mg/L in the YRB. However, that in lakes, reservoirs, and other water is lower than that in rivers.

3.3. Surface Water Extraction Method Considering SPM

The variation curves of different water indexes and SPM concentrations are illustrated in Figure 8. It is evident that the extraction accuracy of all water indexes decreases significantly with the increasing SPM. When the SPM is in the range of [0, $10^{2.8}$], all nine indexes achieve high extraction accuracy. Among them, the MBWI has the highest accuracy. When the SPM is in the range of ($10^{2.8}$, $10^{3.1}$], the extraction accuracy of the NDWI and MBWI decreases significantly. Among them, the WI2021 has the highest accuracy. When the SPM is in the range of ($10^{3.1}$, 10^{4}], the AWEInsh significantly outperforms the other water indexes.

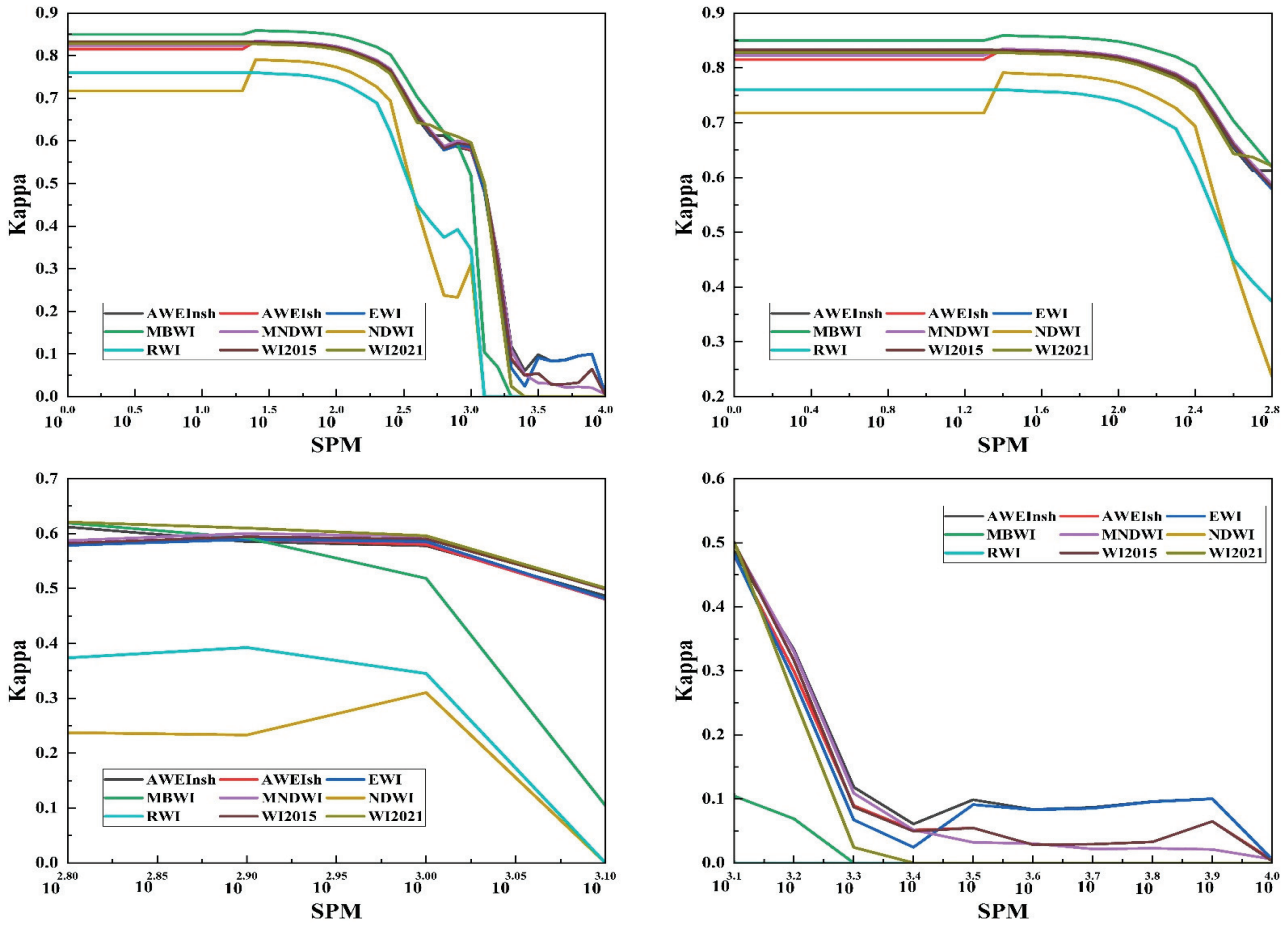

Figure 8. Change curve of water extraction accuracy (kappa coefficient) of each water index with the increase in SPM.

Based on the relationship between the extraction accuracy of each water index and SPM concentration, the SWE-CSPM is proposed. The model is as follows:

$$SWE_{SPM} = \begin{cases} MBWI \geq -0.15 & \left(0 \leq SPM \leq 10^{2.8}\right) \\ WI_{2021} \geq 0.04 & \left(10^{2.8} \leq SPM \leq 10^{3.1}\right) \\ AWEI_{nsh} \geq 0.05 & \left(10^{3.1} \leq SPM \leq 10^{4}\right) \end{cases} \quad (11)$$

When the SPM concentration of surface water is in the range of $[0, 10^{2.8}]$, surface water is identified based on the index model $MBWI \geq -0.15$. When the SPM concentration is in the range of $(10^{2.8}, 10^{3.1}]$, the index model $WI_{2021} \geq 0.04$ is used. When the SPM concentration is in the range of $(10^{3.1}, 10^{4}]$, the index model $AWEI_{nsh} \geq 0.05$ is used. These threshold parameters are determined by repeated tests.

Although this scheme can largely eliminate the interference of buildings and vegetation on water extraction, snow and mountain shadows are still easily misidentified as water. To solve these interference factors, this study constructs post-processing rules based on the spectral characteristics of different land cover types in Section 2.2.2. High-reflective features are excluded using the rule that the spectral reflectance of the red, green, and blue bands is less than 0.3. Furthermore, we exclude mountain shadows by applying the slope rule of less than 8°, which is in line with existing research findings.

3.4. Accuracy Evaluation

In order to scientifically evaluate the extraction accuracy of the water index, this study adopts the traditional accuracy evaluation criteria based on a confusion matrix,

including the overall accuracy (OA), kappa coefficient (kappa), commission errors (CEs), and omission errors (OEs). These formulas are as follows:

$$OA = \frac{\sum O_{ii}}{N} \tag{12}$$

$$Kappa = \frac{\frac{\sum_{i=1}^{k} O_{ii}}{N} - \sum_{i=1}^{k}\left(\frac{\sum_{j=1}^{k} O_{ij}}{N} \cdot \frac{\sum_{j=1}^{k} O_{ji}}{N}\right)}{1 - \sum_{i=1}^{k}\left(\frac{\sum_{j=1}^{k} O_{ij}}{N} \cdot \frac{\sum_{j=1}^{k} O_{ji}}{N}\right)} \tag{13}$$

$$CE_i = \frac{\sum_{j=1 j\neq i}^{k} O_{ji}}{\sum_{j=1}^{k} O_{ji}} \tag{14}$$

$$OE_i = \frac{\sum_{j=1 j\neq i}^{k} O_{ij}}{\sum_{j=1}^{k} O_{ij}} \tag{15}$$

where O represents the confusion matrix, N represents the total number of samples, O_{ij} represents the element in the i-th row and j-th column of the confusion matrix, O_{ji} represents the element in the j-th row and i-th column of the confusion matrix, and k is the number of categories.

In addition, this study also combines the MIWER by Zou et al. [19] for verification. The formula of MIWER is as follows:

$$\begin{gathered} MIWER = ((MNDWI > EVI)\ or\ (MNDWI > NDVI))\ and\ (EVI < 0.1) \\ EVI = 2.5 \times \frac{\rho_{NIR} - \rho_{Red}}{\rho_{NIR} + 6 \times \rho_{Red} - 7.5 \times \rho_{Blue} + 1} \\ NDVI = \frac{\rho_{NIR} - \rho_{Red}}{\rho_{NIR} + \rho_{Red}} \end{gathered} \tag{16}$$

among those, MNDWI is the water index, EVI and NDVI are the vegetation indexes. ρ_{Blue}, ρ_{Red}, ρ_{NIR} represent the reflectance of the blue, red, and near-infrared bands in the Landsat series images, respectively.

3.5. Water Inundation Frequency (WIF)

The WIF is a universal indicator that can monitor long-term changes in water. The WIF refers to the proportion of the number of times a pixel is judged to be water in a year to the total number of valid observations in that year. This study uses the WIF to classify surface water bodies into the largest, permanent, and seasonal water. The WIF is usually expressed as a percentage, and the calculation formula is shown below:

$$WIF = \frac{W}{N} \times 100\% \tag{17}$$

where W represents the count of a pixel identified as water. N represents the count of valid observations for a pixel in a year. Based on the existing research [52,55,56], the $WIF > 25\%$, $25\% < WIF \leq 75\%$, $WIF \geq 75\%$ and are defined as the maximum, seasonal, and permanent water, respectively.

4. Results

4.1. Water Extraction Accuracy

Based on the synthetic images in 2021, Appendix A Figure A1 illustrates the surface water extraction of various methods. Table 2 presents the water extraction accuracy. Among the nine water indexes, the MBWI demonstrates the highest accuracy, followed by the AWEInsh and WI2021, while the NDWI shows the lowest accuracy. Compared with the nine water indexes and the MIWER [19,55], the SWE-CSPM achieves the highest accuracy. The detailed information on the SWE-CSPM extraction accuracy is that the overall accuracy (OA) is 95.44% and the kappa coefficient is 90.65%. The overall accuracy of the SWE-CSPM increases by 2.84% and 1.44% compared to the MBWI and MIWER, respectively, while

the kappa coefficient increases by 5.64% and 2.88%. Notably, both the SWE-CSPM and the MIWER significantly reduce the commission error (CE), albeit with a slight increase in the omission error (OE). The reason for this improvement may be that the utilization of slope data and spectral characteristics of ground features in the post-processing stage effectively decreases the interference of high-reflective features and mountain shadows. To further validate the effectiveness of our approach, we also evaluate the accuracy before post-processing. The overall accuracy, kappa coefficient, commission error (CE), and omission error (OE) are 94.00%, 87.74%, 6.59%, and 7.45%, respectively. Both the overall accuracy and kappa coefficient exceed those of the individual water indexes, indicating that the proposed SWE-CSPM can effectively improve the extraction accuracy of surface water in the YRB.

Table 2. Extraction accuracy of surface water based on 2021 synthetic images using various methods.

Water Extraction Method	Overall Accuracy	Kappa	Commission Error	Omission Error
AWEInsh	91.71%	83.18%	11.76%	6.95%
AWEIsh	90.92%	81.52%	11.72%	9.13%
EWI	91.31%	82.33%	11.43%	8.46%
MBWI	92.60%	84.98%	10.35%	6.45%
MNDWI	91.49%	82.79%	12.70%	6.20%
NDWI	85.85%	71.75%	21.59%	7.54%
RWI	86.82%	73.61%	20.01%	7.62%
WI2015	91.45%	82.65%	11.70%	7.71%
WI2021	91.53%	82.81%	11.80%	7.37%
SWE-CSPM	95.44%	90.62%	2.58%	8.21%
MIWER	94.00%	87.74%	6.59%	7.45%

Figure 9 illustrates the water extraction of various methods in high mountainous regions (Scenario 1). This region is located at the source of the Yellow River, and the ice–snow and mountain shadows are the main interference factors for surface water extraction. It is obvious that the SWE-CSPM outperforms the nine water indexes and the MIWER, effectively decreasing the misclassification of shadow and ice–snow features as water. Figure 10 shows the water extraction of various methods in urban regions (Scenario 2). This region exhibits complex surface features with significant interferences, such as high-reflective buildings, low-reflective buildings, and building shadows. The SWE-CSPM demonstrates the most effective water extraction method, whereas the NDWI and AWEIsh performed poorly, with numerous ground objects misclassified as water. The water areas of the full image, Scenario 1, and Scenario 2 are shown in Figure 11.

4.2. Surface Water Area Changes in the YRB

4.2.1. Surface Water Area Changes at the Global Scale in the YRB

Figure 12 illustrates the area changes in the maximum, permanent, and seasonal water at the global scale of the YRB from 1991 to 2023. It is evident that the maximum water has exhibited a fluctuating downward trend during the study period, but the decreasing range is small. The area of permanent water initially decreases (1991–2001) and then increases (2001–2023), showing an overall uptrend. The seasonal surface water area exhibits a downtrend, with a reduction of 624 km^2 by 2023 compared to 1991. The average annual maximum water area is 8414 km^2, accounting for only 1.05% of the total area of the YRB, which is significantly lower than that in the Yangtze River Basin (approximately 2%) [56] and Hai River Basin (approximately 1.3%) [57]. This indicates that the visible surface water in the YRB is relatively small, closely due to the region's climatic characteristics of low precipitation and high evaporation. The average annual areas of permanent and seasonal water are 4662 km^2 and 3751 km^2, respectively, comprising 55% and 45% of the maximum surface water area, indicating that permanent water dominates in the YRB.

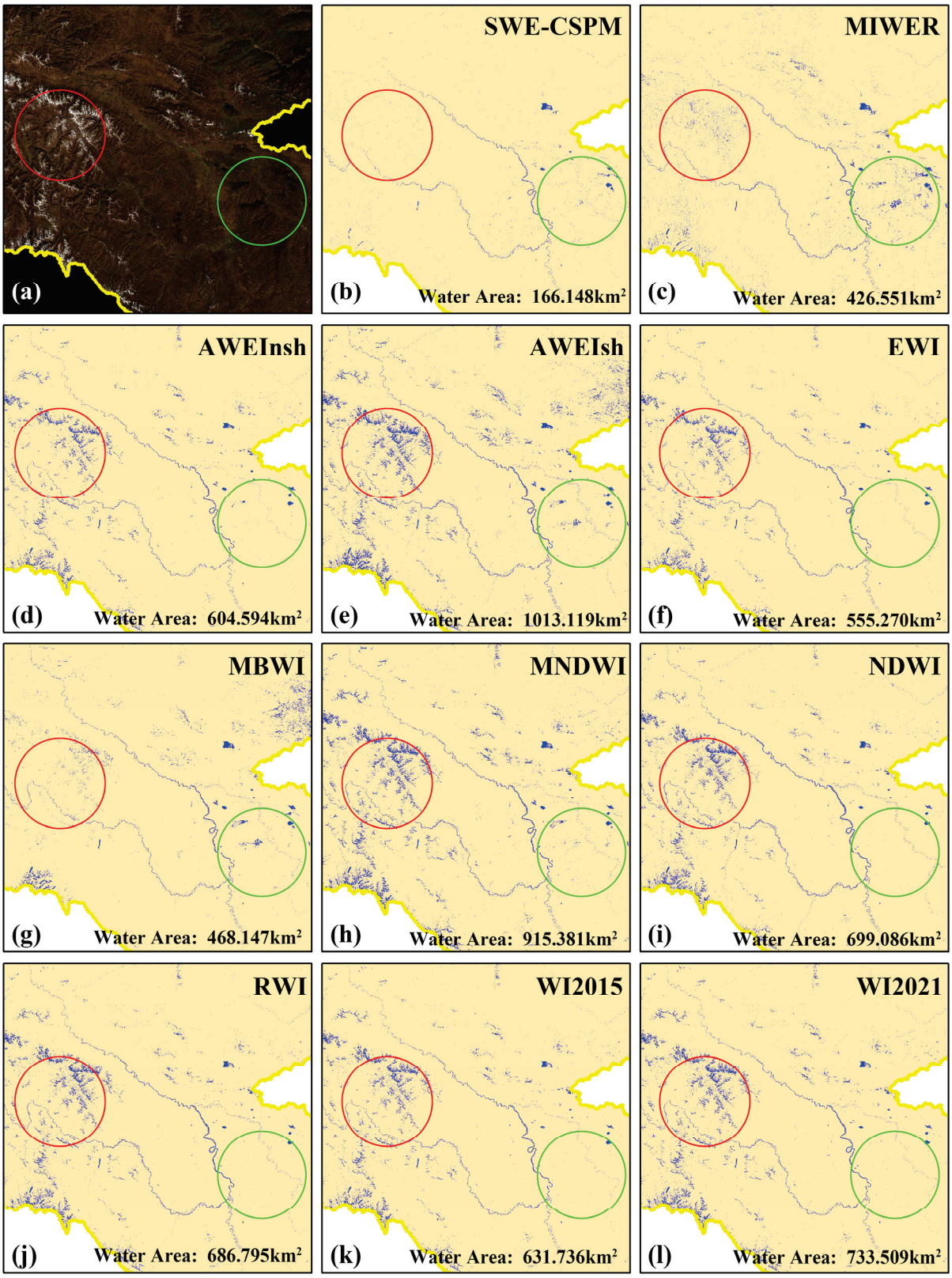

Figure 9. Surface water extraction of various methods in high mountain regions. The red circle is the area of ice–snow and the green circle is the area of shadow. (**a**) Landsat 8 true colour images of the area. (**b**–**l**), respectively the extraction effect of SWE-CSPM MIWER, AWEInsh, AWEIsh, EWI, MBWI, MNDWI, NDWI, RWI, WI2015 and WI2021.

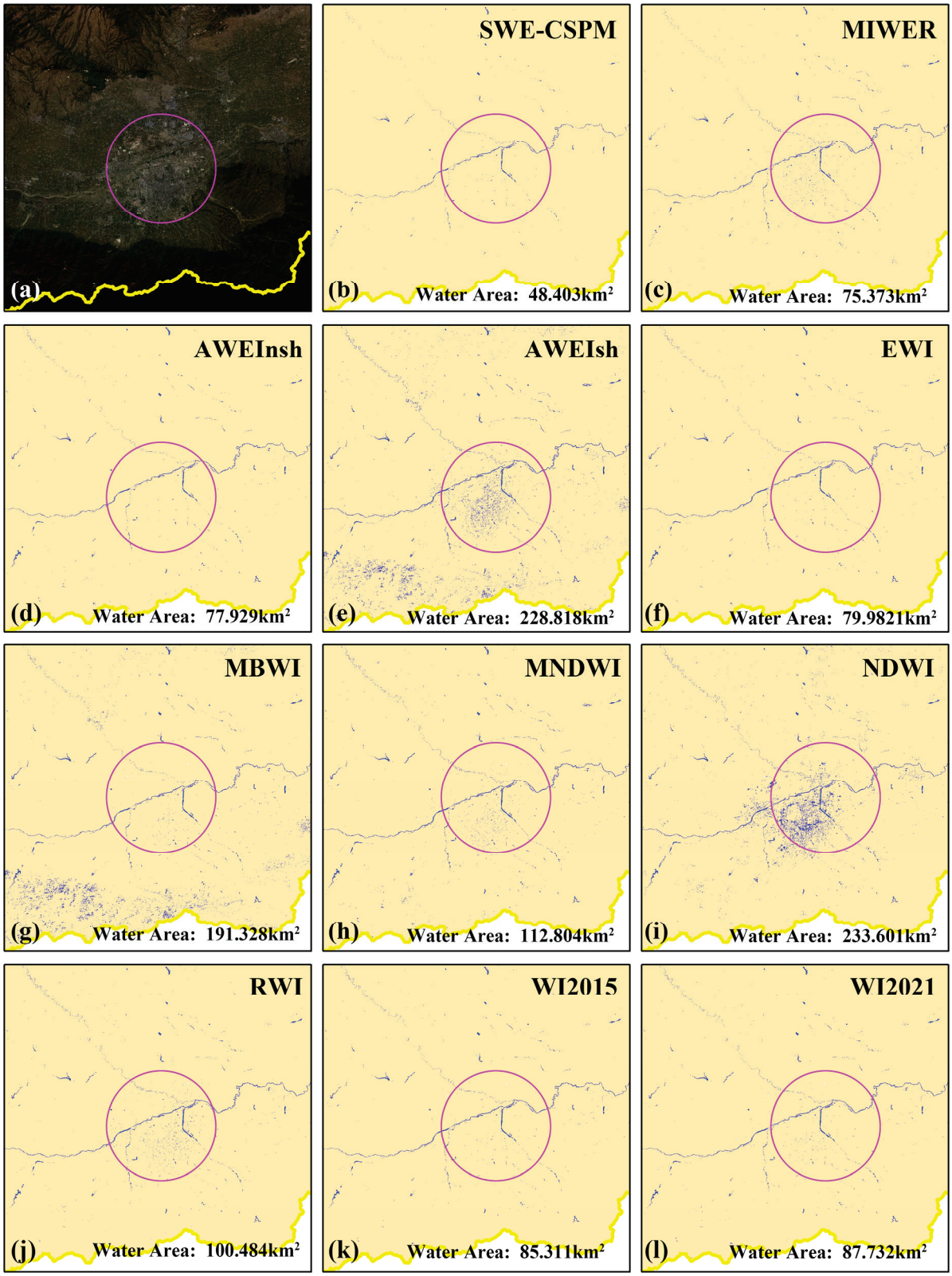

Figure 10. Surface water extraction of various methods in urban areas. The purple circle is the area of buildings. (**a**) Landsat 8 true colour images of the area. (**b**–**l**), respectively the extraction effect of SWE-CSPM MIWER, AWEInsh, AWEIsh, EWI, MBWI, MNDWI, NDWI, RWI, WI2015 and WI2021.

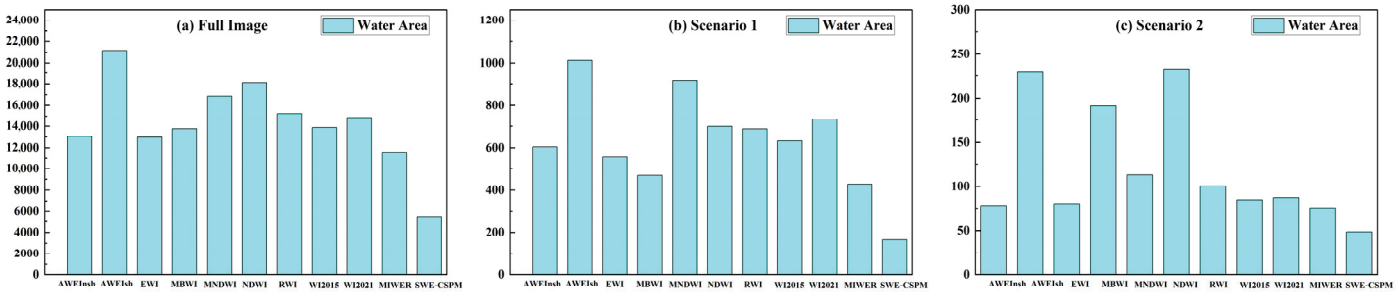

Figure 11. The water area of full image, Scenario 1, and Scenario 2.

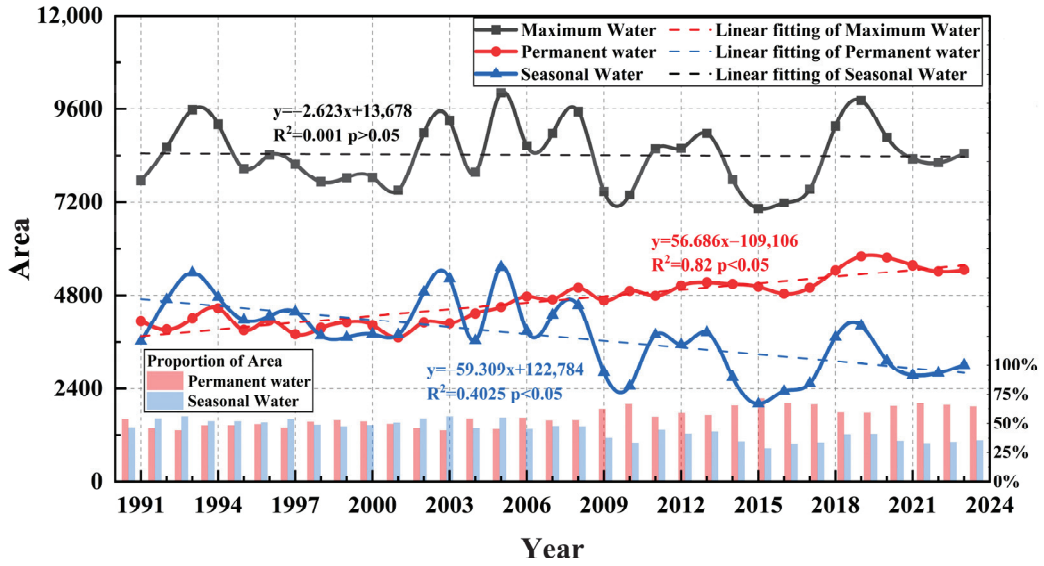

Figure 12. Surface water area changes in maximum, permanent, and seasonal water at the global scale in the YRB (1991–2023). The black curve and dashed line represent the area change trend and linear fitting relationship of the maximum water; the red curve and dashed line represent the area change trend and linear fitting relationship of the permanent water; the blue curve and dashed line represent the area change trend and linear fitting relationship of the seasonal water.

4.2.2. Surface Water Area Changes at the Secondary Water Resource Zoning Scale

Water resource zoning refers to the scientific division of water resources in a certain area based on the natural distribution characteristics of water resources, social and economic conditions, and ecological and environmental needs. Figure 13 shows the maximum, permanent, and seasonal water area changes for each secondary water resource zoning. The maximum surface water area at the secondary water resource zoning scale of the YRB is as follows: Above Longyangxia > Lanzhou City to Hekou Town > Below Huayuankou > Longmen County to Sanmenxia > Longyangxia to Lanzhou City > Sanmenxia to Huayuankou > Hekou Town to Longmen County > Interior Drainage Area. Above Longyangxia has the largest maximum surface water area, due to it being a major water-producing area with abundant water resources and widespread rivers and lakes. The Interior Drainage Area has the smallest water area, primarily due to it being part of the Mu Us Desert, characterized by an arid climate with low precipitation and high evaporation.

Except for the Interior Drainage Area, the permanent surface water area in other secondary water resource zonings increases slowly to varying degrees, with the growth rate from large to small as follows: Above Longyangxia > Lanzhou City to Hekou Town > Be-low Huayuankou > Longmen County to Sanmenxia > Sanmenxia to Huayuankou > Hekou Town to Longmen County > Longyangxia to Lanzhou City > Interior Drainage Area. The growth rate ranges from 0 to 12 km^2/a. Overall, the western and southern secondary water resource zonings exhibit higher growth rates of permanent surface water

area compared to the central and northern zonings. Seasonal surface water areas in all secondary water resource zonings show a fluctuating downward trend, and the downward rate of Longmen County to Sanmenxia is the highest. In 2022, the seasonal surface water areas in Lanzhou City to Hekou Town and the Interior Drainage Area exhibit sudden increases, which are likely due to significant precipitation increases in the northwest region of the YRB.

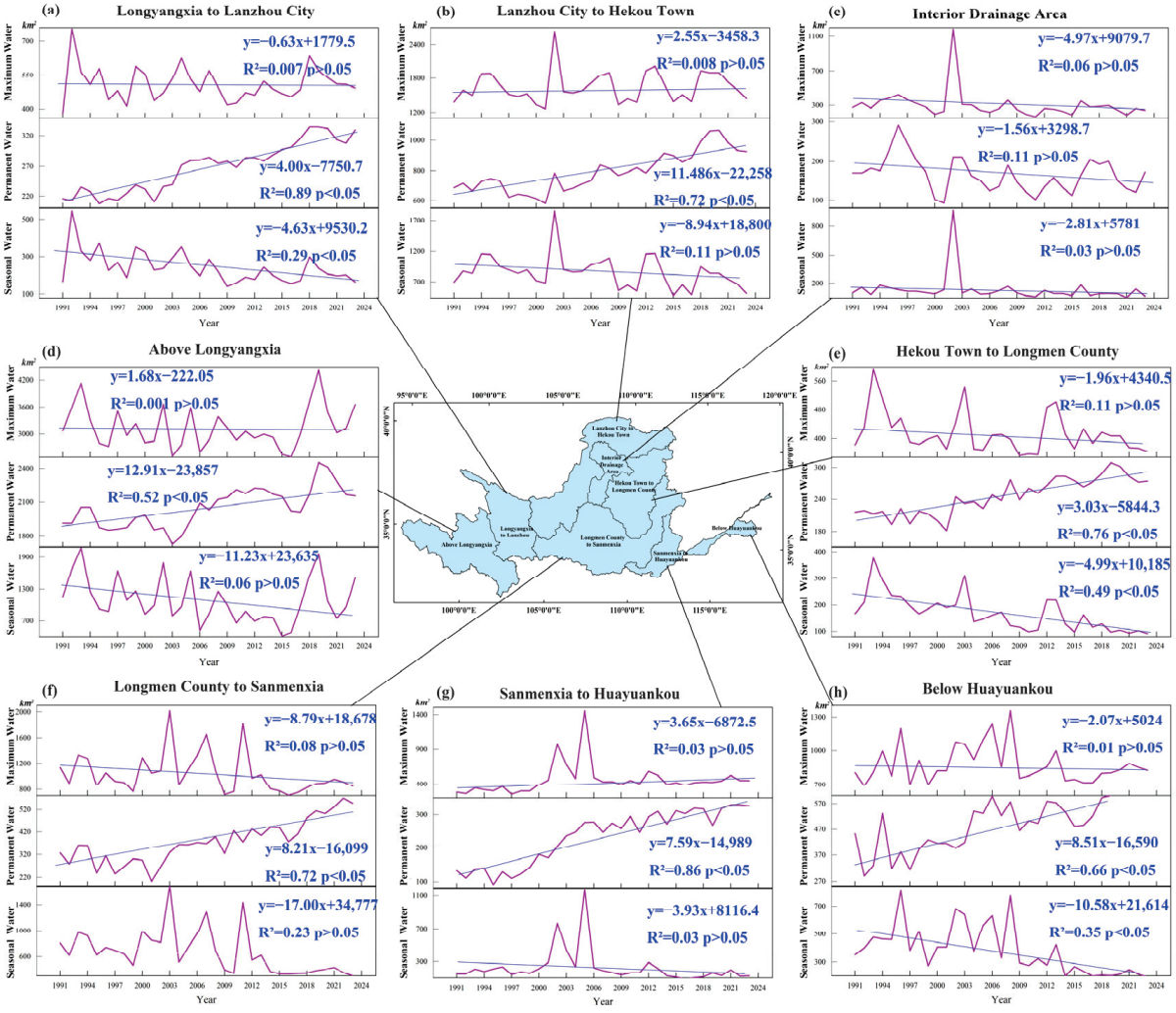

Figure 13. Surface water area changes in maximum, permanent, and seasonal surface water for each secondary water resource zoning (1991–2023). (**a**–**h**) respectively represent the three statistical water areas in Longyangxia to Lanzhou City, Lanzhou City to Hekou Town, Interior Drainage Area, Above Longyangxia, Hekou Town to Longmen County, Longmen County to Sanmenxia, Sanmenxia to Huayuankou and Be-low Huayuankou.

4.2.3. Surface Water Area Changes at the Provincial Scale

Figure 14 illustrates the changes in the maximum, permanent, and seasonal water areas for the nine provinces within the YRB. It is crucial to note that the provinces considered in this study only represent the areas within the YRB, not the entire provincial units. It is evident that, for the maximum surface water, only Shandong Province, Inner Mongolia Autonomous Region, and Qinghai Province exhibit a slow increase from 1991 to 2023. Other provinces show a downtrend, with Shaanxi Province having the highest rate of decrease. For permanent surface water, all provinces exhibit a trend of increasing in different degrees, with Qinghai Province having the highest growth rate at 15.16 km^2/a. Sichuan Province has the smallest water area and the smallest annual growth rate of only 0.096 km^2/a. For

seasonal surface water, all provinces exhibit varying degrees of fluctuating decreases, with Shaanxi Province showing the highest rate of decrease.

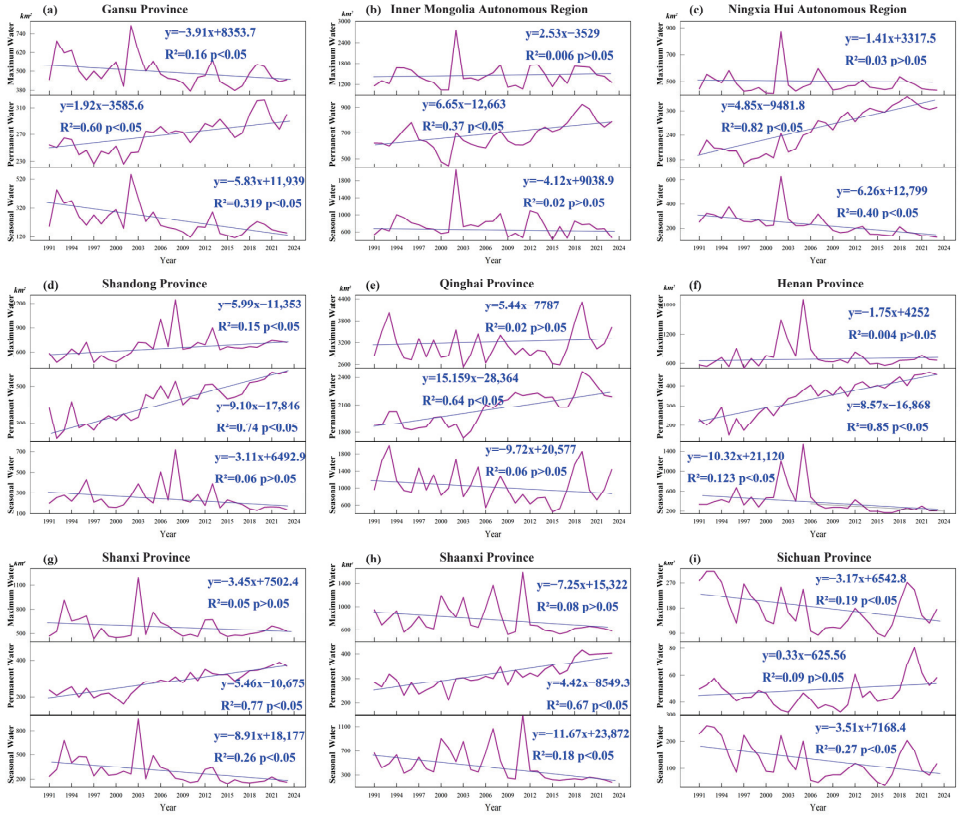

Figure 14. Surface water area changes in maximum, permanent, and seasonal surface water areas for the nine provinces within the YRB. (**a**–**i**) respectively represent the three statistical water areas in Gansu Province, Inner Mongolia Autonomous Region, Ningxia Hui Autonomous Region, Shandong Province, Qinghai Province, Henan Province, Shanxi Province, Shaanxi Province and Sichuan Province.

4.2.4. Surface Water Area Changes at the Typical Water Bodies

This study selects five typical lakes (Zhaling Lake, Eling Lake, Wuliangsuhai, Hongjiannao, and Dongping Lake) from the upper, middle, and lower reaches to analyze their surface water area changes. Zhaling Lake and Eling Lake are two typical natural lakes in the source region of the YRB. Wuliangsuhai and Hongjiannao are representative of natural lakes in the middle reaches of the Yellow River. Wuliangsuhai is located in Urad Front Banner, Bayannur City, Inner Mongolia Autonomous Region. It is a large multifunctional lake with high ecological value, rare in desert and semi-desert regions globally. To maintain the ecosystem health in the Wuliangsuhai, the Inner Mongolia Autonomous Region has provided 3.648 billion m^3 of ecological water replenishment since 2007 [58]. Hongjiannao is located between Shenmu City in Shaanxi Province and Ejin Horo Banner in the Inner Mongolia Autonomous Region. It is the largest desert lake in China. To improve the water environment of the Hongjiannao Nature Reserve, 1 million m^3 of ecological water replenishment has been provided since 2017 from the Erdos Zhasake Reservoir. Dongping Lake, located in Dongping County, Shandong Province, is the only significant flood storage area in the lower reaches of the Yellow River. It is a significant hub for the Eastern Route of the South-to-North Water Diversion Project and the Beijing–Hangzhou Grand Canal.

Figure 15 illustrates the surface water area changes in the five typical lakes. The processes of surface water area changes differ among lakes. For the maximum water, Zhaling Lake exhibits an initial decrease (1991–2001) followed by an increase (2001–2023). Eling Lake exhibits fluctuating changes initially (1991–2001), followed by an increase

(2001–2023). Wuliangsuhai exhibits overall fluctuating changes, with relatively small variations. Hongjiannao exhibits an initial decrease (1991–2015) followed by an increase (2015–2023). Dongping Lake exhibited fluctuating changes before 2012, with an initial decrease followed by an increase from 2012 to 2023.

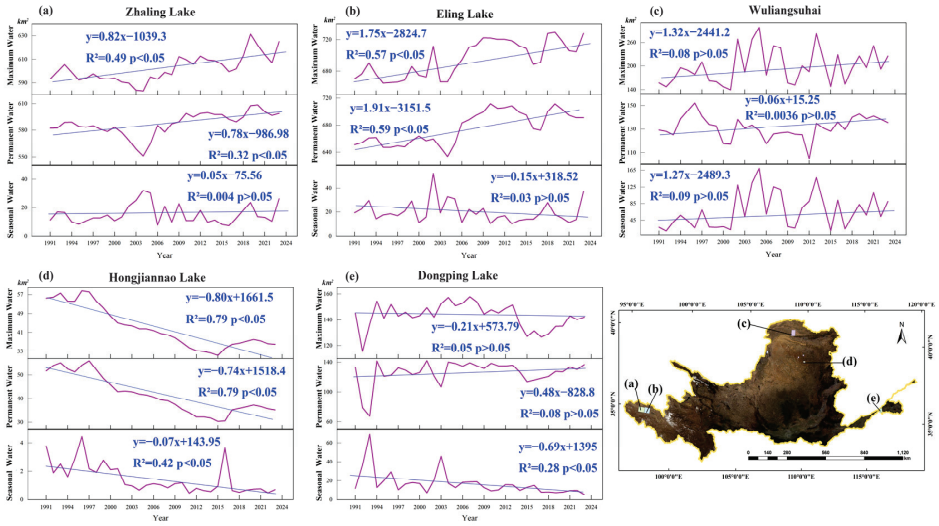

Figure 15. Surface water area changes in maximum, permanent, and seasonal water for typical five lakes in the YRB. (**a**–**e**) respectively represent the three statistical water areas of Zhaling Lake, Eling Lake, Wuliangsuhai, Hongjiannao Dongping Lake.

The changes in the permanent water areas of the five lakes generally mirror those of the maximum water areas, indicating that permanent water dominates the changes in the maximum surface water areas. For seasonal water, the changes are relatively small, but the variation trends among the lakes are slightly different. Zhaling Lake and Wuliangsuhai show a slow uptrend, while Eling Lake, Hongjiannao, and Dongping Lake exhibit a slow downtrend.

5. Discussion

5.1. The Applicability of Water Indexes in the YRB

The surface water of YRB has the characteristics of a large sediment content, and the sediment content has large spatial heterogeneity. They pose a great extraction challenge to surface water. The accuracy of the nine typical water indexes is in order from large to small (Table 2) as follows: MBWI > AWEInsh > WI2021 > MNDWI > WI2015 > EWI > AWEIsh > RWI > NDWI. Therefore, it is recommended to prioritize the MBWI, AWEInsh, and WI2021 when using a single water index to extract surface water in the entire YRB. All nine water indexes have good extraction results in the mainstream of the YRB, tributaries with large river widths, and large lakes and reservoirs. However, for narrow rivers and tiny streams, the identification effect of each water index is poor due to the limitations of Landsat images' spatial resolution (Appendix A Figure A1). Therefore, when extracting surface water in the northwest region of the YRB with narrow rivers and tiny streams, it is recommended to use images with higher spatial resolution such as Sentinel, GF, and Worldview images. As shown in Figure 9, compared with other water indexes, the MBWI can more effectively distinguish between water and ice–snow (Figure 9g). For the areas covered with ice–snow (such as the source region of the YRB), it is recommended to prioritize the MBWI for surface water extraction. In Figure 10, the MNDWI, AWEInsh, and WI2021 can effectively decrease the interference of built-up areas to water extraction (Figure 10d,h,l). Therefore, for areas containing built-up areas, it is recommended to prioritize the MNDWI, AWEInsh, and WI2021.

5.2. The Effectiveness of the SWE-CSPM

The spectral characteristics of water are usually related to their various components. As shown in Figure 5, the spectral characteristics of water in different sections of the YRB undergo significant changes with the sediment content. Figure 8 illustrates that the most applicable water index for surface water with different SPM concentrations is also different. Therefore, based on the concept of classification and grading, surface water is initially categorized into several types according to the SPM concentration. Subsequently, the optimal water index is chosen for each type of water to facilitate water extraction. The scheme is theoretically reasonable and feasible. This study introduces the SPM concentration inversion algorithm proposed by Liu et al. [47], which has been successfully applied to the inversion of the SPM concentration in the Yellow River estuary and extended to the whole YRB in this study. Appendix A Figure A1 and Table 2 demonstrate that in terms of water extraction accuracy, the SWE-CSPM significantly outperforms the nine water indexes and the MIWER. The above experimental results reveal that the SWE-CSPM is effective in improving the extraction accuracy of surface water throughout the YRB. The main reason is that this SWE-CSPM simplifies complex surface water into multiple single types, which improves the separation of water from other surface features and reduces the commission error.

5.3. Spatiotemporal Variation Characteristics of Water Area

This study analyzes the change characteristics of the water area in the YRB at the global scale, the secondary water resource zoning scale, the provincial scale, and the typical water scale. At the global scale, the maximum water area fluctuates slightly downward, the permanent water area shows an uptrend, and the seasonal water area shows a downtrend annually. These trends are generally consistent with the results of Zhang et al. [3] and Hu et al. [55], but the water area is slightly smaller than that of Hu et al. The main reason for the difference is that the SWE-CSPM improves the surface water extraction accuracy and reduces the commission error. According to the previous results [59,60], the permanent water area has increased annually, mainly due to the increase in precipitation and glacial meltwater caused by climate warming. The seasonal water area shows a downtrend annually, which may be due to the transformation of some seasonal water into permanent water. This shift may be attributed to the construction of reservoir projects and the replenishment of lake wetlands [52]. These changes greatly indicate the substantial spatial heterogeneity of surface water.

At the secondary water resource zoning scale, the permanent water area of the Interior Drainage Area remains stable, while other zones show an uptrend. Among them, the permanent water area of Above Longyangxia has the largest growth rate and the largest maximum water area. The reason is that the zoning is the main water source of the YRB, and the water resources are abundant. At the provincial scale, the permanent water area of each province shows an increasing trend to varying degrees. Among them, the water area of Qinghai Province has the largest growth rate, and the reason is similar to that of the secondary water resource zonings, both of which have large lakes in the upper reaches. The seasonal water area of each province shows a fluctuating downtrend. In terms of the maximum water area, only Shandong Province, Inner Mongolia Autonomous Region, and Qinghai Province have a slow increase; the rest of the provinces show a downtrend.

At the typical water scale, there are great differences in the process of water area change in five lakes. Over the past decade, Zhaling Lake, Eling Lake, Wuliangsuhai Lake, Hongjiannao, and Dongping Lake have all shown an uptrend in their permanent water area and maximum water area. On the one hand, climate change has led to an increase in the natural inflow runoff of lakes. On the other hand, water conservancy management departments actively promote river and lake protection policies. Through these policies, numerous ecological water replenishment projects have been implemented for rivers and lakes that are important for ecological functions and whose water areas have seriously shrunk.

5.4. Limitation and Future Work

This study analyzes the dynamic variations in surface water in the YRB at various scales but has not yet conducted an in-depth analysis of the driving mechanisms of climate change and human activities on the spatiotemporal variations at different scales. In addition, this study has not yet involved research on surface water area prediction, early warning, and dynamic changes in water storage. In subsequent studies, we will plan to use higher-resolution terrain data, radar imagery, and optical imagery to conduct a surface water classification, which includes the mainstream, first-level tributaries, second-level tributaries, reservoirs, natural lakes, ponds, wetlands, and more. After analyzing the spatiotemporal variation characteristics of each type of water, we will combine meteorological data and human activity data to explore the driving mechanism of the spatiotemporal variation in the YRB. Then, we will construct water area prediction and early warning models. Moreover, we will combine satellite altimetry data and high-precision terrain data to carry out dynamic monitoring of water storage in typical lakes and reservoirs in the YRB. Subsequently, we will provide detailed decision-supporting data for the planning, management, and servicing of water resources in the YRB.

6. Conclusions

Aiming to address the problems of a large concentration and spatiotemporal heterogeneity of SPM in surface water in the YRB, this study proposes the SWE-CSPM, which is based on the concept of classification and grading and considers the SPM concentration. Compared with nine typical water indexes and the MIWER, the SWE-CSPM significantly reduces the commission error, and the extraction accuracy is the highest (overall accuracy 95.44%, kappa coefficient 90.62%). This study examines the dynamic variations in the water area in the YRB from 1991 to 2023 at the global scale, the secondary water resource zoning scale, the provincial scale, and the typical water scale. This study finds that at the global scale, the area of maximum water shows a fluctuating downtrend, although the change range is small. The permanent water area shows an uptrend, whereas the seasonal water area shows a downtrend year by year. At the secondary water resource zoning scale, the permanent water area increases to varying degrees, except that the Interior Drainage Area remains stable. Among zonings, the zoning of Above Longyangxia experiences the most significant increase in the permanent water area. At the provincial scale, the permanent water area of each province has shown an uptrend, while the seasonal water area has shown a fluctuating downtrend. Only the maximum water area in Shandong Province, Inner Mongolia Autonomous Region, and Qinghai Province increases slowly, while the rest of the provinces show a downtrend. At the water bodies scale, the water area changes in Zhaling Lake, Eling Lake, Wuliangsuhai, Hongjiannao, and Dongping Lake are quite different. However, the permanent water area and maximum water area of the above water bodies have increased in the past decade, and the seasonal water area changes are small. Based on the above research results, we will further carry out surface water classification in the YRB and combine meteorological data and human activity data to explore the driving mechanism of the spatiotemporal variation in the YRB. Then, we will construct water area prediction and early warning models. Moreover, we will combine satellite altimetry data and high-precision terrain data to carry out dynamic monitoring of water storage in typical lakes and reservoirs in the YRB. Subsequently, we will provide detailed decision-supporting data for the planning, management, and servicing of water resources in the YRB.

Author Contributions: Overall design, Z.Z.; methodology, X.G. and Z.Z.; software, X.G. and Y.F.; formal analysis, L.C. and X.L.; writing—original draft preparation, Z.Z. and X.G.; writing—review and editing, X.Z., L.Y., H.Z. and X.X.; funding acquisition, L.C. All authors have read and agreed to the published version of the manuscript.

Funding: This research was funded by the National Key Research and Development Program of China (2022YFC3201703), the Open Fund of Key Laboratory of Geospatial Technology for the Middle and Lower Yellow River Regions (Henan University), Ministry of Education (GTYR202106), North China

University of Water Resources and Electric Power New Era Water Control Social Science Research Institute "Open list" project (24JB-01-02), Henan Province's 2023 Water Conservancy Science and Technology Research Project (GG202338), the Henan Province science and technology research and development plan joint fund project (232103810102), the Research Fund project of Key Laboratory of Water Management and Water Security in Yellow River Basin, Ministry of Water Resources (2023-SYSJJ-04), and the National Natural Science Foundation of China (42007423; 42201097).

Data Availability Statement: The data that support the findings of this study are available on request from the corresponding author. The data are not publicly available due to privacy restrictions. The data will be used for further exploration and analysis.

Acknowledgments: We would like to express our respect and gratitude to the anonymous reviewers and editors for their professional comments and suggestions.

Conflicts of Interest: The authors declare no conflicts of interest.

Appendix A

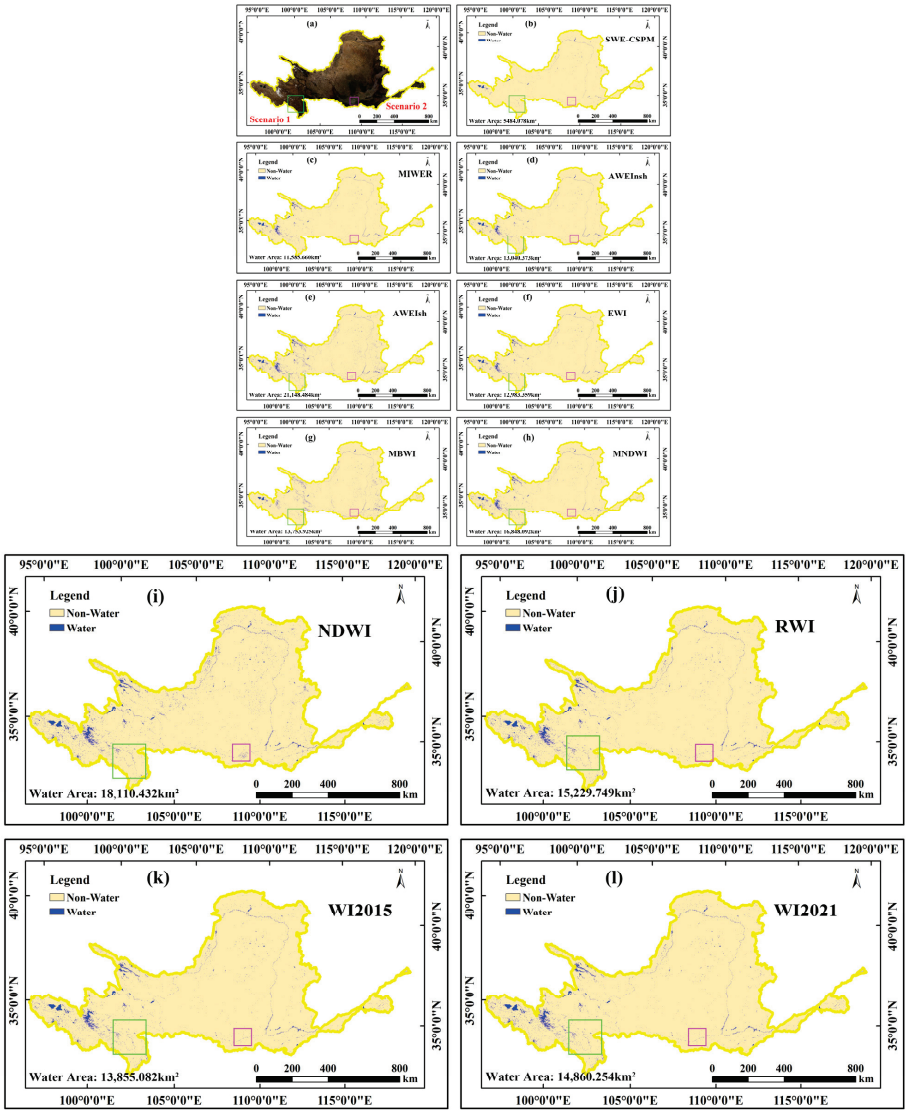

Figure A1. Surface water extraction based on 2021 synthetic images using various methods. Scenario 1 and scenario 2 are the high mountainous regions and urban regions, respectively. The green square in the figure represents scenario 1, and the purple square represents scenario 2. (**a**) Landsat 8 true colour images of the area. (**b**–**l**), respectively the extraction effect of SWE-CSPM MIWER, AWEInsh, AWEIsh, EWI, MBWI, MNDWI, NDWI, RWI, WI2015 and WI2021.

References

1. Yue, L.; Li, B.; Zhu, S.; Yuan, Q.; Shen, H. A fully automatic and high-accuracy surface water mapping framework on google earth engine using landsat time-series. *Int. J. Digit. Earth* **2023**, *16*, 210–233. [CrossRef]
2. Yamazaki, D.; Trigg, M.A. The dynamics of earth's surface water. *Nature* **2016**, *540*, 348–349. [CrossRef]
3. Zhang, Y.; Du, J.; Guo, L.; Fang, S.; Zhang, J.; Sun, B.; Mao, J.; Sheng, Z.; Li, L. Long-term detection and spatiotemporal variation analysis of open-surface water bodies in the Yellow River Basin from 1986 to 2020. *Sci. Total Environ.* **2022**, *845*, 157152. [CrossRef]
4. Cooley, S.W.; Ryan, J.C.; Smith, L.C. Human alteration of global surface water storage variability. *Nature* **2021**, *591*, 78–81. [CrossRef] [PubMed]
5. Scanlon, B.R.; Fakhreddine, S.; Rateb, A.; de Graaf, I.; Famiglietti, J.; Gleeson, T.; Grafton, R.Q.; Jobbagy, E.; Kebede, S.; Kolusu, S.R.; et al. Global water resources and the role of groundwater in a resilient water future. *Nat. Rev. Earth Environ.* **2023**, *4*, 87–101. [CrossRef]
6. Sogno, P.; Klein, I.; Kuenzer, C. Remote sensing of surface water dynamics in the context of global change—A review. *Remote Sens.* **2022**, *14*, 2475. [CrossRef]
7. Tulbure, M.G.; Broich, M.; Stehman, S.V.; Kommareddy, A. Surface water extent dynamics from three decades of seasonally continuous landsat time series at subcontinental scale in a semi-arid region. *Remote Sens. Environ.* **2016**, *178*, 142–157. [CrossRef]
8. Wang, X.; Xiao, X.; Zou, Z.; Dong, J.; Qin, Y.; Doughty, R.B.; Menarguez, M.A.; Chen, B.; Wang, J.; Ye, H.; et al. Gainers and losers of surface and terrestrial water resources in China during 1989–2016. *Nat. Commun.* **2020**, *11*, 3471. [CrossRef]
9. Guo, J.; Wang, X.; Liu, B.; Liu, K.; Zhang, Y.; Wang, C. Remote-Sensing Extraction of Small Water Bodies on the Loess Plateau. *Water* **2023**, *15*, 866. [CrossRef]
10. McFeeters, S.K. The use of the normalized difference water index (NDWI) in the delineation of open water features. *Int. J. Remote Sens.* **1996**, *17*, 1425–1432. [CrossRef]
11. Fisher, A.; Flood, N.; Danaher, T. Comparing landsat water index methods for automated water classification in eastern australia. *Remote Sens. Environ.* **2016**, *175*, 167–182. [CrossRef]
12. Xu, H. Modification of normalised difference water index (NDWI) to enhance open water features in remotely sensed imagery. *Int. J. Remote Sens.* **2006**, *27*, 3025–3033. [CrossRef]
13. Wang, S.; Baig, M.H.A.; Zhang, L.; Jiang, H.; Ji, Y.; Zhao, H.; Tian, J. A simple enhanced water index (EWI) for percent surface water estimation using landsat data. *IEEE J. Sel. Top. Appl. Earth Obs. Remote Sens.* **2015**, *8*, 90–97. [CrossRef]
14. Feyisa, G.L.; Meilby, H.; Fensholt, R.; Proud, S.R. Automated water extraction index: A new technique for surface water mapping using landsat imagery. *Remote Sens. Environ.* **2014**, *140*, 23–35. [CrossRef]
15. Wang, X.; Xie, S.; Zhang, X.; Chen, C.; Guo, H.; Du, J.; Duan, Z. A robust multi-band water index (MBWI) for automated extraction of surface water from landsat 8 OLI imagery. *Int. J. Appl. Earth Obs. Geoinf.* **2018**, *68*, 73–91. [CrossRef]
16. Hu, R.; Yao, Z.; LI, P.; Sun, Y.; Jia, Y. Construction and stability study of water index of Landsat-8 images. *Sci. Surv. Mapp.* **2022**, *47*, 150–155. [CrossRef]
17. Wu, Q.; Wang, M.; Shen, X.; Yao, Y.; Li, J.; Zhang, F.; Zhou, Y. Small water body extraction method based on Sentinel-2 satellite multi-spectral remote sensing image. *Natl. Remote Sens. Bull.* **2022**, *26*, 781–794. [CrossRef]
18. Zhang, D.-D.; Xu, J. Long-Term Monitoring of Surface Water Dynamics and Analysis of Its Driving Mechanism: A Case Study of the Yangtze River Basin. *Water* **2024**, *16*, 677. [CrossRef]
19. Zou, Z.; Xiao, X.; Dong, J.; Qin, Y.; Doughty, R.B.; Menarguez, M.A.; Zhang, G.; Wang, J. Divergent trends of open-surface water body area in the contiguous United States from 1984 to 2016. *Proc. Natl. Acad. Sci. USA* **2018**, *115*, 3810–3815. [CrossRef]
20. Xie, G.; Bai, X.; Peng, Y.; Li, Y.; Zhang, C.; Liu, Y.; Liang, J.; Fang, L.; Chen, J.; Men, J.; et al. Aquaculture ponds identification based on multi-feature combination strategy and machine learning from landsat-5/8 in a typical inland lake of China. *Remote Sens.* **2024**, *16*, 2168. [CrossRef]
21. Hibjur Rahaman, M.; Roshani; Masroor, M.; Sajjad, H. Integrating remote sensing derived indices and machine learning algorithms for precise extraction of small surface water bodies in the lower *thoubal* river watershed, India. *J. Clean. Prod.* **2023**, *422*, 138563. [CrossRef]
22. Si, Y.; Gong, D.; Guo, Y.; Zhu, X.; Huang, Q.; Evans, J.; He, S.; Sun, Y. An advanced spectral–spatial classification framework for hyperspectral imagery based on DeepLab v3+. *Appl. Sci.* **2021**, *11*, 5703. [CrossRef]
23. Qi, Z.; Wang, B.; Tian, Y.; Zhang, P. When ensemble learning meets deep learning: A new deep support vector machine for classification. *Knowl. Based Syst.* **2016**, *107*, 54–60. [CrossRef]
24. Li, Y.; Dang, B.; Zhang, Y.; Du, Z. Water body classification from high-resolution optical remote sensing imagery: Achievements and perspectives. *ISPRS J. Photogramm. Remote Sens.* **2022**, *187*, 306–327. [CrossRef]
25. Wangchuk, S.; Bolch, T. Mapping of glacial lakes using sentinel-1 and sentinel-2 data and a random forest classifier: Strengths and challenges. *Sci. Remote Sens.* **2020**, *2*, 100008. [CrossRef]
26. Li, J.; Ma, R.; Cao, Z.; Xue, K.; Xiong, J.; Hu, M.; Feng, X. Satellite Detection of Surface Water Extent: A Review of Methodology. *Water* **2022**, *14*, 1148. [CrossRef]
27. Xu, Y.; Lin, J.; Zhao, J.; Zhu, X. New method improves extraction accuracy of lake water bodies in central asia. *J. Hydrol.* **2021**, *603*, 127180. [CrossRef]
28. Irvin, B.J.; Ventura, S.J.; Slater, B.K. Fuzzy and isodata classification of landform elements from digital terrain data in pleasant valley, wisconsin. *Geoderma* **1997**, *77*, 137–154. [CrossRef]

29. Liu, Z. Identifying urban land use social functional units: A case study using OSM data. *Int. J. Digit. Earth* **2021**, *14*, 1798–1817. [CrossRef]
30. Xing, H.; Niu, J.; Feng, Y.; Hou, D.; Wang, Y.; Wang, Z. A coastal wetlands mapping approach of yellow river delta with a hierarchical classification and optimal feature selection framework. *Catena* **2023**, *223*, 106897. [CrossRef]
31. Mao, D.; Wang, Z.; Du, B.; Li, L.; Tian, Y.; Jia, M.; Zeng, Y.; Song, K.; Jiang, M.; Wang, Y. National wetland mapping in China: A new product resulting from object-based and hierarchical classification of landsat 8 OLI images. *ISPRS J. Photogramm. Remote Sens.* **2020**, *164*, 11–25. [CrossRef]
32. Jiang, W.; He, G.; Long, T.; Ni, Y.; Liu, H.; Peng, Y.; Lv, K.; Wang, G. Multilayer perceptron neural network for surface water extraction in landsat 8 OLI satellite images. *Remote Sens.* **2018**, *10*, 755. [CrossRef]
33. Zhang, Z.; Zhang, X.; Jiang, X.; Xin, Q.; Ao, Z.; Zuo, Q.; Chen, L. Automated surface water extraction combining sentinel-2 imagery and OpenStreetMap using presence and background learning (PBL) algorithm. *IEEE J. Sel. Top. Appl. Earth Obs. Remote Sens.* **2019**, *12*, 3784–3798. [CrossRef]
34. Li, K.; Wang, J.; Cheng, W.; Wang, Y.; Altansukh, O. Deep learning empowers the google earth engine for automated water extraction in the lake baikal basin. *Int. J. Appl. Earth Obs. Geoinf.* **2022**, *112*, 102928. [CrossRef]
35. Li, K.; Wang, J.; Yao, J. Effectiveness of machine learning methods for water segmentation with ROI as the label: A case study of the tuul river in Mongolia. *Int. J. Appl. Earth Obs. Geoinf.* **2021**, *103*, 102497. [CrossRef]
36. Li, L.; Yan, Z.; Shen, Q.; Cheng, G.; Gao, L.; Zhang, B. Water body extraction from very high spatial resolution remote sensing data based on fully convolutional networks. *Remote Sens.* **2019**, *11*, 1162. [CrossRef]
37. Fu, G.; Liu, C.; Zhou, R.; Sun, T.; Zhang, Q. Classification for High Resolution Remote Sensing Imagery Using a Fully Convolutional Network. *Remote Sens.* **2017**, *9*, 498. [CrossRef]
38. Li, Z.; Zhang, X.; Xiao, P. Spectral index-driven FCN model training for water extraction from multispectral imagery. *ISPRS J. Photogramm. Remote Sens.* **2022**, *192*, 344–360. [CrossRef]
39. Cao, H.; Tian, Y.; Liu, Y.; Wang, R. Water body extraction from high spatial resolution remote sensing images based on enhanced U-Net and multi-scale information fusion. *Sci. Rep.* **2024**, *14*, 16132. [CrossRef]
40. Sun, D.; Gao, G.; Huang, L.; Liu, Y.; Liu, D. Extraction of water bodies from high-resolution remote sensing imagery based on a deep semantic segmentation network. *Sci. Rep.* **2024**, *14*, 14604. [CrossRef]
41. Chen, L.-C.; Papandreou, G.; Kokkinos, I.; Murphy, K.; Yuille, A.L. DeepLab: Semantic image segmentation with deep convolutional nets, atrous convolution, and fully connected CRFs. *arXiv* **2017**, arXiv:1606.00915. [CrossRef]
42. Tao, Y.; Xu, M.; Zhong, Y.; Cheng, Y. GAN-assisted two-stream neural network for high-resolution remote sensing image classification. *Remote Sens.* **2017**, *9*, 1328. [CrossRef]
43. Chang, L.-C.; Wang, W.-H.; Chang, F.-J. Explore training self-organizing map methods for clustering high-dimensional flood inundation maps. *J. Hydrol.* **2021**, *595*, 125655. [CrossRef]
44. Yuan, Q.; Shen, H.; Li, T.; Li, Z.; Li, S.; Jiang, Y.; Xu, H.; Tan, W.; Yang, Q.; Wang, J.; et al. Deep learning in environmental remote sensing: Achievements and challenges. *Remote Sens. Environ.* **2020**, *241*, 111716. [CrossRef]
45. Cheng, G.; Xie, X.; Han, J.; Guo, L.; Xia, G.-S. Remote sensing image scene classification meets deep learning: Challenges, methods, benchmarks, and opportunities. *IEEE J. Sel. Top. Appl. Earth Obs. Remote Sens.* **2020**, *13*, 3735–3756. [CrossRef]
46. Sekertekin, A. A survey on global thresholding methods for mapping open water body using sentinel-2 satellite imagery and normalized difference water index. *Arch. Comput. Methods Eng.* **2021**, *28*, 1335–1347. [CrossRef]
47. Liu, Z.; Cui, T.; Zhang, S.; Zhao, W. Landsat8 OLI piecewise linear inversion of suspended matter concentration in the Yellow River Estuary. *Spectrosc. Spectr. Anal.* **2018**, *38*, 2536–2541. [CrossRef]
48. Yang, Y.; Lü, Y.; Fu, B.; Wu, X.; Wang, S.; Wu, T. The potential for carbon sequestration by afforestation can be limited in dryland river basins under the pressure of high human activity. *Sci. Total Environ.* **2023**, *858*, 159817. [CrossRef]
49. Mehta, P.; Siebert, S.; Kummu, M.; Deng, Q.; Ali, T.; Marston, L.; Xie, W.; Davis, K.F. Half of twenty-first century global irrigation expansion has been in water-stressed regions. *Nat. Water* **2024**, *2*, 254–261. [CrossRef]
50. Qu, L.; Lei, T.; Ning, D.; Civco, D.; Yang, X. A spectral mixing algorithm for quantifying suspended sediment concentration in the yellow river: A simulation based on a controlled laboratory experiment. *Int. J. Remote Sens.* **2016**, *37*, 2560–2584. [CrossRef]
51. Zhao, Z.; Li, H.; Song, X.; Sun, W. Dynamic monitoring of surface water bodies and their influencing factors in the yellow river basin. *Remote Sens.* **2023**, *15*, 5157. [CrossRef]
52. Cao, H.; Han, L.; Li, L. Changes in extent of open-surface water bodies in China's Yellow River Basin (2000–2020) using Google Earth Engine cloud platform. *Anthropocene* **2022**, *39*, 100346. [CrossRef]
53. Jiang, L.; Liu, Y. Response of Runoff-Sediment System to Vegetation Variation in the Yellow River Basin in the Last 20 Years. *Land* **2023**, *12*, 428. [CrossRef]
54. Li, P.; Ke, Y.; Wang, D.; Ji, H.; Chen, S.; Chen, M.; Lyu, M.; Zhou, D. Human impact on suspended particulate matter in the Yellow River Estuary, China: Evidence from remote sensing data fusion using an improved spatiotemporal fusion method. *Sci. Total Environ.* **2021**, *750*, 141612. [CrossRef] [PubMed]
55. Hu, Q.; Li, C.; Wang, Z.; Liu, Y.; Liu, W. Continuous Monitoring of the Surface Water Area in the Yellow River Basin during 1986–2019 Using Available Landsat Imagery and the Google Earth Engine. *ISPRS Int. J. Geo-Inf.* **2022**, *11*, 305. [CrossRef]
56. Deng, Y.; Jiang, W.; Tang, Z.; Ling, Z.; Wu, Z. Long-Term Changes of Open-Surface Water Bodies in the Yangtze River Basin Based on the Google Earth Engine Cloud Platform. *Remote Sens.* **2019**, *11*, 2213. [CrossRef]

57. Li, Z.; Xu, Y.; Sun, Y.; Wu, M.; Zhao, B. Urbanization-driven changes in land-climate dynamics: A case study of haihe river basin, China. *Remote Sens.* **2020**, *12*, 2701. [CrossRef]
58. Jia, X.; Jin, Z.; Mei, X.; Wang, D.; Zhu, R.; Zhang, X.; Huang, Z.; Li, C.; Zhang, X. Monitoring and effect evaluation of an ecological restoration project using multi-source remote sensing: A case study of wuliangsuhai watershed in China. *Land* **2023**, *12*, 349. [CrossRef]
59. Jing, W.; Yao, L.; Zhao, X.; Zhang, P.; Liu, Y.; Xia, X.; Song, J.; Yang, J.; Li, Y.; Zhou, C. Understanding Terrestrial Water Storage Declining Trends in the Yellow River Basin. *J. Geophys. Res. Atmos.* **2019**, *124*, 12963–12984. [CrossRef]
60. Lin, M.; Biswas, A.; Bennett, E.M. Spatio-temporal dynamics of groundwater storage changes in the Yellow River Basin. *J. Environ. Manag.* **2019**, *235*, 84–95. [CrossRef]

water

MDPI

Article

Surface Water Resource Accessibility Assessment of Rural Settlements in the Yellow River Basin

Heying Li [1,2,3,4,5], Huiling Ma [2,3,4,5], Jianchen Zhang [2,3,4,5,*], Xueye Chen [6] and Xuefei Hong [1,6]

[1] Key Laboratory of Urban Land Resources Monitoring and Simulation, Ministry of Natural Resources, Shenzhen 518040, China; 10130155@vip.henu.edu.cn (H.L.); hannah-dm@hotmail.com (X.H.)
[2] College of Geography and Environmental Science, Henan University, Kaifeng 475004, China; mhling@henu.edu.cn
[3] Key Laboratory of Geospatial Technology for the Middle and Lower Yellow River Regions, Henan University, Ministry of Education, Kaifeng 475004, China
[4] Henan Industrial Technology Academy of Spatio-Temporal Big Data, Henan University, Zhengzhou 450046, China
[5] Henan Technology Innovation Center of Spatio-Temporal Big Data, Henan University, Zhengzhou 450046, China
[6] Shenzhen Data Management Center of Planning and Nature Resource (Shenzhen Geospatial Information Center), Shenzhen 518040, China; xueye31@163.com
* Correspondence: jczhang@vip.henu.edu.cn

Abstract: Analyzing the spatial relationship between humans and water is crucial for regional development and water allocation schemes, particularly in the face of extreme water scarcity in the Yellow River Basin. A quantitative evaluation model of surface water resource accessibility (*SWRA*) has been developed, with rural settlements serving as the research unit. This model is built upon three key dimensions: topography, distance, and surface water resources within the Yellow River Basin. The results show that: (1) The *SWRA* range spans from 0.13 to 0.88, with an average value of 0.47 and a standard deviation of 0.05. Higher SWRA values are concentrated in the eastern and western regions, while lower values are predominantly found in the central area. (2) The gradient of *SWRA* across the 12 catchments, from low to high, is as follows: Sanmenxia station, Lanzhou station, Shizuishan station, Longmen station, Tongguan station, Toudaoguai station, Xiaolangdi station, Huayuankou station, Lijin station, Gaocun station, Ai Shan station, and Tangnaihai station. (3) At the city scale, the *SWRA* values are generally higher in the eastern areas of 10 cities, with one exception being higher in the west. Conversely, in the western areas of nine cities, the *SWRA* values are lower. The remaining cities exhibit *SWRA* values at a medium level. The correlation coefficient between primary industry gross domestic product (GDP) and *SWRA* is 0.271 (N = 56, Sig = 0.043, in 0.05 level, the correlation is significant), which confirms that *SWRA* serves as a factor influencing GDP and is appropriately designed for assessing water accessibility. Consequently, managers can utilize *SWRA* results to make informed decisions regarding regional development and water allocation.

Keywords: rural settlement; surface runoff; surface water resource accessibility; the Yellow River Basin

1. Introduction

Rivers are closely related to the living environment. To facilitate production and life, such as agricultural irrigation, laundry, and cooking, most of the original settlements appear along the river. However, rivers not only block people's activities but also connect people's activities. Although it can provide water for human beings, it is also prone to floods, devouring people's lives and property. Water resources are rich in China, and the total amount ranks at the forefront of the world. However, the per capita possession is low, and the spatial and temporal distributions are uneven in China. This imbalanced situation leads to a mismatch in spatial distribution between water resources and population. The Yellow River is the mother river of China. It feeds 12% of the population in China, among

which the rural population accounts for about 75%. However, the Yellow River Basin is in an arid and semi-arid climate zone. Thus, it only accounts for 2% of the river runoff in China. Therefore, the water resources strongly restrict the existence and development of rural settlements. As an important economic region in China, the water resources in the Yellow River are an important support for the economic development of this region. However, the lack of water resources has become a key factor restricting the high-quality development of this region. With the continuous influence of human activities and climate change, the contradiction between the supply and demand of water resources in the Yellow River is prominent [1]. Article 3 of the Regulations of the People's Republic of China on Water Dispatching of the Yellow River stipulates that the state implements unified dispatching of the Yellow River, following the principles of total amount control, cross-section flow control, hierarchical management, and hierarchical responsibility. In 2011, the State Council started the water allocation program in inter-provincial river basins in an all-around way, which gradually solved the problem of cut-off of the Yellow River [2]. In previous work, the water allocation scheme relied on statistical data, mostly neglecting the spatial distribution characteristics of rural settlements. Consequently, this approach led to inaccuracies in allocating water resources to individual rural residents, exacerbating the challenge of water scarcity in regions marked by intense competition for water resources. Moreover, water availability significantly influences the suitability of human settlements [3]. Therefore, amid the acute water scarcity in the Yellow River Basin, it becomes imperative to scrutinize the spatial relationship between rural settlements and water resources [4]. Such analysis is crucial for fostering the coordinated development of both human settlements and water resources within the basin. By doing so, the evaluation of surface water resource accessibility will not only enhance the rationality of water resource allocation programs but also facilitate regional development efforts [5].

Previous studies on water resource accessibility are mostly based on the grid-scale water resource accessibility evaluation model (SHRD) or improved on this model. The indicators of these studies mainly include runoff, slope, relative height difference, and distance [6]. Li et al. added land use resistance or water intake space resistance to evaluate water resource accessibility in southwest China [7]. Xu et al. added a location attribute factor to the SHRD model to evaluate water prices [8]. Besides the SHRD model, Li et al. constructed a grid-scale water resource accessibility evaluation model (LRV) to evaluate water resource accessibility based on the cumulative probability distribution of three variables, namely length, runoff, and sight of the water network [9]. Assefa et al. evaluated the water resource accessibility based on the accessibility distance of water resources [10]. Li and Gao put forward a water resource accessibility analysis method based on network and water intake cost, considering topography, land use, and road factors [11]. Therefore, topography, water resources, and distance are the key factors affecting the accessibility of water resources. Surface runoff is an important part of water resources and plays a vital role in the production and life of rural settlements. Although Zhao et al. found that the main influencing factor affecting the change of surface runoff is precipitation. The surface runoff in the SHRD model is calculated according to the precipitation and runoff coefficient of each basin [12]. However, the accuracy of choosing a runoff coefficient for a large area is fuzzy. The global land data simulation system (GLDAS) provides a long-term global distributed runoff, which is highly demanded in water cycle research and water resources management [13]. The correlation coefficient between the surface runoff provided by these data and the observed surface runoff data in the Liuxi River Basin reaches 0.81 [14]. Therefore, these data can roughly represent large-scale surface runoff.

Water resources play an important role in economic development. Usually, the lower reaches of rivers or deltas are densely populated and economically developed areas where water intake is convenient, with developed agriculture, water conservancy, shipping, and other comprehensive transportation. Therefore, there is a correlation between water resources and economic development. It is generally believed that the richer the water resources, the more developed the economy. Especially for agriculture, the higher the

accessibility of water resources, the more developed the agriculture. Farmers in rural settlements depend on agriculture, and most of them in China are living near fields. Therefore, there is a certain correlation between the surface water resource accessibility of rural settlements and the GDP of the primary industry. Xie and Qin quantitatively analyzed the correlation between water resource accessibility and the economy based on the SHRD model [6,15]. The experimental results show that there is a significant positive correlation between water resource accessibility and regional GDP in China. The development of the regional economy is not only constrained by water resource accessibility in China but also in foreign countries, such as Bhutan [16]. Indeed, the interplay between water resources and rural settlements holds considerable sway over regional sustainable development.

Furthermore, previous research has often overlooked the assessment of surface water resource accessibility concerning the spatial distribution characteristics of rural settlements, particularly in regions like the Yellow River Basin, and using rural settlements as the research unit. This paper seeks to address this gap by introducing the *SWRA* model. The subsequent sections of this manuscript are structured as follows: Section 2 provides an overview of the study area, the dataset collected, and the methods employed in constructing the surface water resource accessibility model. Section 3 presents the assessment results across three different scales, which are further discussed in Section 4. Finally, we conclude our work in Section 5.

2. Materials and Methods

2.1. Study Area

The Yellow River originates from the Bayan Har Mountains in Qinghai Province, China, and extends to Dongying City, Shandong Province. From the source of the Yellow River to the estuary, it passes through 9 provinces and 56 cities in Qinghai Province, Sichuan Province, Gansu Province, Ningxia Hui Autonomous Region, Inner Mongolia Autonomous Region, Shaanxi Province, Shanxi Province, Henan Province, and Shandong Province. The total length of the Yellow River is about 5464 km. According to the Yellow River Conservancy Commission of the Ministry of Water Resources, the total area of the Yellow River Basin is 795,000 km^2. As the birthplace of Chinese civilization, the Yellow River Basin has a total land area of 21,911.23 km^2 in urban and rural areas, industrial and mining areas, and residential areas, accounting for 2.8% of the total area of the Yellow River Basin. Rural residential areas account for about 75% of the total land area. And most residential areas are distributed along rivers. The Yellow River sustains approximately 12% of China's population. According to the Yellow River Water Resources Bulletin, agricultural water use accounts for an average of 67.3% of water usage in the basin [17]. The surface water development utilization rate in the Yellow River Basin stands at a staggering 86%, significantly surpassing the internationally recognized ecological warning line of 40% for water resource development [18]. Consequently, ensuring the rational utilization and allocation of water resources in the Yellow River Basin is imperative. The spatial correlation between rural settlements and water resources plays a pivotal role in water resource allocation. This paper aims to quantitatively evaluate this relationship.

There are many hydrological stations in the Yellow River Basin. This paper selected 12 important control hydrological stations in the mainstream of the Yellow River recorded in the Yellow River Sediment Bulletin [19]. They are Tangnaihai station, Lanzhou station, Shizuishan station, Toudaoguai station, Longmen station, Tongguan station, Sanmenxia station, Xiaolangdi station, Huayuankou station, Gaocun station, Ai Shan station, and Lijin station from upstream to downstream (Figure 1).

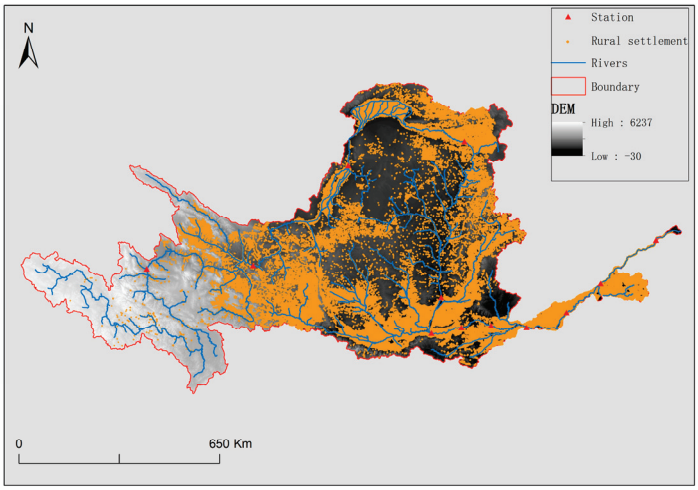

Figure 1. Overview map of the study area.

This paper utilized land use data from 2020 to extract spatial distribution vector data of rivers and residential areas within the Yellow River Basin. Subsequently, the area and number of rural settlement patches within river buffers at varying distances were quantified using the ArcGIS 10.3 spatial statistical analysis tool. This facilitated the qualitative and quantitative revelation of the spatial relationship between rural settlements and rivers. Additionally, by integrating surface water resources, topography, and distance, a surface water resource accessibility model (*SWRA*) was constructed using the Geographic In-formation System (GIS) platform. The *SWRA* model was then employed to analyze the spatial distribution characteristics of rural settlement surface water resource accessibility across the entire Yellow River Basin, as well as at catchment and city scales. Finally, the rationality of the *SWRA* model proposed in this paper was validated through Pearson correlation analysis between the primary industry output value of cities and *SWRA* at the city scale.

Based on the method of buffer zone analysis, this paper first reveals the overall spatial distribution characteristics of rural settlements and rivers in the Yellow River Basin by counting two landscape pattern indices, including the number and area of rural settlements. According to the previous calculation, the area of rural settlements in the Yellow River Basin increased slowly from 1980 to 2020, with little increase in the number of rural settlement areas [20]. Therefore, this paper uses rural settlement vector data and the river network map of 2020 in the study. Then, this paper takes 2 km, 4 km, 6 km, 8 km, and 10 km away from the rivers as buffer zones. Furthermore, the numbers and areas of rural settlements in each buffer zone are counted respectively, as shown in Table 1.

Table 1. The proportion of rural settlement areas and numbers in different buffer zones.

Buffer Distance /km	Number of Rural Settlements	Proportion	Rural Settlement Area/km^2	Proportion
2	21,442	20.73	3388.47	21.37
2–4	13,660	13.21	2481.18	15.65
4–6	11,583	11.20	1966.23	12.40
6–8	9621	9.30	1606.71	10.13
8–10	8235	7.96	1251.94	7.89
>10	38,881	37.59	5164.47	32.56
Total	103,422	100.00	15,858.99	100.00

It can be seen from Table 1 that the proportion of rural settlement areas and numbers are 67.44% and 62.41% in the 10 km buffer distance away from the river. Furthermore, the proportion of rural settlement areas and numbers are 37.02% and 33.94% in the 4 km buffer

distance away from the river. Compared with other residential areas and numbers in the buffer zone with the same distance, the rural residential areas and numbers in the buffer zone of 2 km away from the rivers account for the largest proportion. It can be seen that there is a certain correlation of the spatial distribution between rural settlements and rivers in the Yellow River Basin. Therefore, the spatial distribution relationship between rural settlements and surface water resources is further revealed by constructing the surface water resource accessibility model.

2.2. Materials

2.2.1. Data

The rural settlement data involved in this paper come from the land use data with 30 m resolution in the National Earth System Science Data Center (http://www.geodata.cn/, accessed on 1 May 2023) of 2020. The river network system was extracted by DEM data with a 30 m resolution in 2010. The origin control upstream catchment area of each hydrological station was derived from DEM data on the ArcGIS 10.3 platform. Then, it was corrected by the subbasin boundary in the Yellow River network system of the Atlas of the Yellow River Basin [21] (Figure 1).

Surface runoff data (*Qs_acc*) is derived from the Global Land Data Assimilation System (GLDAS) [22]. GLDAS is a global hydrological model developed and established by NASA's Goddard Space Flight Center and the National Center for Ocean and Atmospheric Prediction. Its data include surface runoff (kg/m^2), snow depth (m), soil moisture (kg/m^2), snow depth water equivalent (kg/m^2), and so on. According to Zheng et al. and Lv et al., the surface runoff data can reflect the change in surface runoff [13,14]. Therefore, this paper directly uses these data to represent surface runoff. We extracted and processed GLDAS-2.1 data (with a spatial solution of 0.25°, equal to 25 km, and a temporary solution of 24 h) in Google Earth Engine (GEE) in 2020 [23]. Then, the average value of surface runoff for 12 periods in 2020 was obtained by the grid calculator tool of ArcGIS 10.3.

The economic data select the output value of the primary industry, which comes from the provincial statistical yearbooks in 2020. According to the standards of the National Economical Industry Classification (GB/T4754-2011) [24] and the Regulations on the Division of Three Industries, the primary industry refers to agriculture, forestry, animal husbandry, and fishery (excluding agriculture services, forestry services, animal husbandry services, and fishery services). The gross output value of agriculture, forestry, animal husbandry, and fishery refers to the total value of all products of agriculture, forestry, animal husbandry, and fishery in monetary terms and various supporting service activities for agriculture, forestry, animal husbandry, and fishery production activities, which reflects the total scale and achievements of agriculture, forestry, animal husbandry, and fishery production in a certain period [25].

2.2.2. Construction of Surface Water Resource Accessibility Model

To quantitatively analyze the accessibility of rural settlements to surface water resources, this paper takes rural settlements as the research unit and constructs the surface water resource accessibility (*SWRA*) model to analyze the water resource accessibility of rural settlements in the Yellow River Basin. The specific indicators include the elevation difference between rural settlements and the nearest water intake point (*E*) reflecting the topographic characteristic, the distance between rural settlements and the nearest water intake point (*D*) reflecting the distance characteristic, and the surface runoff (*Qs_acc*) reflecting the characteristic of surface water resources (Figure 2).

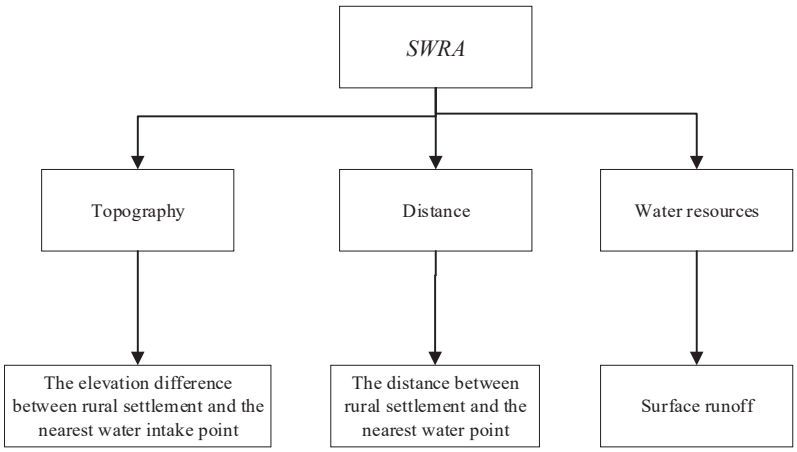

Figure 2. Index system diagram of surface water resource accessibility.

The elevation difference between the rural settlement and nearest water intake point (*E*): the elevation difference between the rural residential area and the nearest water intake point was calculated by DEM data on ArcGIS 10.3 platform using a spatial statistical analysis tool.

The distance between rural settlement and the nearest water intake point (*D*): the distance between each centroid of rural settlement and the nearest water point was calculated by using the proximity analysis tool in ArcGIS 10.3 spatial analysis.

Surface runoff (*Qs_acc*): this paper assigns surface runoff value to the centroid of rural settlement by using the tool of "value extraction to point" in the ArcGIS 10.3 spatial analysis toolbox.

Generally speaking, the higher the *Qs_acc*, the higher the accessibility of water resources. The lower the E, the higher the accessibility of water resources. The smaller the D, the higher the accessibility of water resources. Based on the previous research achievements, the experts in water resource management achieved an agreement that *Qs_acc* and *E* had a higher impact on the accessibility of water resources in rural settlements. The weights of *Qs_acc* and *E* are relatively higher. Then, the weight of *D* is relatively lower. Finally, the weights of *Qs_acc*, *E*, and *D* are set to 0.4, 0.4, and 0.2, respectively, according to the Delphi method.

The water resource accessibility model of each rural settlement is constructed using the method of weighted summation, as shown in Formula (1).

$$SWRA = \sum \left(E \times W_E + D \times W_D + Qs\_acc \times W_Q \right) \tag{1}$$

In Equation (1), W_E is the weight of E, W_D is the weight of D, and W_Q is the weight of Qs_acc.

Since the dimensions of each index in Formula (1) are different, the following standardization method is adopted [26].

$$X_i^* = \frac{X_{max} - X_i}{X_{max} - X_{min}} \tag{2}$$

$$X_i^* = \frac{X_i - X_{min}}{X_{max} - X_{min}} \tag{3}$$

In Formulas (2) and (3), X_i^* is the normalized variable value, X_i is the original variable, and X_{max} and X_{min} are the maximum and minimum values of X_i. For the inverse index, Formula (2) is used for standardization; for positive indicators, Formula (3) is used for standardization.

3. Results

The results of *SWRA* are examined in the whole basin, at catchment scale, and at the city scale. Because the catchments are important components of the basin, the characteristics of *SWRA* values at the catchment scale are delivered. In addition, the characteristics of *SWRA* values at the city scale are examined. Furthermore, in order to verify the rationality of *SWRA*, the correlation between *SWRA* and the GDP of the primary industry is explored.

3.1. The Results of SWRA in the Yellow River Basin

After calculation, the range of surface water runoff in the Yellow River Basin is 0–3.10 kg/m^2. At the same time, the surface runoff of rural settlements is extracted. The range of surface runoff values in rural settlements is 0–0.17 kg/m^2 (Figure 3). Based on the nearest distance, the distance between the rural settlement and the nearest water intake point is calculated. Its value range is 0.13–67,038.47 m (Figure 4). Then, the elevation difference between the rural settlement and the nearest water intake point is calculated based on DEM data combined with the nearest neighbor point. The values range from −515 to 1608 m (Figure 5). It can be seen from Figure 3 that the surface runoff of rural settlements is mostly lower than 0.05 km/m^2, reaching 99.83% by statistics. In other words, the Yellow River Basin is extremely short of water resources. The distribution characteristics of rural settlements are along rivers, which can be seen clearly in Figure 4. There are 10.93% of rural settlements whose elevation is lower than the nearest water intake point through attribute query statistics. There are 3.77% of rural settlements whose elevation is higher than the nearest water intake point by 500 m, reaching a maximum of 1608 m. The positive elevation difference greatly increases the difficulty of water intake.

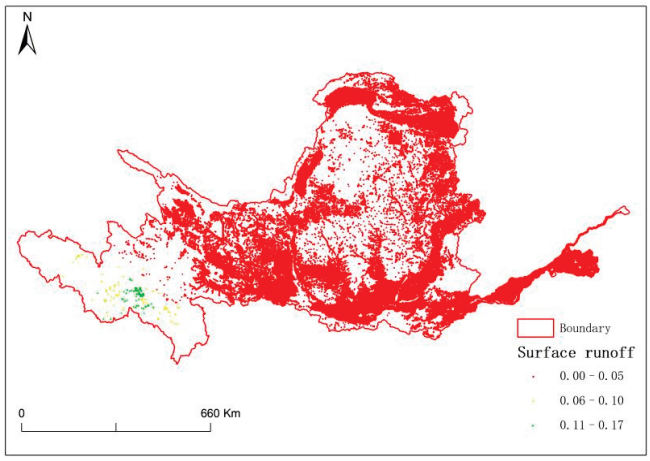

Figure 3. Surface runoff thematic map.

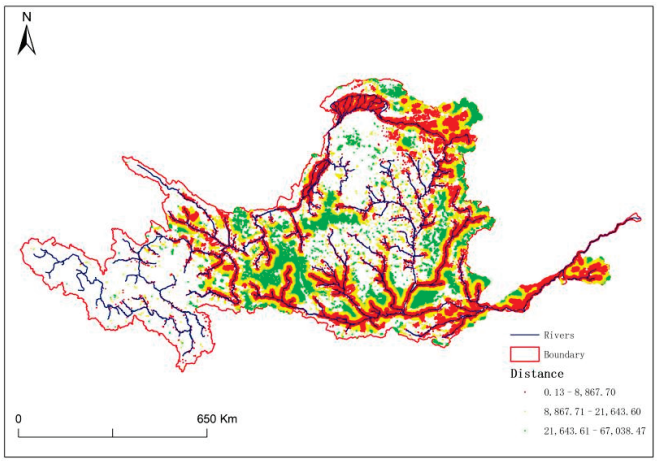

Figure 4. Distance thematic map.

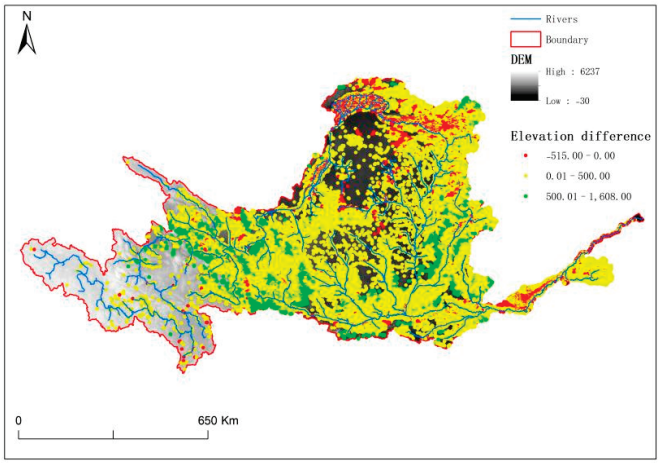

Figure 5. The elevation difference thematic map.

The SWRAS values of each rural settlement were achieved by a weighted sum of the three standardized indicators by Equation (1). The *SWRA* values range from 0.13 to 0.88, with an average value of 0.47 and a standard deviation of 0.05 (Figure 6). The *SWRA* values are divided into three levels, namely high, middle, and low, by 0.45 and 0.51, according to the spatial distribution characteristics of *D*, *E*, and *Qs_acc* by the Delphi method. It can be seen from Figure 6 that the *SWRA* in the Yellow River Basin is higher in the east and west and lower in the middle.

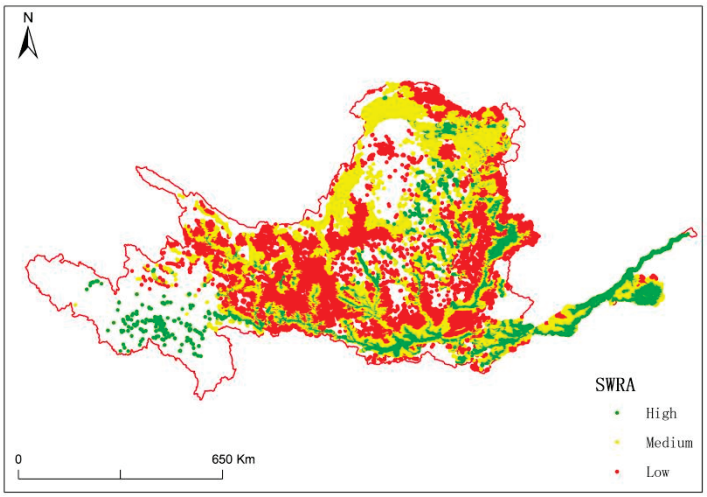

Figure 6. The surface water resource accessibility thematic map.

The distribution characteristics of *SWRA* values are further analyzed at the catchment scale and the city scale.

3.2. Spatial Distribution Characteristics of SWRA at the Catchment Scale

The average value of *SWRA* in each catchment is counted based on the intersect analysis between *SWRA* and catchment boundaries. At the same time, the average values of the distance and elevation difference between rural settlements and the nearest water intake point are counted in Table 2. The results show that the *SWRA* values of the 12 catchments from low to high are Sanmenxia station, Lanzhou station, Shizuishan station, Longmen station, Tongguan station, Toudaoguai station, Xiaolangdi station, Huayuankou station, Lijin station, Gaocun station, Aishan station, and Tangnaihai station. According to the classification standard of Section 3.1, the catchment *SWRA* value in high grade only appears in the catchments of Aishan Station and Tangnaihai Station. The SWRA values in the other catchments are at a medium level. The difference in *SWRA* values is a minor among

these catchments because the catchment *SWRA* value is the average value of all the *SWRA* values of these rural settlements in each catchment. It should be noted that the *SWRA* calculation results of this paper are only the relative level under the state of water shortage. Furthermore, the high-grade ratio of *SWRA* values in Tangnaihai station is 78.55%, while the high-grade ratio of *SWRA* values in Sanmenxia station is only 10.36%. It can be seen from Table 2 that *D* of Tangnaihai station reaches the smallest value, while *D* of Sanmenxia station gains the largest value. In other words, it is relatively difficult for rural settlements in the Sanmenxia catchment to obtain water resources, while it is relatively easy for the Tangnaihai catchment from the perspective of spatial distance. The highest value of elevation difference between rural settlement and the nearest water intake point appears in the Lanzhou catchment, with a value of 210.04 m, while the smallest elevation difference is in the Gaocun catchment, with a value of 0.95 m.

Table 2. Statistical characteristics of rural settlements and water resources at the catchment scale.

Station	*D*/km	*Qs_acc*/kg/m^2	*E*/m	*SWRA*
Tangnaihai station	6.15	0.067	96.87	0.62
Lanzhou station	7.87	0.010	210.04	0.45
Shizuishan station	10.68	0.003	114.88	0.46
Toudaoguai station	8.70	0.004	54.15	0.48
Longmen station	9.93	0.009	146.87	0.46
Tongguan station	10.78	0.013	188.06	0.47
Sanmenxia station	16.53	0.012	160.52	0.45
Xiaolangdi station	6.06	0.013	155.74	0.49
Huayuankou station	10.26	0.017	149.63	0.49
Gaosun station	9.14	0.013	0.95	0.50
Aishan station	6.74	0.020	35.61	0.52
Lijin station	7.99	0.020	80.59	0.50

3.3. Spatial Distribution Characteristics of SWRA at the City Scale

The *SWRA* value of each city is equal to the mean value of all the *SWRA* values in the city. Firstly, it is calculated by the intersection of *SWRA* and the city boundary. Then, the values are summarized by the city boundary. The result shows that the *SWRA* values of the city range from 0.41 to 0.69, with an average value of 0.48 and a standard deviation of 0.04. The city *SWRA* values are divided into three levels according to the classification standard of 3.1.

It can be seen from Figure 7 that the *SWRA* values of nine cities are at a low level and are distributed in the western part of the Yellow River Basin, namely Tongchuan City, Guyuan City, Baiyin City, Xining City, Hainan Tibetan Autonomous Prefecture, Yuncheng City, Dingxi City, Lanzhou City, and Haidong District. The GDP of primary industries in these cities tends to be relatively lower. In the Hainan Tibetan Autonomous Prefecture, several rural settlements are situated at a considerable distance from rivers and with minimal surface runoff. Similarly, in cities like Dingxi, Guyuan, Tongchuan, and Yuncheng, there are few river sections, leading to lower *SWRA* values. Conversely, rural settlements in Xining, Haidong, Lanzhou, and Baiyin are located along rivers, with others scattered across the region. Despite some settlements being close to rivers, a larger number are situated farther away, resulting in a high average value of distance (*D*). Additionally, these rural settlements experience low levels of surface runoff. Therefore, the *SWRA* values of these cities are at a low level. The SWRA values of 11 cities mainly distributed in the east of the study area are in high grade. They are Dongying City, Binzhou City, Dezhou City, Kaifeng City, Liaocheng City, Tai'an City, Jiaozuo City, Heze City, Puyang City, and Jinan City. Besides these cities, the high-grade city distributed in the west is Golog Tibetan Autonomous Prefecture. The GDP of primary industries in the ten eastern cities tends to be relatively higher. This observation suggests a discernible correlation between *SWRA* and GDP. However, in Golog Tibetan Autonomous Prefecture, the *SWRA* value is notably high due to the region's elevated surface runoff levels in the western area.

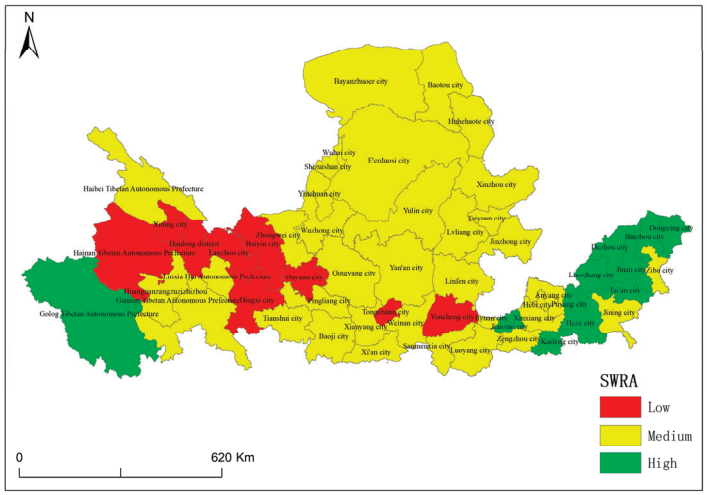

Figure 7. Surface water resource accessibility on an urban scale.

Furthermore, the correlation between the *SWRA* values of the city and the GDP of primary industry is revealed in SPSS 25. The results show that the correlation coefficient between city *SWRA* values and the GDP of primary industry is 0.271 (N = 56, Sig = 0.043, at 0.05 level (double tails), and the correlation is significant). It can be seen that there is a linear positive correlation between *SWRA* and the GDP of the primary industry, which indicates that *SWRA* serves as an influential indicator affecting the GDP of primary industries. Furthermore, it lends credence to the rationality of *SWRA* to some extent. However, the correlation coefficient is not high. The main reason is that the western region with abundant water resources is sparsely populated. For example, the rural settlement is less distributed in the area of the Tangnaihai catchment (e.g., Golog Tibetan Autonomous Prefecture) with a lower GDP of the primary industry, while the water resources there are abundant and with a relatively higher value of *SWRA*. The economic development of this region is affected by other factors such as climate, transportation, and population. In other words, *SWRA* is the secondary influencing factor of the economic development of this region.

4. Discussion

4.1. The Uncertainty of Indicators of SWRA

With the development of infrastructure and the improvement of the tap water supply network, some rural residents gradually give up the water in natural rivers [27]. Then, rivers gradually lose their original functions [28]. Moreover, with the development of the social economy, the water quality in the rivers is gradually polluted by domestic sewage and agricultural sewage [29,30]. After inheritance, interweaving, replacement, connection, and other ways to promote the development of settlements, a coordinated relationship between settlements and rivers is formed [31], and in a long-term evolution, the relationship gradually matures. Therefore, from the perspective of surface water resource accessibility to analyze the accessibility of rural residential water resources, the accuracy needs to be improved. Furthermore, human factors such as the tap water network and pumping stations should be considered in the construction of *SWRA*.

The surface runoff data provided by GLDAS serve as a relative measure of surface water resources. While previous studies have indicated its rough representation of surface runoff, its accuracy is not absolute. Nonetheless, this paper conducts a quantitative evaluation of water resource accessibility in rural residential areas across the Yellow River Ba-sin under conditions of water scarcity. The surface runoff data from GLDAS captures the surface water resources of the entire region under uniform conditions. Through standardization of each indicator during calculation, even if the data's accuracy is not optimal, it remains viable as an indicator for assessing water resources within *SWRA*.

4.2. The Implications of SWRA

The findings underscore the significance of water resource accessibility for the regional development of rural communities. This accessibility serves as a guide for both the water allocation program of the Yellow River and broader regional sustainable development efforts. For instance, in regions with poor surface runoff, it is imperative for managers to allocate more water resources. Additionally, for scattered rural settlements characterized by low *SWRA* values, a strategic relocation to concentrated areas is recommended. This relocation would enable managers to efficiently provide water resources through the implementation of tap water networks and pumping stations.

4.3. The Implications of the Relationship of SWRA and GDP of Primary Industry

The correlation coefficient between city *SWRA* values and the GDP of the primary industry may appear low due to the multifaceted nature of economic development, influenced by both natural and social factors. Natural factors encompass climate, terrain, rivers, and water resources, while social factors include population, transportation, policies, location, and demographics. Particularly in regions with abundant water resources, such as the Yellow River source area, despite high surface runoff and water accessibility, the primary industry's GDP tends to be relatively low. This discrepancy is primarily attributed to the challenging nature of water resource development in such regions, which impedes economic progress. Nonetheless, the significant correlation coefficient underscores the role of water resource accessibility as a factor influencing regional economies. Quantitative data derived from this correlation can offer valuable support for formulating regional economic policies and strategies. By leveraging the relationship between *SWRA* and economic development, regional development strategies can be tailored effectively. Water resources play a pivotal role in economic development, and exploring the connection between water resource accessibility and economic progress can provide crucial data for optimizing water resource allocation, enhancing utilization efficiency, and fostering equitable distribution in China [32]. This paper introduces the *SWRA* model for the first time to assess water resource accessibility in rural residential areas across the Yellow River Basin and its correlation with primary industry economic development. Building upon this foundation, future research will delve into the relationship between water resource accessibility and economic development at various scales (e.g., county scales and upstream, midstream, and downstream scales), contributing to the fair and rational allocation of water resources in the Yellow River Basin.

5. Conclusions

Based on the GIS platform, the spatial distribution characteristics of rural settlements and river networks in the Yellow River Basin are studied qualitatively at first. Then, a quantitative evaluation model of surface water resource accessibility is constructed by using the GIS network analysis method, taking rural settlements as the research unit, based on three dimensions of topography, distance, and surface water resources. The surface water resource accessibility of rural settlements in the Yellow River Basin is evaluated quantitatively. Finally, the rationality of *SWRA* is verified by the Pearson correlation analysis between surface water resource accessibility and the GDP of primary industry. The following conclusions are obtained: (1) The surface runoff of rural residential areas in the Yellow River Basin is mostly less than 0.05 km/m^2, reaching 99.83%. In other words, the Yellow River Basin is extremely short of water resources. The grade of surface water resource accessibility is relatively high only at the source and estuary of the Yellow River, while it is relatively low in the central region of the Yellow River Basin. (2) The average value of surface water resource accessibility at the catchment scale has minor difference. However, from the ratio of high, middle, and low grades of *SWRA* in each catchment area, the high-grade ratio of Sanmenxia station is only 10.36%, while the high-grade ratio of Tangnaihai station is 78.55%. (3) The value of surface water resource accessibility at the city scale is higher in the east of ten cities and in the west of one city. However, it is lower in

the west of nine cities, and the *SWRA* value of the other cities is at a medium level. (4) The water resource is the key factor that restricts the development of the rural economy. There is a correlation between *SWRA* and the primary industry economy in the Yellow River Basin. Indeed, while the correlation coefficient between *SWRA* and GDP may be low, its significance underscores the importance of *SWRA* as a factor influencing GDP. This suggests that *SWRA* is constructed reasonably to assess water accessibility. Consequently, managers can leverage SWRA results to make informed decisions regarding regional development and water allocation strategies.

Author Contributions: Conceptualization, H.L.; methodology, H.L. and J.Z.; software, H.M.; visualization, X.C.; formal analysis, X.H.; investigation, J.Z.; resources, H.L.; data curation, H.M.; writing—original draft preparation, H.L. and H.M.; writing—review and editing, J.Z. and H.M.; visualization, H.L.; supervision, J.Z.; project administration, X.C.; funding acquisition, H.L. All authors have read and agreed to the published version of the manuscript.

Funding: This research was funded by the Open Fund of Key Laboratory of Urban Land Resources Monitoring and Simulation, Ministry of Natural Resources (KF-2022-07-020), the National Natural Science Foundation of China (U21A2014), Natural Science Foundation of Henan (232300420436), Key Scientific Research Projects in Colleges and Universities of Henan Province (24B170002), and Henan Collaborative Innovation Center of Geo-Information Technology for Smart Central Plains (2023C001).

Data Availability Statement: Data are contained within the article.

Conflicts of Interest: The authors declare no conflicts of interest.

References

1. Li, Y.; Huang, S.; Kong, X.; Han, M.; Wang, M.; Hui, H. Ecological Effects of Surface Water Evolution in the Yellow River Delta. *Sustainability* **2022**, *14*, 13544. [CrossRef]
2. Li, X.Q. Study on measures to enhance integrated water resources management of Yellow River. *China Water Resour.* **2011**, *7*, 35–38. [CrossRef]
3. Song, F.; Yang, X.; Wu, F. Suitable Pattern of the Natural Environment of Human Settlements in the Lower Reaches of the Yangtze River. *Atmosphere* **2019**, *10*, 200. [CrossRef]
4. Zuo, Q.T.; Wu, B.B.; Zhang, W.; Ma, J.X. A method of water distribution in transboundary rivers and the new calculation scheme of the Yellow. *Resour. Sci.* **2020**, *42*, 37–45.
5. Wang, Z.Y.; Huang, J.Y. Research on Spatial Distribution Characteristics of Rural Residential Areas Based on GIS: Taking Fuyu City as an Example. *Mod. Agric. Sci. Technol.* **2023**, *21*, 205–208.
6. Qin, X. The Relationship between Water Accessibility and Economic Development in China. Master's Thesis, Central China Normal University, Shanghai, China, 2017.
7. Li, T.; Qiu, S.; Mao, S.; Bao, R.; Deng, H.B. Evaluating Water Resource Accessibility in Southwest China. *Water* **2019**, *11*, 1708. [CrossRef]
8. Xu, L.L.; Tu, Z.F.; Yang, J.; Zhang, C.L.; Chen, X.X.; Gu, Y.X.; Yu, G.M. A water pricing model for urban areas based on water accessibility. *J. Environ. Manag.* **2023**, *327*, 116880. [CrossRef]
9. Li, F.W.; Liu, H.F.; Chen, X.; Yu, D. Trivariate Copula Based Evaluation Model of Water Accessibility. *Water Resour. Manag.* **2019**, *33*, 3211–3225. [CrossRef]
10. Assefa, T.; Jha, M.; Reyes, M.; Srinivasan, R.; Worqlul, A. Assessment of Suitable Areas for Home Gardens for Irrigation Potential, Water Availability, and Water-Lifting Technologies. *Water* **2018**, *10*, 495. [CrossRef]
11. Li, F.W.; Gao, F. Accessibility evaluation of water networks based on network analysis. *Water Resour. Hydropower Eng.* **2023**, 1–13. Available online: https://link.cnki.net/urlid/10.1746.TV.20230922.1452.002 (accessed on 15 June 2023).
12. Zhao, L.; Zhang, Z.; Dong, F.; Fu, Y.C.; Hou, L.; Liu, J.Q.; Wang, Y.B. Research on the Features of Rainfall Regime and Its Influence on Surface Runoff and Soil Erosion in the Small Watershed, the Lower Yellow River. *Water* **2023**, *15*, 2651. [CrossRef]
13. Lv, M.Z.; Lu, H.; Yang, K.; Xu, Z.F.; Lv, M.F.; Huang, X.M. Information of Runoff Components Simulated by GLDAS against UNH-GRDC Dataset at Global and Hemispheric Scales. *Water* **2018**, *10*, 969. [CrossRef]
14. Zheng, J.H.; Wang, H.L.; Liu, B.J. Impact of the long-term prevention and land use changes on runoff variations in a humid subregional river base of China. *J. Hydrol. Reg. Stud.* **2022**, *42*, 101136. [CrossRef]
15. Xie, X.Q. The Relationship between Water Accessibility and Economic Development in China. Master's Thesis, Central China Normal University, Shanghai, China, 2019.
16. Imiya, M.C.; Erandi, S.; Phub, Z.; Miyuru, B.G.; Denkar, D.; Nitin, M.; Amila, A.; Komali, K.; Upaka, R. Assessing the water quality and status of water resources in urban and rural areas of Bhutan. *J. Hazard. Mater. Adv.* **2023**, *12*, 100377.
17. Yellow River Conservancy Commission of the Ministry of Water Resources. Yellow River Water Resources Bulletin. 2020. Available online: http://www.yrcc.gov.cn/other/hhgb/ (accessed on 22 May 2023).

18. Sun, J.W.; Cui, Y.Q.; Zhang, H. Spatio-temporal pattern and mechanism analysis of coupling between ecological protection and economic development of urban agglomerations in the Yellow River Basin. *J. Nat. Resour.* **2022**, *37*, 1673–1690. [CrossRef]
19. Yellow River Conservancy Commission of the Ministry of Water Resources. Yellow River Sediment Bulletin. 2020. Available online: http://www.yrcc.gov.cn/nishagonggao/2020/mobile/index.html#p=1 (accessed on 20 May 2023).
20. Shan, Y.M.; Li, H.Y.; Zhang, J.C.; Tang, L.J.; Guo, J.Z.; Wang, G.X.; Wang, J.Y.; Zhang, H.W.; Zheng, H.H. Temporal and spatial evolution and driving force analysis of rural residential distribution pattern in the Yellow River Basin under the background of rural revitalization. *Surv. Mapp. Bull.* **2024**, *1*, 96–101. [CrossRef]
21. Yellow River Conservancy Commission of the Ministry of Water Resources. *Atlas of the Yellow River Basin*; SinoMaps Press: Beijing, China, 1987; pp. 20–21.
22. Wang, Q.Q.; Zheng, W.; Yin, W.J.; Kang, G.H.; Huang, Q.H.; Shen, Y.F. Improving the Resolution of GRACE/InSAR Groundwater Storage Estimations Using a New Subsidence Feature Weighted Combination Scheme. *Water* **2023**, *15*, 1017. [CrossRef]
23. Rodell, M.; Houser, P.R.; Jambor, U.; Gottschalck, J.; Mitchell, K.; Meng, C.J.; Arsenault, K.; Cosgrove, B.; Radakovich, J.; Bosilovich, M.; et al. The global land data assimilation system. *Bull. Am. Meteorol. Soc.* **2004**, *85*, 381–394. [CrossRef]
24. *GB/T4754-2011*; The National Economical Industry Classification. China, 2011. Available online: https://www.cas.cn/ggfw/tzgg_1/201201/P020120120521186361137.pdf (accessed on 15 June 2023).
25. National Bureau of Statistics of the People's Republic of China. *2021 China Statistical Yearbook*; China Statistics Publishing: Beijing, China, 2021.
26. Li, H.Y.; Fan, Y.B.; Gong, Z.N.; Zhou, D.M. Water accessibility assessment of freshwater wetlands in the Yellow River Delta National Nature Reserve, China. *Ecohydrol. Hydrobiol.* **2020**, *20*, 21–30. [CrossRef]
27. Bao, R.; Wu, J.; Li, T.; Deng, H. Assessment and Influencing Factors of Water Supply Capacity and Water Resource Utilization Efficiency in Southwest China. *Water* **2023**, *15*, 144. [CrossRef]
28. Wu, Y.Q.; Xu, Y.; Zhao, Y.; Luo, Y.Z.; Lu, J.Y.; Chen, Y.C. Evolution of river network due to urbanization in the Southeast Yinzhou Plain of Yongjiang River Basin, China. *J. Clean. Prod.* **2022**, *379*, 134718. [CrossRef]
29. Anh, N.T.; Can, L.D.; Nhan, N.T.; Schmalz, B.; Luu, T.L. Influences of key factors on river water quality in urban and rural areas: A review. *Case Stud. Chem. Environ. Eng.* **2023**, *8*, 100424. [CrossRef]
30. Liu, J.; Cheng, F.; Zhu, Y.; Zhang, Q.; Song, Q.; Cui, X. Urban Land-Use Type Influences Summertime Water Quality in Small- and Medium-Sized Urban Rivers: A Case Study in Shanghai, China. *Land* **2022**, *11*, 511. [CrossRef]
31. Cao, W.F.; Liu, J.G.; Ceola, S.; Mao, G.Q.; Macklin, M.G.; Montanari, A.; Ciais, P.; Yao, Y.Z.; Tarolli, P. Landform-driven human reliance on rivers in imperial China. *J. Hydrol.* **2023**, *620*, 129353. [CrossRef]
32. Espinoza, S.; Forni, L.; Lavado, A.; Olivera, M.; Tapia, C.; Vega, B.; Balderrama, M.; Escobar, M. Connecting Water Access with Multidimensional Poverty: The Case of Tupiza River Basin in Bolivia. *Water* **2022**, *14*, 2691. [CrossRef]

water

MDPI

Article

Optimization Study on Sequential Emptying and Dredging for Water Diversity Reservoir Group

Yujun Wang, Changsai Han and Xiping Zhao *

College of Water Resource Science and Engineering, Taiyuan University of Technology, Taiyuan 030024, China; tigersix1998@163.com (Y.W.); 18649225224@163.com (C.H.)
* Correspondence: zxplzy@126.com

Abstract: Reservoir sediment severely impacts water supply in water-scarce regions, making reservoir dredging an urgent global issue. The investment required for deep-water dredging far exceeds that for dry land dredging. Therefore, against the backdrop of the national water network construction, this study focuses on a typical inter-basin water transfer project in Northern China. To increase the proportion of dry land dredging volume and save costs, this study uses compensation reservoirs to replace the emptied reservoir in undertaking water supply tasks as a constraint. Single-objective optimization models for single reservoirs and multi-objective optimization models for reservoir groups are established, using game theory comprehensive subjective and objective weighting methods to select the optimal solution. The following conclusions are drawn from comparing the water supply effects under various emptying sequences: the optimal sequence for emptying reservoirs should be determined through precise quantitative analysis; as the dredging is completed, the water supply tends to stabilize; the satisfaction with the water supply and the variance of the water shortage rate are primarily related to reservoirs with a large inflow and storage capacity; dredging occurs according to the descending order of the storage capacity of reservoirs; and the startup proportion of pump stations shows an increasing trend.

Keywords: reservoir dredging; inter-basin water transfer; economic operation; joint dispatching of reservoir groups

1. Introduction

The problem of reservoir dredging has plagued the water conservancy industry for many years. The gradual development of sedimentation leads to the extension of backwater, the inundation of land, an impact on navigation, and the weakening of the flood control and water supply functions due to the encroachment of the reservoir capacity. The reduction in the sediment transport of the river also leads to an increase in erosion in the downstream channel and seawater erosion in the estuary [1–3]. In Northern China, where water resources are relatively scarce, the issue of reduced water supply reliability due to sedimentation is particularly pressing [4].

To maintain a substantial effective reservoir capacity over the long term and delay the onset of siltation equilibrium, researchers have explored strategies such as joint sediment discharge scheduling of cascade reservoirs [5,6], single-reservoir sediment discharge scheduling [7–9], and deep-water dredging technology [10,11]. In terms of the joint dispatching of sediment discharge in cascade reservoirs, some researchers [12,13] have conducted extensive theoretical and experimental studies on density flow sediment discharge and riverbed erosion and deposition. Currently, the artificial shaping of density flows for sediment discharge has been successfully applied in the sediment dispatching of the Wanjiazhai–Sanmenxia–Xiaolangdi cascade reservoir system on the Yellow River. In terms of sediment discharge scheduling in a single reservoir, researchers have conducted significant research on the influence mechanism with multiple objectives, including sediment discharge, water supply, power generation, flood control scheduling, and flood

resource utilization, which provide valuable references for solving the optimal scheduling scheme of reservoirs with comprehensive utilization requirements built on sediment-rich rivers [14–18]. Regarding deep-water dredging technology, researchers have primarily focused on enhancing pipeline sediment discharge, reducing water consumption rates, minimizing wear, lowering power consumption, and mitigating the impact of cutterheads on the dispersion of underwater pollutants [19,20]. In order to ensure that the water supply is not compromised during the flood season when sediment is being discharged by lowering the water level in the main reservoir, the authors of [21,22] investigated the utilization of natural reservoir conditions or the construction of a new reverse-regulating reservoir to ensure water supply security for users during the sediment discharge periods of main water supply reservoirs. They transformed the issue into an optimization problem of water quantity dispatching for a group of reservoirs.

However, except for deep-water dredging, none of the above-mentioned dredging methods are suitable for dams without bottom outlets. Numerous reservoirs constructed in the 1950s and 1960s were driven by the urgent need for flood control and water supply. To minimize investment and expedite project completion for immediate benefits, the impact of sedimentation was rarely considered in the design process; many reservoirs did not equip the bottom hole for sediment discharge, relying solely on reserved sedimentation storage to extend their service life. This rendered measures such as emptying for sediment discharge, density current sediment removal, clear-water storage and sediment discharge, and high-channel sand dragging ineffective, all of which depend on bottom outlets for sediment removal [23]. In recent years, among the reinforcement projects for medium and small reservoirs, it is common to add low-level outlets such as sediment discharge bottom outlets, flood discharge tunnels, and drain tunnels to enhance flood discharge capacity and increase sediment removal. However, the water cost of using water flow to flush and remove sediment is too high, making it difficult to apply in water-scarce regions. Particularly in the reservoirs constructed in Shaanxi and Shanxi provinces, located on the Loess Plateau, the vegetation coverage remains low even after implementing the "Grain for Green" policy. The soil erosion caused by heavy rainstorms is exceptionally severe. The reserved sediment storage capacity has been nearly depleted after several infrequent floods, with some heavily silted reservoirs becoming effectively obsolete. Those tasked with flood control are forced to further lower their flood limit levels, resulting in increased water abandonment and reduced water supply reliability. The utility of these reservoirs in serving economic and social development needs is gradually falling behind.

Therefore, the sedimentation issues in reservoirs without bottom outlets can only be resolved through investment in dredging. The investment-to-return ratio of reservoir dredging plans is a critical indicator in determining the feasibility of dredging projects. However, the future social, economic, and flood prevention benefits of dredging cannot be accurately measured in monetary terms. Therefore, the current substantial investment amount is the main reason why reservoir dredging projects struggle to get off the ground. Reducing the investment amount for dredging is a key focus in the design of dredging plans [24–26]. Generally, the higher the proportion of dry land dredging, the lower the total investment in dredging and the higher the dredging efficiency. Compared with deep-water dredging, dry land dredging is simple and low in cost, making it the most cost-effective aspect among the three major investments in dredging, transportation, and disposal. However, the biggest drawback of dry land dredging is the suspension of reservoir functions, which is unacceptable for water supply reservoirs in Northern China. Some design proposals suggest that utilizing reverse-regulating reservoirs to temporarily take over the water supply tasks of reservoirs undergoing dredging can further lower the operational water level during the dredging process, thereby increasing the proportion of dry land dredging. In a sediment dredging plan for Reservoir A in Northern China, which involves the removal of 40 million m^3 of sediment, the construction of a water supply tunnel from downstream Reservoir B to the water users has been proposed. This would enable Reservoir B to substitute for the 26 million m^3 of drinking water previously supplied by Reservoir A. Consequently,

the operating water level of Reservoir A could be reduced, leading to a decrease in the dredging investment from CNY 3.785 billion to CNY 3.12 billion. However, this plan has not yet been implemented. Utilizing reservoirs with certain hydraulic connections for compensatory regulation, coupled with a modest investment in supporting projects, can reduce the cost of sediment dredging while enhancing the regional capacity for water allocation. This approach presents an intriguing solution.

China is advancing the construction of its national water network project, which, based on natural and artificial water bodies, will gradually enhance hydraulic connections between them through engineering measures. This initiative aims to strengthen water resource allocation capabilities, achieve mutual water supply across basins, address the uneven spatial distribution of water resources on a larger scale, and accelerate the management of groundwater over-extraction. The construction of the national water grid primarily encompasses water transfer projects and storage facilities. Beyond the newly constructed single water diversion projects, establishing a network-like framework is gradually achieved by adding key interconnection projects and integrating with previously built inter-basin water transfer systems. This network extends artificial, controllable water conveyance pipelines, tunnels, channels, reservoirs, and natural rivers to cover human settlements, akin to the distribution of nerve endings. If these water transfer projects can be fully utilized, complemented by necessary investment in supporting facilities to establish more complex water volume connections between reservoirs and enhance their mutual compensation capabilities, completely draining severely silted reservoirs for dry land dredging might be feasible.

Based on the above analysis, this study presents a research approach for siltation reservoir groups in water-scarce areas through compensatory regulation to achieve dry land dredging. Using a typical inter-basin water diversion project in Northern China as the research object, we address the optimization of sequential emptying and dredging strategies for water supply reservoir groups. First, we clarify the hydraulic connections between reservoirs and then select a typical dry year group for the basin. By employing a two-step optimization method, we construct both single-reservoir optimal scheduling models and multi-reservoir joint multi-objective optimal scheduling models. Through optimization calculations under different emptying sequences, we utilized a subjective–objective comprehensive weighting method to select the optimal solution [27]. By analyzing the water supply effects under various emptying sequences, we obtain the mechanism of influence between the characteristics of the reservoir, the sequence of emptying, and the operation indicators. The research findings offer new methods for dredging siltation reservoirs in water-scarce regions, providing valuable references for reservoir managers, river basin managers, dredging service industries, and policy makers in relevant departments.

2. Overview of the Study Area

Figure 1 illustrates a water supply project in Northern China that transfers water from a relatively abundant basin to a water-scarce region, addressing the shortfall in industrial, domestic, and agricultural water needs. For clarity, this study divides the project into the transfer area and the receiving area. The transfer area has a per capita water resource volume of 820 m^3, while the receiving area has 257 m^3. Although the per capita water resource volume in China is 2100 m^3, it only accounts for 28% of the global average. Therefore, objectively speaking, the water resource in the transfer area is not abundant. Consequently, this project connects four reservoirs (ZC, YZ, GH, and SX) to achieve the designed annual water transfer target of 112 million m^3. However, three of these source reservoirs were constructed in the 1950s and 1960s and are now severely silted. This has weakened their flood control and water storage capabilities, resulting in a low fill rate. The actual water supply capacity of the project is significantly lower than the designed requirements.

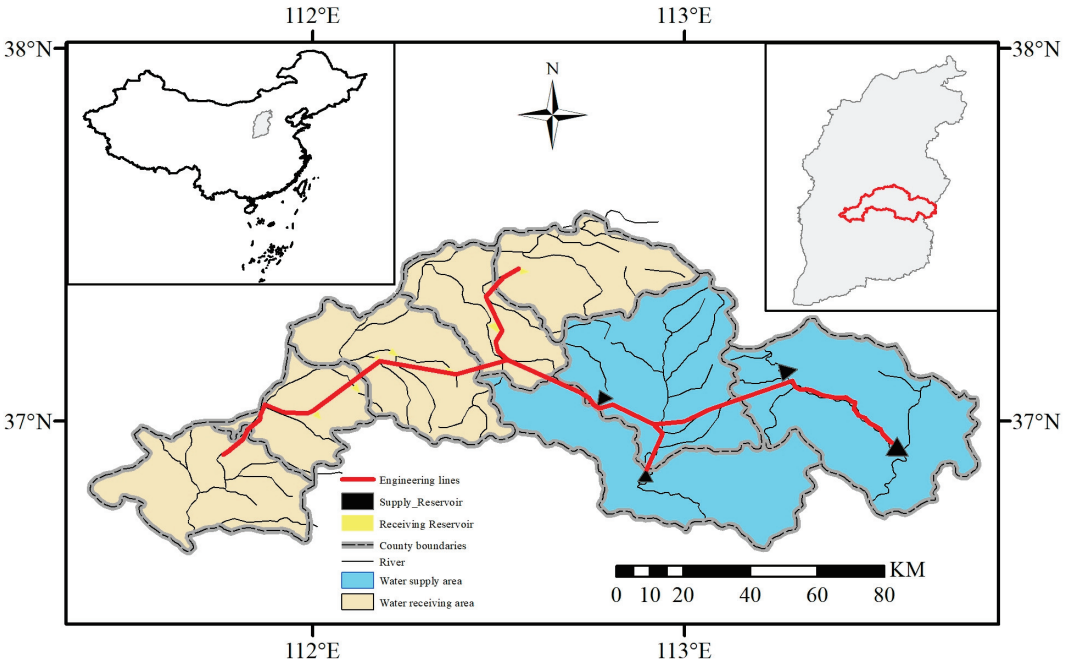

Figure 1. The general arrangement of the project.

Figure 2 illustrates the hydraulic connections among four source reservoirs in the transfer area. Among them, the ZC reservoir is a newly constructed reservoir that has not yet begun to store water, while the YZ, GH, and SX reservoirs have varying degrees of sedimentation. The water from the YZ and SX reservoirs can flow by gravity to the receiving area, resulting in lower water supply costs. In contrast, the GH and ZC reservoirs, due to their lower altitudes, require pumping through 1- and 2-stage pumping stations, respectively, to be transported to the receiving area, leading to higher water supply costs. To clarify the current storage capacity curves of each reservoir, the research team conducted an oblique survey of the ZC reservoir (empty) using a drone equipped with a visible light camera in June 2022. Measurements of the YZ, GH, and SX reservoirs were conducted in March and April 2023 using drones with visible light cameras and unmanned boats equipped with multi-beam echo sounders [28]. Upon analyzing the sedimentation conditions of three reservoirs based on the design data from the time of their construction, it was concluded that each reservoir had accumulated sediments equivalent to 21.2%, 50.5%, and 13.1% of their originally designed total storage capacities, respectively.

The four water source reservoirs in the transfer area each are responsible for supplying water to their respective regions. Industrial, domestic, and agricultural water demands are projected based on the assessments of future population growth and economic development by government planning departments. The ecological water demand within river channels is calculated using the Qp method after fitting long-series monthly average inflow data with a P-III-type curve [29]. The receiving area is a concentrated water-deficient region comprising five towns, where groundwater has long been one of the primary water sources. Prolonged overexploitation has led to severe groundwater depression cones. In terms of total volume, this inter-basin water supply project cannot replace the local groundwater source and can only replace a portion of the groundwater to mitigate the ecological and environmental degradation caused by the overexploitation of groundwater.

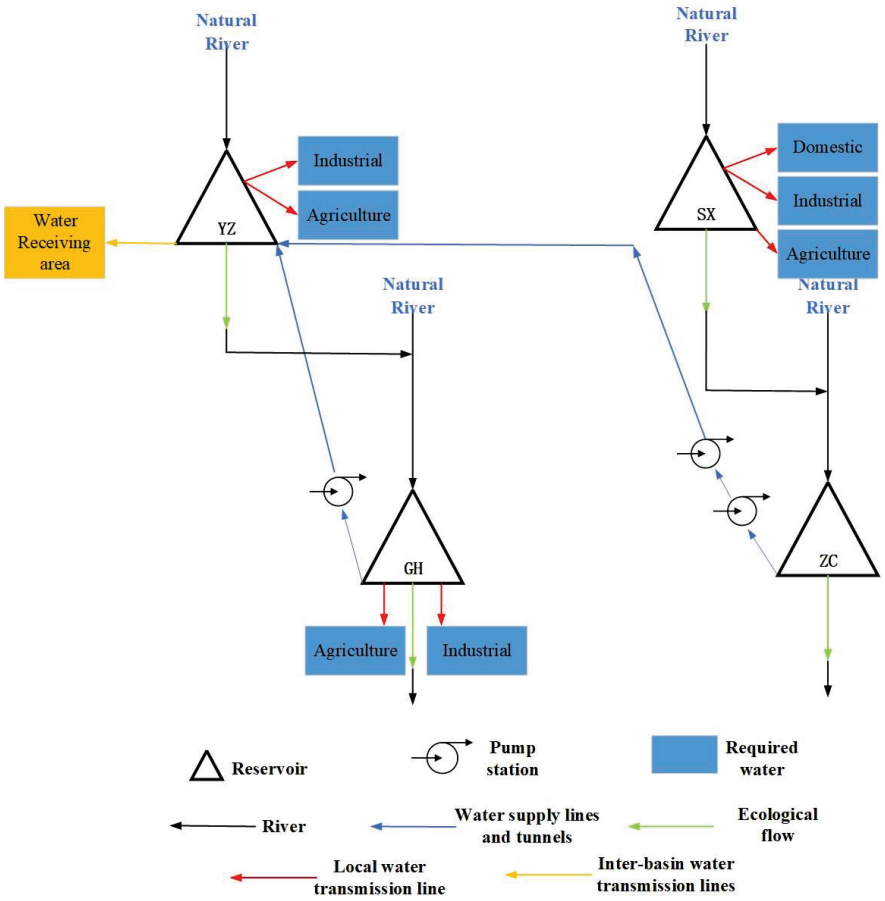

Figure 2. Hydraulic connection of the water supply reservoir group in the transfer area. YZ: Yunzhu reservoir; SX: Shixia reservoir; GH: Guanhe reservoir; ZC: Zecheng reservoir.

3. Methodology

It is widely acknowledged that the lower the reservoir water level, the greater the proportion of the dry land dredging volume and the higher the efficiency of dredging. However, lowering the water level can impact the reservoir's water supply function. Therefore, this study proposes the concept of sequential dry land dredging by emptying reservoirs in rounds. As shown in Figure 3, the process involves sequentially draining reservoirs with severe siltation for dry land dredging, with the water supply tasks during the draining period compensated by reservoirs hydraulically connected to the ones being dredged. This approach ensures efficient dry land dredging without compromising the water supply function of the reservoirs. Hydraulic connections can be categorized into natural and artificial types. Natural hydraulic connections involve the compensation of downstream reservoirs by upstream reservoirs. In contrast, artificial hydraulic connections are achieved by constructing pipes, tunnels, and channels to enable upstream reservoirs to compensate for downstream reservoirs. Additionally, pump stations and pipelines can be constructed to allow downstream reservoirs to compensate for upstream reservoirs.

However, the decision on the sequence for emptying the reservoir group with the lowest risk cannot be made directly. This is due to the following reasons: the water transfer company possesses its own constructed pipelines, tunnels, canals, valves, and pumping stations. However, the ownership of the reservoirs and water resources does not belong to the water transfer company. The company only holds the right to dispatch a portion of the water volume under the premise of reaching a consensus with each reservoir to ensure the supply of water resources to the receiving area. It should be clearly stipulated that the benefits generated from replacing dredging reservoirs with compensation reservoirs for water supply should accrue entirely to the management entity

of the compensation reservoirs, with water prices maintained at the original price, and the water transfer company shall not have a share. Additionally, the electricity costs incurred during the water compensation process when utilizing pumping stations should be borne by the water transfer company. Therefore, the water transfer company requires an optimal emptying sequence plan and a joint-dispatching scheme for reservoir groups to reduce its operational costs and ensure a stable water supply to the receiving area. Obviously, the initial phase of dredging is the most challenging period, characterized by a reduced number of reservoirs involved in water supply, the weakest capacity for water transfer, difficulties in profitability, the highest costs, and the greatest risks in compensation regulation. As more reservoirs complete dredging and the overall water supply capacity increases, the difficulty in profitability decreases, and the risks associated with compensation regulation also diminish. The ideal sequence for emptying and dredging should enhance profits at the initial stage of dredging while reducing compensation risks. However, the profitability at the early stage of dredging is related to water prices, transferred water volumes, and electricity costs. High-value water users have high requirements for reliability, which determines whether users will be willing to purchase water.

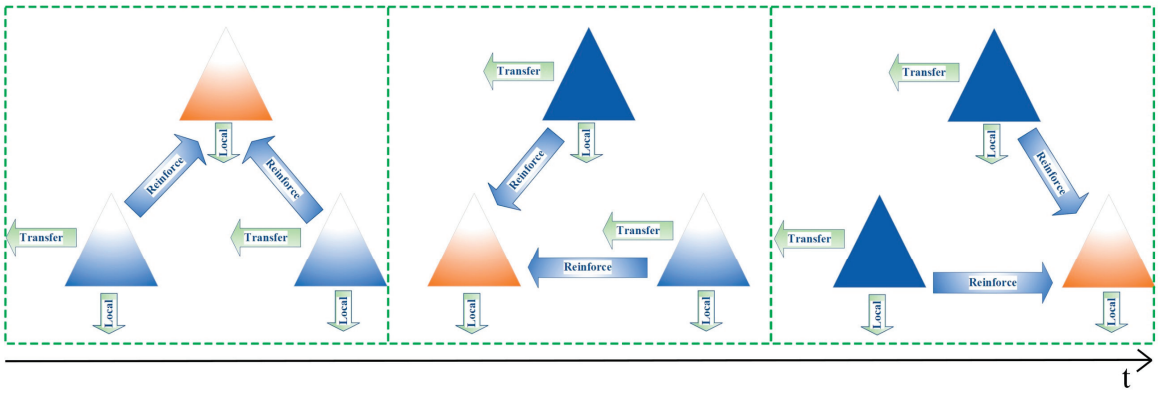

Figure 3. Schematic diagram of the water supply reservoir group for rounds of emptying and dredging.

Should the SX reservoir be the first to release water, its water supply responsibilities would solely fall on the ZC reservoir. However, during the initial period when the overall water supply capacity is at its lowest, the electricity costs incurred by the ZC reservoir to compensate for water supply through pumping stations appear relatively high compared to the profit from the water supply.

If the YZ reservoir is the first to be emptied, its water supply responsibilities can be jointly undertaken by SX, GH, or ZC reservoirs. Among these, both GH and ZC reservoirs require pumping stations, while the SX reservoir can flow naturally to the vicinity of the YZ reservoir through a tunnel. However, the storage capacity of the SX reservoir is relatively small, and the pressure of simultaneously supplying water to both the local area and the YZ reservoir is significant, resulting in a high risk of water supply disruption. Therefore, it is likely that the pumping stations of the ZC and GH reservoirs will need to be activated.

Should the GH reservoir be the first to release water, its supply duties can be jointly undertaken by SX, YZ, and ZC reservoirs. Utilizing the gravity-fed supply from YZ and SX reservoirs offers the lowest cost. However, if the inflow to YZ and SX reservoirs is insufficient to meet both local demand and the demand of the GH reservoir, water must be drawn from the ZC reservoir, necessitating a rational allocation between gravity-fed and pumped water.

Based on the above discussion, it may be most rational to discharge the GH reservoir first, as the support from the water volumes of the two reservoirs might render it unnecessary to activate the pump station at the ZC reservoir. Additionally, given that the GH reservoir has the largest storage capacity, initiating sediment removal can enhance the subsequent amount of water available for external transfer. From a profit perspective,

the most cost-effective approach is to first dredge reservoirs capable of gravity-fed water supply. However, in this case, the two reservoirs that can utilize gravity-fed water may not achieve a stable outflow for external water transfer, or the stable outflow may be minimal.

From the perspective of the social benefits of dredging, there should be no distinction between priority and delay in the dredging sequence. However, these arguments are merely qualitative and have not been simulated with typical inflow data and scheduling plans, lacking quantitative results for reference. Moreover, it is not rigorous to simply determine which reservoir to empty first based on cost-effectiveness and then directly decide to empty that reservoir first. The sequence of emptying and dredging silted reservoirs is a sequential decision-making process, and its merits need to be judged based on the water supply index performance and the trend of water supply index changes throughout the whole dredging period.

4. Optimization Dispatching Model of Emptying Dredging

4.1. Optimization Strategies and Decision Variables

The volume of soil is a primary factor in determining the duration of dredging projects; ascertaining the volume of dredging can roughly establish the project timeline. However, even with advance planning of the dredging volume and construction period, it is difficult to accurately predict the actual duration. The probability of occurrence of factors such as funding issues, weather conditions, epidemic outbreaks, and mechanical failures that lead to work stoppages, as well as additional risk mitigation and slope-rectification tasks that may be added during the reservoir dredging period is considered to be the same in this study. Therefore, different emptying sequences are not expected to impact the overall construction period.

Consequently, water supply indices can be calculated under the conditions of a typical dry year. However, due to the varying dredging durations of individual reservoirs, the results calculated over a single typical year are highly contingent. Extending the scheduling period would significantly increase the dimensionality of decision variables, thereby increasing the difficulty of finding a global optimal solution. This study ultimately selected a 3-year scheduling period with monthly scheduling intervals. Utilizing long-series inflow data for each reservoir, the P-III curve was employed to rank the total 3-year runoff volumes, resulting in the design of dry year groups for each reservoir. Finally, the total sum of squared deviations was minimized to select the typical dry year group for the transfer area [30].

This article does not consider shipping and power generation flows because reservoirs with shipping functions and significant power generation benefits are mostly located in regions abundant in water resources. These reservoirs are constructed to a high standard, with complete hub engineering, and most possess the capability to discharge sediment at low water levels, thus not requiring consideration under the background of this article. However, the impact on flood prevention during the emptying and desilting process is significant. In the event of rare heavy rainstorms, to ensure the flood discharge safety of downstream river channels, the emptied reservoirs will be refilled to store floodwaters and then emptied again after the flood season. This will inevitably reintroduce some sediment.

The outflow from the compensating reservoir group consists of three types of flows: external transfer, compensatory, and discharge (local water demand). Consequently, at least the end-of-period water level and two types of flows need to be considered as decision variables. However, due to the numerous constraints, random search algorithms prove inefficient when faced with the vast solution space and the potential fragmentation of the feasible domain by constraints. Therefore, this paper uses two-step optimization to reduce the dimensionality of the model, as shown in Figure 4.

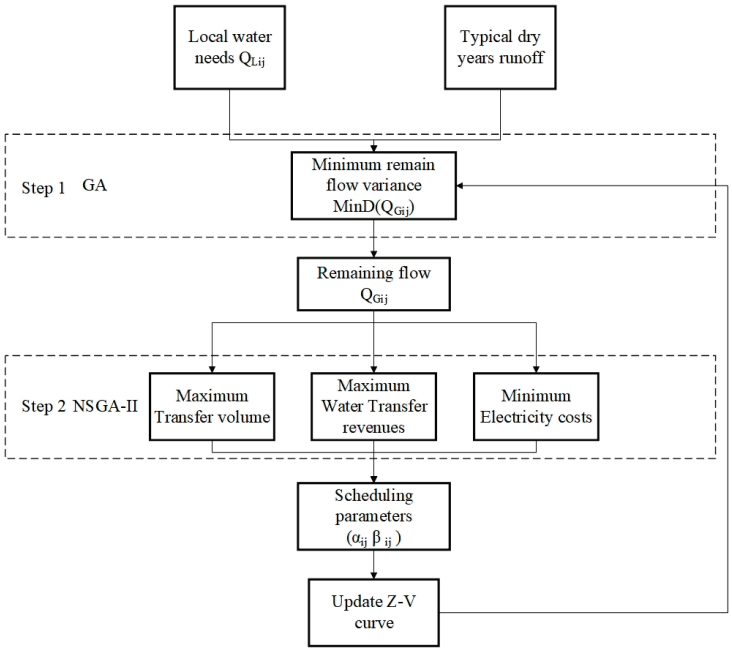

Figure 4. Optimization strategy.

The first step is taking the water level at the end of the period as the decision-making variable and optimizing each reservoir individually to minimize the variance of the remaining flow Q_{Gij}, subject to the constraint of meeting the local water demand. Here, Q_{Gij} represents the total of transferred and compensatory flows, resulting in the optimal remaining flow process that each reservoir can provide through individual regulation.

In the second layer, the optimal remaining flow of each reservoir serves as the upper limit, dividing the remaining flow into two parts: external transfer flow and compensatory flow. These are distinguished by the proportion coefficient α for external transfer flow and the utilization coefficient β for drawing water from different reservoirs, transforming the decision variables into the α, β values for each reservoir and time period. The values of α and β range from 0 to 1, undergoing multi-objective optimization.

4.2. Objective Function

The objective function of the second step involves three aspects: the total water supply, revenue, and cost. The revenue is calculated by multiplying the price of water by the total amount of water transferred. The water pricing for inter-basin water transfer projects should be determined under the coordination of the government, considering both the construction costs of the project and the local development context, ensuring that the water price fluctuates within a reasonable range. This approach aims to secure a certain profit for the inter-basin water transfer companies while reducing the water costs for users.

The study area suffers from widespread water scarcity and reservoir siltation, leading to a low water supply guarantee rate. This situation has dampened the enthusiasm of high-value water users to utilize transferred water while creating a conflict between the water fee payment capacity of agricultural users and the costs incurred by the water transfer company [31].

When a floating water price is employed to attract high-value water users, it is necessary to base the pricing on the supply effectiveness of the water transfer company. This approach draws on the broad and shallow damage principle, which evenly distributes water deficits across time periods [32].

This study defines floating water prices as follows: even when the total water supply is substantial, it cannot replace the groundwater sources in the water-receiving area. Assuming that water fees are settled at the end of the year if the water scarcity rate in the receiving area is more uniform, it indicates that the water supply trend aligns with the water usage

trend, signifying better water supply effectiveness. Thus, the corresponding water price should be increased. Conversely, if the variance of the water scarcity rate in the receiving area is larger, it indicates that the water supply trend does not meet the water usage trend, and the corresponding water price should be reduced [33]. In reducing electricity costs, drawing water from different reservoirs implies varying extraction costs, and to minimize these costs, it is essential to avoid using pump stations as much as possible.

In the first step, in addition to the reservoir that has been emptied, the local water supply tasks of each reservoir are independently undertaken, serving as constraints for individual reservoir optimization; in the second step, the water supply tasks assigned to the emptied reservoir are compensated by other reservoirs, acting as constraints for joint optimization.

The objective function for the single-objective optimization model for a single reservoir is as follows:

$$Q_{Gij}=Q_{Oij}-Q_{Lij} \tag{1}$$

$$\min F = \min D(Q_{Gij}) \tag{2}$$

where Q_{Gij} represents the remaining flow of the reservoir j during time period i, and Q_{Oij} and Q_{Lij} represent the outflow and local water demand flow of period i, respectively.

The objective function for the multi-objective optimization model of the reservoir group is as follows:

(1) Maximum external water transfer

$$\max F1 = \max \sum_{i=1}^{N}\sum_{j=1}^{M} \beta_{ij}\alpha_{ij}Q_{Gij} \tag{3}$$

where α_{ij} represents the proportion of remaining flow that reservoir j allocates for external transfer during period i; and β_{ij} represents the proportion of remaining flow that reservoir j utilizes during period i.

(2) Highest income

$$\max F2 = \max Pri \cdot \sum_{i=1}^{N}\sum_{j=1}^{M} \beta_{ij}\alpha_{ij}Q_{Gij} \tag{4}$$

$$Pri = 5 \cdot \left(\frac{1}{Var+1}\right) \tag{5}$$

$$Var = D\left(\frac{\beta_{ij}\alpha_{ij}Q_{Gij}-Q_{Ri}}{Q_{Ri}}\right) \tag{6}$$

where Pri represents the unit price of the water supply; Var represents the variance of water scarcity rate in the receiving area, where the smaller the variance of the water scarcity rate, the higher the unit price. The base water price is set at 5 CNY/m^3.

(3) Lowest electricity rates

$$\min F3=\min C \cdot 30.4 \cdot 24 \cdot \left(\sum_{h=1}^{K} P_h\right) \tag{7}$$

$$P_h=Q_{Gij} \cdot \beta_{ij} \tag{8}$$

where C represents the electricity price, P_h represents the total power consumption of pump station h over the entire scheduling period, and K represents the number of pump stations.

4.3. Constraints

(1) Water balance constraint

$$V_{ij} = V_{i+1j} + V_{Nij} - V_{Lij} - V_{Tij} - V_{Sij} - V_{Aij} - V_{Eij} \quad (9)$$

$$V_{Eij} = E_{ij} \times S_{ij} \quad (10)$$

where V_{ij} and V_{i+1j} represent the reservoir j capacities for time periods i and i + 1, respectively; V_{Nij} represents the inflow volume during time period i; V_{Lij} represents the local water supply volume during time period i; V_{Tij} represents the volume of water transferred from external sources at time period i; V_{Sij} represents the compensatory water volume at time period i; V_{Aij} represents the discharge of water abandoned during time period i; V_{Eij} represents the amount of water lost by way of evaporation at time period i of reservoir j; E_{ij} represents the water surface evaporation depth of reservoir j at time period i, derived from the design report of each reservoir; S_{ij} represents the average water surface area of the reservoir at time period i of reservoir j, which can be obtained by querying the water level–area curve, because the water level–area curve after dredging is difficult to estimate, so the same curve is adopted as before dredging.

(2) Water transport capacity constraints

$$0 \leq Q_{Tij} + Q_{Sij} \leq Q_{Uj} \quad (11)$$

where Q_{Tij} represents the transfer flow from reservoir j during time period i; Q_{Sij} represents the compensatory flow from reservoir j during time period i; and Q_{Uj} represents the maximum value of the tunnel and pumping station water conveyance capacity allocated to reservoir j by the inter-basin water transfer project.

(3) Water level operation constraints

$$X_{Lij} \leq X_{ij} \leq X_{Uij} \quad (12)$$

where X_{ij} represents the water level of reservoir j during time period i; X_{Lij} and X_{Uij} represent the permissible minimum and maximum water levels of reservoir j during time period i, respectively; the value of X_{Lij} is set at the dead storage level of each reservoir; and X_{Uij} is determined by the flood limit level during the flood season and the normal storage level during the non-flood season. These controls are applied irrespective of whether the reservoir has been dredged, adhering to the current characteristic water level regulations.

(4) Compensation for water supply constraints

$$Q_{Sij} = \beta_{ij}(1 - \alpha_{ij})Q_{Gij} \quad (13)$$

$$\sum_{j=1}^{M} Q_{Sij} \geq Q_{Li} \quad (14)$$

where Q_{Li} represents the water demand flow of the reservoir during emptying and dredging.

4.4. Initial Conditions

To maximize the assurance of water demand during consecutive dry years, it is advisable to commence the emptying construction of a specific reservoir when all reservoirs are fully stocked or at their highest water levels, typically after the flood season, which marks the peak water level within a year. In this study, the starting time is the beginning of October, the dispatch period is from the beginning of October of the first year to the end of September of the third year, and the starting water level is set at the normal storage level, which means that the compensation reservoir group should ensure that the reservoir group is full at the end of the flood season through accurate meteorological forecasting and scheduling during the flood season of the current year.

4.5. Solution Selection

Figure 5 shows the weighting process for sorting Pareto sets in this paper. The game theory-based approach that integrates subjective and objective weighting is employed [27], and the Pareto set obtained from the second-step optimization is scored and ranked. The subjective weighting employs triangular fuzzy numbers to represent the comparative judgments of the importance between pairwise indicators [34,35], forming a Fuzzy Analytic Hierarchy Process. If only the subjective weights are considered, the indicator with a more concentrated distribution of solutions may obtain larger weights, thereby increasing the probability of selecting the local optimal solution. Therefore, objective weighting utilizes a method based on the degree of interval separation, characterizing the degree of separation of the solution set under each indicator. Appendix B shows the method for converting indicator values into intervals. Finally, a comprehensive weighting method based on game theory is introduced [36], which seeks a balanced and consistent solution between the subjective and objective weights, minimizing the deviation between the final possible weights and the individual basic weights, thereby obtaining the final comprehensive weighting value. The specific formula for calculating the basic weights Γ, ζ, and the coefficient α_e of the base weight are shown in Appendix A.

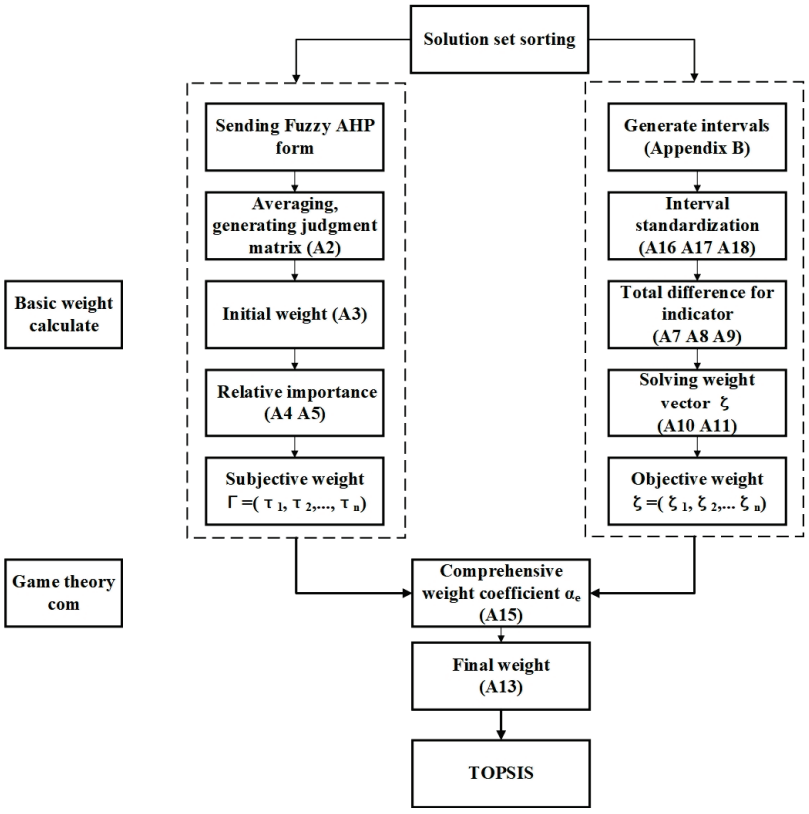

Figure 5. Flow chart of solution set sorting.

5. Results and Discussion

5.1. Typical Dry Year Group

The specific drought frequency was set at 95%, and the least squares approximation method was employed to calculate the typical dry year group for the watershed, yielding the hydrological years of 1991 to 1993. As Figure 6 shows, the inflow to the two reservoirs that rely on gravity-fed water supply was relatively small, whereas the inflow to the two reservoirs supplied by pumping stations was significantly larger.

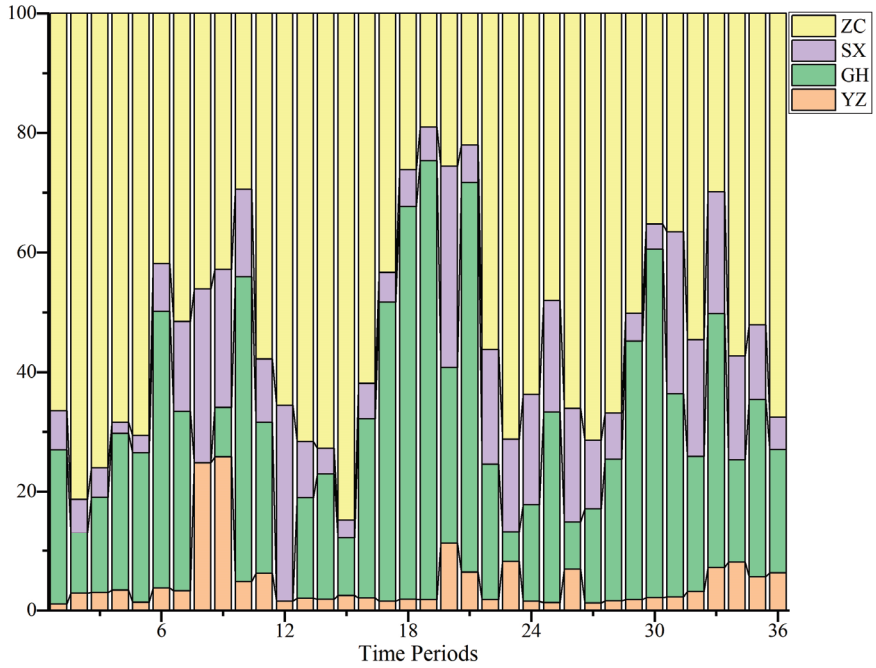

Figure 6. Percentage accumulation chart of each reservoir's runoff from 1991 to 1993. ZC: Zecheng Reservoir; SX: Shixia Reservoir; GH: Guanhe Reservoir; YZ: Yunzhu Reservoir.

5.2. The Volume of Sediment Removal and the Curve of Reservoir Capacity Post-Dredging

When the sedimentation in a reservoir becomes so severe that investment in dredging is deemed necessary, it is common to not fully restore the original storage capacity. Particularly, sedimentation below the dead storage level is often not considered for removal, not only due to the high costs associated with deep-water dredging but also because the legal status of the dead storage level renders the loss of dead storage capacity acceptable. Dredging operations in reservoirs typically focus on increasing the beneficial storage capacity, with the dredging elevation generally exceeding that of the intake structures. Additionally, a significant portion involves dry excavation of areas exposed in the middle to latter sections of the reservoir. The minimum operational water level during the dredging period determines the proportion of deep-water dredging to dry land excavation.

Among the three reservoirs studied in this paper, YZ is a lake-type reservoir with a large water surface area and relatively shallow depth, GH is a river-type reservoir with a small water surface area but greater depth, and SX is intermediate between the two. The design of the dredging scheme must ensure that the dredged material falls within the ultimate effective storage capacity and minimize the areas of ineffective dredging to reduce the amount of backfill [37].

Because the three reservoirs in this study were built many years ago, the original riverbed elevation data are missing, making it difficult to determine an accurate longitudinal river profile. Additionally, dredging entails significant investment, and during the design phase, it is crucial to consider cost issues comprehensively, not merely aiming for the highest dredging volume.

Table 1 presents the design schemes and internal reports on sediment accumulation and dredging volumes of completed and planned reservoir dredging projects collected in this study. Considering that there is competition between dredging volumes and costs in any reservoir, and this competition intensity is generally consistent across different regions and times, the schemes have already balanced dredging volumes and costs during design. Through statistical analysis of the proportion of dredging volumes to total sediment accumulation in these cases, the dredging volumes for the three reservoirs in this study were determined.

Table 1. Several design schemes for sediment removal projects.

Reservoir Name	Original 10^4 m^3	Type	Siltation 10^4 m^3	Clearance 10^4 m^3	Dredging Proportion
Caizhuang	2070	River	1260	300	23.8%
Fenhe	73,300	River	37,700	2000	5.3%
Suyahu		Lake	7710	9506	123.3%
Guanting	103,000	River	65,600	15,000	22.8%
Xiamizhuang	1144.8	River	229.4	147.1	64.1%
Wangyao	20,300	River	14,200	1650	11.6%
Linghe	3990	River	2065	350	16.9%
Shuangta	24,000	Lake	10,000	3006	30.6%

This study ultimately determined the dredging volume to be 25% of the total sediment accumulation, focusing on clearing the beneficial storage capacity to expand the reservoir capacity within the normal operational water level range. The post-dredging new storage capacity curve was obtained by superimposing an exponential function (water level–storage recovery) curve on the existing storage capacity curve. Figure 7 illustrates the water level–storage capacity curves before and after dredging. It should be emphasized that under the joint operation of reservoir groups, the dredging volume of each reservoir is a value that can be optimized, although the dredging volume is set to a uniform ratio in this study, which does not hinder the exploration of the change law of each index.

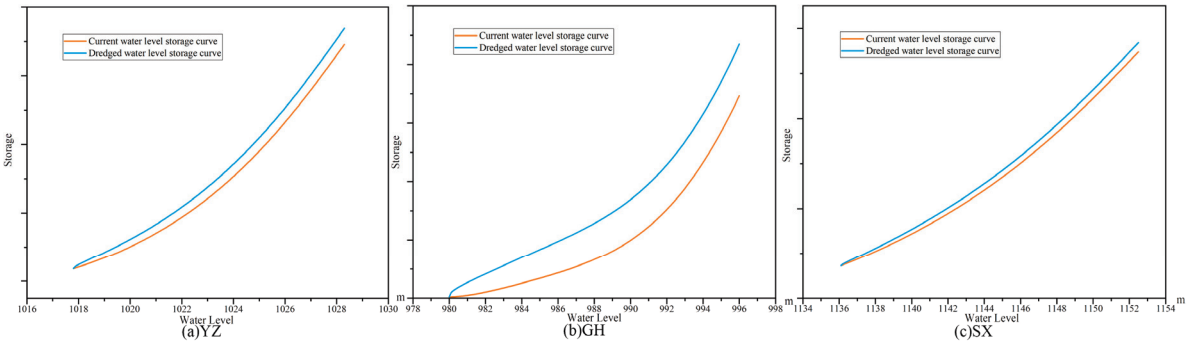

Figure 7. Z-V curve before and after dredging.

5.3. Optimization Results

Figure 8a,b, respectively, illustrate the optimization results of the first step and the optimization results of the second step in the first phase with the order GH-SX-YZ. Figure 9 shows the correlation relationships between each pair of objectives. The remaining flow after dredging in each reservoir has slightly increased. Under the conditions of the extremely dry year group, the remaining flow of YZ, SX, and GH reservoirs can be increased by 7.58%, 0.85%, and 5.4%, respectively, after dredging compared with before dredging; the competitive relationships between total water transfer volume, water transfer revenues, and power cost are quite evident.

The optimal solution is selected from the Pareto set obtained by the second-step optimization. Initially, the subjective weighting is conducted using the Fuzzy Analytic Hierarchy Process, where multiple experts are invited to score the importance levels of three objectives. Each scoring session provides the upper and lower bounds of relative importance as well as the median, forming a judgment matrix.

$$F_T = \begin{bmatrix} [1.00, 1.00, 1.00] & [0.43, 0.50, 1.00] & [0.43, 0.50, 0.90] \\ [1.00, 2.00, 2.40] & [1.00, 1.00, 1.00] & [0.80, 0.90, 1.00] \\ [1.20, 2.00, 2.40] & [1.00, 1.20, 1.40] & [1.00, 1.00, 1.00] \end{bmatrix} \quad (15)$$

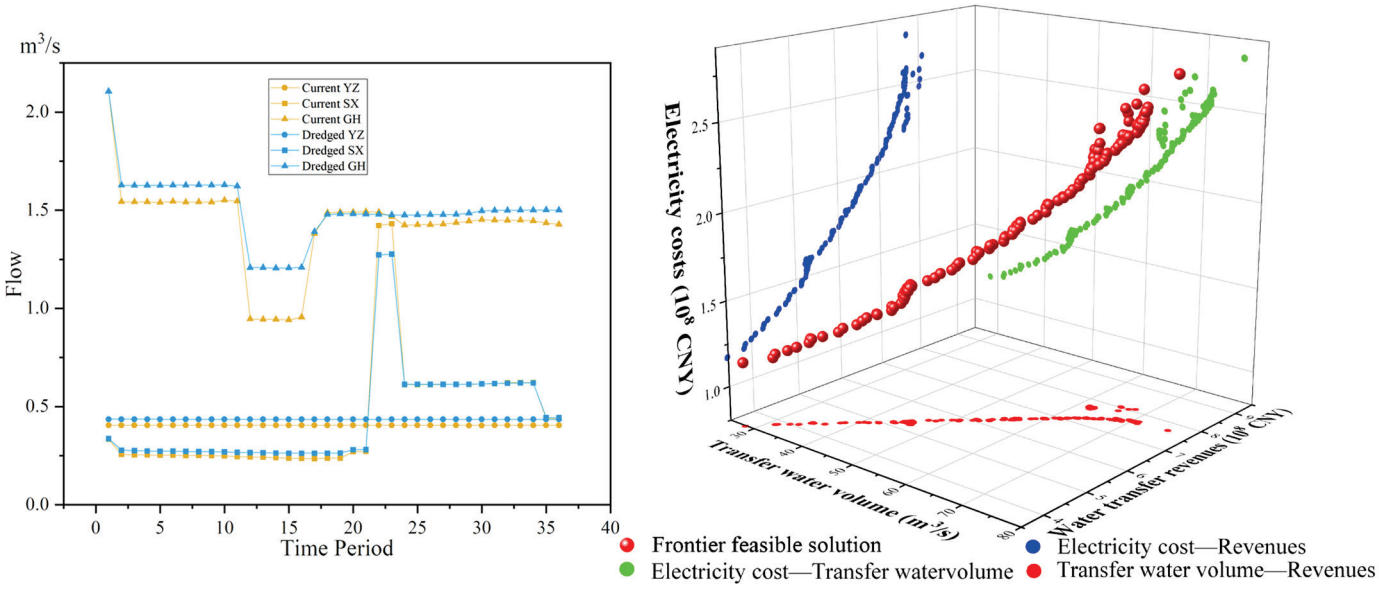

(**a**) (**b**)

Figure 8. (**a**) Optimal remaining flow of each reservoir; (**b**) Pareto frontier solution set of the first phase in the sequence GH-SX-YZ.

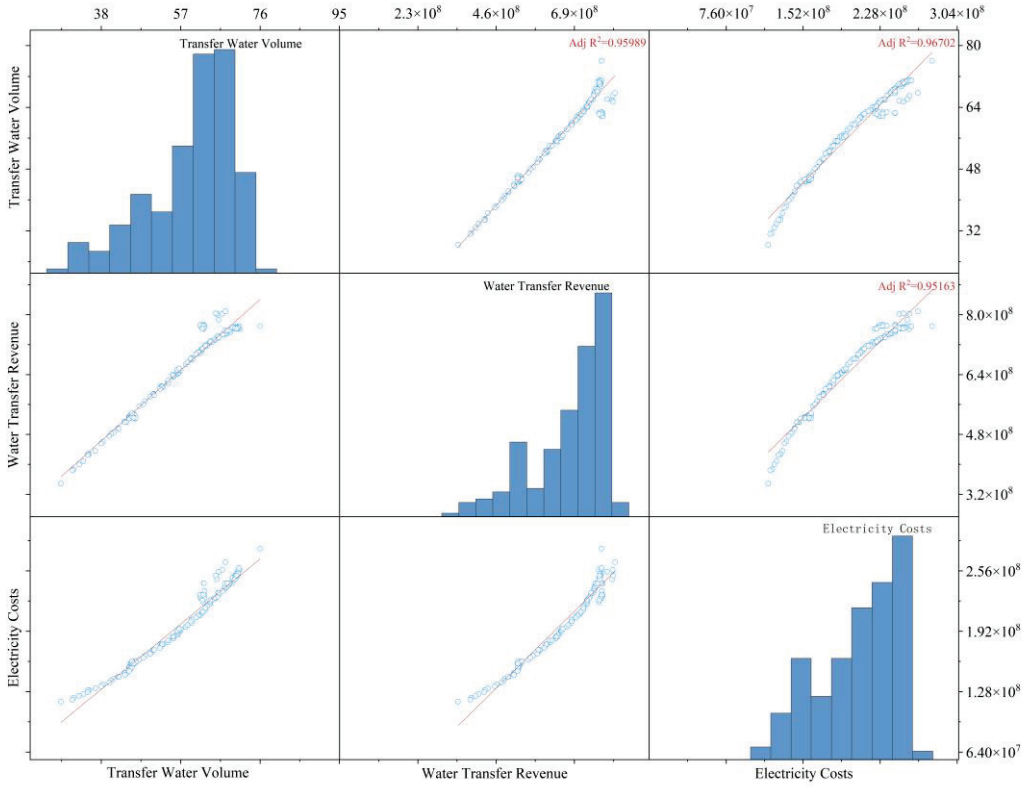

Figure 9. Matrix correlation diagram of the first phase in the sequence GH-SX-YZ.

The subjective weights obtained through the Fuzzy Analytic Hierarchy Process are as follows:

$$\Gamma = (0.58, 0.25, 0.17) \tag{16}$$

Based on the weights assigned by multiple experts, the water supply volume is deemed the most significant, followed by the income, with the costs considered the least important. The weights of income and costs are relatively close. This indicates that people

pay more attention to the total amount of water supplied during the dispatch period, which means that the receiving area is in a state of severe water shortage, and the benefits and costs of the water supply company will not be of concern for the time being.

Taking ±0.2% as the expansion range of the upper and lower bounds of the index fuzziness, the objective weight calculated based on the distancing degree of the interval number is (taking the order GH-SX-YZ as an example) as follows:

$$\xi = (0.317, 0.327, 0.356) \tag{17}$$

The comprehensive weight obtained by integrating subjective and objective weights based on game theory is as follows:

$$\omega = (0.556, 0.257, 0.187) \tag{18}$$

The solution set obtained based on the calculation of the separation degree of interval exhibits a relatively uniform distribution under the three objectives, with weights approaching each other. The result, after integrating both subjective and objective weights, remains predominantly influenced by subjective weights.

Based on the comprehensive weights obtained, the TOPSIS method is employed to score and rank the solution set [38], thereby identifying the optimal solution under each sequence.

As shown in Figure 10, the disparities in water prices are primarily evident during the period when the first two reservoirs are being emptied for dredging. Subsequently, the differences in water prices gradually diminish, indicating a decreasing variance in water scarcity rates in the receiving area. This trend suggests that water transfers stabilize as the reservoir dredging is completed. Regarding the trend of water price changes, societal development tends to gradually reduce water prices, while water users prefer lower average water prices. The difference between the water price and the end of the water price is calculated, and the more the water price is reduced, the more favorable the water price change trend is. Therefore, the ranking of various schemes based on the advantages and disadvantages of water price trends and average water prices is presented in Table 2.

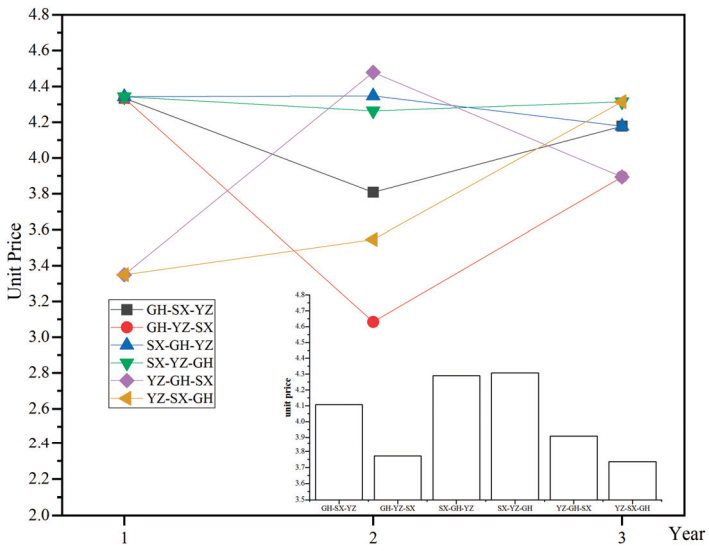

Figure 10. Transfer water unit price (CNY).

Figure 11b illustrates the transfer flow under various sequences. The trend of transfer flow is similar to that of the water demand process. Figure 11a shows the water supply satisfaction under different sequences. During the dredging period of the YZ reservoir, the water supply satisfaction maintained a high level across all orders. In contrast, the GH

reservoir experienced lower levels during its dredging period. This clearly demonstrates the decisive role of large reservoirs and abundant water rivers in determining water supply satisfaction.

Table 2. Scheme ranking.

	Unit Price	Unit Price Trend	Total Water Transfer	Total Power	Pumping Proportion Trend	Total Profit	Profit Trend
GH-SX-YZ	4	3	4	3	1	3	6
GH-YZ-SX	2	1	1	5	2	5	3
SX-GH-YZ	5	2	5	1	4	1	5
SX-YZ-GH	6	4	6	2	6	2	4
YZ-GH-SX	3	5	3	4	3	4	2
YZ-SX-GH	1	6	2	6	5	6	1

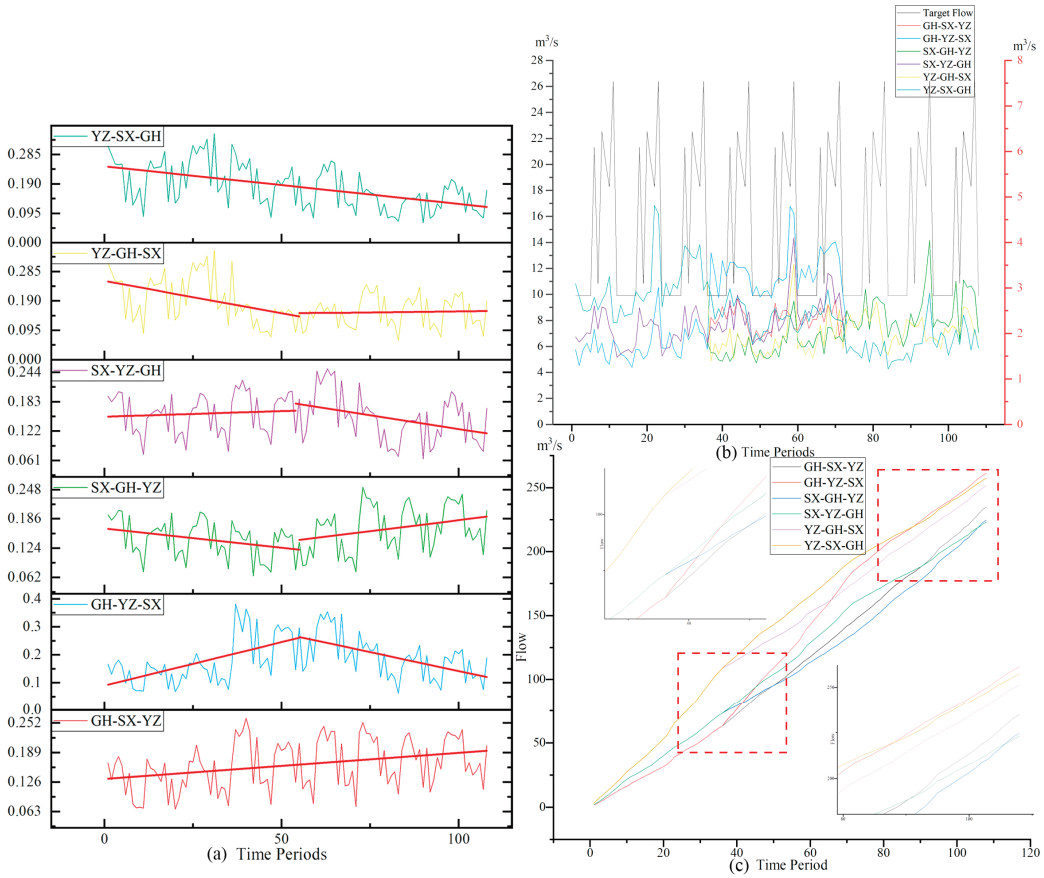

Figure 11. (**a**) Water supply satisfaction in receiving area; (**b**) water supply process in receiving area; (**c**) cumulative transfer volume.

Figure 11c illustrates the cumulative transfer flow diagrams under six sequences. (1) The two schemes that were the first to empty the GH reservoir grew the slowest in the first phase. After the first phase, the GH-YZ-SX gradually surpasses other schemes to become the one with the greatest water supply volume, attributable to the large reservoir capacity and abundant inflow of GH. (2) The GH-SX-YZ scheme, after the first phase, does not experience the rapid growth seen in the GH-YZ-SX scheme; instead, its growth accelerates starting from the third phase due to the natural inflow at the SX reservoir section being greater than that at the YZ reservoir. (3) The SX-YZ-GH scheme, after the first phase, accelerates its growth more rapidly than the SX-GH-YZ scheme because it first empties YZ

and, with a larger GH reservoir capacity, has a stronger capability for transfer flow. (4) The two schemes led by YZ emptying have a larger water transfer volume in the first phase, with stable growth rates in the second and third phases. This indicates that the overall increase in water supply caused by emptying SX first and emptying GH first is close. This is because the water from the GH reservoir is limited by the maximum flow rate of the pumping station, while the water from the SX reservoir is transported through a tunnel with a high upper limit, resulting in a similar actual water supply capacity between the two reservoirs. From the curve perspective, the total water supply of YZ-SX-GH is superior to that of YZ-GH-SX. The ranking based on the total water supply is shown in Table 2.

Figure 12 illustrates the cumulative power values of pump stations with different sequences. From the second stage to the conclusion, the ranking of cumulative power values among the various scenarios remains largely unchanged. The scheme with the lowest total power is SX-GH-YZ, while the scheme with the highest total power is YZ-SX-GH.

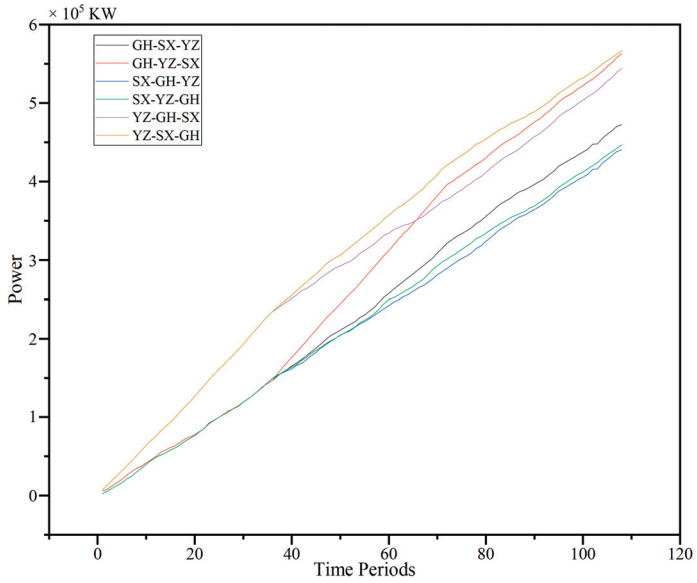

Figure 12. Cumulative power of pumping stations.

Empirically, the earlier the dredging of the gravity-fed water reservoir is completed, the lower the proportion of using pumping stations should be, and the total cumulative power would be lower compared to dredging the pumping station reservoir first. However, the calculation results show the opposite conclusion. This is because the objective function is not a fixed value that needs to be met, nor does this paper specify the total amount or process of water transfer; rather, it uses the water transfer volume and the variance of the water shortage rate as the evaluation criterion. In actual operation, the specified water transfer flow may lead to water abandonment, which should be avoided as much as possible in optimization scheduling. This also underscores the significance of quantitative analysis. The ranking according to the total power of each scheme is shown in Table 2.

Figure 13 illustrates the profit curves estimated with varying water prices and fixed electricity costs. It can be observed that the periods with higher profits across all sequences coincide with the periods when the YZ reservoir is emptied for dredging. This is due to the relatively small natural inflow of water to the YZ reservoir, which increases the overall instability of the water supply when it participates in the supply. Given the significant instability factors associated with transfers and compensations during the initial dredging phase, it is preferable for the water supply profit to exhibit a declining trend. If the reservoir is desilted in order of runoff from small to large, the overall water supply profit will show a downward trend. The ranking obtained based on the trend of water supply profits is presented in Table 2.

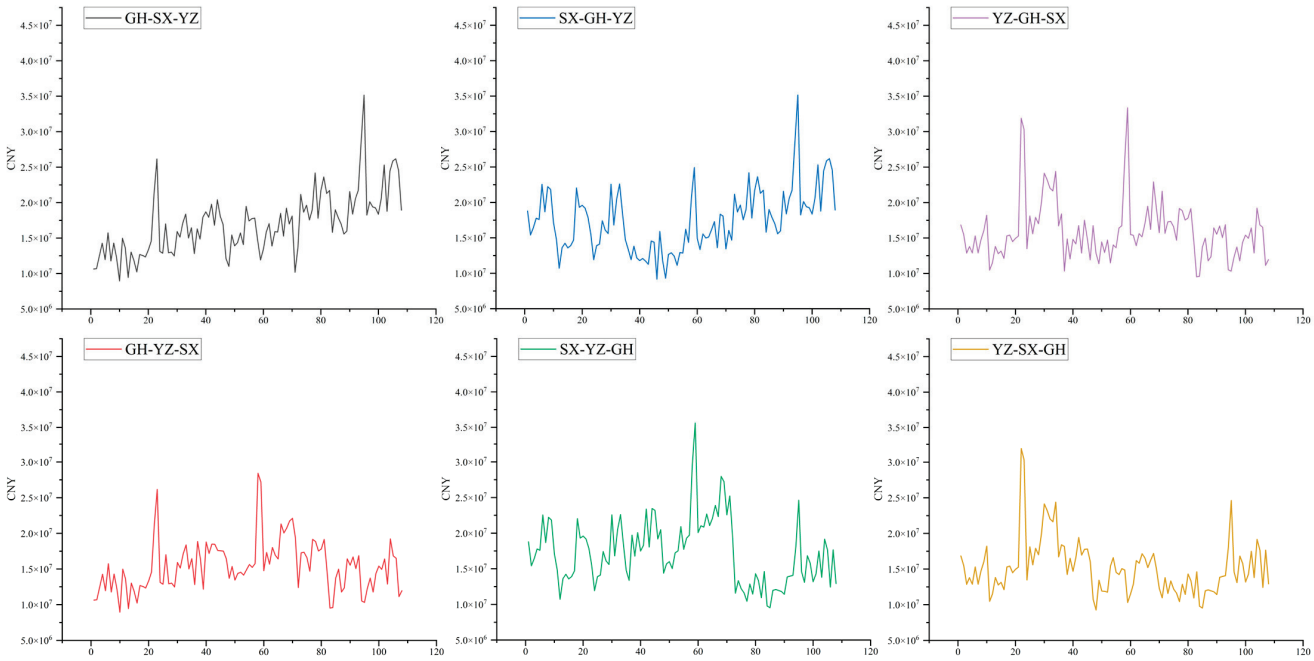

Figure 13. Profit curve.

Figure 14 illustrates the proportion of gravitational and pumping stations across various schemes. During the dredging periods of GH across various schemes, the proportion of water transfer by pumping stations has significantly decreased. The optimal sequence for emptying should aim to reduce the usage proportion of pumping stations in the early stages, indicating that the GH-SX-YZ sequence is the most favorable. In comparing the GH-SX-YZ and GH-YZ-SX schemes, it is evident that emptying in the order of reservoir inflow from largest to smallest facilitates a more pronounced trend of increasing the proportion of pump station usage.

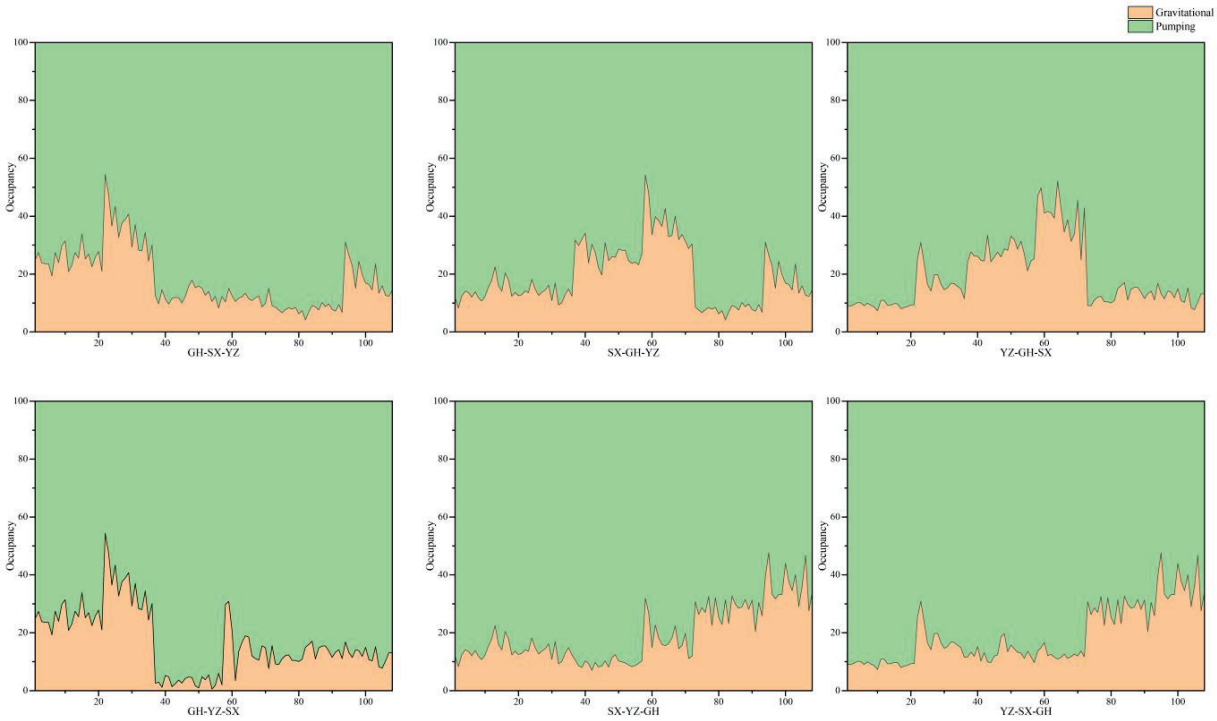

Figure 14. Ratio of gravitational water supply to pumped water supply.

Table 2 shows the metrics further extracted from the results of multi-objective optimization and ranks them based on the advantages and disadvantages of each scheme under these indicators. It can be seen that GH-YZ-SX and SX-GH-YZ are two schemes with more obvious characteristics. GH-YZ-SX is beneficial for water users to save water costs, and SX-GH-YZ is beneficial for water transfer companies to obtain more profits and save water transfer costs.

6. Conclusions

The issue of reservoir dredging has long plagued the water conservancy industry. With the implementation of the national water network strategy, new solutions to reservoir dredging have emerged. To explore the optimal sequence for emptying and dredging multiple reservoirs in rotation, this study established a two-step optimization scheduling model. Using a typical dry year group as the input, the optimal operation schemes under individual reservoir scheduling were solved. On this basis, the optimal schemes for joint reservoir group scheduling under different emptying sequences were solved and selected. Through comparative analysis of the water supply effects under various sequences, the following main conclusions were drawn:

1. Under the conditions of 25% dredging and extremely dry years, the remaining flow of YZ, SX, and GH reservoirs increased by 7.58%, 0.85%, and 5.4%, respectively;
2. As the dredging process nears completion, the water supply's stability gradually improves, reducing the variance of water scarcity rates. Consequently, the disparity in water prices diminishes accordingly;
3. The level of satisfaction with water supply and the variance of water shortage rates are determined by reservoirs with large runoff and substantial storage capacity, which decisively influence the profit value;
4. According to the descending order of the storage capacity of reservoirs, emptying and dredging the reservoirs can facilitate an increasing trend in the utilization ratio of pumping stations, thereby reducing the relative usage ratio of pumping stations in the initial phase;
5. Emptying and dredging the reservoir according to the order of the amount of water coming from the reservoir from small to large is more conducive to reducing the profit;
6. The optimization results, which aim to minimize the variance of water scarcity rates, contradict empirical judgments, underscoring the critical importance of quantitative analysis in the optimal scheduling of reservoir groups;
7. Reservoir managers and water transfer managers pay more attention to the total amount of water transferred, and the profits and costs of water transfer companies are not a concern for the time being.

This research offers a new idea for the dredging projects of reservoir groups, serving as a reference for reservoir dispatchers and dredging service industry professionals; however, there are areas for improvement in the present study, including the following: (1) The selection of a typical dry year group for the basin at a 95% guarantee rate was based on the method of minimizing the sum of squared deviations. However, inflow to some reservoirs in this group exceeds their own frequency discharge results. Therefore, it is necessary to continuously monitor new inflow data to select a more representative typical year group that aligns with the design guarantee rate. (2) Given the many feasible solutions, the optimal solution obtained through the weighting method is somewhat contingent, leading to contradictory conclusions when general patterns are analyzed. Future research should enhance the study of indicators for the optimization of scheduling schemes involving rounds of emptying and sediment removal. To clearly understand the impact of sediment removal in each reservoir on various indicators, it is advisable to select mutually independent indicators for evaluation. (3) Rounds of emptying and dredging are projects involving social stability and economic development, and there are still many vague indicators in the evaluation of the program that have not been considered in this paper. If these indicators are weighted according to Chang's method, some indicators with

a weight of 0 may be generated. Subsequently, the method of reference to [39] can be used to synthesize the relative importance calculation methods of Mikhailov [40] and Wang and Chin [41] and to use Mamdani's FIS method to rank the alternatives [42].

Author Contributions: Conceptualization, Methodology, Writing—original draft, Y.W.; Investigation, Writing—review and editing, X.Z.; Data curation, C.H. All authors have read and agreed to the published version of the manuscript.

Funding: This research received no external funding.

Data Availability Statement: The data presented in this study are available on request from the corresponding author.

Conflicts of Interest: The authors declare no conflicts of interest.

Appendix A

The steps of the multi-metric decision-making method are provided below [27].

Subjective weighting:

Since the relative importance of the different objectives is a vague concept, the invited experts were asked to give the upper bound, the median, and the lower levels of relative importance between the objectives. Assume the set of indicators $U=\{u_1, u_2, \cdots, u_n\}$. The relative importance given by the experts is in the following form:

$$F_{ij}=(l_{ij} \quad m_{ij} \quad u_{ij}) \tag{A1}$$

where F_{ij} represents the fuzzy trigonometric function of the importance comparison between the indicators u_i and u_j; i, j = 1,2,. . .n; l_{ij}, m_{ij}, and u_{ij} represent the upper, median, and lower bounds of the possible importance of the index u_i relative to u_j, respectively; and the 1~9 scale method in the traditional AHP method is used to represent the degree of importance, If the importance of u_i to u_j is λ, the importance of u_j to u_i is $1/\lambda$.

Judgment Matrix F:

$$F = \begin{bmatrix} F_{11} & \cdots & F_{1n} \\ \vdots & & \vdots \\ F_{n1} & \cdots & F_{nn} \end{bmatrix} \tag{A2}$$

The initial weights of each indicator are calculated as follows:

$$\gamma_i = \begin{pmatrix} l_{ij} & m_{ij} & u_{ij} \end{pmatrix} = \frac{\sum_{j=1}^{n} F_{ij}}{\sum_{i=1}^{n}\sum_{j=1}^{n} F_{ij}} \tag{A3}$$

where γ indicates the initial weight of the indicator u_i, and u_{ij}, m_{ij}, and l_{ij} represent the upper, median, and lower bounds of the initial weights of the indicator u_i, respectively.

The following formula is used to calculate the importance of each indicator relative to the others [35]:

$$\tau_i = V(\gamma \geq \gamma_1, \gamma_2, \cdots, \gamma_n) = \min V(\gamma \geq \gamma_i) \tag{A4}$$

$$V(\gamma_i \geq \gamma_j) = \begin{cases} 1 & m_i > m_j \\ \frac{l_j - u_j}{(m_i - u_i)-(m_j - l_j)} & m_i \leq m_j, u_i \geq l_j \\ 0 & \text{else} \end{cases} \tag{A5}$$

where τ_i indicates the importance of the indicator u_i relative to all other indicators; V is the general formula used for calculating the relative importance.

Finally, the subjective weights are obtained by means of normalization:

$$\Gamma = (\tau_1, \tau_2, \cdots, \tau_n) \tag{A6}$$

Objective Weight:

The indicator values are expressed in the form of intervals. Suppose the Pareto set is $S = \{s_1, s_2, \cdots s_z\}$. The objective weight vector to be solved is $\zeta = (\zeta_1, \zeta_2, \cdots, \zeta_n)$; then, the index value of the scheme s_i about u_j is expressed as an interval $(x_{ij,L}, x_{ij,U})$. The interval algorithm is used to standardize the benefit index and the cost index, and the value of the processed index is $[r_{ij,L}, r_{ij,U}]$, which is specifically used in the following interval operation.

Use the following formula to calculate the phase separation between each interval:

$$d(r_{ij}, r_{kj}) = \left\| r_{ij} - r_{kj} \right\|_2 = \sqrt{(r_{ij,L} - r_{kj,L})^2 + (r_{ij,U} - r_{kj,U})^2} \tag{A7}$$

The following formula is used to calculate the degree of difference between the decision scheme s_i and all other schemes for the indicator u_j:

$$D_{ij}(\zeta) = \sum_{k=1}^{z} d(r_{ij}, r_{kj}) \zeta_j \tag{A8}$$

Use the following formula to calculate the total difference between all decision schemes and other schemes for indicator u_j:

$$D_{ij}(\zeta) = \sum_{i=1}^{z} \sum_{k=1}^{z} d(r_{ij}, r_{kj}) \zeta_j \tag{A9}$$

where i, k = 1, 2, . . ., Z.

The selection of the weight vector ζ should make the total difference of all indicators to all decision schemes the maximum so as to make the distribution of solutions as uniform as possible. Then, solving ζ turns into a single-objective optimization problem as shown below:

$$\max D(\zeta) = \sum_{j=1}^{n} \sum_{i=1}^{z} \sum_{k=1}^{z} d(r_{ij}, r_{kj}) \zeta_j \tag{A10}$$

$$\text{s.t.} \begin{cases} \sum\limits_{j=1}^{n} \zeta_j^2 = 1 \\ \zeta_j \geq 0, j \in N \end{cases} \tag{A11}$$

The optimal objective weights of each index are obtained via normalization of the optimized ζ:

$$\zeta = (\zeta_1, \zeta_2, \cdots, \zeta_n) \tag{A12}$$

Comprehensive subjective and objective weights:

According to the comprehensive weighting method of game theory, the purpose is to find the most balanced solution among different weights so that the deviation between the final weight and each basic weight is minimal. That is, by optimization of the coefficients α in the following formula means that the deviation between ω and ω_l calculated via different methods is minimal, $\omega_1 = \Gamma, \omega_2 = \zeta$ in this study.

$$\omega = \sum_{e=1}^{2} \alpha_e \omega_e^T \tag{A13}$$

This can be translated into an optimization problem as shown below:

$$\min \left\| \sum_{e=1}^{2} \alpha_e \omega_e^T - \omega_e \right\|_2 \tag{A14}$$

According to the properties of the matrix, this problem can be converted into solving the following equations:

$$\begin{bmatrix} \omega_1\omega_1^T & \omega_1\omega_2^T \\ \omega_2\omega_1^T & \omega_2\omega_2^T \end{bmatrix} \begin{bmatrix} \alpha_1 \\ \alpha_2 \end{bmatrix} = \begin{bmatrix} \omega_1\omega_1^T \\ \omega_2\omega_2^T \end{bmatrix} \quad \text{(A15)}$$

After the equations are solved, ω is calculated using (A13), and the final weight can be obtained after normalization.

Appendix B

Assuming that the minimum value of the original index value is fmin, and its interval is (fmin-αfmin, fmin + αfmin), abbreviated as [$fmin_L$,$fmin_U$], the maximum value is fmax, and its interval is (fmax-αfmax, fmax + αfmax), abbreviated as [$fmax_L$, $fmax_U$], and α is the range of up and down fluctuations set artificially. The interval of the maximum minus minimum value is [$fmax_L$-$fmin_U$, $fmax_U$-$fmin_L$], denoted as [$Range_L$,$Range_U$]. Set the interval of an index value P as [P_L,P_U], and use the following formula to calculate the distance interval between P and the minimum value:

$$[P_{disL},P_{disU}]=[P_L-fmin_U,P_U-fmin_L] \quad \text{(A16)}$$

Use the following formulas to calculate the normalized value of P:

$$NormP_L=\min\left(\frac{P_{disL}}{Range_L},\frac{P_{disL}}{Range_U},\frac{P_{disU}}{Range_L},\frac{P_{disU}}{Range_U}\right) \quad \text{(A17)}$$

$$NormP_U=\max\left(\frac{P_{disL}}{Range_L},\frac{P_{disL}}{Range_U},\frac{P_{disU}}{Range_L},\frac{P_{disU}}{Range_U}\right) \quad \text{(A18)}$$

References

1. Randle, T.J.; Morris, G.L.; Tullos, D.D.; Weirich, F.H.; Kondolf, G.M.; Moriasi, D.N.; Annandale, G.W.; Fripp, J.; Minear, J.T.; Wegner, D.L. Sustaining United States reservoir storage capacity: Need for a new paradigm. *J. Hydrol.* **2021**, *602*, 126686. [CrossRef]
2. Perera, D.; Williams, S.; Smakhtin, V. Present and Future Losses of Storage in Large Reservoirs due to Sedimentation: A Country-Wise Global Assessment. *Sustainability* **2023**, *15*, 219. [CrossRef]
3. Xu, J.; Zhao, Y.; Chen, Y.; Du, P.; Qu, L. Hydrological Changes and Sediment Dynamics in the Inner Mongolia Section of the Yellow River: Implications for Reservoir Management. *Water* **2024**, *16*, 810. [CrossRef]
4. Foster, S.; Garduno, H.; Evans, R.; Olson, D.; Tian, Y.; Zhang, W.; Han, Z. Quaternary Aquifer of the North China Plain—Assessing and achieving groundwater resource sustainability. *Hydrogeol. J.* **2004**, *12*, 81–93. [CrossRef]
5. Bai, T.; Wei, J.; Chang, F.-J.; Yang, W.; Huang, Q. Optimize multi-objective transformation rules of water-sediment regulation for cascade reservoirs in the Upper Yellow River of China. *J. Hydrol.* **2019**, *577*, 123987. [CrossRef]
6. Jin, W.; Chang, J.; Wang, Y.; Bai, T. Long-term water-sediment multi-objectives regulation of cascade reservoirs: A case study in the Upper Yellow River, China. *J. Hydrol.* **2019**, *577*, 123978. [CrossRef]
7. Elzinga, L. Dredging of Reservoirs. Master Thesis, Delft University of Technology (TU Delft), Delft, The Netherlands, 2017.
8. Qiu, J.; Li, F.-F. Multiobjective Reservoir Optimization Considering Sedimentation Applied to the Three Gorges Reservoir. *J. Water Resour. Plan. Manag.* **2021**, *147*, 05021004. [CrossRef]
9. Ren, S.; Zhang, B.; Wang, W.-J.; Yuan, Y.; Guo, C. Sedimentation and its response to management strategies of the Three Gorges Reservoir, Yangtze River, China. *Catena* **2021**, *199*, 105096. [CrossRef]
10. Vercruijsse, P.; van Muijen, H.; Verichev, S. Dredging Technology for Deep Sea Mining Operations. In Proceedings of the Offshore Technology Conference, Houston, TX, USA, 2–5 May 2011. [CrossRef]
11. Ren, S.; Hu, X.-E.; Long, X.; Lü, C.-N.; Gao, Y. Aerodynamic Dredging Technology for Deep Water in front of Three Gorges Reservoir. *J. Yangtze River Sci. Res. Inst.* **2023**, *40*, 24–28. [CrossRef]
12. Qiwei, H. Study on preliminary operation of Xiaolangdi Reservoir and flow-sediment regulation of the Yellow River. *J. Sediment Res.* **2008**, *3*, 1–18. (In Chinese) [CrossRef]
13. Fan, J.; Qi, W.; Dai, Q. Investigation of density current plunging I: Review of previous flume experiment works and theoretical analysis. *J. Hydraul. Eng.* **2018**, *49*, 404–418. (In Chinese) [CrossRef]
14. Tang, X.; Tong, S.; Xu, G.; Huang, G.; Wang, T. Delayed response of sedimentation in the flood seasons to the pool level of the Three Gorges Reservoir. *Adv. Water Sci.* **2019**, *30*, 528–536. (In Chinese) [CrossRef]
15. Wu, W.; Zhou, X.; Wang, X.; Cheng, W. Research and application on water-sediment coordinative optimized dispatch of water-supply reservoir in the sediment-laden river. *J. Northwest AF Univ. Nat. Sci. Ed.* **2010**, *38*, 221–229. (In Chinese) [CrossRef]

16. Ha, Y.; Bai, T.; Huang, Q.; Jin, W. Transformation of multi-objectives inwater and sediment joint regulation of cascade reservoirs. *J. Hydroelectr. Eng.* **2017**, *36*, 23–33. (In Chinese) [CrossRef]
17. Li, J.; Li, H.; Wang, Y.; Jiang, E. Construction and application of a multi-objective collaborative model of water and sediment regulation in the Yellow River. *Adv. Water Sci.* **2023**, *34*, 708–718. (In Chinese) [CrossRef]
18. Zhao, H.; Ren, S.; Yan, J.; Zhang, C.; Liu, Z.; Gao, Y. The influence of flood resource utilization on sediment deposition in three Gorges Reservoir. *J. Lake Sci.* **2024**, *36*, 634–644. (In Chinese) [CrossRef]
19. Tang, D.; Weng, H.; Shen, J. Impact of Reamer Operation Parameters on Pollutant Dispersion in Reservoir Dredging. *Water Resour. Power* **2018**, *36*, 41–43+5. (In Chinese)
20. Yan, Z.; Jiang, S.; Li, K.; Wang, Y.; Li, T.; Li, X. Study on Sediment Dredging Experiment of Plain Reservoir. *Yellow River* **2019**, *41*, 14–17. (In Chinese)
21. Wang, X.; Gong, L.; Wu, W.; Tang, Y. Reservoir operation patterns of water-supply reservoir in sediment-laden river: A case study on the Wangyao Reservior. *J. Sediment Res.* **2018**, *43*, 33–39. (In Chinese) [CrossRef]
22. Yang, L.; Wang, X.H.; Hou, J.M.; Liu, J.L.; Chai, J.; Tong, Y.; Wang, T.; Li, D.L. Research on water and sediment regulation of reservoir with high sediment content under reverse regulation reservoir: Case of Tingkou Reservoir. *J. Basic Sci. Eng.* **2022**, *30*, 530–540. (In Chinese) [CrossRef]
23. Wang, H.-W.; Kondolf, M.; Tullos, D.; Kuo, W.-C. Sediment Management in Taiwan's Reservoirs and Barriers to Implementation. *Water* **2018**, *10*, 1034. [CrossRef]
24. Kawashima, S. Conserving reservoir water storage: An economic appraisal. *Water Resour. Res.* **2007**, *43*. [CrossRef]
25. Smith, C.; Williams, J.; Nejadhashemi, A.P.; Woznicki, S.; Leatherman, J. Cropland management versus dredging: An economic analysis of reservoir sediment management. *Lake Reserv. Manag.* **2013**, *29*, 151–164. [CrossRef]
26. Bagarani, M.; De Vincenzo, A.; Ievoli, C.; Molino, B. The Reuse of Sediments Dredged from Artificial Reservoirs for Beach Nourishment: Technical and Economic Feasibility. *Sustainability* **2020**, *12*, 6820. [CrossRef]
27. Dong, Z.C.; Chen, M.F.; Ni, X.K.; Yao, H.; Jia, W.; Yang, G. Decision method of optimal operation of reservoir group considering fuzzy interval. *J. Hohai Univ. Nat. Sci.* **2021**, *49*, 233–240. (In Chinese) [CrossRef]
28. Hilgert, S.; Sotiri, K.; Fuchs, S. Review of methods of sediment detection in reservoirs. *Int. J. Sediment Res.* **2024**, *39*, 28–43. [CrossRef]
29. Hu, K.; Ailihazi, W.; Danierhan, S. Ecological Base Flow Characteristics of Typical Rivers on the North Slope of Kunlun Mountains under Climate Change. *Atmosphere* **2023**, *14*, 842. [CrossRef]
30. Tang, D. Optimization of typical hydrologic years and typical series of the yellow river basin. *J. Hehai Univ.* **1994**, *22*, 15–19. (In Chinese)
31. Zhang, C.-Y.; Oki, T. Water pricing reform for sustainable water resources management in China's agricultural sector. *Agric. Water Manag.* **2023**, *275*, 108045. [CrossRef]
32. Wei, R.; Yan, Z.; Zhou, Z.; Jiang, Y.; Wang, K. Optimal method of reservoir drought-limited water level based on principle of wide and shallow damage. *Water Resour. Prot.* **2023**, *39*, 152–158, 166. (In Chinese)
33. Chen, Z.; Wang, H.; Qi, X. Pricing and Water Resource Allocation Scheme for the South-to-North Water Diversion Project in China. *Water Resour. Manag.* **2013**, *27*, 1457–1472. [CrossRef]
34. Huang, Z.; Luo, J. Possibility Degree Relation Model for Decision Making Objects with Multiple Criteria Values as Triangular Fuzzy Number. *Control Decis.* **2018**, *33*, 1931–1940. (In Chinese) [CrossRef]
35. Chang, D.-Y. Applications of the extent analysis method on fuzzy AHP. *Eur. J. Oper. Res.* **1996**, *95*, 649–655. [CrossRef]
36. Liu, B.; Huang, J.J.; McBean, E.; Li, Y. Risk assessment of hybrid rain harvesting system and other small drinking water supply systems by game theory and fuzzy logic modeling. *Sci. Total Environ.* **2020**, *708*, 134436. [CrossRef] [PubMed]
37. Yang, L.; Zhao, W.; Zhang, X. Research on Desilting Scheme for Large and Medium-Sized Reservoirs in the Loess Plateau Area. *Shaanxi Water Resour.* **2023**, *12*, 110–113+119. (In Chinese) [CrossRef]
38. García-Cascales, M.S.; Lamata, M.T. On rank reversal and TOPSIS method. *Math. Comput. Model.* **2012**, *56*, 123–132. [CrossRef]
39. Papadopoulos, C.; Spiliotis, M.; Pliakas, F.; Gkiougkis, I.; Kazakis, N.; Papadopoulos, B. Hybrid Fuzzy Multi-Criteria Analysis for Selecting Discrete Preferable Groundwater Recharge Sites. *Water* **2022**, *14*, 107. [CrossRef]
40. Mikhailov, L. Deriving priorities from fuzzy pairwise comparison judgements. *Fuzzy Sets Syst.* **2003**, *134*, 365–385. [CrossRef]
41. Wang, Y.-M.; Chin, K.-S. Fuzzy analytic hierarchy process: A logarithmic fuzzy preference programming methodology. *Int. J. Approx. Reason.* **2011**, *52*, 541–553. [CrossRef]
42. Mamdani, E.H.; Assilian, S. An Experiment in Linguistic Synthesis with a Fuzzy Logic Controller. *Int. J. Mach. Stud.* **1975**, *7*, 1–13. [CrossRef]

water

MDPI

Article

Innovative Adaptive Multiscale 3D Simulation Platform for the Yellow River Using Sphere Geodesic Octree Grid Techniques

Bingxuan Li , Jinxin Wang *, Yan Zhang and Yongkang Sun

School of Geoscience & Technology, Zhengzhou University, Zhengzhou 450001, China; alinww@126.com (B.L.); zy15565509353@gs.zzu.edu.cn (Y.Z.); sunykyx@163.com (Y.S.)
* Correspondence: jxwang@zzu.edu.cn

Abstract: Earth system simulation technology is fundamental for ecological protection and high-quality development in the Yellow River Basin. To address the lack of a Yellow River simulation platform, this study proposes an adaptive multiscale true 3D crust simulation platform using the Sphere Geodesic Octree Grid (SGOG). Twelve models in four categories were designed: single fine-scale models, geomorphic zone-based models, and models using both top-down and bottom-up approaches. The models were evaluated based on terrain feature representation and computational efficiency. The results show that single fine-scale models preserve detailed terrain features but are computationally intensive. They are suitable for the precise simulation of surface processes. Top-down and bottom-up models balance terrain detail and efficiency, and are thereby widely applicable. Geomorphic zone-based models provide detailed focal area representation and higher computational efficiency, being more targeted. Various methods offer flexible scale transformations, each with its own strengths, allowing researchers to select a method according to practical application needs. Consequently, this research demonstrates that spherical discrete grids offer reliable support for constructing basin simulation platforms, providing new technological and scientific insights for the Yellow River Basin's ecological protection and development.

Keywords: global discrete grid; Sphere Geodesic Octree Grid; true 3D geographic scene; adaptive multiscale; Yellow River Basin

1. Introduction

The Yellow River, known as the mother river of the Chinese nation, represents the history of Chinese development [1]. The evolution of the ideas and wisdom of flood control and river management in China can be traced back to evasion, embankment filling, dredging, diversion, embankment reinforcement, coordination, harmony, and protection and development [1]. With the advancement of flood control technologies, from manual labor, animal power, machinery, and electricity to computers, concepts such as the real Yellow River, model Yellow River, digital Yellow River [2], and Yellow River simulators [3] have emerged. Flood control technologies have propelled and guided the scientific and technological development in China. Thus, the philosophy of flood control profoundly influences national governance. Water control is akin to state governance, and the advanced water management civilization of the Chinese nation to a certain extent determines the path to the country's prosperity, comprehensive national strength, and global standing [4].

The watershed simulator represents a new conceptual framework and a significant undertaking in digital water management in the context of contemporary spatial big data and information technology. The Yellow River simulator, designed specifically for the Yellow River Basin, focuses on the Yellow River Basin and serves as an integrated watershed simulation system, with scientific apparatus developed and deployed throughout the basin. It revolves around the natural and social water cycles within the basin, with a focus on addressing key issues related to the Yellow River by coupling multiple systems, coordinating

multiple actors/parties, achieving multiple functionalities, simulating multiple processes, and ensuring integration [3]. The Yellow River simulator enables a comprehensive process simulation of various natural and human factors within the basin, as well as their coupled interactions. It particularly focuses on addressing distinctive Yellow River issues, such as soil erosion, sediment deposition, ecological vulnerability, limited development quality, and social governance capacity [3]. Simulating watershed-scale geographical processes represents the core task of the simulator, with the coupling of temporal and spatial scales being a key and challenging scientific problem [5]. From a conceptual standpoint, watershed simulation can be divided into comprehensive simulation (simulating the response of a watershed system to geographic variable changes) and scenario analysis (analyzing and evaluating the economic and ecological effects of various element combinations, thereby facilitating decision-making in management) [6]. Both the simulations and analyses require a simulation platform as a foundation. In summary, the simulation platform serves as the catalyst, key, and core of the watershed simulator, and all the work of the simulator revolves around the simulation platform.

Watershed simulation belongs to the domain of Earth system simulation, which is an application of Earth simulation at the watershed scale [5]. The Earth's system encompasses various spheres, including the near-Earth space, atmosphere, oceans, land surface, biosphere, and solid Earth (including the lithosphere, mantle, and core). Mathematical equations have been established based on the physical, chemical, and biological processes within these spheres, and large-scale comprehensive computational programs, known as Earth system models, have been developed to solve these equations using numerical methods [7]. Earth system models are among the most complex and comprehensive scientific numerical simulation tools. Their advancement reflects a country's core competitiveness in Earth systems' science research, and serves as an important indicator for assessing the country's overall level of Earth science research and comprehensive national strength [8]. Internationally, the United States, United Kingdom, Germany, Japan, and France hold leading positions in Earth system model development and simulation research. Examples include the Community Earth System Model (CESM) in the United States (National Center for Atmospheric Research, Boulder, CO, USA), the European Network for Earth System Modeling (ENES) (EUDAT Ltd, Keilaranta, Finland), and the Frontiers Research System for Global Change (FRSGC) in Japan (Japan Agency for Marine-Earth Science and Technology (JAMSTEC), Yokohama, Japan) [7]. China's Earth System model, CAS-ESM2.0 (Chinese Academy of Sciences (CAS), Beijing, China), is at an advanced global level [8]. Three fundamental elements constitute the basic models of Earth system simulation: System Dynamics (SD) models, Cellular Automata (CA) models, and Agent-Based (AB) models. Each has its own characteristics and complementary nature, allowing for organic integration into the basic model of Earth system simulations, with CA being an essential component [9]. The spherical grid model used in this study is a type of CA model.

The Earth Tessellation Grid (ETG) belongs to the traditional research field of Earth system science. An ETG is a spherical (ellipsoidal) grid that can be subdivided infinitely without changing its shape, providing a fitting mesh for the Earth [10]. Recently, the study of grids for digital earth platforms has emerged as a new research field. It emphasizes the establishment of a unified and rigorous global positioning reference system, the fusion and integration of multi-source and heterogeneous spatial data and related thematic data, the construction and analysis of three-dimensional virtual geographic environments, and the simulation and inference of various geographical spatial processes. There are two types of grids used in digital Earth platforms: two-dimensional spherical surface grids (DGGs, Discrete Global Grids) and three-dimensional spherical grids (ESSG). Nearly 20 DGG schemes [11] are used for organizing surface spatial data. This study mainly involves three-dimensional spherical grids. The main achievements in this field include three types: Spheroid Degenerated Octree Grid (SDOG) [12], Sphere Geodesic Octree Grid (SGOG) [13,14], and Sphere Shell Space Grid (S3G) [15], all proposed by Chinese scholars. SDOG and S3G belong to the Latitude–Longitude Hexahedral Grids, while

SGOG belongs to the Geodesic Tetrahedron Grid, which have certain advantages in a true three-dimensional modeling of geographic space, especially in the true three-dimensional modeling of the Earth's crust, and SGOG grids can be directly extended to ellipsoids. Therefore, in this study, the SGOG grid was selected as the basic model for watershed crustal modeling. It should be noted that the computational grids (vectors) of Earth system models and the grids (rasters) of digital Earth platforms do not fundamentally differ. The organic integration of the two can be achieved [16–18]. In recent years, despite strong interest in research and commercial applications of Discrete Global Grid Systems (DGGS), participation from the GIS scientific community has remained focused on relatively narrow topics, such as grid specifications and refinement improvements [19]. Recent advancements include: theoretical developments in multi-resolution encoding for hexagonal discrete grids [20,21]; the optimization and extension of grid subdivision and encoding methods [22–27]; the analysis of grid metrics and their applications [28,29]; reviews and challenges in DGGS research [19,30]; spatial analysis [31,32]; coastal environment and maritime applications [33,34]; terrain analysis [35,36]. See Table 1.

Table 1. Characteristics of different types of grids.

Grid Type	Representative References	Advantages	Disadvantages	Application
Triangle	Alborzi and Semmet, 2000 [37]; Bartholdi, 2001 [38]; Baumgarder, 1985 [39]; Dutton, 1984 [40], 1999 [41]; Fekete and Treinish, 1990 [42]; Goodchild and Yang, 1992 [43]; Song, 2002 [44]; White, 1998 [45]	Can be combined into arbitrary polygons; completely cover spherical surfaces; easy for texture mapping; effectively fits curved surfaces; addresses convergence issues at poles; preservation of similarity, edge length, and area equality.	Non-uniformly adjacent units; not unique directions; do not align with traditional square conventions and output devices.	Modeling and visualization of large-scale geographic spatial data
Quadrilateral	Sahr, 2003 [46]; White 2000 [47]; Bjørke, 2003 [48]; Gibb, 2016 [49]	Simpler geometric structures; consistent directional, radial symmetry, and translational congruence properties; can directly leverage many algorithms based on plane quadtrees; well-matched with traditional output devices.	Non-uniform adjacency; inability to cover the entire globe; inability to directly generate spherical grids; significant distortion or degeneration of units in high-latitude regions.	Storage and management of spatiotemporal big data
Hexagon	Heikes, 1995 [50]; Sadourny, 1968 [51]; Sahr, 2003 [46]; Thuburn, 1997 [52]; Peterson, 2006 [53]; Vince, 2006 [54]; Jin Ben, 2018 [20]	The most regular structure, highest plane coverage and angular resolution; consistent topology; topological distance closely matches Euclidean linear distance; highest spatial sampling rate;	Cannot fully cover the spherical surface; faces challenges in encoding efficiency of grid cells and compatibility with constructing multi-resolution data models.	Certain advantages in dynamic modeling and Earth system model computations

The Earth's surface serves as the interface between the atmosphere and lithosphere, and is the focal area for various geographical phenomena and processes. Geomorphology is pivotal to Earth's surface science and tightly integrates disciplines such as human dynamics, biology, biogeochemistry, geochemistry, geology, hydrology, geomorphology, and atmospheric dynamics [55]. Information regarding the topography of the Earth is a critical parameter for nearly all Earth science analyses, precise land use, and planning [56]. Understanding surface processes relies on modern digital terrain representation [57], and contemporary ground, aerial, and space remote sensing technologies have enabled the detailed geographic analyses of large regions, or even globally [58].

In the field of global discrete grids, there exists a predominance of theoretical research over applied studies. Issues in digital watershed three-dimensional spatial modeling and geographical process simulation include traditional watershed 2.5D spatial modeling, which prioritizes surface over subsurface, focusing mostly on surface geographical pro-

cesses, thereby posing challenges in simulating and analyzing sub-surface spatial processes and phenomena within watersheds. Moreover, existing three-dimensional simulation platforms are segmented and disconnected, failing to integrate surface, near-surface, and subsurface spaces into unified modeling. Traditional geographical simulation methods often operate at fixed scales, aiming primarily for single-scale simulations, with intricate complexities in scale integration and variation. From the perspective of river simulators, macro-level framework studies predominate, with limited attention to specific technical mechanisms. Spherical grid partitioning effectively addresses scale issues. Its recursive subdivision mechanism facilitates the construction of models at single scales and hybrid multi-level scales, thus enabling the flexible and on-demand simulation of watershed geographical processes.

In summary, this study focuses on the construction of a true three-dimensional computational platform for the Yellow River Simulator based on SGOG grids, globally shared Digital Elevation Model (DEM) data and watershed terrain and landform data. It tackles key technical challenges in building a spherical grid multi-scale model and dynamic simulation computing technology for watershed geographical processes. The study verifies these technologies through experiments, particularly in simulating groundwater point source pollution diffusion, aiming to provide essential technical support and foundations for constructing the Yellow River Simulator.

2. Technical Foundations of True 3D Yellow River Simulation Platform Construction

2.1. SGOG Subdivision Theory

The Earth Tessellation Grid fundamentally treats the Earth system as a regular geometric fluid, recursively dividing the flow surface or fluid into quasi-uniform segments, organically encoding (indexing) and organizing them to simulate Earth phenomena and processes. Each grid consists of grid points, edges, centers, and elements (surface and volume elements). The SGOG adopts a method of large circular arc median QTM octree division (spherical quadtree and radial binary tree), where the spherical quadtree can utilize any existing QTM encoding scheme (this study uses directional encoding), and the radial aspect employs binary tree encoding (Figure 1). The SGOG grid (tile) system was relatively evenly distributed, and symmetric with respect to the center of the sphere, exhibiting simple regularity and consistent topological relationships. The intralayer deformation is minimal, whereas the radial deformation is significant [13,14]. Matching the grid points of the Earth's surface with the basin's DEM elevation through interpolation (this study employs the nearest neighbor method), and subsequently connecting the grid edges, can express the basin's landform. Introducing basin geological strata data (assumed data in this study) and matching them with the underground grid can convey information related to the basin's underground geological strata, thereby establishing a truly three-dimensional crustal simulation platform for the Yellow River Basin.

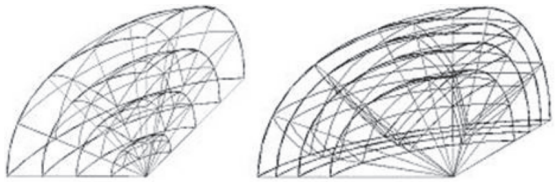

Figure 1. Spherical Quadtree (QTM) Grid.

2.2. Study Area and Source Data

The Yellow River originates from the northern foot of the Bayan Har Mountains on the Qinghai–Tibet Plateau, has a total length of approximately 5464 km, and flows through more than 370 counties in nine provinces before emptying into the Bohai Sea. The basin covers an area of 795,000 square kilometers, making it the fifth-longest river in the world and the second-longest river in China. It is considered one of the most difficult rivers to manage globally. The Yellow River Basin traverses three major terraces spanning vast distances,

with numerous mountain ranges and significant east–west elevation differences, leading to marked variations in landforms. Sediment deposition poses a prominent challenge, exacerbating the sharp conflict between human activities and water resources within fragile ecological environments. Historically, the Yellow River has served as the cradle of Chinese civilization, representing a hub for political, economic, and cultural activities. However, the overall socioeconomic development of the region lags behind the national average in today's comprehensive societal and economic context.

Considering the computational and storage capabilities of a single machine, the modeling is based on the SGOG 9th, 10th, 11th, and 12th level subdivision tiles (corresponding to approximate grid surface edge lengths of 19.49 km, 9.75 km, 4.87 km, and 2.44 km, respectively). DEM data covering the Yellow River basin area were downloaded from the shared website (http://www.ncdc.ac.cn/, accessed on 1 March 2023), specifically the SRTM v4.1 data with a 30 m resolution. The basic parameters included the UTM/WGS-84 projection, GeoTIFF format, 84,467 × 34,894 pixels, with elevations relative to the geoid of the WGS-84 ellipsoid.

2.3. Technical Approach for Simulation Platform Construction

This study adopts Visual Studio 2017 (VS2017) as the development platform, utilizes the open-source 3D graphics toolkit Open Scene Graph(OSG) as the graphics engine, employs standard C++ as the development language, and utilizes the Interactive Data Language (IDL) to process the DEM source data to establish the experimental environment. Initially, we conducted computations and conversions of the SGOG tile grid point coordinates, matched the longitude and latitude coordinates with the DEM grid, and then proceeded with grid point elevation interpolation calculations and stratigraphic data matching. Subsequently, hybrid multiscale grid modeling was performed, followed by hierarchical color rendering. The overall technical approach is illustrated in Figure 2.

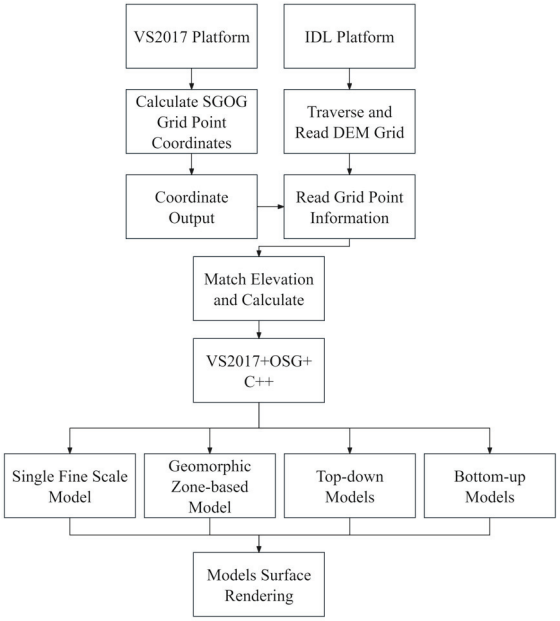

Figure 2. Overall technical approach for constructing the adaptive multiscale three-dimensional crustal simulation platform for the Yellow River.

3. Construction Process of Adaptive Multiscale True 3D Simulation Platform

The characteristics of the large-volume, multidimensional spatiotemporal nature, heterogeneous multi-source, and dynamic variability of Earth's spatiotemporal big data, as well as the complexity and comprehensiveness of Earth system simulation, demand that the Earth system simulation platform be targeted, adaptive, and flexible, enabling agile spatiotemporal multiscale, multidimensional simulations for specific simulation

requirements. This section introduces the construction process and the results of the construction of an adaptive multiscale true three-dimensional simulation platform for spherical grids. The experimental environment for this study includes: 12th Gen Intel Core i5-12450H 2.00 GHz processor, 3200 MHz 32 GB RAM, NVIDIA GeForce RTX 3050 graphics processor, 512 GB PCIe solid state drive; Windows 11 operating system, Visual Studio 2017 Professional, OSG 3.4.1 open source library, QT 5.12.0 open source library, QT Visual Studio Tools v2.10.1.2 extension tools; and is developed using C++ as the programming language.

3.1. Establishment of Single Fine-Scale Grid Simulation Platform

DEM and ETG are essentially based on the discrete representation of geographic space through sampled points. Naturally, a higher sampling density leads to a higher expression accuracy. Owing to the limitations of the computational power available in this study, the maximum level of SGOG grid partitioning allowed the entire Yellow River Basin crustal simulation to be at the 12th level. To provide a comparative benchmark for the various modeling methods, the results of the Yellow River simulation platform were obtained following the aforementioned technical approach, as shown in Figure 3. Using the mean elevation of each surface triangular grid point as an index, the corresponding thresholds were set and hierarchical color rendering was performed based on different threshold levels, resulting in the rendering of the Yellow River Basin, as shown in Figure 4. A side view of the rendering is displayed in Figure 5, where the curvature of the Yellow River Basin's crust and the vertical stratigraphic structure can be observed. A local zoomed-in view is shown in Figure 6.

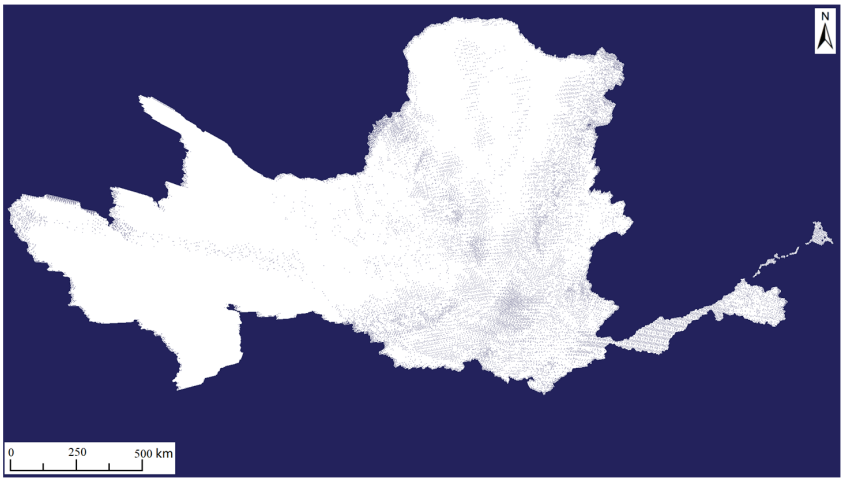

Figure 3. Modeling results of the 12th layer single-scale grid in the Yellow River Basin.

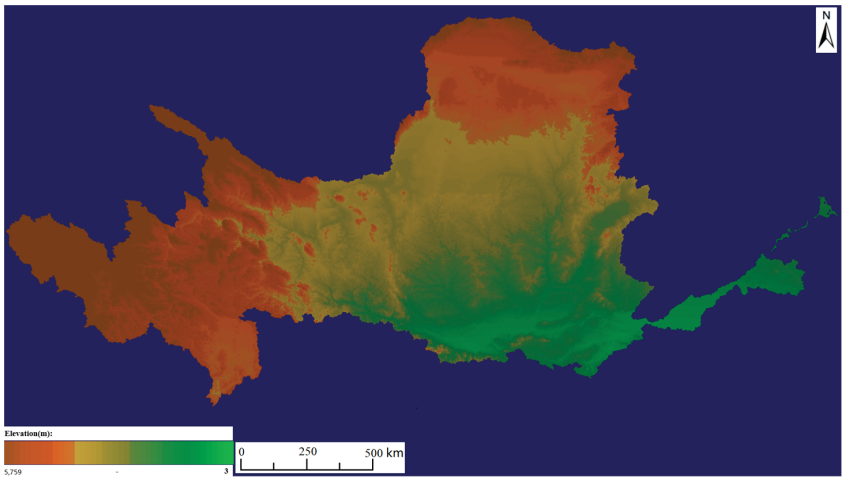

Figure 4. Rendering of the 12th layer single-scale grid model in the Yellow River Basin.

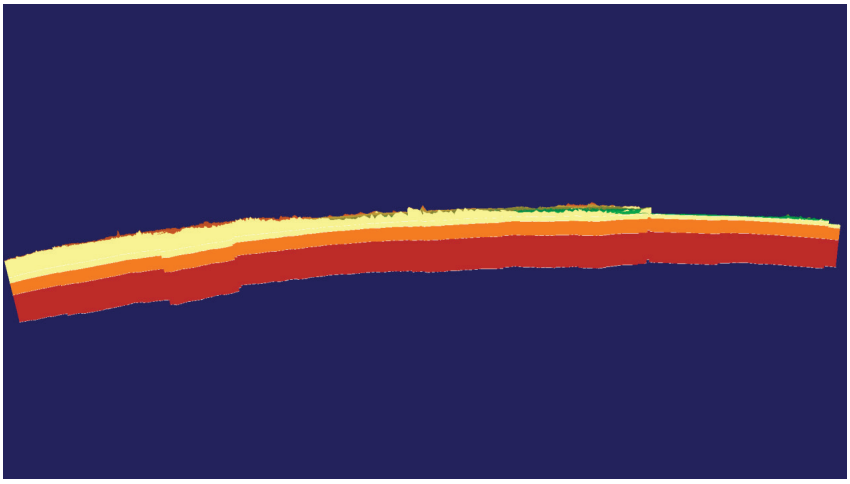

Figure 5. Side view of the rendering effect of the 12th layer single-scale model in the Yellow River Basin (stratigraphic data are hypothetical).

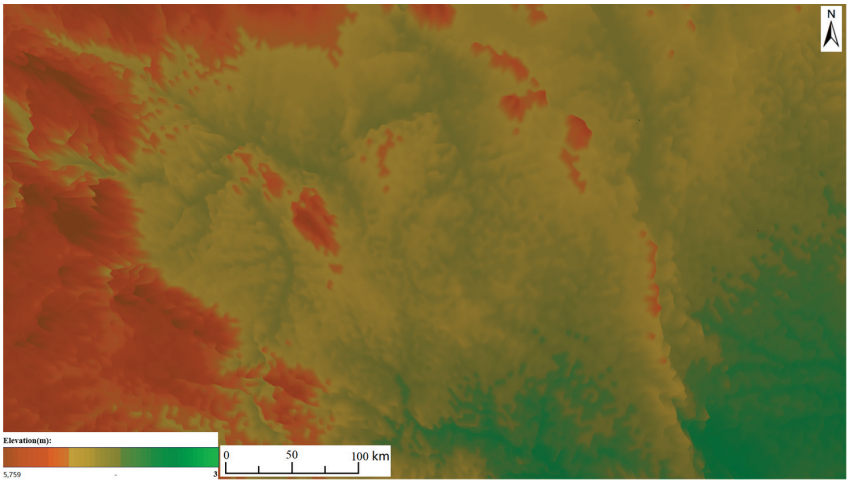

Figure 6. Local magnification of the rendering effect of the 12th layer single-scale model in the Yellow River Basin.

3.2. Establishment of Adaptive Multiscale Simulation Platform Based on Geomorphic Zoning

The Yellow River Basin has a fixed geomorphic pattern and structure. The boundaries of the geomorphic divisions in the Yellow River Basin were downloaded from the National Cryosphere Desert Data Center (http://www.ncdc.ac.cn/, accessed on 1 March 2023) and overlaid with the DEM. The geomorphic divisions were then clipped according to the DEM. Based on different geomorphic types, the corresponding grid layers were manually designated and adjacent layers were merged to create an adaptive multiscale Yellow River simulation platform based on divisions, as shown in Figure 7. On this platform, the Qinghai–Tibet Plateau, Qinling Mountains, and downstream areas were divided into 12 layers, whereas the Loess Plateau, Yinshan Mountains, Liupan Mountains, Lvliang Mountains, and Taihang Mountains were divided into 11 layers. The Ordos Plateau, Hetao Plain, Guanzhong Basin, Fen River Valley, and Taiyuan Basin were divided into 10 layers, and the downstream North China Plain was divided into the 9th layer. It should be noted that because of the narrow channel area in the downstream region, even with the use of a 12-layer grid for matching, there are still a few places where matching is unsuccessful, resulting in discontinuities.

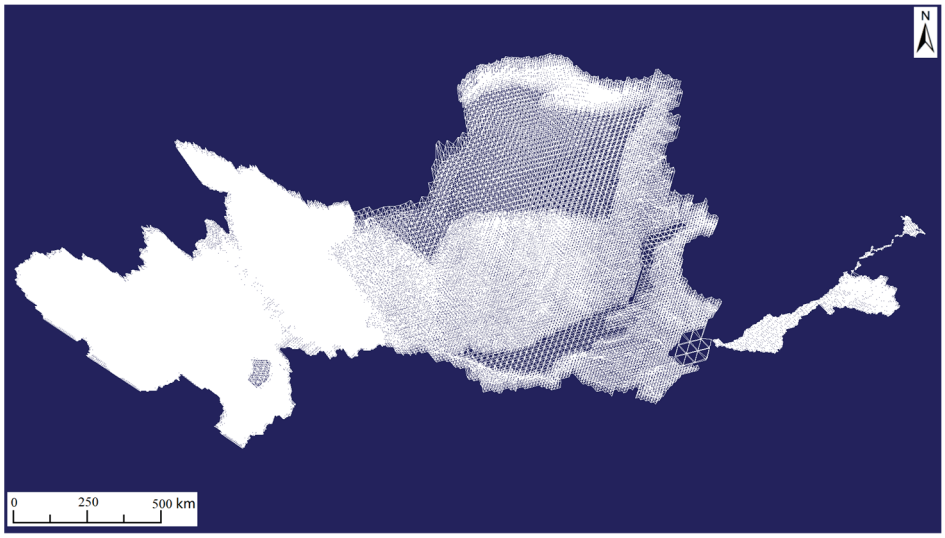

Figure 7. Hybrid multiscale grid modeling results in the Yellow River Basin, based on geomorphic zoning.

The technical approach for grid model edge matching in different geomorphic regions is as follows: The boundary portions of the grid model of each division were extended outward by a certain distance and overlaid. Duplicate grids were identified and removed.

3.3. Establishment of Top-Down Adaptive Multiscale Simulation Platform

A top-down modeling approach was implemented, starting from coarser grids and automatically subdividing them into finer grids according to specific rules until the desired level of detail is achieved. In this method, the 9th to 12th layers of the SGOG grid were selected to model the entire basin.

(1) Initially, an appropriate subdivision level n was selected to model the entire Yellow River Basin. This subdivision level was determined based on the specific scale of the study area, with $n = 9$ (approximating a triangle edge length of 19.49 km) chosen for the initial modeling of the entire basin.

(2) After elevation matching, a threshold value Δ for the maximum height difference between grid points is set as the criterion for further subdivision. The threshold Δ is determined based on the overall topography of the current basin. In this study, threshold values of 50 m, 100 m, and 150 m were used for Δ. If the height difference exceeded this threshold, the grid was further subdivided; otherwise, the subdivision was halted. The specific method for subdivision involved connecting the midpoints of the three edges of triangles at the current level to create four new triangles at level n + 1.

(3) The elevation differences between pairs of vertices on the outer grid are calculated, and the values are compared against the threshold Δ to determine whether to retain or subdivide. A technical roadmap for this method is shown in Figure 8.

To facilitate model comparison, this study employed two methods: the fixed and variable threshold step methods.

(a) Fixed threshold step method: This method consists of three variations ranging from the 9th layer to the 12th layer. The elevation difference threshold between adjacent layers was set at 50 m, 100 m, and 150 m to model the Yellow River simulation platform.

(b) Variable threshold step method: This method includes two variations. The first variation starts with a 50 m threshold at the 9th–10th layers and increases by 50 m at each step, until reaching a 150 m threshold at the 11th–12th layers. The second variation begins with a 150 m threshold at the 9th–10th layers and decreases by 50 m at each step, until reaching a 50 m threshold at the 11th–12th layers.

The results of the aforementioned experiments are illustrated in Figure 9.

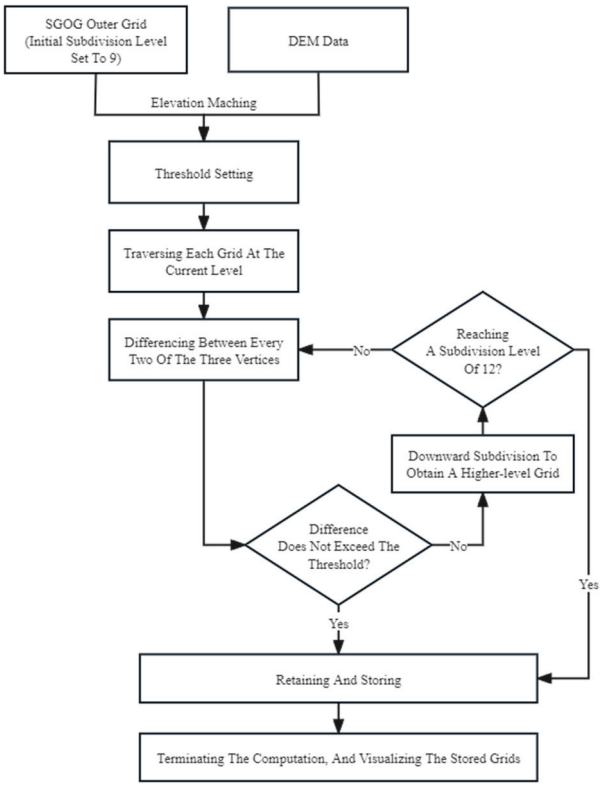

Figure 8. Technical roadmap for the top-down approach.

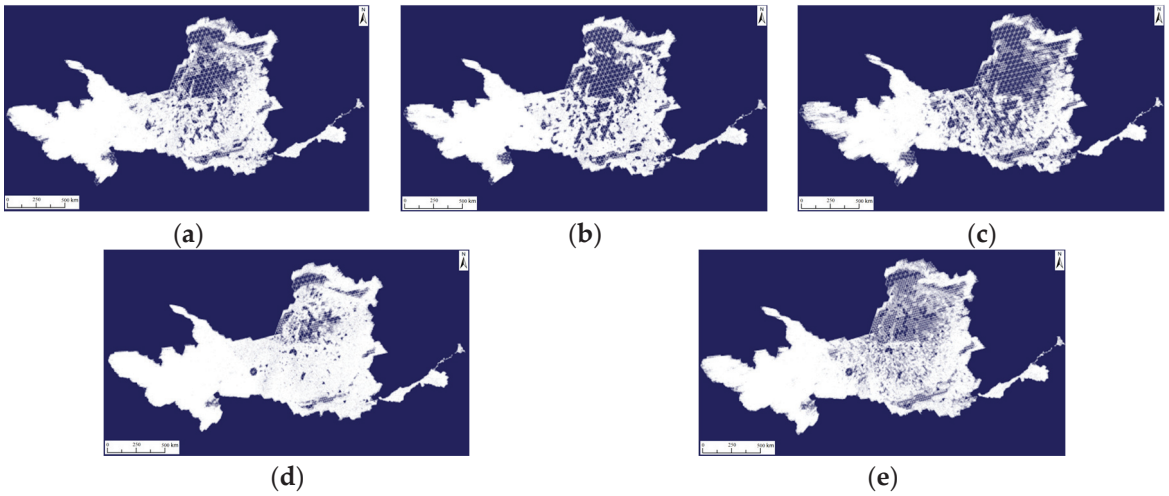

Figure 9. Crustal grid modeling results in the Yellow River Basin under different elevation difference thresholds in the top-down approach. (**a**). Fixed threshold at 50 m. (**b**). Fixed threshold at 100 m. (**c**). Fixed threshold at 150 m. (**d**). Variable threshold range: 50 m–100 m–150 m. (**e**). Variable threshold range: 150 m–100 m–50 m.

In the top-down approach, the magnitude of the threshold determines grid density. A larger threshold resulted in sparser grids, whereas a smaller threshold resulted in denser grids. Furthermore, the different geomorphic types exhibited varying grid density patterns. In practical applications, the choice of threshold values can be based on specific requirements.

The partial subdivision code statements for the top-down algorithm are as follows:

// The three points with height differences greater than the threshold, as well as their three child points, will be divided.

$$
\begin{aligned}
&\text{if } (\text{abs}(H1 - H2) >= HD \,||\, \text{abs}(H2 - H3) >= HD \,||\, \text{abs}(H3 - H1) >= HD) \{ \\
&B4 = (B1 + B2)/2; \\
&B5 = (B2 + B3)/2; \\
&B6 = (B3 + B1)/2; \\
&L4 = (L1 + L2)/2; \\
&L5 = (L2 + L3)/2; \\
&L6 = (L3 + L1)/2; \\
&\}
\end{aligned}
$$

The latitude and longitude coordinates of the grid points with height differences exceeding the threshold are subdivided in the manner described above.

3.4. Establishment of Bottom-Up Adaptive Multiscale Simulation Platform

The bottom-up modeling approach, which progresses from finer to coarser grids, shares the basic principles of the top-down method, but in the opposite direction, merging from higher to lower subdivision levels. Initially, the finest grid model (designated the 12th layer in this study) was established. Starting from the bottom, the maximum height difference between the grid points on the outer layers was evaluated at each level to determine whether it was below a predefined threshold. If this occurred, the grids were merged until an appropriate level was reached. In this method, grids at subdivision levels 9, 10, 11, and 12 were selected to model the entire basin. Threshold values of 50 m, 100 m, and 150 m were used in separate experiments along with the variable threshold experiments. The technical roadmap of this method is shown in Figure 10, and the modeling results are presented in Figure 11.

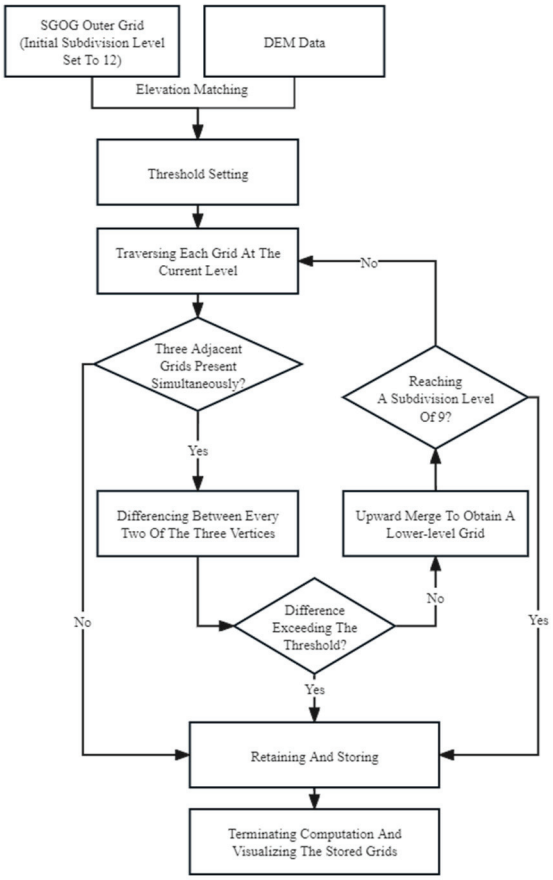

Figure 10. Technical roadmap for the bottom-up approach.

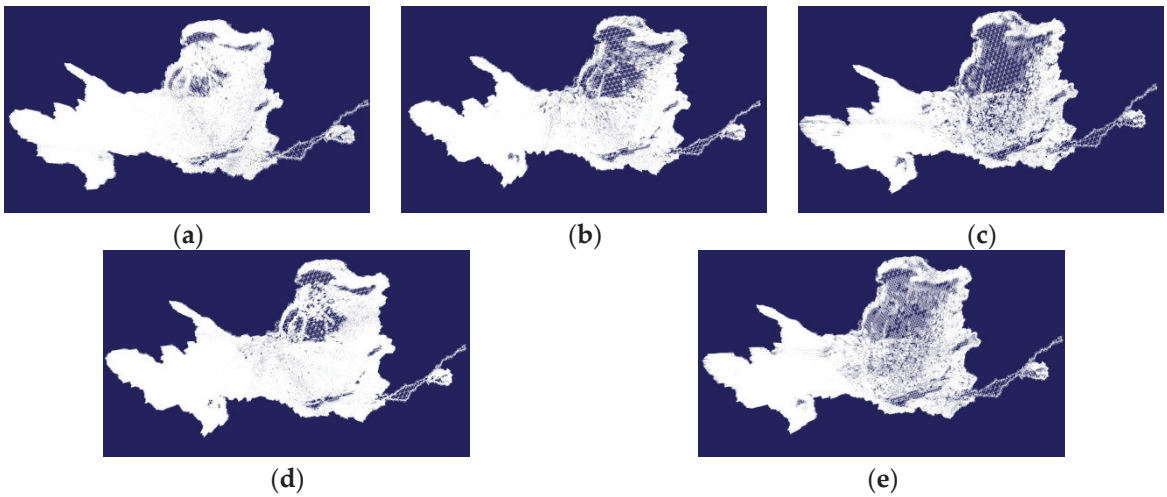

Figure 11. Crustal grid modeling results in the Yellow River Basin under different elevation difference thresholds in the bottom-up approach. (**a**). Fixed threshold at 50 m. (**b**). Fixed threshold at 100 m. (**c**). Fixed threshold at 150 m. (**d**). Variable threshold range: 50 m–100 m–150 m. (**e**). Variable threshold range: 150 m–100 m–50 m.

Compared to Figure 9, the bottom-up approach for crustal modeling in the Yellow River Basin generally produces denser grids, providing a more comprehensive representation of terrain details. The algorithm and code implementation of this method approximate the top-down approach, and will not be reiterated here.

4. Comprehensive Evaluation of Hybrid Multiscale Grid Models in the Yellow River Basin

The above experiments employed four methods, namely single-scale, geomorphic zoning, top-down, and bottom-up, to flexibly construct the 12th layer of the finer SGOG crustal grid model and the 11 other adaptive hybrid multiscale SGOG grid models in the Yellow River Basin. These models exhibit diverse appearances. To objectively evaluate the merits and demerits of each method, this study conducted a quantitative evaluation from two perspectives, terrain information representation and algorithmic consumption, providing scientific references for the construction of a geographic simulation platform for the basin.

4.1. Selection of Evaluation Indicators

In general, the greater the amount of terrain information implied by the surface model, the more realistic and higher quality the effect. Based on the characteristics of the DEM data and the principle of easy calculation, this study selected three indicators, namely, terrain roughness, elevation variation coefficient, and terrain relief, to measure the amount of terrain information contained in the model. For comparison, this study also lists the standard deviation and mean elevation. In addition, to establish a watershed simulation platform, the efficiency of model construction is also an important indicator of its quality from a practical perspective. This study selected four modeling efficiency indicators: grid vertex count, modeling time consumption (calculated uniformly after the grid vertex elevation is matched), grid point coordinate file storage space consumption (hereafter referred to as file storage space consumption), and running memory space consumption. Using the 12th layer grid model as a reference, a quality index calculation, comparison, and ranking of the remaining 11 hybrid scale models were conducted, thus comprehensively evaluating the terrain information expression and model operating efficiency of the aforementioned hybrid multiscale models.

The grid vertex count is the total number of vertices on the outermost surface grid for single-layer or hybrid multiscale modeling. The terrain roughness formula used in this study is as follows:

$$\sigma = \frac{A}{A_p} \tag{1}$$

where A is the sum of the surface area on the watershed grid and Ap is the sum of the lower surface area of the watershed grid, representing the projected area of the watershed surface grid on the sphere.

Mean elevation: The mean elevation is the sum of the elevations of all grid vertices divided by the number of grid vertices, and reflects the average level of elevation in the region.

$$\overline{H} = \frac{\sum_{i=1}^{n} H_i}{n} \tag{2}$$

where H is the elevation of the grid vertex, and n is the number of grid vertices.

Elevation standard deviation:

$$s = \sqrt{\frac{\sum(H - \overline{H})^2}{n-1}} \tag{3}$$

Elevation variation coefficient: the percentage of the ratio of elevation standard deviation to mean elevation, reflecting the degree of deviation of a set of elevation values from the mean.

$$c \cdot v = \frac{s}{\overline{H}} \times 100\% \tag{4}$$

Terrain relief:

$$R = H_{max} - H_{min} \tag{5}$$

In this formula, H_{max} is the highest elevation value in region, and H_{min} is the lowest elevation value in region.

Time consumption refers to the time elapsed from the start of the program to the completion of the generation process after completing grid elevation matching, including processes such as grid data reading, grid data calculation, scene rendering, and generation. File storage space consumption and running memory space consumption refer to the computer hard disk space consumed by storing grid data in file form for different methods and the computer running memory consumed by calculating, drawing, and visualizing grid data in the program for different methods.

4.2. Definition of Quality Indices

The crustal model of the Yellow River Basin constructed in the previous section is most finely represented by the 12th layer grid model. Based on this, the quality standard for the hybrid multiscale model is defined as follows: the model with the closest amount of terrain information to the 12th layer grid model and the highest modeling and computing efficiency is of the best quality.

Definition of the quality index: Let the aforementioned indicators be denoted as m_i and the corresponding indicator for the 12th layer as $m_{n\,=\,12}$. The quality index w_i is defined as the absolute difference between m_i and $m_{n\,=\,12}$ divided by $m_{n\,=\,12}$, that is:

$$w_i = \frac{|m_i - m_{n=12}|}{m_{n=12}} \times 100\% \tag{6}$$

Each indicator has a different influence on the quality of the model relative to the aforementioned quality standards and indicators. The quality index for terrain information-related indicators is better when is smaller, whereas a larger quality index is preferable for efficiency-related indicators. These are referred to as negative and positive indicators,

respectively. Accordingly, the negative and positive quality indices, Q_1 and Q_2, are defined as follows:

$$Q_1 = \sum w, w \in \left\{ w_{TerrainRoughness}, w_{TerrainRelief}, w_{ElevationVariabilityCoefficient} \right\} \quad (7)$$

$$Q_2 = \sum w, w \in \left\{ w_{NumberOfGridVertices}, w_{TimeConsumption}, w_{FileStorageSpace}, w_{RuntimeMemorySpace} \right\} \quad (8)$$

The quality of each hybrid model was comprehensively determined based on the ranking of Q_1 and Q_2.

4.3. Computational Results and Evaluation Analysis

For convenience of analysis and comparison, the experimental numbers for the aforementioned experiments are as follows (Table 2):

Table 2. Model construction experiment labeling.

Labeling	A	B	C	D	E	F
Experiment	Single-scale 12th Layer	Terrain-based Partitioning Method	Top-down Threshold 50 m	Top-down Threshold 100 m	Top-down Threshold 150 m	Top-down Threshold 50–100–150 m
Labeling	G	H	I	J	K	L
Experiment	Top-down Threshold 150–100–50 m	Bottom-up Threshold 50 m	Bottom-up Threshold 100 m	Bottom-up Threshold 150 m	Bottom-up Threshold 50–100–150 m	Bottom-up Threshold 150–100–50 m

4.3.1. Terrain Feature Representation

The calculations of the terrain information-related indicators for various scale models of the Yellow River Basin crust are presented in Table 3. Overall, it can be seen that the terrain information-related parameters for various hybrid scale models are not significantly different from the single 12-layer scale model (Method A). The terrain roughness was slightly lower than that of Model A, indicating that regardless of the hybrid scale used, a certain amount of terrain relief details were omitted. The elevation variation coefficient for Model B based on geomorphic zoning was greater than that of Model A, whereas the rest were lower than that of Model A. This indicates that, in terms of standard deviation and mean elevation, Model B has a larger standard deviation and a smaller mean elevation. The other methods had larger elevation standard deviations and mean elevations, indicating that the continuity of the elevation distribution in Model B was not as good as that in the other models. The terrain relief for the bottom-up approach was equivalent to that of Model A, whereas those of the other methods were slightly lower. In particular, the top-down and bottom-up methods have fixed values, reflecting a certain determinism in the modeling mechanism of each method. Figure 12 is shown below.

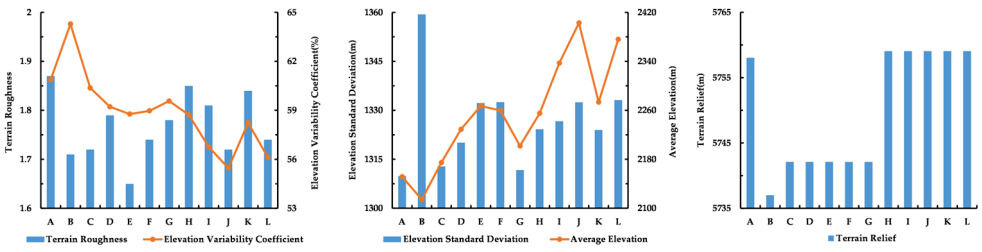

(**a**) (**b**) (**c**)

Figure 12. Terrain feature representation. (**a**): Terrain roughness and elevation variability coefficient. (**b**): Elevation standard deviation and average elevation. (**c**): Terrain relief.

Table 3. Terrain information-related (negative) indicators.

Methods	Labeling	Terrain Roughness	Elevation Standard Deviation (m)	Average Elevation (m)	Elevation Variability Coefficient (%)	Terrain Relief (m)
Single-scale	A	1.87	1309.86	2151.55	60.88	5758.05
Geomorphic Zoning	B	1.71	1359.38	2114.33	64.29	5737.01
Top-down (from coarse to fine)	C	1.72	1312.81	2174.71	60.37	5742.11
	D	1.79	1320.10	2228.97	59.22	5742.11
	E	1.65	1332.22	2267.01	58.77	5742.11
	F	1.74	1332.50	2259.69	58.97	5742.11
	G	1.78	1311.71	2201.86	59.57	5742.11
Bottom-up (from fine to coarse)	H	1.85	1324.20	2255.05	58.72	5759.07
	I	1.81	1326.67	2337.15	56.76	5759.07
	J	1.72	1332.44	2402.66	55.46	5759.07
	K	1.84	1323.98	2273.36	58.24	5759.07
	L	1.74	1333.11	2376.00	56.11	5759.07

4.3.2. Computational Efficiency

The calculations of the model operating efficiency-related indicators for the various scale models of the Yellow River Basin crust are listed in Table 4. It can be observed that the temporal and spatial consumption of the model computation is directly related to the number of grid vertices; the greater the number of vertices, the higher the temporal and spatial consumption. Among them, Model B had the fewest grid vertices, resulting in the lowest temporal and spatial consumption and the highest efficiency. It is important to emphasize that the watershed simulation platform consists of a series of logical steps, as shown in Figure 1. Time consumption refers to the visualization construction time of the grid model after the elevation matching of all grid points, excluding the time consumed for processing the source DEM data, calculating grid point coordinates, matching grid point elevations, overlaying geomorphic boundaries with the source DEM, data clipping, and the hierarchical color rendering of the model. For example, in the experimental environment of this study, single-scale Model A required approximately 3.5 h from grid point coordinate calculation, elevation matching, and grid generation to color rendering. Figure 13 is shown below.

Table 4. Model operating efficiency-related (positive) indicators.

Methods	Labeling	Number of Grid Vertices	Time Consumption (s)	File Storage Space Consumption (MB)	Runtime Memory Space Consumption (MB)
Single-scale	A	91,327	2.95	50.5	1024.0
Geomorphic Zoning	B	51,692	1.73	28.1	626.1
Top-down (from coarse to fine)	C	79,930	2.72	45.3	1009.3
	D	67,521	2.47	41.2	917.9
	E	53,581	2.21	36.8	819.9
	F	65,068	2.46	41.0	913.5
	G	63,496	2.45	40.8	909.0
Bottom-up (from fine to coarse)	H	86,021	2.93	48.9	1016.0
	I	73,544	2.56	42.7	951.4
	J	61,917	2.39	39.9	889.0
	K	85,451	2.87	47.9	1015.2
	L	63,453	2.43	40.5	902.3

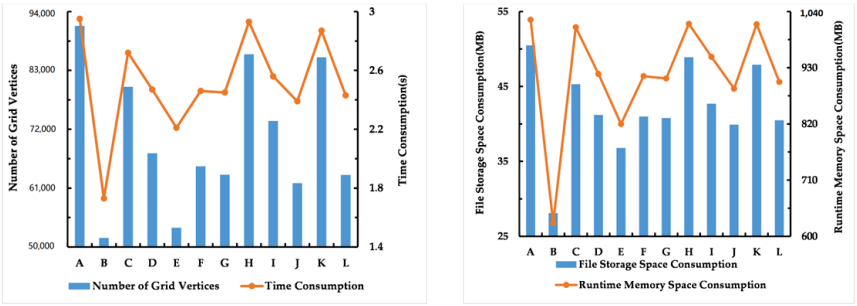

(**a**) (**b**)

Figure 13. Computational efficiency. (**a**): Number of grid vertices and time consumption. (**b**): File storage space consumption and runtime memory space consumption.

4.3.3. Quality Indices

The quality index calculations for these indicators are presented in Tables 5 and 6.

Table 5. Quality index for terrain information-related indicators.

Methods	Labeling	$W_{TerrainRoughness}$ (%)	$W_{ElevationVariabilityCoefficient}$ (%)	$W_{TerrainRelief}$ (%)	Q_1 (%)	Ranking
Geomorphic Zoning	B	8.56	5.60	0.37	14.53	8
Top-down (from coarse to fine)	C	8.02	0.84	0.28	9.14	5
	D	4.28	2.73	0.28	7.29	4
	E	11.76	3.47	0.28	15.51	10
	F	6.95	3.14	0.28	10.37	7
	G	4.81	2.15	0.28	7.24	3
Bottom-up (from fine to coarse)	H	1.07	3.55	0.02	4.64	1
	I	3.21	6.77	0.02	10.00	6
	J	8.02	8.90	0.02	16.94	11
	K	1.60	4.34	0.02	5.96	2
	L	6.95	7.84	0.02	14.81	9

Table 6. Quality index for model operating efficiency indicators.

Methods	Labeling	$W_{NumberOfGridVertices}$ (%)	$W_{TimeConsumption}$ (%)	$W_{FileStorageSpace}$ (%)	$W_{RuntimeMemorySpace}$ (%)	Q_2(%)	Ranking
Geomorphic Zoning	B	43.40	41.36	44.36	38.86	167.98	1
Top-down (from coarse to fine)	C	12.48	7.80	10.30	1.43	32.01	9
	D	26.07	16.27	18.42	10.36	71.12	7
	E	41.33	25.08	27.13	19.93	113.47	2
	F	28.75	16.61	18.81	10.79	74.96	6
	G	30.47	16.95	19.21	11.23	77.86	5
Bottom-up (from fine to coarse)	H	5.81	0.68	3.17	0.78	10.44	11
	I	19.47	13.22	15.45	7.09	55.23	8
	J	32.20	18.98	20.99	13.18	85.35	3
	K	6.43	2.71	5.15	0.86	15.15	10
	L	30.52	17.63	19.80	11.88	79.83	4

From Table 5, it can be observed that from the perspective of terrain information expression, the bottom-up method is superior to the top-down method, with the geomorphic zoning method ranking in the middle and later positions. Specifically, the bottom-up 50 m threshold (H) and the 50–100–150 m dynamic threshold (K) models rank in the top two positions, while the top-down 150–100–50 m dynamic threshold (G) and the 100 m fixed threshold (D) models rank 3rd and 4th, and the scores of the two are basically comparable. The top-down 50 m fixed threshold (C), bottom-up 100 m fixed threshold (I), and top-down

50–100–150 m dynamic threshold (F) models had similar scores, ranking 5th to 7th, and the geomorphic zoning method (B) ranks 8th. Finally, the bottom-up 150–100–50 m dynamic threshold (L), top-down 150m fixed threshold (E), and bottom-up 100m fixed threshold (J) models rank 9th to 11th. The quality indices for rankings 8–11 were all greater than 14 and were essentially in the same category. Figure 14 is shown below.

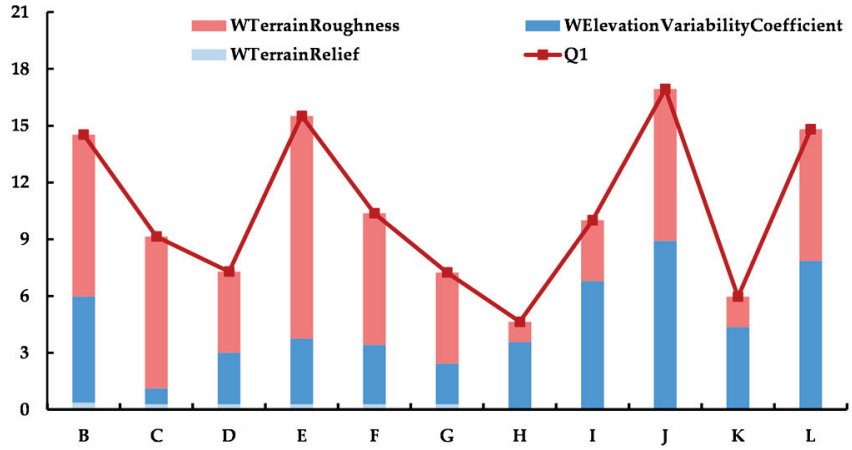

Figure 14. Quality index for terrain information-related indicators.

As shown in Table 6, from the perspective of computational efficiency, the quality ranking is almost the opposite of that in Table 4. The geomorphic zoning method performed the best, and the top-down approach was superior to the bottom-up approach. Specifically, Model B demonstrated an outstanding performance, with the highest score. Model E was on par with Model B, with scores over 100. Models J, L, G, F, and D belonged to the second tier, with scores ranging from 70 to 90. Models I and C fell in the third tier, with scores ranging between 30 and 60. Models K and H were in the lowest tier, with scores below 20. Figure 15 is shown below.

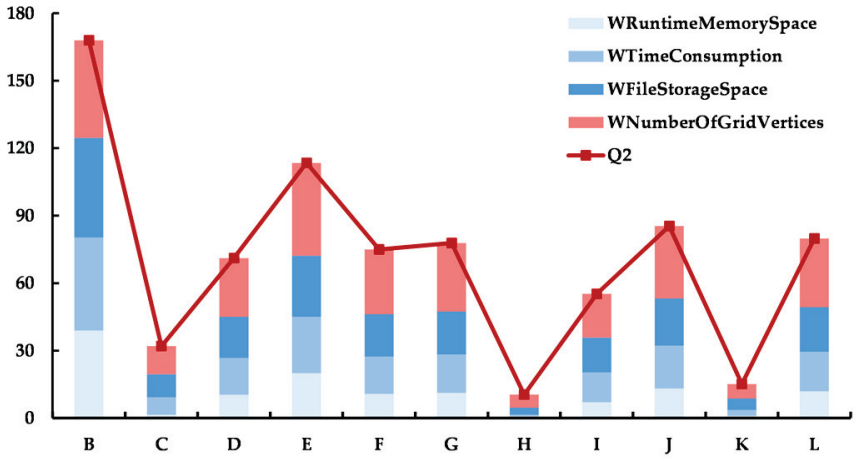

Figure 15. Quality index for model operating efficiency indicators.

From the above analysis, it can be concluded that, under the given conditions, it is impossible to simultaneously achieve both efficient terrain information representation and computational efficiency in the models. It is a natural and objective law. Each method has its own characteristics, and the selection or achievement of a relative balance between the actual applications and environmental conditions should be based on these characteristics.

5. Conclusions

In response to the demands of digital Earth representation and Earth system model computation in the era of spatiotemporal big data, this study utilized SGOG and globally shared DEM data to design and implement a crustal simulation platform for the Yellow River Basin. The platform includes four categories and 12 adaptive multiscale models based on geomorphic zoning, using both top-down and bottom-up approaches. Relevant terrain and computational efficiency indicators were selected to evaluate the quality of grid models in the simulation platforms. The main conclusions are as follows.

(1) The establishment of a single-scale fine-grid model can reflect terrain details more accurately, approximate actual surface conditions, and provide rich terrain information. However, it requires large amounts of data and high computational power, making it suitable for the precise simulation of surface processes and supercomputing environments.

(2) Adaptive multiscale modeling based on characteristic thresholds achieves an organic balance between terrain feature representation and computational efficiency while maintaining the natural continuity of the terrain. Under the same elevation difference threshold, the bottom-up (finer-to-coarser) approach has certain advantages in terms of terrain feature representation, whereas the top-down (coarser-to-finer) approach excels in computational efficiency. Both approaches can achieve desirable results. These methods provide a certain level of terrain accuracy with relatively relaxed requirements for computational environments, making them widely applicable.

(3) Geomorphic zoning-based multiscale modeling incorporates prior knowledge of landforms into the modeling process, resulting in stronger targeting. It achieves maximum terrain fidelity in key areas at minimum spatiotemporal cost and exhibits the highest computational efficiency. However, it needs hard boundaries in prior landform zoning, which disrupts the natural continuity of terrain distribution to some extent. Fine-grained landform zoning is required to achieve highly desirable results, which inevitably reduces computational efficiency. This approach integrates human intelligence and incorporates an "attention" mechanism for key areas and issues. This is a crucial technical means of overcoming the bottlenecks in Earth system modeling and geographic process simulation, satisfying the special requirements of complex geographic computations.

In conclusion, the basin crustal simulation platform is a crucial component of the basin simulator. The spherical discrete grid mechanism provides ample flexibility for establishing and applying the platform. The model can be either an arbitrary single scale or adaptive multiscale. The scale can be manually specified or automatically calculated based on the characteristic thresholds. The thresholds can be fixed or dynamic. The construction strategy can proceed from coarser to finer or finer to coarser. This study introduces the concept of a spherical grid-based Yellow River Basin true three-dimensional multiscale simulator platform, addressing the issue of scale rigidity in traditional geographical simulations. It achieves model construction at both a single scale and multiple hierarchical mixed scales, enabling flexible basin geographic process simulations as needed. The platform can be used to organize spatiotemporal big data in the digital Earth context, as well as for Earth system model computations. It encompasses both the static representation of surface phenomena and dynamic simulation of geographic processes. In summary, the Earth's discrete grid is the core technology of Earth system simulators and represents an important development direction in contemporary Earth information science.

For future research, our team is currently exploring the application of the simulation platform developed in this study to conduct geographic process simulations in the Yellow River Basin, specifically focusing on simulating groundwater point source pollution diffusion based on the Yellow River simulation platform. Other forms of basin geographic process simulations are equally applicable.

Author Contributions: Conceptualization, B.L. and J.W.; data curation, J.W.; funding acquisition, J.W.; methodology, B.L.; resources, B.L.; software, Y.Z. and Y.S.; writing—original draft, B.L.; writing—review and editing, B.L., J.W., Y.Z. and Y.S. All authors have read and agreed to the published version of the manuscript.

Funding: This research was funded by Henan Key R&D and Promotion Special Program (Science and Technology Tackling) (232102320264). Supported by the Department of Science and Technology of Henan Province, China. Grant number 232102320264.

Data Availability Statement: The data presented in this study are openly available in Construction Technique of Spherical Grid-Based Adaptive Multi-scale True 3D Yellow River Simulation Platform Source Code at https://doi.org/10.57760/sciencedb.16536.

Acknowledgments: We would like to thank all editors and reviewers for their insightful comments, which helped us improve the quality of this paper.

Conflicts of Interest: The authors declare no conflicts of interest.

References

1. Zuo, Q.T.; Qiu, X.; Ma, J.X.; Zhang, Z.Z. Evolution of flood control thought and modern flood control strategy in the Yellow-River Basin. *J. Water Resour. Water Eng.* **2023**, *34*, 1–9.
2. Xu, X.Y.; Yang, Z.F. General Discussion on Ecological Environment Water Demand. *China Water Resour.* **2003**, *3*, 20–23+5.
3. Zuo, Q.T.; Qin, X.; Ma, J.X. Framework Design and Development Layout of Yellow River Simulator Construction. *Yellow River* **2023**, *45*, 18–23.
4. Zhang, W. Correctly understand and fully engage with the "River Strategy". *Water Resour. Dev. Res.* **2023**, *23*, 1–3.
5. Xia, J.; Zhan, C.S.; Zeng, S.D.; Zou, L.; She, D.X.; Zuo, Q.T. Theoretical method and practical exploration of Yangtze River Simulator construction. *J. Hydraul. Eng.* **2022**, *53*, 505–514.
6. Zhu, A.X.; Zhu, L.J.; Shi, Y.X.; Qin, C.Z.; Liu, J.Z. Integrated watershed modeling and scenario analysis: A new paradigm for integrated study of physical geography? *Prog. Geogr.* **2019**, *38*, 1111–1122. [CrossRef]
7. Wang, H.J.; Zhu, J.; Pu, Y.F. The earth system simulation. *SCIENTIA SINICA Phys. Mech. Astron.* **2014**, *44*, 1116–1126.
8. Lu, C.K. Earth system simulation large scientific device to diagnose the Earth. *Invent. Innov.* **2021**, *3*, 57.
9. Zheng, X.Q. On the Geographic System Simulation Basic Model. *Chin. J. Nat.* **2012**, *34*, 143–149.
10. Zhao, X.S.; Ben, J.; Sun, W.B.; Tong, X.C. Overview of the Research Progress in the Earth Tessellation Grid. *Acta Geod. Cartogr. Sin.* **2016**, *45*, 1–14.
11. Zhang, Y.S.; Ben, J.; Tong, X.C. *Theory, Algorithm and Application of Spherical Discrete Grid of Earth Spatial Information*, 1st ed.; Science Press: Beijing, China, 2007; pp. 15–20.
12. Wu, L.X.; Yu, J.Q. Global 3D-Grid based on sphere degenerated octree and its distortion features. *Geogr. Geo-Inf. Sci.* **2009**, *25*, 1–4.
13. Wang, J.X.; Lu, F.N.; Chen, J. Comparison of surface and solid discrete global grids. *Sci. Surv. Map* **2012**, *37*, 34–36.
14. Wang, J.X.; Zheng, Y.S.; Li, Y.H.; Lu, F.N.; Liu, J.N. Building the Platform of Digital Earth with Sphere Split Bricks. *Acta Geod. Cartogr. Sin.* **2015**, *44*, 694.
15. Cao, X.F. Research on Earth Sphere Shell Space Grid Theory and Algorithms. Ph.D. Thesis, Information Engineering University, Zhengzhou, China, 2012.
16. Zhao, Z.P. Research on Model-oriented Spherical Rhombus Discrete Grids. Master's Thesis, Nanjing Normal University, Nanjing, China, 2015.
17. Liu, K. A Universal Data Model of Discrete Global Grid System Based on Fiber Bundle Theory. Master's Thesis, Nanjing Normal University, Nanjing, China, 2019.
18. Lin, B.X.; Zhou, L.C.; Xu, D.P.; Zhu, A.X.; Lu, G.N. A discrete global grid system for earth system modeling. *Int. J. Geogr. Inf. Sci.* **2018**, *32*, 711–737. [CrossRef]
19. Hojati, M.; Robertson, C.; Roberts, S.; Chaudhuri, C. GIScience research challenges for realizing discrete global grid systems as a Digital Earth. *Big Earth Data* **2022**, *6*, 358–379. [CrossRef]
20. Ben, J.; Li, Y.L.; Wang, R.; Du, L.Y. Algebraic encoding scheme for aperture 3 hexagonal discrete global grid system. *Sci. Earth Sci.* **2018**, *48*, 340–352. [CrossRef]
21. Zhou, J.B.; Ben, J.; Wang, R.; Zheng, M.Y. Encoding and Operation for the Aperture-4 Hexagonal Discrete Global Grids on Uniform Tiles. *J. Wuhan Univ. Inf. Sci. Ed.* **2023**, *48*, 639–646.
22. Benjamin, U.; Faramarz, S. Toward volume preserving spheroid degenerated-octree grid. *Geoinformatica* **2020**, *24*, 505–529.
23. Liang, X.Y.; Ben, J.; Wang, R.; Liang, Q.S.; Huang, X.H.; Ding, J.J. Construction of rhombic triacontahedron discrete global grid systems. *Int. J. Digit. Earth* **2022**, *15*, 1760–1783. [CrossRef]
24. Zhao, L.; Li, G.; Yao, X.; Ma, Y.; Cao, Q. An optimized hexagonal quadtree encoding and operation scheme for icosahedral hexagonal discrete global grid systems. *Int. J. Digit. Earth* **2022**, *15*, 975–1000. [CrossRef]
25. Zhou, J.B.; Ding, J.J.; Ben, J.; Chen, Y.H.; Liang, Q.S. Multi-mode 3D extension methods for equal-area discrete global grid systems for geospatial data representation. *J. Geod. Geoinf. Sci.* **2024**, *53*, 173–188.

26. Liang, Q.S.; Chen, Y.H.; Ben, J.; Zhou, J.B.; Ding, J.J.; Dai, J.C. Modelling and Storage Method for Hexagonal Remote Sensing Images in Rhombic Triacontahedron Discrete Global Grid System. *J. Geo-Inf. Sci.* **2023**, *25*, 2361–2373.
27. Zhao, L.; Li, G.Q.; Yao, X.C.; Ma, X. Code Operation Scheme for the Icosahedral Hexagonal Discrete Global Grid System. *J. Geoinf. Sci.* **2023**, *25*, 239–251.
28. Wang, Z.; Zhao, X.; Sun, W.; Luo, F.; Li, Y.; Duan, Y. Correlation Analysis and Reconstruction of the Geometric Evaluation Indicator System of the Discrete Global Grid. *ISPRS Int. J. Geo-Inf.* **2021**, *10*, 115. [CrossRef]
29. Alexander, K.; Ivan, V.; Holger, V.; Evelyn, U. Area and shape distortions in open-source discrete global grid systems. *Big Earth Data* **2022**, *6*, 256–275.
30. Wu, Y.T.; Wan, G.; Liu, L.; Mu, Y.; Wei, Z.J.; Wang, S. A Review of the Research on Discrete Global Grid Systems in Digital Earth. In Proceedings of the IEEE International Information Technology and Artificial Intelligence (ITAC), Chongqing, China, 19 June 2022.
31. Kazemi, M.; Wecker, L.; Samavati, F. Efficient Calculation of Distance Transform on Discrete Global Grid Systems. *ISPRS Int. J. Geo-Inf.* **2022**, *11*, 322. [CrossRef]
32. Wang, J.X.; Shi, Y.; Qin, Z.L.; Cao, Z.N. A Three-Dimensional Buffer Analysis Method Based on the 3D Discrete Global Grid System. *ISPRS Int. J. Geo-Inf.* **2021**, *10*, 520. [CrossRef]
33. Bousquin, J. Discrete Global Grid Systems as scalable geospatial frameworks for characterizing coastal environments. *Environ. Model. Softw.* **2021**, *146*, 105210. [CrossRef] [PubMed]
34. Andrew, R.; Zoheir, S.; Mario, B. Geospatial Data Analysis for Global Maritime Risk Assessment Using the Discrete Global Grid System. In Proceedings of the 2021 IEEE International Geoscience and Remote Sensing Symposium, Brussels, Belgium, 16 July 2021.
35. Mingke, L.; Heather, M.; Emmanuel, S. Multi-resolution topographic analysis in hexagonal Discrete Global Grid Systems. *Int. J. Appl. Earth Obs. Geoinf.* **2022**, *113*, 102985.
36. Wang, J.X.; Qin, Z.L.; Zhao, G.C.; Li, B.X.; Gao, C.R. Scale Effect Analysis of Basin Topographic Features Based on Spherical Grid and DEM:Taking the Yangtze River as An Example. *J. Basic Sci. Eng.* **2022**, *30*, 1109–1120.
37. Alborzi, H.; Samaet, H. Augmenting SAND with a spherical data model. In Proceedings of the First International Conference on Discrete Global Grids, Santa Barbara, CA, USA, 28 March 2000.
38. Bartholdi, J.J.; Goldsman, P. Continuous indexing of hierarchical subdivisions of the globe. *Int. J. Geogr. Inf. Sci.* **2001**, *15*, 489–522. [CrossRef]
39. Baumgarder, J.R.; Frederickson, P.O. Icosahedral discretization of the two- sphere. *SIMA J. Numer. Anal.* **1985**, *22*, 1107–1115. [CrossRef]
40. Dutton, G. Geodesic Modelling of Planetary Relief. *Cartographica* **1984**, *21*, 188–207. [CrossRef]
41. Dutton, G. *A Hierarchical Coordinate System for Geoprocessing and Cartography*; Springer: Berlin/Heidelberg, Germany, 1999.
42. Fekete, G. Rendering and Managing Spherical Data with Sphere Quadtrees. In Proceedings of the IEEE Conference on Visualization, San Francisco, CA, USA, 26 October 1990.
43. Goodchild, M.F.; Yang, S. A Hierarchical Spatial Data Structure for Global Geographic Information Systems. *Comput. Vis. Graph. Image Process.* **1992**, *54*, 31–34. [CrossRef]
44. Song, L.; Kimerling, A.J.; Sahr, K. Developing an equal area global grid by small circle subdivision. In *Discrete Global Grids: A Web Book*; Goodchild, M.F., Kimerling, A.J., Eds.; The National Center for Geographic Information and Analysis: Santa Barbara, CA, USA, 2002.
45. White, D.; Kimerling, A.J.; Sahr, K.; Song, L. Comparing Area and Shape Distortion on Polyhedral-Based Recursive Partitions of the Sphere. *Int. J. Geogr. Inf. Sci.* **1998**, *12*, 805–827. [CrossRef]
46. Sahr, K.; White, D.; Kimerling, A.J. Geodesic Discrete Global Grid Systems. *Cartogr. Geogr. Inf. Sci.* **2003**, *30*, 121–134. [CrossRef]
47. White, D. Global Grids from Recursive Diamond Subdivisions of the Surface of an Octahedron or Icosahedron. *Environ. Monit. Assess.* **2000**, *64*, 93–103. [CrossRef]
48. Bjørke, J.T.; Kindlmann, J.K.; Holt, M. A Global Grid Model Based on "Constant Area" Quadrilaterals. In Proceedings of the 9th Scandinavian Research Conference on Geographical Information Science, Espoo, Finland, 4–6 June 2003; pp. 239–250.
49. Gibb, R.; Raichev, A.; Speth, M. The rHEALPix Discrete Global Grid System. 2016. Available online: https://datastore.landcareresearch.co.nz/dataset/rhealpix-discrete-global-grid-system (accessed on 17 July 2018).
50. Heikes, R.; Randall, D.A. Numerical Integration of the Shallow-Water Equations on a Twisted Icosahedral Grid. Part II: A Detailed Description of the Grid and an Analysis of Numerical Accuracy. *Mon. Weather Rev.* **1995**, *123*, 1881–1887.
51. Sadourny, R.; Arakawa, A.; Mintz, Y. Integration of the Nondivergent Barotropic Vorticity Equation with an Icosahedral-Hexagonal Grid for the Sphere. *Mon. Weather Rev.* **1968**, *96*, 392–399. [CrossRef]
52. Thuburn, J. A PV-Based Shallow-Water Model on a Hexagonal Icosahedral Grid. *Mon. Weather Rev.* **1997**, *125*, 2328–2347. [CrossRef]
53. Peterson, P. Close-Packed Uniformly Adjacent, Multi-resolution Overlapping Spatial Data Ordering. U.S. Patent US8018458B2, 13 September 2011.
54. Vince, A.; Zheng, X. Arithmetic and Fourier Transform for the PYXIS Multi-Resolution Digital Earth Model. *Int. J. Digit. Earth.* **2009**, *2*, 59–79. [CrossRef]

55. Murray, A.B.; Lazarus, E.; Ashton, A.; Baas, A.; Coco, G.; Coulthard, T.; Fonstad, M.; Haff, P.; McNamara, D.; Paola, C. Geomorphology, complexity, and the emerging science of the Earth's surface. *Geomorphology* **2009**, *103*, 496–505. [CrossRef]
56. Dech, S. The Earth surface. In *Utilization of Space*, 1st ed.; Feuerbacher, B., Stoewer, H., Eds.; Springer: Berlin/Heidelberg, Germany, 2005; Volume 1, pp. 53–90.
57. Tarolli, P.; Arrowsmith, J.R.; Vivoni, E.R. Understanding earth surface processes from remotely sensed digital terrain models. *Geomorphology* **2009**, *113*, 1–3. [CrossRef]
58. Yue, T.X. Progress in earth surface modeling. *J. Remote Sens.* **2011**, *15*, 1105–1124.

water

MDPI

Article

A Harmony-Based Approach for the Evaluation and Regulation of Water Security in the Yellow River Water-Receiving Area of Henan Province

Zhiqiang Zhang [1,2], Weiwei Wang [1], Xiuyu Zhang [3,*], Hui Zhang [1], Li Yang [1], Xizhi Lv [4] and Xu Xi [5,*]

[1] College of Surveying and Geo-Informatics, North China University of Water Resources and Electric Power, Zhengzhou 450001, China; zhangzhiqiang@ncwu.edu.cn (Z.Z.); 15293594642@163.com (W.W.); huihui945726@163.com (H.Z.); zhyl@ncwu.edu.cn (L.Y.)
[2] Key Laboratory of Geospatial Technology for Middle and Lower Yellow River Regions (Henan University), Ministry of Education, Kaifeng 475000, China
[3] College of Water Resources, North China University of Water Resources and Electric Power, Zhengzhou 450001, China
[4] Yellow River Institute of Hydraulic Research, Zhengzhou 450003, China; nihulvxizhi@163.com
[5] School of Geography Science and Geomatics Engineering, Suzhou University of Science and Technology, Suzhou 215009, China
* Correspondence: zhangxiuyu@ncwu.edu.cn (X.Z.); xixu@mail.usts.edu.cn (X.X.)

Abstract: Water security, as a crucial component of national security, plays a significant role in maintaining regional stability and ensuring the healthy and rapid development of the economy and society. The Yellow River water-receiving area of Henan Province (YRWAR-HN) is selected as the research area in this study. Firstly, a comprehensive evaluation index system is constructed based on the actual water security problems of the research area, and the single index quantification–multiple indices syntheses–poly-criteria integration method (SMI-P) is introduced to quantify the water security degree of 14 cities in the YRWAR-HN from 2010 to 2021. Then, the obstacle degree model is used to identify the key obstacle indexes that restrict the improvement of water security. Finally, the harmonious behavior set optimization method is adopted to carry out the regulation of water security, and the improvement path of water security in the YRWAR-HN is formulated. The results indicate the following: (1) the water security degree of the YRWAR-HN shows a fluctuating upward trend, increasing from 0.4348 (2010) to 0.6766 (2021), a significant rise of 55.61%. The water security level improves from the relatively unsafe level to the relatively safe level. Hebi City exhibits the fastest rate of water security improvement, while Xinxiang City shows the slowest rate. (2) The density of the river network (X1) and the proportion of investment in water conservancy and environmental protection in the total investment (X15) are the two indexes with the highest obstacle degree, with the average obstacle degrees being 15.09% and 10.79%, respectively. (3) The combination of the composite regulation scenario and improvement Path 2 is the optimal regulation strategy for water security in the YRWAR-HN. From the implementation process, Luoyang, Sanmenxia, Jiyuan, Xuchang, and Shangqiu may prioritize improving their flood and drought disaster defense capabilities and emergency response capabilities, continuously enhancing the flood prevention and disaster reduction system. Zhengzhou, Kaifeng, Xinxiang, Jiaozuo, Anyang, Hebi, Pingdingshan, and Zhoukou may prioritize resolving the regional water supply and demand conflicts, balancing development and conservation, actively seeking transboundary and external water transfers, and strengthening the capacity for water conservation and intensive utilization. Puyang City may prioritize enhancing its comprehensive water environment management capabilities, increasing investment in water conservancy and the environment, improving production processes, reducing pollutant emissions, and mitigating agricultural non-point source pollution.

Keywords: water security; evaluation and regulation; obstacle factors recognition; harmony-based approach

1. Introduction

Water resources, as the source of life, essential for production, and the foundation of ecology, are critical to national food security, economic security, and ecological security. They are important strategic resources and security guarantees [1]. In the context of rapid urbanization and economic development, the demand for water resources development and utilization has increased greatly [2]. Since the 1980s, global freshwater use has been growing at a rate of about 1% per year, but the living water needs of more than 1 billion people remain unmet [3]. The global future water security situation is not optimistic. In 1999, the United Nations warned the world that if measures were not taken promptly, nearly 30% of the global population would be unable to access safe drinking water by 2025. Since the 21st century, water security has gradually become a research hotspot in the field of water resources [4–6], attracting the attention of many government and non-government organizations, including the United Nations, the World Bank, and the Asian Development Bank [7,8]. The World Ministerial Conference held in The Hague, Netherlands, in March 2000 [9], and the 10th discussion of the World Water Forum held in Stockholm, Sweden, in August 2000, both set "21st Century Water Security" as their conference theme. At the 2005 International Water Science Conference, water security was elevated to the level of national security. On World Water Day in 2013, the UN Water Organization released the "Water Security Analytical Brief," discussing the inclusion of a water-related sustainable development goal in the United Nations' Sustainable Development Goals [10]. The United Nations 2023 Water Conference held in New York, USA, in March 2023 called for countries to unite in addressing the water resource crisis and adopted a milestone "Water Action Agenda".

At present, the definition of water security is not fully unified. WaterAid defines water security from the perspective of water demand assurance and water disaster risk management, considering it as the reliability of obtaining sufficient quantity and quality of water to meet basic human needs, small-scale livelihoods, and local ecosystem services, while ensuring good risk management of water-related disasters [11]. Xia et al. [12] believes that water security is the ability to provide an adequate and quality-assured water supply needed for human production and living, to ensure society is protected from the erosion of water and drought disasters and water environment pollution, and to maintain the health of the natural environment and people's living conditions within the basin. Deng et al. [13] defines water security as the ability to sustainably supply sufficient and quality-compliant water at an affordable cost, ensuring the needs of human life, socioeconomic and ecological health, and guaranteeing the safety of water-related disaster prevention and control. Wang et al. [14] points out from a national perspective that water security is the state and capacity to ensure the stability of the nation, enhance people's well-being, eliminate water and drought threats, and ensure sustainable social development and ecological environment health. Although the definition of water security is not unified, it is generally agreed that water security involves water systems, socioeconomic systems, and ecological environment systems [15–17]. It primarily includes the ability to meet the water demands of economic, social, and ecological environments [18], the sustainability of the water system itself, and the risk management capabilities for water-related disasters such as droughts and floods [19].

Water security evaluation is fundamental to addressing water security issues and is an important branch of water security research. The key to water security evaluation lies in constructing a scientifically comprehensive water security evaluation index system without deviating from the core connotations of water security. Early water security evaluations focus on using single indicators to evaluate the sustainability of water systems. Widely used indicators include the Water Resources Stress Index (WRSI), the Water Resources Vulnerability Index (WRVI), and the development and utilization degree of water resources. For instance, Falkenmark et al. [20] developed the Water Scarcity Index (IWS) based on per capita water resources to measure the degree of regional water scarcity, which has been widely used in global water security evaluation [21–23]. Raskin et al. [24] introduced the

coefficient of variation of the precipitation to construct the IWRV, assessing the vulnerability and sustainability of water resources at both national and regional scales. As the concept of water security has been continuously refined, existing studies have constructed comprehensive water security evaluation systems from different evaluation dimensions. According to different concepts of constructing indicator systems, they can be roughly divided into two categories. One category approaches water security from a systems theory perspective, dividing the complex system into different subsystems, each of which selects representative indicators to construct a water security evaluation system. The advantage of this method is the clear connotation of water security, emphasizing the coordination between subsystems, facilitating the analysis of key indicators affecting water security, and the formulation of regulation plans. For example, Deng et al. [13] constructed a water security evaluation index system based on water quantity, water quality, sustainability, water price and supply affordability, and flood safety. Wang et al. [25] developed an indicator system from the dimensions of water resources balance capacity, water resources pressure and driving force, and water resources development and utilization capacity, evaluating the comprehensive water resource carrying capacity of 31 provinces in China. Another category is centered around water systems, considering the pressures from the economic–social–ecological system on the water system, the state and response of the water system itself, and human management of the water system; this approach uses fixed models as the framework for constructing indicator systems. These models include the Driver-State-Response (DSR) model [26], the Pressure-State-Response (PSR) model [27], the Driver-Pressure-State-Impact-Response (DPSIR) model [28], and the Driver-Pressure-State-Impact-Response-Management (DPSIRM) model [29].

On the basis of the index system construction, the appropriate comprehensive evaluation method is usually selected to quantify the degree of regional water security. Widely used comprehensive evaluation methods include fuzzy mathematics, artificial neural networks, set pair analysis (SPA), the cloud entropy model, and the SMI-P. Cai et al. [30] used the fuzzy comprehensive evaluation and entropy weight methods to establish a water security evaluation model based on the water footprint. Deng et al. [31] utilized the SPA to establish a comprehensive evaluation index system covering water resources, socioeconomics, and the ecological environment, and systematically quantified the water resource carrying capacity for the current and future periods of the Hanjiang River Basin in China. Qiu et al. [32] constructed a water ecological security evaluation index system for the Yellow River Basin based on the PSR model and calculated the water ecological security index for 62 cities using the SMI-P method. It is worth noting that due to influencing factors, regional water security is usually at a low level, necessitating optimization and regulation research to develop strategies for improving regional water security. The behavior set optimization method is a commonly used optimization and regulation method. Its basic idea is to establish the constraints and objective functions for optimization and regulation, build the optimization and regulation behavior set, and finally determine the optimal regulation behavior based on the principle of maximizing the objective function [33]. For example, Zuo et al. [34,35] treated the human and water systems as a composite system and constructed a harmonious behavior set of human–water relationships based on the quantitative evaluation of human–water relationships, with the objective function of maximizing harmony.

The Yellow River water-receiving area of Henan Province (YRWAR-HN) is a densely populated and economically significant area in the basin, playing a crucial role in implementing the national strategy for the Yellow River [36]. Due to long-term sediment deposition, the riverbed elevation has continually risen, resulting in the famous elevated river in the Henan section, which frequently suffers from flood disasters, making water security issues particularly prominent [37]. To determine the water resource carrying capacity in the YRWAR-HN, Zhang et al. [38] developed an index system encompassing three criteria: water resources, ecological environment, and socioeconomic factors. They applied a TOPSIS model with combined weights based on the analytic hierarchy process (AHP)

and the entropy weight method (EWM) to evaluate the water resource carrying capacity in the region from 2010 to 2021. Additionally, Zhang et al. [39] constructed a high-quality development evaluation index system from four perspectives: resources, ecology, economy, and society. They employed the SMI-P method to assess the development level of the YRWAR-HN, and used an embedded system dynamics approach to develop and apply a regional high-quality development regulation model. However, there are few studies on water security evaluation and regulation for the YRWAR-HN, and the spatiotemporal characteristics and enhancement strategies of water security in this section remain unclear, necessitating in-depth research. Given this, this study selects the YRWAR-HN as a study area, and introduces the harmony-based method (including the SMI-P and the HBSO) to conduct water security evaluation and regulation research. It analyzes the spatiotemporal characteristics and key obstacle factors of water security in the YRWAR-HN from 2010 to 2021 and proposes pathways for improving water security in this section, aiming to provide guidance for enhancing water security in the YRWAR-HN.

2. Study Area

The YRWAR-HN includes 14 prefecture-level cities: Zhengzhou, Kaifeng, Luoyang, Pingdingshan, Anyang, Hebi, Xinxiang, Jiaozuo, Puyang, Xuchang, Sanmenxia, Shangqiu, Zhoukou, and Jiyuan (Figure 1). This area covers a total of approximately 104,000 km^2, accounting for 62.3% of the total area of Henan Province. The terrain is higher in the southwest and lower in the northeast. The southwestern part belongs to the Funiu Mountain, characterized mainly by mountains and hills. The central and northeastern parts are relatively flat, forming part of the North China Plain, which is a major grain-producing area in China. Most of the YRWAR-HN are located in the warm temperate, semi-humid, and semi-arid regions, characterized by a temperate continental monsoon climate with distinct transitional features. Due to the influence of the monsoon climate, rainfall distribution is uneven, with humid and rainy summers and dry winters. Precipitation is concentrated mainly between June and September, accounting for 55% to 75% of the annual total, with a long-term average precipitation of 658.46 mm and an average annual temperature ranging from 12.1 °C to 15.7 °C [40]. The summer season is sometimes affected by typhoons, bringing extreme heavy rainfall events, such as the extreme downpour in July 2021, which led to severe urban flooding [41].

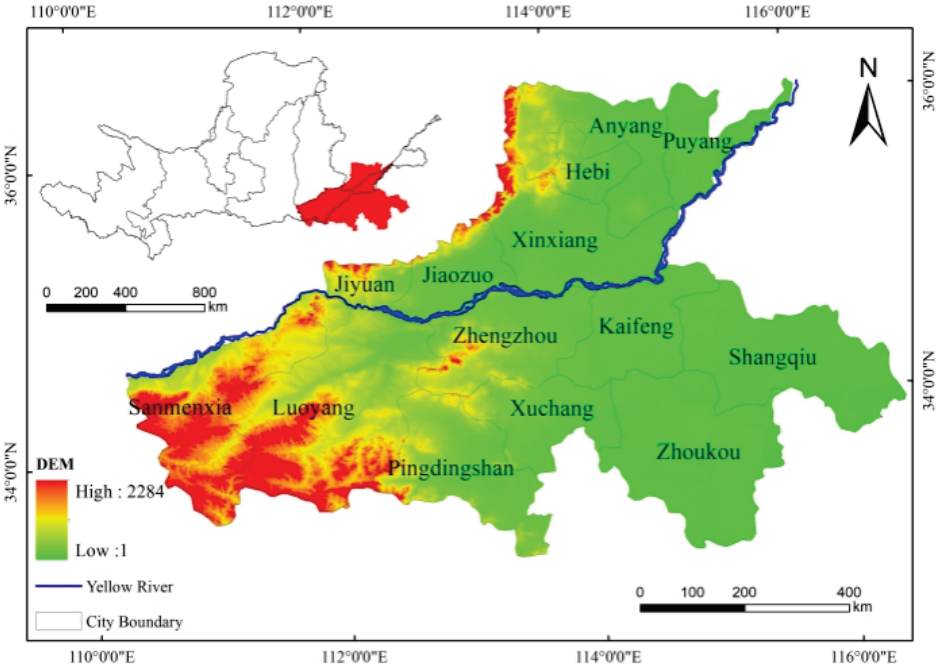

Figure 1. Overview Map of the Study Area.

The YRWAR-HN is a densely populated area and a major economic belt in the Yellow River Basin, playing a significant role in implementing the national strategy for the Yellow River. However, due to long-term sediment deposition, the riverbed elevation has continuously risen, forming an above-ground "hanging river," which frequently subjects the region to flood disasters. According to incomplete statistics, over the recorded history of more than 2000 years, the lower reaches of the Yellow River have breached and flooded over 1500 times, with more than twenty major course changes and six significant course alterations. Simultaneously, with the rapid economic and social development, the region's water consumption and pollutant discharge have continuously increased, leading to prominent contradictions between water supply and demand, and severe water environment pollution issues.

3. Methodology

3.1. Evaluation Index System

This study, based on the actual issues of the YRWAR-HN, constructs a comprehensive water security evaluation index system with a four-tier hierarchical structure (Table 1). First, the evaluation objective is determined, which is to calculate the water security degree of the YRWAR-HN. Then, considering the prominent water security issues in this area—flood disasters, water supply–demand imbalances, and water environment pollution—the evaluation dimensions are determined as flood and drought disaster defense, water supply–demand conflict, and water environment pollution. In the flood and drought disaster defense dimension, the focus is on evaluating the flood disaster defense capability, drought defense capability, and emergency disaster response capability. In the water supply–demand conflict dimension, emphasis is placed on the regional characteristics of water resources, the development and utilization degree of water resources, and water use efficiency. In the water environment pollution dimension, the focus is on the pressure and response regarding water environment pollution prevention. Based on the determination of the evaluation content, the corresponding evaluation indicators are comprehensively established by integrating existing research [42–46] and adhering to the principles of systematicity, representativeness, and operability. For example, when selecting the evaluation indicators of regional characteristics of water resources, per capita water resources, the water yield modulus and the precipitation are usually selected in the reference [43,44]. In this study, the per capita water resources are finally selected as the evaluation index according to the data availability of the YRWAR-HN.

3.2. Calculation of Evaluation Index Data

The indicator data for river network density is derived from satellite remote sensing images. First, cloud-free landsat TM/ETM+/OLI images (2010–2021) of the YRWAR-HN from March to May are downloaded from the USGS website and preprocessed. The Modified Normalized Difference Water Index (MNDWI) is used to extract annual surface water bodies, and the results are corrected through human–machine interaction. Then, the river network centerline is extracted by mathematical morphology, and the river length of each city in the YRWAR-HN from 2010–2021 is calculated. Finally, the river network density for each city in the YRWAR-HN is calculated. The calculation formula is shown in Appendix A (Equation (A1)).

The other indicator data are obtained from the "Statistical Yearbook", "Water Resources Bulletin", and "Economic and Social Development Bulletin" of Henan Province and its cities from 2010 to 2021. A small amount of missing data is obtained through interpolation and extended calculations.

Table 1. Comprehensive Evaluation Index System for Water Security.

Objective Layer	Dimension Layer	Content Layer	Indicator Layer	Index Number	Unit
water security evaluation in the YRWAR-HN	flood and drought disaster defense	flood disaster defense capability	river network density	X1	km^{-1}
			drainage pipeline density in built-up areas	X2	km^{-1}
		drought defense capability	number of electromechanical wells per unit area of cultivated land	X3	number/10^3 hm^2
		emergency disaster response capability	hospital beds per capita	X4	number/10^4 capita
	water supply and demand	regional characteristics of water resources	per capita water resources	X5	m^3/capita
		development and utilization of water resources	utilization rate of surface water resources	X6	%
			exploitation rate of groundwater resources	X7	%
		water use efficiency	per capita comprehensive water consumption	X8	m^3/capita
			water consumption per 10^4 CNY GDP	X9	t/10^4 CNY
			water consumption per 10^4 CNY of industrial value added	X10	t/10^4 CNY
	water environment pollution	pressure	per capita COD emissions	X11	t/capita
			per capita SO_2 emissions	X12	t/capita
			fertilizer application per unit of sown area	X13	t/10^3 hm^2
		response	urban sewage treatment rate	X14	%
			the proportion of investment in water conservancy and environmental protection in the total investment	X15	%

3.3. Single Index Quantification–Multiple Indices Syntheses–Poly-Criteria Integration Method (SMI-P)

The SMI-P is a widely used comprehensive evaluation method [47], and it has been extensively applied in the fields of water resources management [48], environmental health evaluation, economic management, and more. This study extends its application to water security evaluation, and introduces the concept of "water security degree (WSD)" to measure the water security level of each city in the YRWAR-HN. Correspondingly, each evaluation dimension has a sub-water security degree (SWSD), and each indicator has an index water security degree (IWSD), with values ranging from [0, 1].

3.3.1. Single Index Quantification

Based on the fuzzy mathematics theory, this study establishes a piecewise linear membership function to calculate the SWSD for each indicator. It is assumed that each indicator has five characteristic values: (a) the worst value, (b) the worse value, (c) the medium value, (d) the better value, and (e) the optimal value [49–51]. Table 2 shows the characteristic values of each indicator. For positive indicators, the SWSD corresponding to the five characteristic values are 0, 0.3, 0.6, 0.8, and 1.0, respectively. For negative indicators, the SWSD corresponding to the five characteristic values are 1.0, 0.8, 0.6, 0.3, and 0, respectively. The calculation formula is shown in Appendix A, Equations (A2) and (A3).

Table 2. Quantitative Indicator Node Characteristic Values and Indicator Weights.

Index Number	Worst Value	Worse Value	Medium Value	Better Value	Optimal Value	Indicator Weights	Indicator Type
X_1	0.01	0.02	0.03	0.05	0.22	0.31	↑
X_2	3.47	6.78	8.00	9.00	18.70	0.22	↑
X_3	19.35	145.96	200.46	246.36	933.03	0.23	↑
X_4	23.10	42.94	51.78	63.08	147.57	0.24	↑
X_5	57.78	168.60	212.37	295.66	1304.09	0.22	↑
X_6	0.65	0.55	0.40	0.25	0.10	0.12	↓
X_7	0.90	0.70	0.55	0.40	0.20	0.19	↓
X_8	628.46	466.88	305.30	231.99	158.69	0.16	↓

Table 2. *Cont.*

Index Number	Worst Value	Worse Value	Medium Value	Better Value	Optimal Value	Indicator Weights	Indicator Type
X_9	80.00	65.00	50.00	30.00	15.00	0.17	↓
X_{10}	70.00	55.00	40.00	25.00	10.00	0.15	↓
X_{11}	0.0402	0.0142	0.0096	0.0031	0.0001	0.15	↓
X_{12}	0.0899	0.0175	0.0062	0.0026	0.0001	0.18	↓
X_{13}	619.90	607.40	584.10	564.40	481.20	0.23	↓
X_{14}	60.00	70.00	85.00	90.00	100.00	0.18	↑
X_{15}	4.00	7.00	12.00	17.00	22.00	0.26	↑

Notes: "↑" indicates a positive indicator, meaning the higher the indicator value, the higher the water security degree. Conversely, "↓" indicates a negative indicator, meaning the higher the indicator value, the lower the water security degree.

3.3.2. Weighted Calculation of Multiple Indicators

Based on single index quantification, a multi-indicator weighted average model is established to calculate the SWSD of each evaluation dimension. The calculation formula is shown in Appendix A (Equation (A4)). In this study, the entropy weight method is used to determine the weights of each indicator, and the results are shown in Table 2.

3.3.3. Multi-Criteria Integrated Calculation

Based on the evaluation results of all dimensions, a multi-dimensional integration model is established to calculate the water security degree of each city for each year. The calculation formula is shown in Appendix A (Equation (A5)). Based on existing research [52], the water security levels of the YRWAR-HN are divided into six levels using the equal interval principle, as shown in Table 3.

Table 3. Classification Standards for Water Security Levels.

Serial Number	Water Security Level	Range of Wsd Values
1	Safe	$0.83 < WSD \leq 1.00$
2	Relatively Safe	$0.67 < WSD \leq 0.83$
3	Basically Safe	$0.50 < WSD \leq 0.67$
4	Relatively Unsafe	$0.33 < WSD \leq 0.50$
5	Unsafe	$0.17 < WSD \leq 0.33$
6	Severely Unsafe	$0.00 < WSD \leq 0.17$

3.4. Obstacle Degree Model

The obstacle degree model can identify factors that have significant restrictive effects on the evaluation results and has been widely used in ecological security research [53]. In this study, it is applied to identify key obstacle indicators for water security improvement in the YRWAR-HN. The calculation formula is shown in Appendix A (Equations (A6)–(A8)).

3.5. Water Security Regulation

This study draws on the Harmony Behavior Optimization Method and proposes a water security regulation method based on the optimization of solution sets. The core idea of this method is to first establish a set of water security regulation strategies, then calculate the water security degree of each strategy, and finally determine the optimal or relatively optimal regulation strategy with the objective function of maximizing the water security degree.

This study initially sets up five water security regulation schemes, with each scheme having five improvement paths (increasing key obstacle indicators by 10%, 20%, 30%, 40%, and 50% based on the increments in Scheme 1). Taking Path 1 as an example, the five regulation schemes are introduced as follows, which are detailed in Appendix B. Scheme 1 (baseline scenario): maintain the current development model, with each evaluation indicator keeping the original growth rate over the past 12 years (2010–2021). Scheme 2

(enhanced flood and drought disaster defense scenario): increase the top 50% of the indicators in the flood and drought disaster defense dimension by 1.1 times the growth rate of Scheme 1, with the remaining indicators maintaining their original growth rates. Scheme 3 (optimized supply and demand scenario): increase the top 50% of the indicators in the water supply and demand dimension by 1.1 times the growth rate of Scheme 1, with the remaining indicators maintaining their original growth rates. Scheme 4 (ecological protection scenario): increase the top 60% of the indicators in the water environment pollution dimension by 1.1 times the growth rate of Scheme 1, with the remaining indicators maintaining their original growth rates. Scheme 5 (composite regulation scenario): increase the eight indicators enhanced in Schemes 2–4 by 1.1 times the growth rate of Scheme 1, with the remaining indicators maintaining their original growth rates. Based on data from 2010–2021, the water security degree of each city in the YRWAR-HN in 2030 is simulated and calculated for the five schemes under the five improvement paths to determine the optimal regulation scheme.

4. Result

4.1. Spatiotemporal Variation in Water Security in the YRWAR-HN

4.1.1. Spatial Pattern

This study selects three representative years, 2010, 2015, and 2021, to reveal the spatial pattern of water security in the YRWAR-HN, as shown in Figure 2. It is evident that in all three years, the spatial pattern of water security in the YRWAR-HN exhibits significant regional characteristics, generally showing a spatial aggregation that decreases radially from the provincial capital, Zhengzhou. In 2010, the areas with basically safe water security levels are concentrated in the western part of Zhengzhou, gradually forming a basically safe spatial cluster around Jiyuan and Luoyang. The surrounding cities, however, formed a relatively unsafe spatial cluster, with the northern cluster around Jiaozuo-Xinxiang-Puyang-Anyang centered around Zhengzhou, and the southern cluster around Pingdingshan-Xuchang-Zhoukou-Shangqiu, with Anyang and Kaifeng at the outer edge of the study area falling into the unsafe spatial cluster. In 2015, water security in the YRWAR-HN presents a patchy distribution. With Luoyang as the center, the basically safe spatial cluster expanded further, gradually forming a basically safe spatial cluster centered around Sanmenxia-Luoyang-Jiyuan-Zhengzhou-Xuchang. The relatively unsafe areas are primarily located to the northeast and east of Zhengzhou. By 2021, the water security in the YRWAR-HN exhibits a core–periphery distribution, forming a relatively safe spatial cluster with dual centers of Zhengzhou and Hebi, involving Sanmenxia-Luoyang-Jiyuan and Pingdingshan-Xuchang-Zhoukou-Shangqiu. The surrounding areas gradually formed basically safe spatial clusters around Jiaozuo-Xinxiang-Kaifeng-Anyang-Puyang.

4.1.2. Temporal Variation

Figure 3 shows the temporal variation in water security in all cities in the YRWAR-HN from 2010 to 2021. It is evident that the water security levels of all cities in the YRWAR-HN exhibit an overall upward trend. Among them, Hebi City has the fastest growth rate (0.0388 yr^{-1}), while Xinxiang City has the slowest growth rate (0.0130 yr^{-1}). Hebi City shows the largest increase, rising from an unsafe level to a relatively safe level. Xinxiang City shows the smallest increase, rising from a relatively unsafe level to a basically safe level. During the study period, the water security degree of Hebi City increased by 35.11% from 2020 to 2021, mainly due to a 106.53% improvement in the supply–demand balance of water resources in 2021 compared to 2020. Notably, the per capita water resources saw the most significant increase, rising by 626.92%. According to relevant data [54], the total water resources in all prefecture-level cities within the YRWAR-HN increased in 2021 compared to the long-term average. Hebi City experienced the largest increase, reaching 321.1%. Sanmenxia City experienced a trend of first increasing and then decreasing, with the highest degree recorded in 2020 (0.7267). This is likely due to a significant increase in the proportion of investments in water conservancy and environmental protection in 2020 compared to

2019, which rose by 17.48%. Zhengzhou, Luoyang, Sanmenxia, and Jiyuan consistently maintained a high level, with values exceeding 0.5 since 2015. In contrast, Kaifeng City had generally low water security levels, with values below 0.5 in all years before 2019.

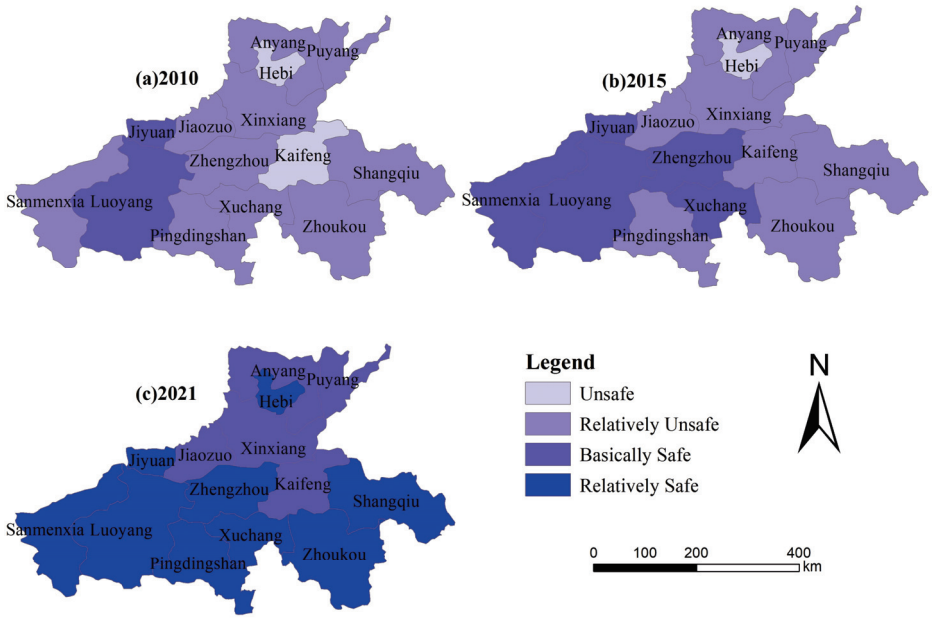

Figure 2. Spatial Distribution of Water Security in the YRWAR-HN.

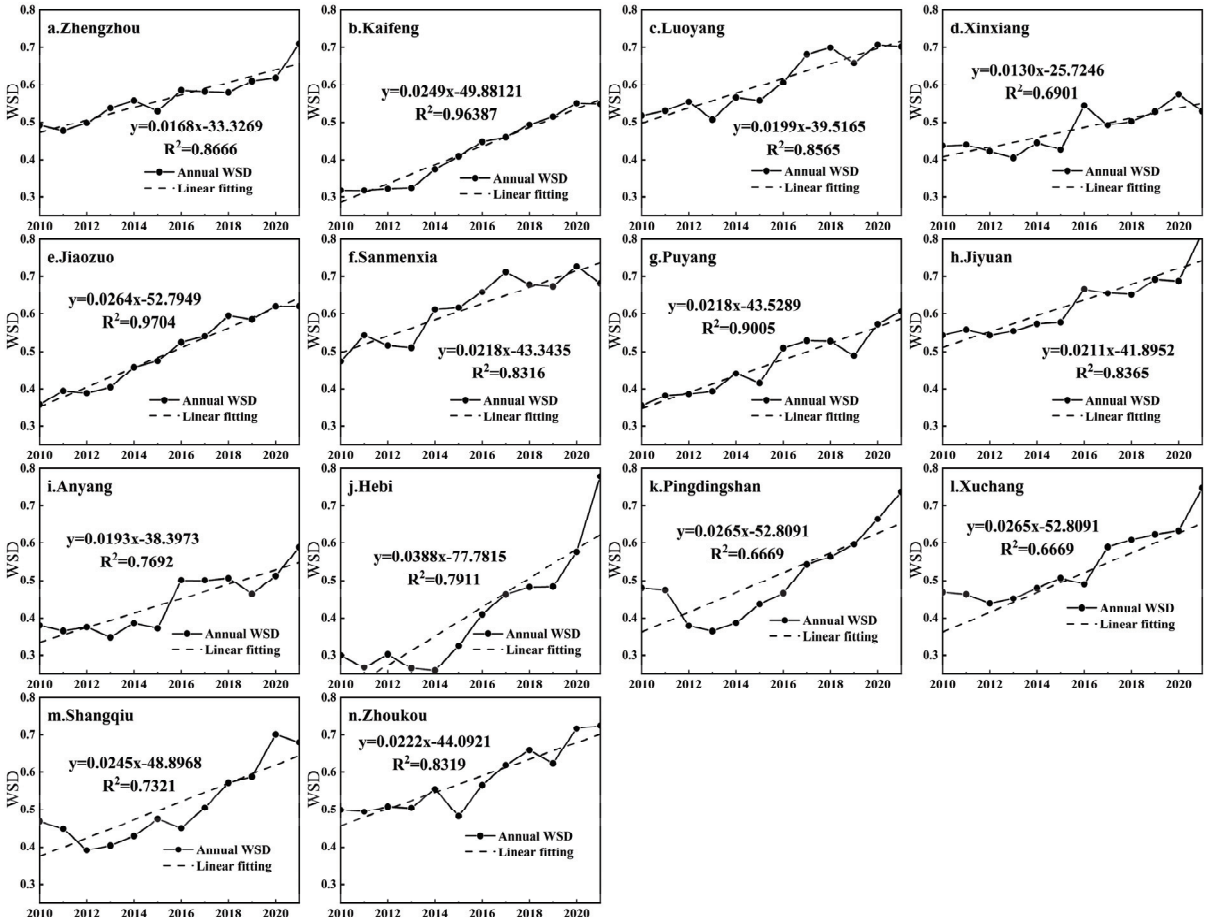

Figure 3. Temporal Variation in Water Security in the YRWAR-HN from 2010 to 2021.

4.2. Diagnosis of Water Security Obstacle Factors in the YRWAR-HN

Figure 4 shows the obstacle degrees of water security evaluation indicators for all cities in the YRWAR-HN. It is evident that the key obstacle indicators vary slightly among different cities, and the proportions of the same indicator differ between cities. Overall, the key indicators affecting water security in the YRWAR-HN include river network density (X1), hospital beds per capita (X4), per capita water resources (X5), groundwater exploitation rate (X7), water consumption per 104 CNY GDP (X9), fertilizer application per unit sown area (X13), urban sewage treatment rate (X14), and the proportion of investment in water conservancy and environmental protection in the total investment (X15). Comparing the proportions of the key obstacle indicators across all cities, X1 is the primary obstacle indicator for all cities except Zhengzhou, Jiaozuo, Jiyuan, and Puyang, indicating that X1 is a significant constraint on water security in the YRWAR-HN. The obstacle degree of X15 is greater than 10% in all cities except Luoyang, Jiyuan, and Hebi, reflecting that efforts to control water environment pollution need to be improved, making this proportion another constraint on water security. As the capital of Henan Province, Zhengzhou has a high population density and a per capita water resource obstacle degree of 16.21%, making it the primary factor restricting water security in the city. This is consistent with the results of Zhang et al. [38], who also find that Zhengzhou has a low water resource carrying capacity rating, with limited per capita water resources and severe water shortages. This indicates that the supply–demand imbalance of water resources in Zhengzhou is particularly acute, highlighting the severity of the water scarcity issue.

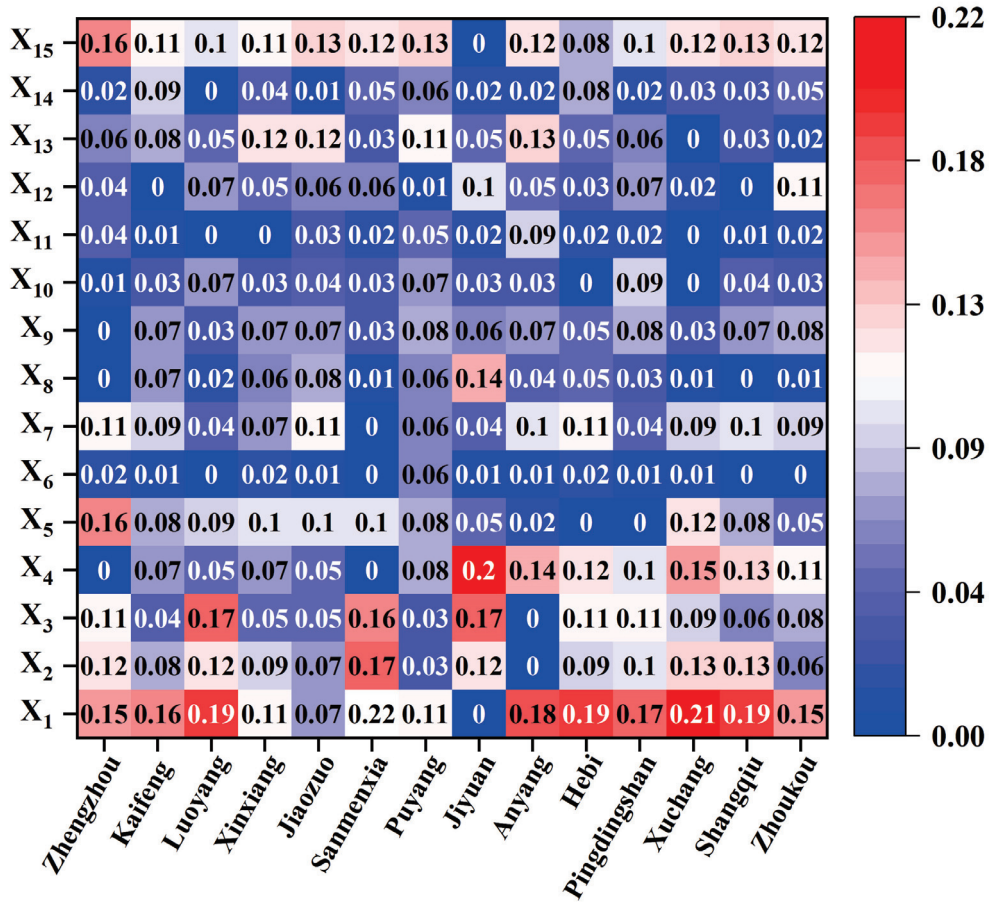

Figure 4. Obstacle Degrees of Water Security Evaluation Indicators for All Cities in the YRWAR-HN.

4.3. Water Security Regulation in the YRWAR-HN

Figure 5 compares the water security degree in 2030 for all cities along the YRWAR-HN under five improvement paths and five schemes, while Table 4 displays the average water

security degree for these cities under the different schemes and improvement paths by 2030. It is evident that there has been a significant improvement in water security across different paths and schemes for all cities compared to 2021. The composite scenario (Scheme 5) achieves the highest water security degree, indicating that improving indicators with greater obstacles can effectively enhance the water security degree. Comparing Schemes 2, 3, and 4, Zhengzhou, Kaifeng, Xinxiang, Jiaozuo, Anyang, Hebi, Pingdingshan, and Zhoukou cities show optimal results under Scheme 3, suggesting a priority to resolve water supply and demand issues. Luoyang, Sanmenxia, Jiyuan, Xuchang, and Shangqiu cities show optimal results under Scheme 2, indicating a need to prioritize the enhancement of regional flood and drought disaster defense capabilities. Puyang City performs best under Scheme 4, suggesting a priority to strengthen ecological environment construction, increase investment in ecological efforts, improve production processes, and reduce pollutant emissions. Among the different improvement paths in the composite scenario, the order of performance from highest to lowest is Path 5 > Path 4 > Path 3 > Path 2 > Path 1, with average increases of 0.32%, 0.37%, 0.48%, and 0.63%, respectively. This shows that a 20% increase in key obstacle indicators results in the largest water security improvement and cost-effectiveness for the YRWAR-HN, with diminishing returns as investments continue to rise.

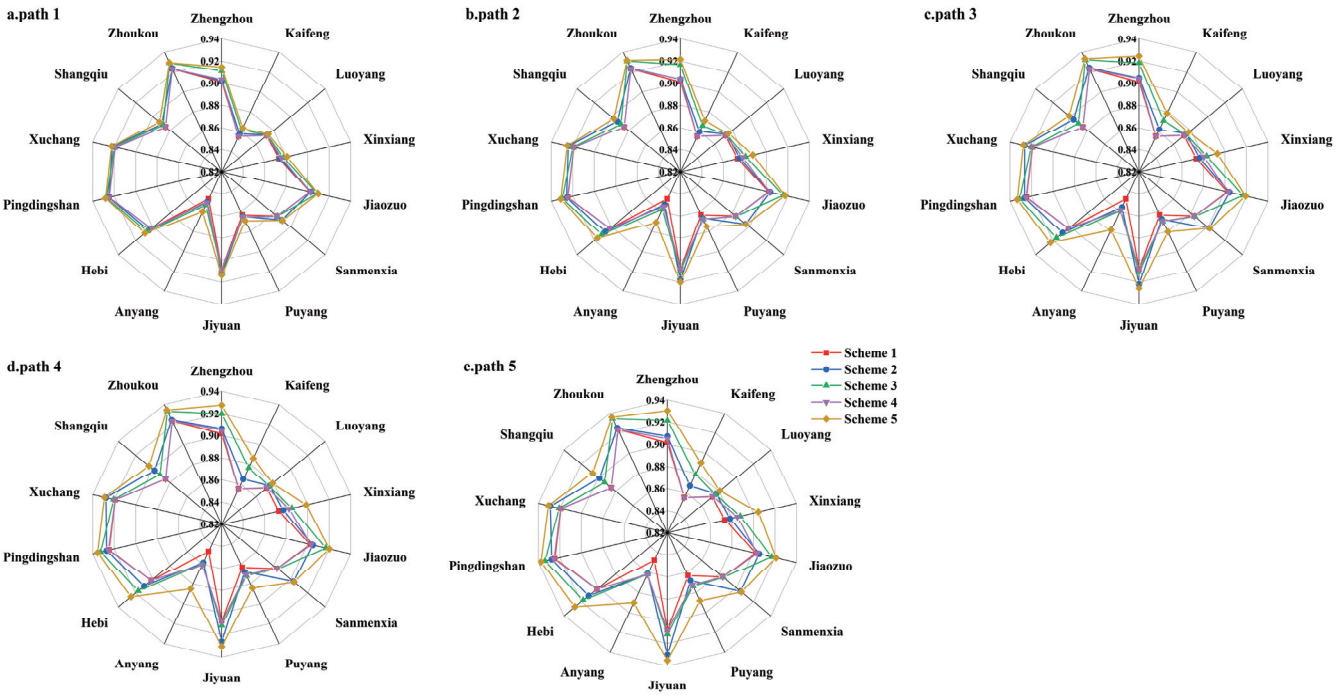

Figure 5. Water Security Degree in 2030 for All Cities along the YRWAR-HN under Different Regulation Strategies.

Table 4. Average Water Security Degree by 2030 for the YRWAR-HN under Different Regulation Strategies.

	Scheme 1	Scheme 2	Scheme 3	Scheme 4	Scheme 5
Path 1	0.8901	0.8923	0.8939	0.8909	0.8970
Path 2	0.8901	0.8945	0.8967	0.8915	0.9026
Path 3	0.8901	0.8965	0.8984	0.8922	0.9069
Path 4	0.8901	0.8980	0.8998	0.8927	0.9103
Path 5	0.8901	0.8993	0.9009	0.8931	0.9132

Notes: Scheme 1 represents the baseline scenario. Scheme 2 corresponds to the enhanced flood and drought disaster defense scenario. Scheme 3 represents the scenario with optimized supply and demand. Scheme 4 corresponds to the ecological protection scenario. Scheme 5 represents the composite regulation scenario. Detailed regulation schemes can be found in Section 3.5 on Water Security Regulation.

5. Discussion

This study, based on an analysis of the prominent water security issues in the YRWAR-HN, constructs a water security evaluation index system. This system is significant for quantifying the water security status in these areas, identifying key factors that constrain improvements in water security, and developing scientifically sound optimization and regulation strategies. Although the applicability of this index system to other study areas requires further validation, the concepts underlying its construction, the selection of indicators, and the methods of calculation can serve as a reference for the development of comprehensive water security evaluation systems in other regions.

Overall, the water security degree in the YRWAR-HN shows a fluctuating upward trend, and the conclusion is basically consistent with that of Zuo et al. [42]. Compared to 2010 (0.4348), the water security degree of the YRWAR-HN in 2021 has significantly improved, with the average water security degree reaching 0.6766, upgrading from a relatively unsafe level to a relatively safe level. Since 2010, China's water affairs have rapidly developed, with the national level formulating water security plans for the "12th Five-Year Plan" and "13th Five-Year Plan". Henan Province has thoroughly implemented the national water security plans and issued a series of planning documents, such as the "Henan Province Comprehensive Disaster Prevention and Reduction Plan" and the "13th Five-Year Plan for Building a Water-Saving Society in Henan Province", leading to a significant enhancement in disaster defense capabilities and water use efficiency. This may be the fundamental reason for the significant improvement in overall water security in the YRWAR-HN. Among the all cities in the YRWAR-HN, Hebi City has seen the largest increase in water security during the study period. This could be due to the city's water security being at a relatively unsafe level in 2010 with substantial potential for improvement, and the significant increase in water conservancy construction investment in recent years, where the proportion of X15 increased from 6.75% in 2010 to 19.7% in 2021, a rise of 191.77%.

There is still considerable room for improvement in the water security of all cities along the YRWAR-HN. According to the water security evaluation results of 2021, no city has reached a safe level, while Jiaozuo, Kaifeng, Xinxiang, Anyang, and Puyang cities remained at a basically safe level, indicating significant water security challenges in the YRWAR-HN, particularly in Kaifeng and Xinxiang. Through the analysis of obstacle degree, it is found that X1, X5, and X15 are the top three indexes of obstacle degree in Kaifeng City. Therefore, it is imperative for Kaifeng to increase investment in water conservancy projects, implement river–lake connectivity projects, dredge congested rivers, and excavate new channels. Meanwhile, Kaifeng City should actively seek external water transfers and through-flow water via water rights trading to increase the regional available water resources. For Xinxiang City, X1, X13, and X15 are the top three indexes of obstacle degree. Xinxiang City should therefore focus on improving its capabilities in flood and drought disaster defense and water environment pollution control, including carrying out river–lake connectivity projects, increasing the regional river network density, and advancing the comprehensive management of agricultural non-point source pollution by implementing precise fertilization and replacing chemical fertilizers with organic ones. For Zhengzhou City, X5, X15, and X1 are the top three obstacle indexes. Therefore, Zhengzhou City should prioritize obtaining more external water resources (such as South-to-North Water Transfer Project water and Yellow River water) through increased water conservancy investment and water rights trading. Meanwhile, it should also increase the number of agricultural irrigation wells to enhance the drought resistance of agricultural production.

According to the regulation results, employing Scheme 5 will allow the achievement of the maximum increase in water security across all cities in the YRWAR-HN, albeit with substantial investment costs. Given limited investment capacity, priority should be given to enhancing flood and drought disaster defense capabilities and emergency response systems in Luoyang, Sanmenxia, Jiyuan, Xuchang, and Shangqiu. This includes continuously improving flood prevention and disaster mitigation systems, advancing the construction of stormwater drainage channels in urban areas, dredging and clearing drainage ditches, and

enhancing monitoring, forecasting, early warning, rehearsal, contingency planning, and flood control scheduling. Zhengzhou, Kaifeng, Xinxiang, Jiaozuo, Anyang, Hebi, Pingdingshan, and Zhoukou should prioritize resolving regional water supply and demand conflicts by improving water conservancy projects, water network operation scheduling plans, and emergency water dispatch plans, as well as implementing inter-basin and inter-regional water resource scheduling projects. A long-term mechanism for the integrated regulation of atmospheric water, surface water, and groundwater should be established. Puyang should focus on enhancing its water environment management capabilities, strengthening collaboration with neighboring cities and counties, promoting integrated ecological management and restoration of trans-regional river basins, increasing investments in water and environmental projects, improving production processes, reducing pollutant emissions, and mitigating agricultural non-point source pollution.

6. Conclusions

This study focuses on the actual water security issues in the YRWAR-HN. By establishing a water security evaluation index system and employing the SMI-P evaluation methodology, a quantitative evaluation of the water security degrees of 14 prefecture-level cities in the YRWAR-HN from 2010 to 2021 is conducted. Furthermore, using the obstacle model, key obstacle indicators are identified. Through comparative analysis of regulation strategies, an optimized strategy for water resources in the YRWAR-HN is formulated. The main conclusions are as follows:

(1) From 2010 to 2021, the water security degree in the YRWAR-HN shows a fluctuating upward trend. The water security degree increases from 0.4348 in 2010 to 0.6766 in 2021, an increase of 55.61%, with the water security level improving from relatively unsafe to relatively safe. Hebi City experiences the fastest increase in water security degree, rising from 0.2997 in 2010 to 0.7788 in 2021, an increase of 159.86%. Xinxiang City has the slowest rate of improvement, with water security degree of 0.4372 in 2010 and 0.5294 in 2021, an increase of 21.1%.

(2) As of 2021, Jiaozuo, Xinxiang, Kaifeng, Anyang, and Puyang remain at a basically safe level. Spatially, a relatively safe cluster is centered around Zhengzhou and includes Sanmenxia, Luoyang, Jiyuan, Pingdingshan, Xuchang, Zhoukou, and Shangqiu. Notably, the water security levels of Xinxiang and Kaifeng remain below 0.55.

(3) Based on the average obstacle degree of each indicator, river network density (X1) and the proportion of investment in water conservancy and environmental protection in the total investment (X15) are the two indicators with the highest obstacle degree, with average obstacle degrees of 15.09% and 10.79%, respectively. Therefore, it can be inferred that increasing water conservancy and environmental investments, and carrying out scientifically sound river–lake connectivity projects, can significantly enhance the water security level of the YRWAR-HN.

(4) The optimal water security regulation strategy for the YRWAR-HN is a combination of Regulation Scheme 5 and Enhancement Path 2. In terms of implementation, Luoyang, Sanmenxia, Jiyuan, Xuchang, and Shangqiu should prioritize improving their flood and drought disaster prevention capabilities and emergency response capacity, continuously refining their flood control and disaster mitigation systems. Zhengzhou, Kaifeng, Xinxiang, Jiaozuo, Anyang, Hebi, Pingdingshan, and Zhoukou should focus on resolving regional water supply–demand conflicts by balancing water sourcing and conservation, actively securing transboundary and external water transfers, and enhancing the efficient use of water resources. Puyang should prioritize improving its comprehensive water environment management capacity by increasing investment in water conservancy and environmental protection, improving production processes, reducing pollutant emissions, and mitigating agricultural non-point source pollution.

This study addresses the actual water security issues in the YRWAR-HN and, based on data availability in the study area, establishes a water security evaluation index system. This provides a reference and guidance for water security evaluation in other regions. It is

important to note that water security challenges and data availability vary across regions, so the applicability of this index system in other areas requires further validation. In future research, we aim to develop a more universally applicable water security evaluation index system and to further refine the water security regulation strategies for the YRWAR-HN, offering more specific regulation recommendations tailored to different prefecture-level cities.

Author Contributions: Overall design, Z.Z.; methodology, W.W. and X.Z.; software, H.Z. and L.Y.; formal analysis, X.L. and X.X.; writing—original draft preparation, W.W.; writing—review and editing, Z.Z.; funding acquisition, X.Z. All authors have read and agreed to the published version of the manuscript.

Funding: This research was funded by the Open Fund of Key Laboratory of Geospatial Technology for the Middle and Lower Yellow River Regions (Henan University), Ministry of Education (GTYR202106); the Henan Province science and technology research and development plan joint fund project (232103810102); the Science and Technology Research Project of Henan Province (212102311156); the Open Research Fund Project of Key Laboratory of Yellow River Sediment of Ministry of Water Resources (HHNS202005), the Research Fund Project of Key Laboratory of Water Management and Water Security in Yellow River Basin, Ministry of Water Resources (2023-SYSJJ-04); and the National Natural Science Foundation of China (42007423; 42201097).

Data Availability Statement: Data available on request due to privacy: The data presented in this study are available on request from the corresponding author.

Acknowledgments: We would like to express our respect and gratitude to the anonymous reviewers and editors for their professional comments and suggestions. In addition, thanks to Yongfeng Zhao, Zhiwei Xu, Wenzhe Wang, and Yuyang Qi for collecting and preprocessing the experimental data.

Conflicts of Interest: The authors declare no conflicts of interest.

Appendix A

$$RD_{i,t} = \frac{RL_{i,t}}{Area_{i,t}} \tag{A1}$$

where $RD_{i,t}$, $RL_{i,t}$, and $Area_{i,t}$ denote the river network density, river length, and area of city i in year t, respectively.

$$IWSD_{i,j}^{t} = \begin{cases} 0 & x_{i,j}^{t} \le a_j \\ 0.3 \times \frac{x_{i,j}^{t} - a_j}{b_j - a_j} & a_j < x_{i,j}^{t} \le b_j \\ 0.3 + 0.3 \times \frac{x_{i,j}^{t} - b_j}{c_j - b_j} & b_j < x_{i,j}^{t} \le c_j \\ 0.6 + 0.2 \times \frac{x_{i,j}^{t} - c_j}{d_j - c_j} & c_j < x_{i,j}^{t} \le d_j \\ 0.8 + 0.2 \times \frac{x_{i,j}^{t} - d_j}{e_j - d_j} & d_j < x_{i,j}^{t} \le e_j \\ 1 & x_{i,j}^{t} > e_j \end{cases} \tag{A2}$$

$$IWSD_{i,j}^{t} = \begin{cases} 1 & x_{i,j}^{t} \le e_j \\ 0.8 + 0.2 \times \frac{x_{i,j}^{t} - d_j}{e_j - d_j} & e_j < x_{i,j}^{t} \le d_j \\ 0.6 + 0.2 \times \frac{x_{i,j}^{t} - c_j}{d_j - c_j} & d_j < x_{i,j}^{t} \le c_j \\ 0.3 + 0.3 \times \frac{x_{i,j}^{t} - b_j}{c_j - b_j} & c_j < x_{i,j}^{t} \le b_j \\ 0.3 \times \frac{x_{i,j}^{t} - a_j}{b_j - a_j} & b_j < x_{i,j}^{t} \le a_j \\ 0 & x_{i,j}^{t} > a_j \end{cases} \tag{A3}$$

where $IWSD_{i,j}^{t}$ and $x_{i,j}^{t}$ are the SWSD and the indicator value of indicator j for the city i in year t, respectively. a_j, b_j, c_j, d_j, and e_j denote the worst value, the worse value, the medium value, the better value, and the optimal value of indicator j, respectively.

$$SWSD_{i,k}^{t} = \sum_{j=1}^{n} \omega_j \times IWSD_{i,j}^{t} \tag{A4}$$

In the formula, $SWSD_{i,k}^{t}$ represents the SWSD of evaluation dimension k for the city i in year t. n denotes the number of evaluation indicators in evaluation dimension k. ω_j represents the weight of indicator j, with the sum of the weights of all indicators in each evaluation dimension equaling 1.

$$WSD_{i}^{t} = \sum_{k=1}^{3} \omega_k \times SWSD_{i,k}^{t} \tag{A5}$$

In the formula, WSD_{i}^{t} represents the water security degree of city i in year t. ω_k denotes the weight of evaluation dimension k.

$$r_j = \frac{\alpha_j \times \beta_j}{\sum_{j=1}^{15} (\alpha_j \times \beta_j)} \times 100\% \tag{A6}$$

$$\alpha_j = 1 - X_j \tag{A7}$$

$$\beta_j = \omega_j \times \omega_k \tag{A8}$$

In the formula, r_j, α_j, and β_j represent the obstacle degree, deviation degree, and factor contribution degree of indicator j, respectively. A larger obstacle degree indicates a greater restrictive effect of the indicator on the final evaluation result. X_j represents the standardized result of indicator j. ω_j and ω_k denote the weights of indicator j and its corresponding evaluation dimension k, respectively.

Appendix B

Table A1. Water Security Regulation Schemes for the YRWAR-HN under Path 1.

City	Scheme 1	Scheme 2	Scheme 3	Scheme 4	Scheme 5
Zhengzhou	All indicators adjusted by 1 times the growth rate from 2010–2021	X1, X2 adjusted by 1.1 times the growth rate, with the remaining indicators maintaining their original growth rates	X5, X6, X7 adjusted by 1.1 times the growth rate, with the remaining indicators maintaining their original growth rates	X11, X13, X15 adjusted by 1.1 times the growth rate, with the remaining indicators maintaining their original growth rates	X1, X2, X5, X6, X7, X11, X13, X15 adjusted by 1.1 times the growth rate, with the remaining indicators maintaining their original growth rates
Kaifeng	All indicators adjusted by 1 times the growth rate from 2010–2021	X1, X2 adjusted by 1.1 times the growth rate, with the remaining indicators maintaining their original growth rates	X5, X7, X9 adjusted by 1.1 times the growth rate, with the remaining indicators maintaining their original growth rates	X13, X14, X15 adjusted by 1.1 times the growth rate, with the remaining indicators maintaining their original growth rates	X1, X2, X5, X7, X9, X13, X14, X15 adjusted by 1.1 times the growth rate, with the remaining indicators maintaining their original growth rates
Luoyang	All indicators adjusted by 1 times the growth rate from 2010–2021	X1, X3 adjusted by 1.1 times the growth rate, with the remaining indicators maintaining their original growth rates	X5, X7, X10 adjusted by 1.1 times the growth rate, with the remaining indicators maintaining their original growth rates	X12, X13, X15 adjusted by 1.1 times the growth rate, with the remaining indicators maintaining their original growth rates	X1, X3, X5, X7, X10, X12, X13, X15 adjusted by 1.1 times the growth rate, with the remaining indicators maintaining their original growth rates

Table A1. *Cont.*

City	Scheme 1	Scheme 2	Scheme 3	Scheme 4	Scheme 5
Xinxiang	All indicators adjusted by 1 times the growth rate from 2010–2021	X1, X2 adjusted by 1.1 times the growth rate, with the remaining indicators maintaining their original growth rates	X5, X7, X9 adjusted by 1.1 times the growth rate, with the remaining indicators maintaining their original growth rates	X12, X13, X15 adjusted by 1.1 times the growth rate, with the remaining indicators maintaining their original growth rates	X1, X2, X5, X7, X9, X12, X13, X15 adjusted by 1.1 times the growth rate, with the remaining indicators maintaining their original growth rates
Jiaozuo	All indicators adjusted by 1 times the growth rate from 2010–2021	X1, X2 adjusted by 1.1 times the growth rate, with the remaining indicators maintaining their original growth rates	X5, X7, X8 adjusted by 1.1 times the growth rate, with the remaining indicators maintaining their original growth rates	X12, X13, X15 adjusted by 1.1 times the growth rate, with the remaining indicators maintaining their original growth rates	X1, X2, X5, X7, X8, X12, X13, X15 adjusted by 1.1 times the growth rate, with the remaining indicators maintaining their original growth rates
Sanmenxia	All indicators adjusted by 1 times the growth rate from 2010–2021	X1, X2 adjusted by 1.1 times the growth rate, with the remaining indicators maintaining their original growth rates	X5, X9, X10 adjusted by 1.1 times the growth rate, with the remaining indicators maintaining their original growth rates	X12, X14, X15 adjusted by 1.1 times the growth rate, with the remaining indicators maintaining their original growth rates	X1, X2, X5, X9, X10, X12, X14, X15 adjusted by 1.1 times the growth rate, with the remaining indicators maintaining their original growth rates
Puyang	All indicators adjusted by 1 times the growth rate from 2010–2021	X1, X4 adjusted by 1.1 times the growth rate, with the remaining indicators maintaining their original growth rates	X5, X9, X10 adjusted by 1.1 times the growth rate, with the remaining indicators maintaining their original growth rates	X13, X14, X15 adjusted by 1.1 times the growth rate, with the remaining indicators maintaining their original growth rates	X1, X4, X5, X9, X10, X13, X14, X15 adjusted by 1.1 times the growth rate, with the remaining indicators maintaining their original growth rates
Jiyuan	All indicators adjusted by 1 times the growth rate from 2010–2021	X3, X4 adjusted by 1.1 times the growth rate, with the remaining indicators maintaining their original growth rates	X5, X8, X9 adjusted by 1.1 times the growth rate, with the remaining indicators maintaining their original growth rates	X11, X12, X13 adjusted by 1.1 times the growth rate, with the remaining indicators maintaining their original growth rates	X3, X4, X5, X8, X9, X11, X12, X13 adjusted by 1.1 times the growth rate, with the remaining indicators maintaining their original growth rates
Anyang	All indicators adjusted by 1 times the growth rate from 2010–2021	X1, X4 adjusted by 1.1 times the growth rate, with the remaining indicators maintaining their original growth rates	X7, X8, X9 adjusted by 1.1 times the growth rate, with the remaining indicators maintaining their original growth rates	X11, X13, X15 adjusted by 1.1 times the growth rate, with the remaining indicators maintaining their original growth rates	X1, X4, X7, X8, X9, X11, X13, X15 adjusted by 1.1 times the growth rate, with the remaining indicators maintaining their original growth rates
Hebi	All indicators adjusted by 1 times the growth rate from 2010–2021	X1, X4 adjusted by 1.1 times the growth rate, with the remaining indicators maintaining their original growth rates	X7, X8, X9 adjusted by 1.1 times the growth rate, with the remaining indicators maintaining their original growth rates	X13, X14, X15 adjusted by 1.1 times the growth rate, with the remaining indicators maintaining their original growth rates	X1, X4, X7, X8, X9, X13, X14, X15 adjusted by 1.1 times the growth rate, with the remaining indicators maintaining their original growth rates
Pingdingshan	All indicators adjusted by 1 times the growth rate from 2010–2021	X1, X3 adjusted by 1.1 times the growth rate, with the remaining indicators maintaining their original growth rates	X7, X9, X10 adjusted by 1.1 times the growth rate, with the remaining indicators maintaining their original growth rates	X12, X13, X15 adjusted by 1.1 times the growth rate, with the remaining indicators maintaining their original growth rates	X1, X3, X7, X9, X10, X12, X13, X15 adjusted by 1.1 times the growth rate, with the remaining indicators maintaining their original growth rates

Table A1. *Cont.*

City	Scheme 1	Scheme 2	Scheme 3	Scheme 4	Scheme 5
Xuchang	All indicators adjusted by 1 times the growth rate from 2010–2021	X1, X4 adjusted by 1.1 times the growth rate, with the remaining indicators maintaining their original growth rates	X5, X7, X9 adjusted by 1.1 times the growth rate, with the remaining indicators maintaining their original growth rates	X12, X14, X15 adjusted by 1.1 times the growth rate, with the remaining indicators maintaining their original growth rates	X1, X4, X5, X7, X9, X12, X14, X15 adjusted by 1.1 times the growth rate, with the remaining indicators maintaining their original growth rates
Shangqiu	All indicators adjusted by 1 times the growth rate from 2010–2021	X1, X4 adjusted by 1.1 times the growth rate, with the remaining indicators maintaining their original growth rates	X5, X7, X9 adjusted by 1.1 times the growth rate, with the remaining indicators maintaining their original growth rates	X13, X14, X15 adjusted by 1.1 times the growth rate, with the remaining indicators maintaining their original growth rates	X1, X4, X5, X7, X9, X13, X14, X15 adjusted by 1.1 times the growth rate, with the remaining indicators maintaining their original growth rates
Zhoukou	All indicators adjusted by 1 times the growth rate from 2010–2021	X1, X4 adjusted by 1.1 times the growth rate, with the remaining indicators maintaining their original growth rates	X5, X7, X9 adjusted by 1.1 times the growth rate, with the remaining indicators maintaining their original growth rates	X12, X14, X15 adjusted by 1.1 times the growth rate, with the remaining indicators maintaining their original growth rates	X1, X4, X5, X7, X9, X12, X14, X15 adjusted by 1.1 times the growth rate, with the remaining indicators maintaining their original growth rates

References

1. Shuval, H.I. Are the conflicts between Israel and her neighbors over the waters of the Jordan River Basin an obstacle to peace? Israel-Syria as a case study. In *Environmental Challenges*; Springer: Berlin/Heidelberg, Germany, 2000; pp. 605–630.
2. Qiu, D.H. Research advances in regional water security strategy. *Adv. Water Sci.* **2005**, *16*, 305–312.
3. UNESCO. *The United Nations World Water Development Report 2021: Valuing Water*; United Nations: San Francisco, CA, USA, 2021.
4. Ait-Kadi, M. Water for development and development for water: Realizing the sustainable development goals (SDGs) vision. *Aquat. Procedia* **2016**, *6*, 106–110. [CrossRef]
5. L, B.; Zeng, Y.; Zhang, B.; Wang, X. A risk evaluation model for karst groundwater pollution based on geographic information system and artificial neural network applications. *Environ. Earth Sci.* **2018**, *77*, 1–14.
6. Fan, L.; Ma, L.; Yu, Y.; Wang, S.; Xu, Y. Water-conserving mining influencing factors identification and weight determination in northwest China. *Int. J. Coal. Sci. Technol.* **2019**, *6*, 95–101. [CrossRef]
7. Cook, C.; Bakker, K. Water security: Debating an emerging paradigm. *Glob. Environ. Change* **2012**, *22*, 94–102. [CrossRef]
8. Gerlak, A.K.; Mukhtarov, F. 'Ways of knowing' water: Integrated water resources management and water security as complementary discourses. *Int. Environ. Agreem. Politics Law Econ.* **2015**, *15*, 257–272. [CrossRef]
9. Jiang, Y. China's water security: Current status, emerging challenges and future prospects. *Environ. Sci. Policy* **2015**, *54*, 106–125. [CrossRef]
10. Escap, U.N. *Water Security & the GLOBAL Water Agenda: A UN-Water Analytical Brief*; United Nations University: Tokyo, Japan, 2013.
11. WaterAid. *Water Security Framework*; WaterAid: London, UK, 2012.
12. Xia, J.; Shi, W. Perspective on water security issue of changing environment in China. *J. Hydraul. Eng.* **2016**, *47*, 292–301.
13. Deng, J.; Jia, S.F. Indicators system construction and application of regional water security. *Adv. Water Sci.* **2022**, *33*, 48–56.
14. Wang, H.; Zuo, Q.; Jiang, Y.Z. Proposition of national water safety discipline and construction of its discipline system. *Adv. Water Sci.* **2022**, *33*, 859–867.
15. Li, B.; Wu, Q.; Zhang, W.; Liu, Z. Water resources security evaluation model based on grey relational analysis and analytic network process: A case study of Guizhou Province. *J. Water Process Eng.* **2020**, *37*, 101429. [CrossRef]
16. Liu, B.; Zhang, F.; Qin, X.; Wu, Z.; Wang, X.; He, Y. Spatiotemporal assessment of water security in China: An integrated supply-demand coupling model. *J. Cleaner Prod.* **2021**, *321*, 128955. [CrossRef]
17. Sun, K.; He, W.; Shen, Y.; Yan, T.; Liu, C.; Yang, Z.; Han, J.; Xie, W. Ecological security evaluation and early warning in the water source area of the Middle Route of South-to-North Water Diversion Project. *Sci. Total Environ.* **2023**, *868*, 161561. [CrossRef] [PubMed]
18. Yomo, M.; Mourad, K.A.; Gnazou, M.D. Examining water security in the challenging environment in Togo, West Africa. *Water* **2019**, *11*, 231. [CrossRef]
19. Zhao, J.; Chen, Y.; Xu, J.; Jin, J.; Wang, G.; Shamseldin, A.; Guo, Y.; Cheng, L. Regional water security evaluation with risk control model and its application in Jiangsu Province, China. *Environ. Sci. Pollut. Res.* **2021**, *28*, 55700–55715. [CrossRef]

20. Falkenmark, M.; Widstrand, C. Population and water resources: A delicate balance. *Popul. Bulletin.* **1992**, *47*, 1–36.
21. Porkka, M.; Kummu, M.; Siebert, S.; Flörke, M. The role of virtual water flows in physical water scarcity: The case of Central Asia. *Int. J. Water Resour. Dev.* **2012**, *28*, 453–474. [CrossRef]
22. Zeng, Z.; Liu, J.; Savenije, H.H. A simple approach to assess water scarcity integrating water quantity and quality. *Ecol. Indic.* **2013**, *34*, 441–449. [CrossRef]
23. Ahammed, S.J.; Chung, E.S.; Shahid, S. Parametric assessment of pre-monsoon agricultural water scarcity in Bangladesh. *Sustainability* **2018**, *10*, 819. [CrossRef]
24. Raskin, P.; Gleick, P.; Kirshen, P.; Pontius, G.; Strzepek, K. *Water Futures: Assessment of Long-Range Patterns and Problems. Comprehensive Assessment of the Freshwater Resources of the World*; Food and Agriculture Organization of the United Nations: Rome, Italy, 1997.
25. Wang, Y.; Wang, Y.; Su, X.; Qi, L.; Liu, M. Evaluation of the comprehensive carrying capacity of interprovincial water resources in China and the spatial effect. *J. Hydrol.* **2019**, *575*, 794–809. [CrossRef]
26. Chen, X. Assessment and prediction of China's ocean strategy resource safety based on DSR model—Take the south china sea oil security for example. *World Reg. Stud.* **2017**, *26*, 46–58.
27. Li, S.; Liu, C.; Ge, C.; Yang, J.; Liang, Z.; Li, X.; Cao, X. Ecosystem health assessment using PSR model and obstacle factor diagnosis for Haizhou Bay, China. *Ocean Coast Manag.* **2024**, *250*, 107024. [CrossRef]
28. Sun, S.; Wang, Y.; Liu, J.; Cai, H.; Wu, P.; Geng, Q.; Xu, L. Sustainability assessment of regional water resources under the DPSIR framework. *J. Hydrol.* **2016**, *532*, 140–148. [CrossRef]
29. Zhang, F.; Zhang, J.; Wu, R.; Ma, Q.; Yang, J. Ecosystem health assessment based on DPSIRM framework and health distance model in Nansi Lake, China. *Stoch. Environ. Res. Risk Assess.* **2016**, *30*, 1235–1247. [CrossRef]
30. Cai, J.; He, Y.; Xie, R.; Liu, Y. A footprint-based water security assessment: An analysis of Hunan province in China. *J. Clean Prod.* **2020**, *245*, 118485. [CrossRef]
31. Deng, L.; Yin, J.; Tian, J.; Li, Q.; Guo, S. Comprehensive evaluation of water resources carrying capacity in the Han River Basin. *Water* **2021**, *13*, 249. [CrossRef]
32. Qiu, M.; Zuo, Q.; Wu, Q.; Yang, Z.; Zhang, J. Water ecological security assessment and spatial autocorrelation analysis of prefectural regions involved in the Yellow River Basin. *Sci. Rep.* **2022**, *12*, 5105. [CrossRef]
33. Zuo, Q.T. *Harmony Theory. Method and Application*; Chinese Science Press: Beijing, China, 2012.
34. Zuo, Q.; Zhao, H.; Mao, C.; Ma, J.; Cui, G. Quantitative analysis of human-water relationships and harmony-based regulation in the Tarim River Basin. *J. Hydrol. Eng.* **2015**, *20*, 05014030. [CrossRef]
35. Li, J.; Ma, J.; Yu, L.; Zuo, Q. Analysis and regulation of the harmonious relationship among water, energy, and food in nine provinces along the Yellow River. *Water* **2022**, *14*, 1042. [CrossRef]
36. Wang, S.; Yang, J.; Wang, A.; Yan, Y.; Liu, T. Coupled coordination of water resources–economy–ecosystem complex in the Henan section of the Yellow River basin. *Water Supply* **2022**, *22*, 8835–8848. [CrossRef]
37. Cao, W.; Gao, Z.; Guo, H.; Pan, D.; Qiao, W.; Wang, S.; Ren, Y.; Li, Z. Increases in groundwater arsenic concentrations and risk under decadal groundwater withdrawal in the lower reaches of the Yellow River basin, Henan Province, China. *Environ. Pollut.* **2022**, *296*, 118741. [CrossRef] [PubMed]
38. Zhang, Z.; Cao, Y.; Bao, T.; Wang, Y.; Shi, F. Assessment of Water Resources Carrying Capacity of the Yellow River Diversion Area in Henan Province Based on TOPSIS Model with Combined Weights. *Yellow River* **2022**, *45*, 73–78.
39. Zhang, X.; Zhou, Y.; Han, C. Research on high-quality development evaluation and regulation model: A case study of the Yellow River water supply area in Henan Province. *Water* **2023**, *15*, 261. [CrossRef]
40. Li, Y.; Sun, K.; Men, R.; Wang, F.; Li, D.; Han, Y.; Qu, Y. Study on the Optimization of Multi-Objective Water Resources Allocation in the Henan Yellow River Water Supply Zone. *Water* **2023**, *15*, 4009. [CrossRef]
41. Zhao, X.; Li, H.; Cai, Q.; Pan, Y.; Qi, Y. Managing Extreme Rainfall and Flooding Events: A Case Study of the 20 July 2021 Zhengzhou Flood in China. *Climate* **2023**, *11*, 228. [CrossRef]
42. Zuo, Q.; Li, W.; Zhao, H.; Ma, J.; Han, C.; Luo, Z. A harmony-based approach for assessing and regulating human-water relationships: A case study of Henan province in China. *Water* **2020**, *13*, 32. [CrossRef]
43. Jiang, L.; Zuo, Q.; Ma, J.; Zhang, Z. Evaluation and prediction of the level of high-quality development: A case study of the Yellow River Basin, China. *Ecol. Indic.* **2021**, *129*, 107994. [CrossRef]
44. Zhang, Y.; Zuo, Q.; Wu, Q.; Han, C.; Tao, J. An integrated diagnostic framework for water resource spatial equilibrium considering water-economy-ecology nexus. *J. Clean Prod.* **2023**, *414*, 137592. [CrossRef]
45. Nie, R.; Tian, Z.; Wang, J.; Zhang, H.; Wang, T. Water security sustainability evaluation: Applying a multistage decision support framework in industrial region. *J. Clean Prod.* **2018**, *196*, 1681–1704. [CrossRef]
46. Octavianti, T.; Staddon, C. A review of 80 assessment tools measuring water security. *Wires Water* **2021**, *8*, e1516. [CrossRef]
47. Liu, L.; He, L.; Zuo, Q. Evaluating the Human–Water Relationship over the Past Two Decades Using the SMI-P Method across Nine Provinces along the Yellow River, China. *Water* **2024**, *16*, 916. [CrossRef]
48. He, G.; Fu, Y.; Zhao, S. Evaluation of water ecological security in Huaihe River Basin based on the DPSIR-EES-SMI-P model. *Water Supply* **2023**, *23*, 1127–1143. [CrossRef]
49. Cheng, R.; Li, W.; Lu, Z.; Zhou, S.; Meng, C. Integrating the three-line environmental governance and environmental sustainability evaluation of urban industry in China. *J. Clean. Prod.* **2020**, *264*, 121554. [CrossRef]

50. Luo, Z.; Shao, Q.; Zuo, Q.; Cui, Y. Impact of land use and urbanization on river water quality and ecology in a dam dominated basin. *J. Hydrol.* **2020**, *584*, 124655. [CrossRef]
51. Taha, A.W.; Sharma, S.; Lupoja, R.; Fadhl, A.N.; Haidera, M.; Kennedy, M. Assessment of water losses in distribution networks: Methods, applications, uncertainties, and implications in intermittent supply. *Resour. Conserv. Recycl.* **2020**, *152*, 104515.
52. Zhao, M.; Wei, J.; Han, Y.; Shi, J.; Wang, S. Water resource security evaluation and obstacle analysis in Henan Province utilizing the DPSIR framework. *Front. Environ. Sci.* **2024**, *12*, 1354175. [CrossRef]
53. Fan, Y.; Fang, C. Evolution process and obstacle factors of ecological security in western China, a case study of Qinghai province. *Ecol Indic.* **2020**, *117*, 106659. [CrossRef]
54. Water Resources Department of Henan Province, People's Republic of China. Henan Water Resources Bulletin. Available online: https://slt.henan.gov.cn/bmzl/szygl/szygb/ (accessed on 30 August 2024).

water

MDPI

Article

Evaluating the Human–Water Relationship over the Past Two Decades Using the SMI-P Method across Nine Provinces along the Yellow River, China

Lu Liu [1], Liuyue He [2,3,*] and Qiting Zuo [4,*]

[1] Yellow River Institute for Ecological Protection and Regional Coordination Development, Zhengzhou University, Zhengzhou 450001, China; doris8370@163.com
[2] Donghai Laboratory, Zhoushan 316021, China
[3] Ocean College, Zhejiang University, Zhoushan 316021, China
[4] School of Water Conservancy and Transportation, Zhengzhou University, Zhengzhou 450001, China
* Correspondence: hely2018@163.com (L.H.); zuoqt@zzu.edu.cn (Q.Z.)

Abstract: The foundation for ensuring the sustainable utilization of natural resources and human well-being lies in achieving a harmonious balance between nature and humans. In the Yellow River basin (YRB), numerous water crises, including floods, droughts, soil erosion, and water pollution, threaten its crucial role as a significant economic belt and ecological barrier. Unfortunately, less comprehension regarding the complex human–water relationship in this region has impeded watershed water management decision-makers from identifying key priorities for intervention. Here, we selected 29 evaluation indicators, including water resources, environment, ecology, society, economy, and science and technology from three dimensions: healthy water systems, sustainable human systems, and synergy of human–water system. We applied the entropy weight method, hierarchical analysis, and Single index quantification, multiple index synthesis, and poly-criteria integration (SMI-P) methods to quantify the spatial–temporal variation of the human–water harmony degree (*HWHD*) in nine provinces of the YRB from 2002 to 2021. We observed a consistent increase in the *HWHD* across all provinces in the YRB in the past two decades. Notably, five provinces have transitioned from Complete disharmony ($0 \leq HWHD \leq 0.2$) to Nearly complete disharmony ($0.2 < HWHD \leq 0.4$). Additionally, the average growth rate of the downstream provinces is faster compared to those upstream. By 2021, the *HWHD* of upstream provinces like Sichuan and Ningxia, constrained by slower growth, became the two lowest provinces of the YRB, at 0.19 and 0.12 respectively. These findings offer valuable guidance for the region and similar areas grappling with the complex challenges of human–water conflicts, providing insights to navigate and address such dilemmas effectively.

Keywords: harmony theory; harmony evaluation; water resources management; spatial–temporal analysis

1. Introduction

Water serves as the fundamental resource for humanity and is indispensable for fostering social development and well-being [1,2]. As the global population and societal development continue to rise, the increasing demand for water resources exacerbates its impact on the water environment [3]. The escalating water crisis, encompassing issues like water scarcity, flood disasters, and polluted groundwater, threatens human survival and sustainable development, posing a significant challenge to global social security [4,5]. The projected global urban population experiencing water scarcity is expected to triple by 2050 compared to the levels observed in 2016 [5]. Moreover, populations exposed to river flooding are predicted to increase by 4–20 fold by the years of 2100 [6]. Therefore, comprehending the interplay between human and water systems and promoting their sustainable development has become both urgent and imperative.

The human system, centered around humanity, encompasses social activities, economic development, scientific and technological progress, and other factors critical to human survival [7]. Accordingly, the water system comprises the water consumption and demand of related sectors, as well as the environmental background conditions of water resources. The interplay between human activities and water environment status is exceptionally intricate [8]. Currently, the quantification of this relationship employs either single or comprehensive indicators. When focusing on single indicators, researchers often construct evaluation metrics based on the contrast between water supply and demand, with commonly employed measures such as water shortage index [9], water stress index [10], water use efficiency [11,12], and others. However, these single indicators reflect only one aspect of the complex relationship. Conversely, comprehensive indicators and integrated assessment models offer a more holistic approach, such as the water poverty index [13,14], water resources carrying capacity index [15], water security index [16], and human–water harmony index [17]. These comprehensive metrics offer a more nuanced understanding of the multifaceted relationship within the human–water system, helping to promote synergies between human development and water environment health.

Related research of human–water harmonious is a forward-looking exploration grounded in the mechanisms of interaction, adaptation, and balance principle within human–water system [17]. Its primary objective is to promote a virtuous cycle within the human–water system. This will enhance the self-maintenance and renewal capabilities of the water system, ensuring that water resources can offer enduring support and assurance sustainable economic growth and social development [18]. Research on human–water harmonious has evolved from qualitative inquiries at the beginning of the 21st century to a more quantitative approach today. Key components of this research now encompass the exploration of interaction mechanisms within human–water systems, the quantitative analysis and simulation of the human–water relationship, and the optimization of schemes promoting such harmony [19–21]. These studies have found widespread application across various scales, including national, provincial, urban, and watershed levels. In this study by Ding et al. [17], 27 indicators related to social development, system coordination, and public satisfaction were utilized to establish the Human–Water Harmony Index (HWHI) grounded in the concept of harmony with its application to five megalopolises of China. Building upon this framework, Zuo et al. [18] determined the harmonious balance constraint and regulation by quantifying the equilibrium state of the human–water relationship of six criteria in 43 countries along the Belt and Road. Duan et al. [19] constructed a human–water-nexus-based evaluation system, in which 13 indicators of 8 sustainable development goals (i.e., SDGs 2, 6, 8, 9, 11, 12, 13, and 17) associated with water, society, and ecology criteria were analyzed. These studies evaluate human–water relationship by examining specific factors related to water resources within human systems, including water quantify, water quality, water use structure, and the dynamic balance between supply and demand. Unfortunately, they primarily focus on enhancing the health of water systems and promoting the sustainable development of human systems, while overlooking the harmonized development of the two [17,22]. The latter aspect is crucial for promoting the healthy, orderly, and sustainable development of both systems simultaneously.

Yellow River Basin (YRB) serves as a representative example of human–water interaction [23,24]. The basin's environment is significantly influenced by human activities, meanwhile, water resource scarcity emerges as a critical constraint for the socio-economic development of the region [25]. Nonetheless, a comprehensive analysis of the evolution of the human–water relationship in the YRB is hindered by the insufficient simulation on key process, vital variables, mutual feedback relationships, and a lack of comprehension regarding common mechanisms. Simultaneously, both domestically and internationally, there is a scarcity of research cases focusing on identifying the evolutionary mechanisms and assessing the external effects of the synergistic mechanism between water resources utilization and human activities in the large river basins [26].

To address these knowledge gaps, we selected 29 evaluation indicators to construct the Human–water harmony degree (*HWHD*) evaluation framework, encompassing three dimensions: healthy water systems, sustainable human systems, and synergy between human and water systems. Meanwhile, we combined the Entropy Weight method (EW) and Analytic Hierarchy Process (AHP) into one framework to determine every indicator's weight. According to the harmony theory, we employed the Single index quantification, multiple index synthesis, and poly-criteria integration (SMI-P) method to quantify the *HWHD*. Generally, we analyzed the intricate relationship between humans and water in YRB from 2002 to 2021 and explore their synergistic development from an integrated perspective. Hence, the systematic quantification of the dynamic evolving process of the *HWHD* in the YRB can serve as a scientific foundation for fostering ecological health and sustainable development within the YRB. Furthermore, it can facilitate to the development of earth system science in China through integrated basin research.

2. Methods

2.1. Calculation of Comprehensive Weight

As an objective weighting method, EW judges the degree of dispersion of the index through the information entropy of the index data, while it neglects the actual demand of decision-makers for indicators [27]. AHP judges the relative importance of each indicator according to the experience of decision makers, however, the evaluation results are prone to fluctuate due to subjective human factors [28]. It is desired an integrated EW-AHP method should be developed to overcome the above issues [29]:

$$w_i = \frac{\alpha_i \times \beta_i}{\sum_{i=1}^{n} \alpha_i \times \beta_i} (i = 1, 2, \ldots, n) \quad (1)$$

w_i, α_i, and β_i are the comprehensive, subjective, and objective weights of the index i, respectively.

2.2. Calculation of HWHD

Here, we utilized the evaluation approach of SMI-P to assess the *HWHD* [30]. *HWHD* is further segmented into the three sub-harmony degrees (*SHD*), named healthy water systems (*HED*), sustainable human systems (*HAD*), and synergy between human and water systems (*DED*), respectively. The *SHD* of each indictor was determined based on the assumed fuzzy membership within the range of [0, 1] as shown in Figure 1 [19]. These *SHD* are detailed in the following calculated equations [31].

$$HED(T) = \sum_{i=1}^{n_1} w_i SHD_1(Y_1^i(T)) \quad (2)$$

$$DED(T) = \sum_{i=1}^{n_1} w_i SHD_2(Y_2^i(T)) \quad (3)$$

$$HAD(T) = \sum_{i=1}^{n_1} w_i SHD_3(Y_3^i(T)) \quad (4)$$

where T and n indicate the time and number of indicator; $Y_n^i(T)$ shows the indicator value; w_i presents the indicator's weight; $SHD_{\alpha i}\left[Y^i(T)\right]$ indicates the sub-harmony degree; and $HED(T)$, $HED(T)$, and $HAD(T)$ represent the sub-harmony of each criterion, respectively.

Then, the final *HWHD* can be achieved as follows:

$$HWHD(T) = HED(T)^{\beta_1} \times DED(T)^{\beta_2} \times HAD(T)^{\beta_3} \quad (5)$$

where $HWHD(T)$ *is* the final human–water harmony degree; β_1, β_2, and β_3 are the weights of each criteria, respectively; generally, the weights of each criteria are assumed as equal (i.e., 1/3). The harmony grading standards were based on the final *HWHD* and were equally segmented into five intervals from 0 to 1 [31].

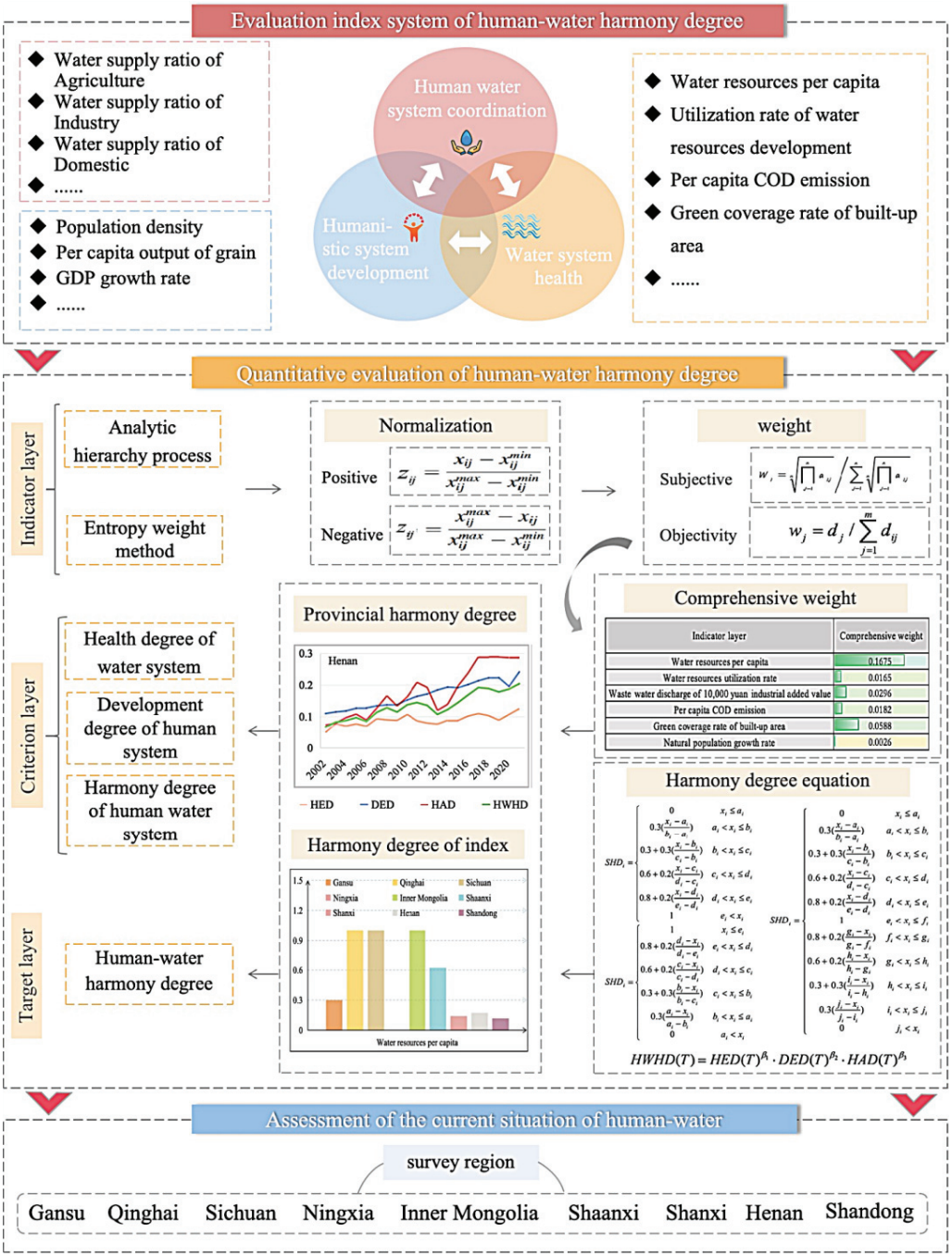

Figure 1. Study framework.

3. Case Study

As the second longest river in China, YRB covers approximately 7950 hm^2. It constitutes 2.56% of the national total water resources, while sustains 12% of the population, irrigates 13% of farmland, and contributes 13% of food and 14% of GDP in China [27]. In 2021, the total population in YRB is 421 million, and the GDP is CNY 28,778.3 billion. However, the per capita water resources in this basin are 26,824 m^3 per person, occupying about 1/4 of the world average level, which evolves into the biggest contradiction in the

YRB. Due to the serious imbalance between social and economic development and natural hydrological process and ecosystem process, the YRB is one of the most prominent and complicated areas in China. It has become a national strategic plan to protect the ecological environment and promote the high-quality development of the YRB. Meanwhile, several national development plans were also published toward the harmonious human–water relationship. In detail, during the 14th Five-Year Plan, the water ecological environmental protection work should pay more attention to human–water harmony by the Ministry of Ecology and Environment of the people's Republic of China. In the year of 2024, opinions of thoroughly promoting the construction of Beautiful China were published by the CPC and State council, aiming at accelerating the modernization of harmonious coexistence between human and nature, especially for building the pilot zone for ecological protection and high-quality development of the YRB.

Thus, we built a comprehensive human–water harmony evaluation system to promote the implementation of national strategies. As shown in Figure 1, the constructed human–water harmony evaluation system encompasses three aspects: the evaluation indicators of *HWHD*, calculation of weights based on AHP and EW, and the spatio-temporal analysis of *HWHD* in the YRB from 2002 to 2021.

To reflect the prominent contradictions between human and water systems in nine provinces of YRB in the past two decades, we employed 29 indicators to construct a human–water harmony evaluation system based on harmony theory, including three dimensions: healthy water systems, sustainable human systems, and synergy between human and water systems [21], as shown in Table 1. A healthy water system necessitates the preservation of ecological functions in rivers, lakes, groundwater, and other water sources, with robust self-repair and renewal capabilities and resistance to shocks. Thus, we chose Water resources per capita, Water resources utilization rate, and Per capita COD emission to express the health conditions. Sustainable water systems require socio-economic development to be managed in a way that doesn't compromise life support on earth. Thus, indicators of Proportion of employees in the tertiary industry, Per capita disposable income of urban residents, and Per capita disposable income of rural residents were presented for development. Synergy between human and water systems mandates that water systems must provide necessary and robust support for human and social economic development. Meanwhile, humans are expected to continually safeguard the health of rivers and take proactive measures to transform the relationship between humans and water into a virtuous cycle. Therefore, the synergy indicators were chosen in terms of Water supply ratio of industry, Water supply ratio of domestic, and Water supply ratio of ecology.

Table 1. Evaluation indicator standard threshold.

Criterion Layer	Classification Layer	Indicator Layer	Unit	Criterion Attribute	Worst Value	Difference Value	Pass Value	Optimal Value	Optimal Value
Health degree of water system	Water resources subsystem	Water resources per capita	Person	Positive	130	1115	2100	2600	3100
		Water resources utilization rate	%	Negative	100	80	60	42	24
	Water environment subsystem	Waste water discharge per CNY 10,000 of industrial added value	Ton	Negative	80	53	26	20	14
		Per capita COD emission	Ton	Negative	0.04	0.03	0.02	0.011	0.002
	Water ecological subsystem	Green coverage rate of built-up area	%	Positive	29	32	35	40	45

Table 1. *Cont.*

Criterion Layer	Classification Layer	Indicator Layer	Unit	Criterion Attribute	Worst Value	Difference Value	Pass Value	Optimal Value	Optimal Value
Development degree of human system	Social development subsystem	Natural population growth rate	‰	Negative	10	8	6	4	2
		Urbanization rate	%	Positive	37	43.5	50	65	80
		population density	Person/km^2	Negative	4000	2300	650	400	148
		Proportion of employees in the tertiary industry	%	Positive	20	34	48	59	70
		Engel's coefficient for urban residents	%	Negative	60	55	50	40	30
		Per capita disposable income of urban residents	Yuan	Positive	7700	16,350	25,000	62,500	100,000
		Per capita disposable income of rural residents	Yuan	Positive	2500	5650	8800	26,900	45,000
		Per capita grain yields	Kilogram	Positive	14	232	450	1225	2000
		Per capita comprehensive water consumption	m^3	Negative	800	610	420	290	160
	Economic development Subsystem	Per capita GDP	Yuan	Positive	39,000	60,000	81,000	190,500	300,000
		Per capita fiscal revenue	Yuan	Positive	3500	8750	14,000	19,500	25,000
		Per capita total social fixed asset investment	Yuan	Positive	17,000	68,500	120,000	1,060,000	2,000,000
		Proportion of output value of tertiary industry in GDP	%	Positive	20	32.5	45	57.5	70
		GDP growth rate	%	Positive	2	3.5	5	7	9
		Growth rate of output value of tertiary industry	%	Positive	7	9	11	12	13
	Science and technology development subsystem	Water consumption per CNY 10,000 of GDP	m^3	Negative	450	250	50	30	10
		Water consumption per CNY 10,000 of industrial added output	m^3	Negative	65	47	28	17	5
		Irrigation water per mu of farmland	Cubic meter	Negative	450	400	350	245	140
		Reuse rate of urban industrial water	%	Positive	22	55	88	93	98
		College students per 10,000 people	Person	Positive	32	181	330	415	500
Harmony degree of human water system	Water supply subsystem	Water supply ratio of Agriculture	%	Negative	91	77	63	46.5	30
		Water supply ratio of Industry	%	Positive	3	11.5	20	32.5	45
		Water supply ratio of Domestic	%	Positive	5	9	13	15	17
		Water supply ratio of Ecology	%	Positive	1	2.5	4	6	8

During the data processing, most data were obtained by the national statistical yearbooks. Some non-uniform data such as water resources per capita, proportion of output value of tertiary industry in GDP, and college students per 10,000 people were obtained by the statistical yearbooks of each province in the YRB. Several indicators such as per capita grain yields, urbanization rate, and irrigation water per mu of farmland were collected from Chinese economic and social big data research platform. A linear interpolation approach was also introduced to address the issue of missing data and fill in the continuous data from 2002 to 2021. All the source data are illustrated in this paper and are available from http://data.stats.gov.cn, https://data.cnki.net, (accessed on 30 December 2023), or the corresponding author upon reasonable request.

4. Results

4.1. Result of Weight

Weight is a parameter used to measure the contribution of each indicator to the system. The accuracy of the weights directly affects the accuracy of the evaluation results. There are many methods to determine weights, including subjective weight and objective weight. Subjective weight is determined by the evaluator's subjective understanding of the index, which is greatly influenced by the evaluator's subjective influences. Objective weight is determined by the objective law between the index data, which is greatly influenced by the original data of the index. In order to avoid the subjectivity and one-sidedness of a single method affecting the evaluation results, this paper adopts a comprehensive weight that uses multiple weights. Its subjective weight uses the analytic hierarchy process, its objective weight uses the entropy weight, and its comprehensive weight is used to synthesize the two weights [31]. Table 2 shows the subjective weights, objective weights, and comprehensive weights of each indicator in the nine provinces studied based on the EW-AHP method. Overall, the indicators with large subjective weights are the green coverage rate of built-up area, water resources utilization rate, and the waste water discharge per CNY 10,000 of industrial added value, which are 0.14, 0.11, and 0.10, respectively. The indicators with large objective weights are Water resources per capita and the water supply ratio of ecology, which are 0.18 and 0.07, respectively. According to the comprehensive weight calculation method which was introduced in 2.1, the comprehensive weights of the water supply ratio of ecology and the water resources per capita are relatively large: 0.22 and 0.17, respectively.

4.2. Temporal Variation of HWHD

Figure 2 illustrates the temporal trend of the *HWHD* in the YRB during 2002–2021. Our analysis reveals that although the *HWHD* of the nine provinces in the Yellow River basin has remained in Nearly complete disharmony or Complete disharmony ($HWHD < 0.4$) over the past 20 years, there has been an upward trend. By 2021, five provinces had transitioned from Complete disharmony ($0 \leq HWHD \leq 0.2$) to Nearly complete disharmony ($0.2 < HWHD \leq 0.4$). Notably, provinces such as Shandong, Inner Mongolia, and Shaanxi exhibit substantial increases in *HWHD*, with variations of 0.18, 0.17, and 0.17, respectively. Conversely, upstream basin provinces like Sichuan and Ningxia experience mitigated increases, rising only by 0.10 and 0.12, respectively, from 2002 to 2021 (as shown in Figure 3). In addition, the *HWHD* in Ningxia is notably lower than that of other provinces, consistent with the findings of Shi et al. (2023) [21]. This can be attributed to Ningxia's lowest water resources per capita among all provinces, which holds the higher weight among all evaluation indicators. It's also related to the disparities in economic and technological development, geographic and climatic factors, as well as pertinent national or local regulations.

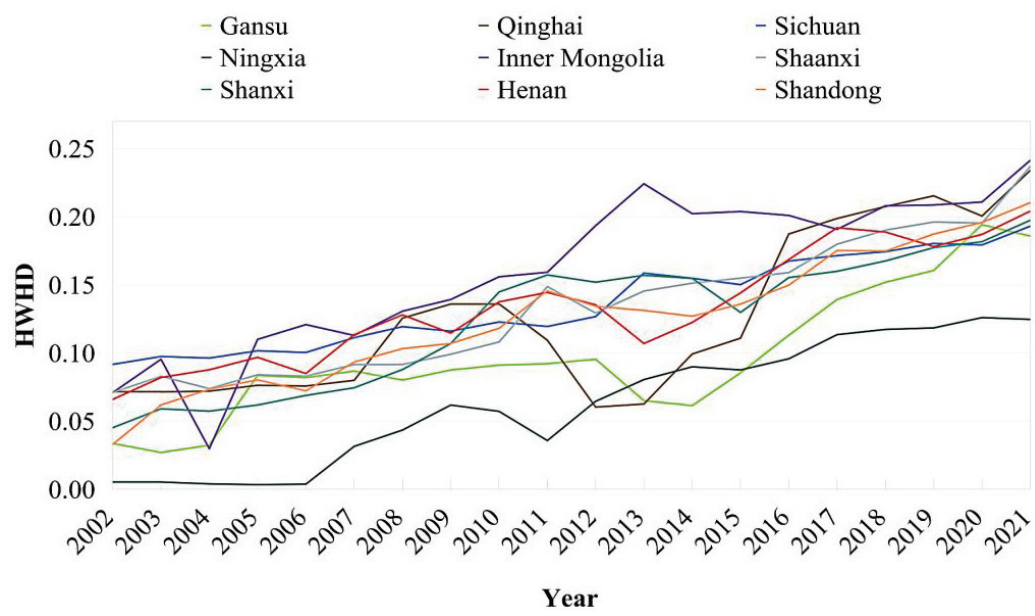

Figure 2. The temporal changes of *HWHD* across nine provinces in the YRB from 2002 to 2021.

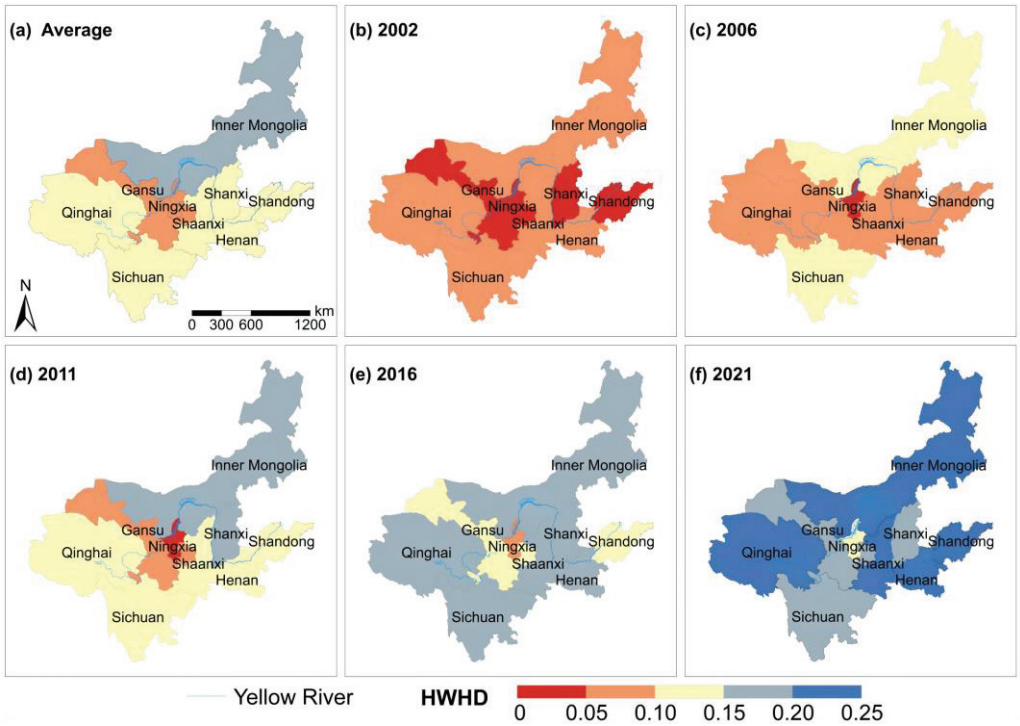

Figure 3. Spatial distribution of *HWHD* across nine provinces for the mean of 2002 to 2021.

Table 2. Comprehensive weights of indicators in nine provinces.

Indicator Layer	Subjective Weight	Objective Weight	Comprehensive Weight
Water resources per capita	0.0238	0.1859	0.1675
Water resources utilization rate	0.1190	0.0037	0.0165
Waste water discharge per CNY 10,000 of industrial added value	0.1071	0.0073	0.0296
Per capita COD emission	0.0357	0.0135	0.0182
Green coverage rate of built-up area	0.1429	0.0109	0.0588

Table 2. *Cont.*

Indicator Layer	Subjective Weight	Objective Weight	Comprehensive Weight
Natural population growth rate	0.0039	0.0178	0.0026
Urbanization rate	0.0317	0.0216	0.0259
population density	0.0025	0.0339	0.0033
Proportion of employees in the tertiary industry	0.0051	0.0294	0.0057
Engel's coefficient for urban residents	0.0204	0.0139	0.0107
Per capita disposable income of urban residents	0.0089	0.0586	0.0197
Per capita disposable income of rural residents	0.0089	0.0634	0.0214
Per capita grain yields	0.0143	0.0550	0.0298
Per capita comprehensive water consumption	0.0470	0.0142	0.0252
Per capita GDP	0.0145	0.0536	0.0294
Per capita fiscal revenue	0.0243	0.0634	0.0584
Per capita total social fixed asset investment	0.0131	0.0674	0.0335
Proportion of output value of tertiary industry in GDP	0.0183	0.0288	0.0199
GDP growth rate	0.0504	0.0206	0.0392
Growth rate of output value of tertiary industry	0.0223	0.0033	0.0028
Water consumption per CNY 10,000 of GDP	0.0251	0.0047	0.0045
Water consumption per CNY 10,000 of industrial added output	0.0381	0.0047	0.0067
Irrigation water per mu of farmland	0.0089	0.0116	0.0039
Reuse rate of urban industrial water	0.0138	0.0135	0.0071
College students per 10,000 people	0.0570	0.0288	0.0621
Water supply ratio of agriculture	0.0168	0.0237	0.0151
Water supply ratio of industry	0.0079	0.0395	0.0117
Water supply ratio of domestic	0.0376	0.0348	0.0496
Water supply ratio of ecology	0.0805	0.0725	0.2209

4.3. Spatial Variation of HWHD

Figure 3 gives the spatial variation of *HWHD* in 2002, 2006, 2011, 2016, and 2021, along with the average *HWHD* over the past two decades. With the exception of 2012−2015, *HWHD* of Ningxia has always been lower than other provinces. However, since 2006, *HWHD* of Ningxia has been significantly improved. It mainly due to the influence of economy, science and technology, and the per capita GDP and per capita financial revenue have notably improved. The water consumption per CNY 10,000 of GDP and growth rate of output value of tertiary industry decreased significantly. Over the past two decades, *HWHD* has notably improved in most of provinces, particularly in Shandong Province. Thanks to the increase in available water resources and the decrease in water consumption, the water resources utilization rate in Shandong province has decreased year by year. Consequently, its *HWHD* increased gradually, and the *HWHD* value reached 0.21 after 2020. In contrast, given the considerably lower value of the water supply ratio of ecology in Sichuan, which acts as the direct driving index of *HWHD*, coupled with its slow growth rate, the overall *HWHD* growth rate in the region is relatively sluggish. As a result, by 2020, Sichuan ranks as the third lowest in *HWHD* after Ningxia and Gansu. Additionally, we observed that the *HWHD* in downstream areas is generally higher than that in upstream areas, but this gap between upstream and downstream has been diminishing in recent years.

4.4. The Evaluation Results of Three Subsystems

The evaluated results in the three sub-criterion, healthy water systems (*HED*), sustainable human systems (*HAD*), and synergy between human and water systems (*DED*), are depicted in Figure 4. Overall, the harmony degrees of each subsystem across the nine provinces improved from 2002 to 2021. Furthermore, the harmony degrees of each subsystem varied among the provinces. For instance, the *HED* in the nine provinces exhibited less fluctuation and maintained consistent increments from 2002 to 2021. Among these

provinces, Inner Mongolia demonstrated the highest growth range, rising from 0.10 to 0.27, with a notable increase observed in 2013. This surge can be attributed to a significant reduction in Water resources utilization rate in the same year. Meanwhile, the *HED* of Sichuan showed a fluctuating upward trend due to changes in the total amount of water resources- and utilization rate.

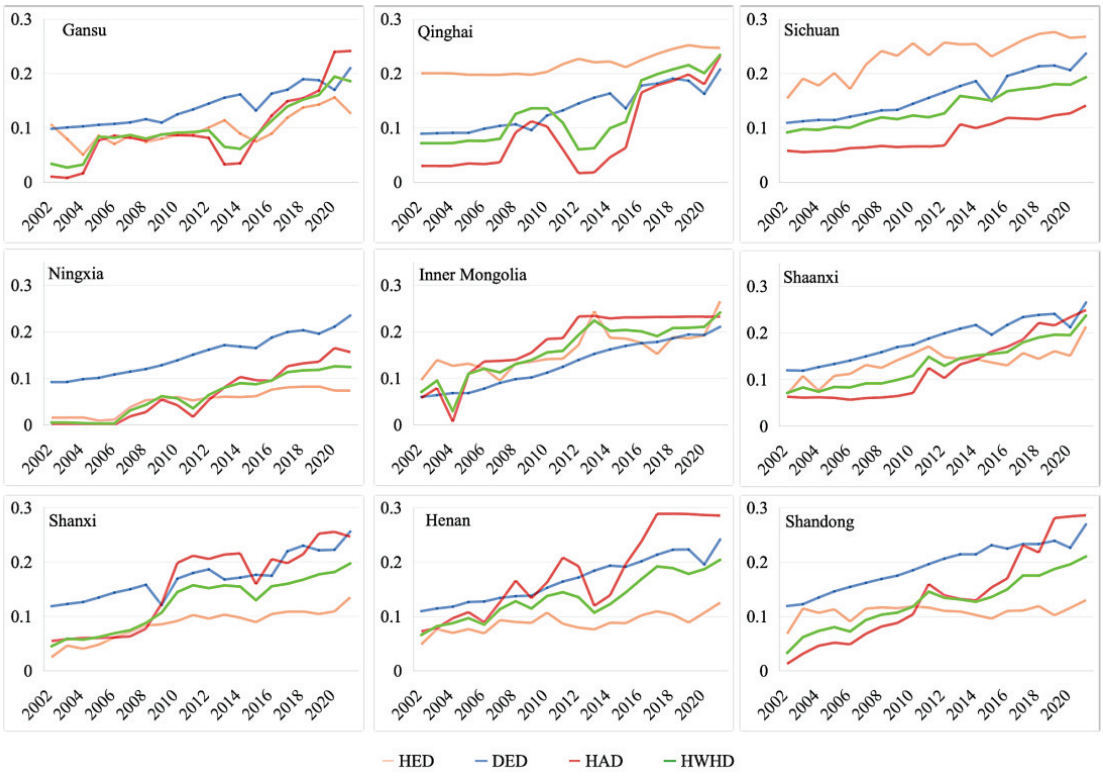

Figure 4. The four dimensions of *HWHD* across the nine provinces in YRB from 2002 to 2021.

The *DED* of nine provinces also maintained upward trends from 2002 to 2021. Notably, these provinces in downstream, such as Inner Mongolia, exhibited the highest incremental change, reaching 0.15. This change is primarily associated with societal, economic, and scientific developments. Specifically, Inner Mongolia's per capita disposable income of urban residents, Green coverage rate of built−up area, and water consumption per CNY 10,000 of industrial added value increased from 0 (Complete disharmony) to 0.7 (Fair harmony), 0.8 (Complete harmony), and 0.8 (Complete harmony), respectively. Moreover, the *DED* of Inner Mongolia experienced Flat growth during 2002–2021, attributed to a series of pragmatic and effective policy measures that enhanced the potential of industrial production and improved market supply−demand relationships.

The *HAD* of Henan experienced significant growth over the past 20 years, with a substantial increase observed from 2013 to 2017. This notable rise can be attributed to the considerable increase in indicators such as domestic water supply and ecological water supply during this period. Specifically, the supplied water resources increased by 6.8×10^8 m^3 and 13.7×10^8 m^3, respectively. The harmony degree associated with water supply ratio of domestic and water supply ratio of ecology increased from 0.6 (Fair harmony) to 1 (Complete harmony) and from 0.3 (Nearly complete disharmony) to 1 (Complete harmony), respectively. These improvements may result from the "Most Stringent Water Resource Management System" in 2013 was put into practice, leading to adjustments in total water utilization and irrigated water.

5. Discussion

Upon quantifying the harmony between humans and water in nine provinces of the YRB, our findings underscore the decisive role of the government's active guidance and investment in enhancing the living environment. For example, the *HWHD* value of Qinghai from 2011 to 2015 was notably lower than its overall change trend, reflecting extreme incoordination issues between the water system and the human system during this period. During this period, Qinghai Province actively increased its number of and investment in agricultural water conservancy projects in large and medium−sized irrigation areas, while vigorously expanding its area of efficient water−saving irrigation. Consequently, its proportion of the agricultural water supply decreased from an average of 80% during the 12th Five−Year Plan period (2011–2015) to less than 75.38% in 2016. As a result, the *HWHD* increased from an average of 0.09 to more than 0.18 after 2016.

Currently, the YRB faces prominent issues such as ecological fragility, water shortage, and weak resources carrying capacity. These issues interact with each other, becoming key restrictions for achieving the national development goals. Thus, it is of great significance to break the boundaries of single factors and single fields, and build a multi−dimensional, multi−objective and multi−system collaborative governance from the perspective of whole basin system. Moreover, water resources are the core factor restricting the protection and development of the YRB. The rigid constraints of water resources should be further implemented, especially for increasing the ecological water rationing in the upstream and adopting the water right replacement in the middle and downstream. Future studies should insist on using water to determine the city, land, people, and production, and improve the promote the intensive and economical water resources utilization.

6. Conclusions and Limitations

To learn about the human–water relationship in large river basins, we studied the changes in the *HWHD* in the YRB over the past two decades. We mainly considered 29 evaluation indicators, encompassing healthy water systems, sustainable human systems, and synergy between human and water systems in the YRB to construct an evaluation framework for human–water harmony. We analyzed the evolution trend of the overall *HWHD* and the above three sub−criterion in nine provinces of the YRB during 2002–2021. The results showed that there was a consistent increase in the *HWHD* across all provinces along the YRB in the last 20 years. Particularly noteworthy is the substantial growth in the *HWHD* observed in downstream provinces like Shanxi, Henan, and Shandong, exceeding 0.20 (Nearly complete disharmony) in 2021. In contrast, upstream provinces such as Ningxia have shown slower growth, at 0.11, resulting in this province having the lowest *HWHD* by 2021, at 0.12 (Complete disharmony).

Our results disclosed that the *HWHD* of the nine provinces showed a consistent increase during the past two decades; these findings provided valuable strategies for dealing with the future human–water relationship in the YRB. However, limitations need to be further considered in the future evaluation works. Due to data limitations, our analysis focused solely on the harmonious relationship between humans and water of nine provinces in the YRB, overlooking regional differences within provinces. Future studies could refine the research to the county scale or even the grid scale with sufficient survey data. This would enable the exploration of spatial differences and correlations of human–water harmony from upstream to downstream of large river basins, considering factors such as nature, climate, geographical conditions, and regional trade.

Author Contributions: L.L. collected the data, designed the evaluation system, performed the results analysis and wrote the original draft; L.H. performed the methodology and results validation, and wrote the original draft; Q.Z. coordinated the project. All authors have read and agreed to the published version of the manuscript.

Funding: This research was funded by the National Key Research and Development Program of China (no. 2021YFC3200201), the National Natural Science Foundation of China (no. 52279027).

Data Availability Statement: All the source data are illustrated in this paper.

Conflicts of Interest: The authors declare no conflicts of interest.

References

1. Vörösmarty, C.J.; McIntyre, P.B.; Gessner, M.O.; Dudgeon, D.; Prusevich, A.; Green, P.; Glidden, S.; Bunn, S.E.; Sullivan, C.A.; Liermann, C.R.; et al. Global threats to human water security and river biodiversity. *Nature* **2010**, *467*, 555–561. [CrossRef]
2. Mehta, L. Water and human development. *World Dev.* **2014**, *59*, 59–69. [CrossRef]
3. Oki, T.; Kanae, S. Global hydrological cycles and world water resources. *Science* **2006**, *313*, 1068–1072. Available online: http://webofscience.clarivate.cn.libproxy.v.zzu.edu.cn/wos/alldb/full%E2%88%92record/INSPEC:13105253 (accessed on 30 December 2023). [CrossRef]
4. Srinivasan, V.; Lambin, E.F.; Gorelick, S.M.; Thompson, B.H.; Rozelle, S. The nature and causes of the global water crisis: Syndromes from a meta−analysis of coupled human−water studies. *Water Resour. Res.* **2012**, *48*, W10516. [CrossRef]
5. He, C.; Liu, Z.; Wu, J.; Pan, X.; Fang, Z.; Li, J.; Bryan, B.A. Future global urban water scarcity and potential solutions. *Nat. Commun.* **2021**, *12*, 4667. [CrossRef]
6. Boulange, J.; Hanasaki, N.; Yamazaki, D.; Pokhrel, Y. Role of dams in reducing global flood exposure under climate change. *Nat. Commun.* **2021**, *12*, 417. [CrossRef]
7. Nerubasska, A.; Palshkov, K.; Maksymchuk, B. A systemic philosophical analysis of the contemporary society and the human: New potential. *Postmod. Open.* **2020**, *11*, 275–292. [CrossRef]
8. Zhou, A.; Zhang, Y.; Xie, S.; Chen, Y.; Li, X.; Wang, J.; Zou, J. Microplastics and their potential effects on the aquaculture systems: A critical review. *Rev. Aquac.* **2021**, *13*, 719–733. [CrossRef]
9. Yoo, C.; Jun, C.; Zhu, J.; Na, W. Evaluation of Dam Water−Supply Capacity in Korea Using the Water−Shortage Index. *Water* **2021**, *13*, 956. [CrossRef]
10. Schlosser, C.A.; Strzepek, K.; Gao, X.; Fant, C.; Blanc, É.; Paltsev, S.; Jacoby, H.; Reilly, J.; Gueneau, A. The future of global water stress: An integrated assessment. *Earth's Future* **2014**, *2*, 341–361. [CrossRef]
11. Mathias, J.M.; Thomas, R.B. Global tree intrinsic water use efficiency is enhanced by increased atmospheric CO_2 and modulated by climate and plant functional types. *Proc. Natl. Acad. Sci. USA* **2021**, *118*, e2014286118. [CrossRef]
12. Yu, L.; Gao, X.; Zhao, X. Global synthesis of the impact of droughts on crops' water−use efficiency (WUE): Towards both high WUE and productivity. *Agric. Syst.* **2020**, *177*, 102723. [CrossRef]
13. Garriga, R.G.; Foguet, A.P. Improved method to calculate a water poverty index at local scale. *J. Environ. Eng.* **2010**, *136*, 1287–1298. [CrossRef]
14. Ladi, T.; Mahmoudpour, A.; Sharifi, A. Assessing impacts of the water poverty index components on the human development index in Iran. *Habitat Int.* **2021**, *113*, 102375. [CrossRef]
15. Jia, Z.; Cai, Y.; Chen, Y.; Zeng, W. Regionalization of water environmental carrying capacity for supporting the sustainable water resources management and development in China. *Resour. Conserv. Recycl.* **2018**, *134*, 282–293. [CrossRef]
16. Assefa, Y.T.; Babel, M.S.; Sušnik, J.; Shinde, V.R. Development of a generic domestic water security index, and its application in Addis Ababa, Ethiopia. *Water* **2018**, *11*, 37. [CrossRef]
17. Ding, Y.; Tang, D.; Dai, H.; Wei, Y. Human−water harmony index: A new approach to assess the human water relationship. *Water Resour. Manag.* **2014**, *28*, 1061–1077. [CrossRef]
18. Zuo, Q.; Diao, Y.; Hao, L.; Han, C. Comprehensive evaluation of the human−water harmony relationship in countries along the "belt and road". *Water Resour. Manag.* **2020**, *34*, 4019–4035. [CrossRef]
19. Zhou, Y.; Zou, S.; Duan, W.; Chen, Y.; Takara, K.; Di, Y. Analysis of energy carbon emissions from agroecosystems in Tarim River Basin, China: A pathway to achieve carbon neutrality. *Appl. Energy* **2022**, *325*, 119842. Available online: http://www.sciencedirect.com.libproxy.v.zzu.edu.cn/science/article/pii/S0306261922011114 (accessed on 30 December 2023). [CrossRef]
20. Zhang, J.; Tang, D.; Wang, M.; Ahamd, I.; Hu, J.; Meng, Z.; Pan, S. A Regional Water Resource Allocation Model Based on the Human–Water Harmony Theory in the Yellow River Basin. *Water* **2023**, *15*, 1388. [CrossRef]
21. Shi, Y.; Yang, S.; Chen, W.; Wang, X.; Feng, C. Research on the construction of a human−water harmony model in the Yellow River Basin. *Water Policy* **2023**, *25*, 742–757. [CrossRef]
22. Ahmad, I.; Waseem, M.; Lei, H.; Yang, H.; Yang, D. Harmonious level indexing for ascertaining human–water relationships. *Environ. Earth Sci.* **2018**, *77*, 125. [CrossRef]
23. Yin, L.; Feng, X.; Fu, B.; Wang, S.; Wang, X.; Chen, Y.; Tao, F.; Hu, J. A coupled human−natural system analysis of water yield in the Yellow River basin, China. *Sci. Total Environ.* **2021**, *762*, 143141. [CrossRef]
24. Zuo, Q.; Zhang, Z.; Ma, J.; Li, J. Solutions to Difficult Problems Caused by the Complexity of Human–Water Relationship in the Yellow River Basin: Based on the Perspective of Human–Water Relationship Discipline. *Water* **2022**, *14*, 2868. [CrossRef]
25. Xie, P.; Zhuo, L.; Yang, X.; Huang, H.; Gao, X.; Wu, P. Spatial−temporal variations in blue and green water resources, water footprints and water scarcities in a large river basin: A case for the Yellow River basin. *J. Hydrol.* **2020**, *590*, 125222. [CrossRef]
26. Liu, S.; Zhao, L. Development and synergetic evolution of the water–energy–food nexus system in the Yellow River Basin. *Environ. Sci. Pollut. Res.* **2022**, *29*, 65549–65564. [CrossRef]

27. Shannon, C.E. A mathematical theory of communication. *Bell Syst. Tech. J.* **1948**, *27*, 379–423. Available online: https://ieeexplore.ieee.org/document/6773024 (accessed on 30 December 2023). [CrossRef]
28. Saaty, T.L. A scaling method for priorities in hierarchical structures. *J. Math. Psychol* **1977**, *15*, 234–281. [CrossRef]
29. Ma, Y.; Shi, T.; Zhang, W.; Hao, Y.; Hung, J.; Lin, Y. Comprehensive policy evaluation of NEV development in China, Japan, the United States, and Germany based on the AHP−EW model. *J. Clean. Prod.* **2019**, *214*, 389–402. Available online: http://www.sciencedirect.com.libproxy.v.zzu.edu.cn/science/article/pii/S0959652618338277 (accessed on 30 December 2023). [CrossRef]
30. Zuo, Q.; Zhang, Y.; Lin, P. Index system and quantification method for human−water harmony. *J. Hydraul. Eng.* **2008**, *39*, 440–447. Available online: http://webofscience.clarivate.cn.libproxy.v.zzu.edu.cn/wos/alldb/full%E2%88%92record/CSCD:3287618 (accessed on 30 December 2023).
31. Zuo, Q.; Zhao, H.; Mao, C.; Ma, J.; Cui, G. Quantitative Analysis of Human−Water Relationships and Harmony−Based Regulation in the Tarim River Basin. *J. Hydrol. Eng.* **2015**, *20*, 1–11. [CrossRef]

water

MDPI

Article

Analysis of the Water Quality Status and Its Historical Evolution Trend in the Mainstream and Major Tributaries of the Yellow River Basin

Zhenzhen Yu [1], Xiaojuan Sun [1,2], Li Yan [1,*], Shengde Yu [3], Yong Li [1] and Huijiao Jin [1]

[1] Yellow River Water Resources Protection Institute, Zhengzhou 450004, China; zzyuhydro@126.com (Z.Y.); sunxiaojuan@gs.zzu.edu.cn (X.S.); 2wi861015@163.com (Y.L.); 13980603356@163.com (H.J.)
[2] School of Water Conservancy and Transportation, Zhengzhou University, 100 Kexue Avenue, Zhengzhou 450001, China
[3] Ecohydrology Research Group, Department of Earth and Environmental Sciences, University of Waterloo, 200 University Avenue West, Waterloo, ON N2L 3G1, Canada; s228yu@uwaterloo.ca
* Correspondence: yanli_5677@163.com

Abstract: The Yellow River basin, an area of extreme water scarcity, has faced significant challenges in water quality management due to rapid economic and social development since the 1980s. This study analyzes the water quality evolution over nearly 40 years, focusing on primary pollutants like chemical oxygen demand (COD), ammonia nitrogen (NH_3-N), and permanganate index (COD_{Mn}). In the 1990s, sections of the river were severely polluted, with some areas failing to meet the lowest national standards. In 2000, 32% of the river water was classified as inferior Class V. However, enhanced water resource management and stricter pollutant regulations introduced after 2000 have significantly improved water quality. By 2010, water quality reached its nadir, with 16% of water classified as inferior Class V and 25% as Class IV–V. By 2020, water quality showed marked improvement, with a significant reduction in segments classified as inferior Class V and Class IV–V. Recent years have seen water quality stabilize, with COD meeting Class I standards and NH_3-N and COD_{Mn} meeting Class II standards based on national criteria. The study also highlights discrepancies in water quality between the mainstream and tributaries of the Yellow River. While the mainstream generally maintains good water quality, many tributaries remain severely polluted. In 2022, 85% of the water in tributaries was classified as Class I to III, 12.3% as Class IV to V, and only 2.7% as Class V. However, all water in the mainstream reached Class I–III, with 86% achieving Class II and 14% achieving Class I. A detailed analysis of the Huayuankou section over the past three decades shows a general decline in pollution indicators. Seasonal water quality fluctuations, correlated with flow rates and temperatures, were observed, often exhibiting normal distribution patterns. These findings underscore the effectiveness of sustained pollution control and the need for continuous, adaptive management strategies to improve and maintain water quality in the Yellow River basin.

Keywords: mainstream and tributaries; water environmental quality status; water quality evolution trend; Huayuankou section; Yellow River basin

1. Introduction

The Yellow River, the mother river of the Chinese nation originating from the Qinghai–Tibet Plateau, is 5464 km long and has a total basin area of 795,000 km^2 [1]. This river is essential not only as a water supply source for the arid regions of northwestern and northern China but also as a linchpin for major agricultural, industrial, and energy production activities [2–4]. The Yellow River basin serves as a critical region for national economic development and supports a significant portion of China's grain production. Specifically in recent years, the basin is responsible for about 13% of China's food production area and 15% of the arable land area, underscoring its importance to food security [5]. The basin

is also responsible for urban water supply to over 50 large-and medium-sized cities [2]. Furthermore, the basin is a vital area for energy resources, including the Longyanxia's hydropower station and the Qinghai power grid [6,7].

Despite its importance, the Yellow River basin faces extreme water scarcity, complicating efforts to protect and manage its water environment. Since the 1990s, there has been a persistent water scarcity characterized by total water withdrawals exceeding the total available water [8]. In the applications of Yellow River water, agriculture, industry, and urban residential areas contributed to a reduction in the water amount by 40%, 26%, and 16%, respectively [2]. Meanwhile, the intricate hydrology of the river, combined with the diverse ecological and economic functions it serves, underscore the urgent need for effective water quality management [9]. Over the past four decades, the Yellow River has experienced significant fluctuations in water quality due to a combination of natural factors and human activities [10]. Natural factors such as climate change and seasonal variability have influenced water flow and quality, while anthropogenic activities, including industrial discharge, agricultural runoff, and urban development, have significantly contributed to pollution levels [11]. Rapid economic and social development, starting in the 1980s and continuing onward, led to substantial increases in water pollution [12]. Industrial discharges surged as factories proliferated along the river, and agricultural activities intensified, leading to the increased runoff of fertilizers and pesticides, thereby elevating the heavy metal pollution in the area [13]. Urbanization further exacerbated the situation, with untreated sewage effluents being one of the major pollutants [14]. Specifically, industrial wastewater, domestic wastewater, phosphorus, and nitrogen accounted for 66%, 21%, 8%, and 5% of the influence on water quality, respectively [2]. During urbanization, deteriorated water quality adversely impacted both the ecosystem's health and the millions of people depending on it. For instance, the migratory fish species in the lower Yellow River have been gradually affected by anthropogenic modifications to the river system since the 1950s, which led to their current rarity [15]. Additionally, 30.1–34.7% of the total population experienced seasonal water scarcity, while 20.2–35.5% faced perennial water scarcity [8].

However, since 2000, enhanced water resource management and stricter pollutant regulations have begun to mitigate water pollution, leading to gradual improvements in water quality [5,15]. Initiatives such as the implementation of the "Action Plan for Prevention and Control of Water Pollution" in 2015, along with increased investment in wastewater treatment facilities, have contributed to these improvements [15,16]. Recent years have seen improvements and stabilization in water quality, which is evident in the decreasing trend of COD_{Mn} and NH_3-N from 2008 [17]. The increased water resource carrying capacity since 2005 also indicates the improving trend of the Yellow River water body [18]. Although water quality has improved in various areas, sustainable water use and comprehensive management still need to be strengthened. Just like the lack of identification and diagnosis technology that leads to little control and insufficient scientific basis in management, achieving the precise identification and diagnosis of water environment problems remain challenging [19].

Studying the water quality status and its historical evolution in the mainstream and major tributaries of the Yellow River basin is essential for understanding the impacts of human activities and natural processes on this vital water resource. Our studies in this article focus on several key investigations regarding the water quality of the Yellow River basin and aim to provide insights into the precise management of the water body. These investigations include examining trends in water usage, wastewater discharge, and pollutant emissions over the period from 1980 to 2015, as well as tracking changes in overall water quality classification from 1980 to 2022 by categorizing water into different quality classes. Additionally, the article observes water quality in the mainstream of the Yellow River from 2011 to 2022 and compares concentrations of pollutants, specifically COD and NH_3-N, in the mainstream between 2000 and 2018. It also analyzes water quality in the tributaries of the Yellow River from 2011 to 2022 and investigates concentrations of COD and NH_3-N

in specific segments of the Yellow River tributaries between 2000 and 2018. Furthermore, the study assesses daily, monthly, and annual fluctuations in primary pollutants in the Huayuankou section from 1992 to 2022. This study also highlights the differences in water quality trends between the mainstream and tributaries of the Yellow River, revealing that while the mainstream's water quality has generally been acceptable, some tributaries continue to suffer from severe pollution.

2. Materials and Methods

2.1. Study Area

The physical characteristics of the Yellow River include a winding and variable mainstream, unevenly distributed tributaries, and a large longitudinal drop in the riverbed (Figure 1). The length of the main river channel is 5464 km, winding eastward from the source with the river channel shaped similar to the Chinese character "几" [1]. The upper reaches are the main runoff area of the Yellow River [20]. From Longyangxia to Xiaheyuan in Ningxia, the river drops are mainly located between gorges, providing sufficient hydraulic resources [21]. From Xiaheyuan to Hepu Town, the Yellow River flows through the wide and flat Ning–Mongolian plain, where large irrigation areas are scattered on both sides [21]. Floods and ice disasters occurred in the plains along the river to different extents. Notably, in the Sanshenggong section, ice jams and ice dams obstruct water flow during the ice flood period, resulting in dike breaches [22]. Most middle reaches are located in Loess Plateau, which is the primary source of floods and silt, characterized by the loss in soil and water [23]. The longest continuous canyon on the mainstream of the Yellow River is the Jinshaan Canyon, which is located from Hepu Town to Yumenkou and offers rich hydraulic resources [24]. From Yumenkou to Tongguan, the Yellow River flows through the Fenwei trench, where the river channel becomes wide and shallow, and the erosion and siltation changes are extremely severe [25]. Valleys gradually widen below the Xiaolangdi, which is the transition section of the Yellow River from mountains to plains [26]. The downstream area is the world-famous suspended river with a serious threat of floods [27]. From Taohuayu to the estuary, with the exception of the hills from the south bank of Dongping Lake to Jinan, the remaining banks rely on dikes to obstruct water [28].

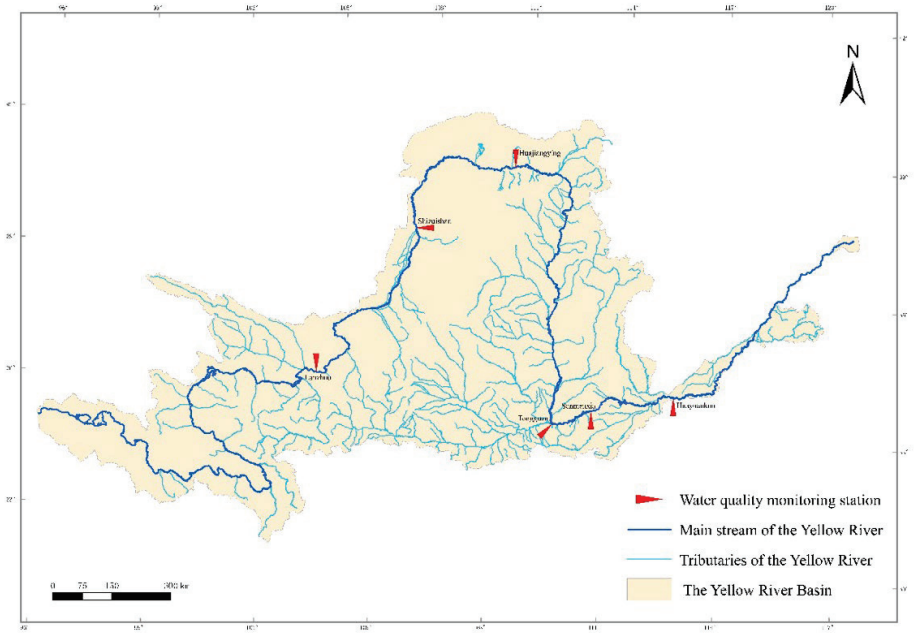

Figure 1. Characteristics of the Yellow River basin.

There are 220 tributaries with a catchment area greater than 100 km^2 in the Yellow River basin [29]. Among these tributaries, there are 76 tributaries with an area greater

than 1000 km^2 (43 in the upper reaches, 30 in the middle reaches, and 3 in the lower reaches) [29]. The basin area is 580,000 km^2, accounting for 77% of the total river catchment area [30]. Moreover, there are 10 tributaries larger than 10,000 km^2, whose basin area reaches 370,000 km^2, accounting for 50% of the total river catchment area [31]. Key tributaries, including the Fen River, Luo River, Qin River, Wei River, and Yi River, constitute the main body of Yellow River basin area [32]. These tributaries originate from various regions and bring with them unique hydrological and sediment characteristics which affect the overall water quality and ecological health of the Yellow River [33].

The Fen River originates from the Luliang Mountains and is a major tributary in Shanxi Province [32]. It is known for its high sediment load due to soil erosion in the Loess Plateau region [34]. The Luo River, another significant tributary, flows through the provinces of Shaanxi and Henan, contributing to the Yellow River's flow and sediment [32]. The Qin River, which flows from the Taihang Mountains, also joins the Yellow River in Henan Province, impacting its hydrological dynamics [32]. The Wei River is one of the largest tributaries, originating from the Longshan Mountains in Gansu Province [32]. It plays a critical role in the agriculture and water resources of the region [35]. The Yi River, flowing through the provinces of Henan and Shandong, is noted for its historical significance and contributions to the Yellow River's sediment and flow [36]. These tributaries, along with others, contribute to the Yellow River's complex hydrology, influencing water quality, sediment transport, and ecological dynamics across different regions [33].

Huayuankou was a significant historical city in the Central Plains of China, known for the establishment, survival, and development of the Yellow River warping irrigation area [37]. The Huayuankou section is an important water quality control point in the lower reaches of the Yellow River [11]. Located downstream from Huayuankou, the river section features a typical wandering channel constrained by large dikes on both sides, resembling an elevated river [38]. The environmental conditions of water bodies in the Huayuankou section are affected not only by upstream tributaries like the Yi River, Luo River, Qin River, Mang River, and direct sewage outlets into the Yellow River, but also constrained by the riverbank conditions, the operation mode of the Xiaolangdi reservoir, and its outflow characteristics [39]. Therefore, this Huayuankou section serves as a typical section for analyzing fluctuations in water quality.

2.2. Methodology

This study focuses on the analysis of water quality in the Yellow River, utilizing nearly four decades of water quality data collected from various monitoring stations [40], with the Huayuankou section serving as a key sampling point. Based on the analysis of national surface water environmental monitoring statistical data, the evaluation metrics of water quality include the pH value, DO, COD_{Mn}, COD, BOD_5, NH_3-N, total phosphorus (TP), copper, zinc, fluoride, selenium, arsenic, mercury, cadmium, hexavalent chromium, lead, cyanide, volatile phenol, petroleum, anionic surfactants, and sulfides [40,41]. Data analysis was performed using Python 3.10 for statistical computations, graph generation, and OriginPro 2024 for graph production and visualization.

In this study, the water quality assessment primarily focuses on the evaluation of primary pollutants, including COD, NH_3-N, and COD_{Mn}. These were analyzed using the dichromate method, salicylic acid spectrophotometry, and titration method, respectively. In addition, water flow rate and temperature were recorded. The single-factor evaluation method was then employed against the national water quality standards (GB3838-2002) [41], where each parameter was compared with the established standard values to determine the water quality class. The overall classification was based on the parameter showing the poorest performance, which determines the final evaluation outcome.

The water quality classification system, ranging from Class I to Class V, offers a structured approach for evaluating and managing the health of rivers, water systems, and watersheds. Supplementary Table S1 provides specific details regarding the classification of water. This system establishes a comprehensive framework for monitoring a wide array of

chemical and physical parameters [41]. These stringent guidelines ensure the preservation of water quality across different classes, thereby protecting aquatic ecosystems and public health by controlling key pollutants and maintaining ecological balance.

Time-series analysis and data visualization techniques—such as bar charts, radar charts, line graphs, and composite graphs—were employed to identify trends and variations in pollutant concentrations from 1980 to 2022. This analysis utilized data from the National Surface Water Quality Automatic Monitoring Real-Time Database and on-site test results from the Yellow River Huayuankou section conducted between 1 March and 30 March 2020, as detailed in Supplementary Table S2. The detection limits for each testing item are provided in Supplementary Table S3 to ensure the accuracy and reliability of the measurements. Statistical tools were employed to calculate the maximum, minimum, range, and average values, enabling the interpretation of data and the exploration of relationships between pollutant levels and different years. Rigorous quality control measures, including regular instrument calibration, ensured data accuracy and consistency. Anomalies were thoroughly investigated and corrected to maintain data integrity. This comprehensive methodology enabled a detailed assessment of water quality and its historical evolution in the Yellow River basin, providing valuable insights for environmental management and policymaking.

3. Results

3.1. Water Quality in the Yellow River Basin

3.1.1. Water Usage, Wastewater Discharge, and Pollutant Emissions in the Yellow River Basin

Figure 2 below presents a comprehensive overview of the trends in water usage, wastewater discharge, and pollutant emissions in the Yellow River basin from 1980 to 2015. The graph highlights significant increases in water usage and wastewater discharge, along with fluctuations in pollutant levels, particularly COD and NH_3-N.

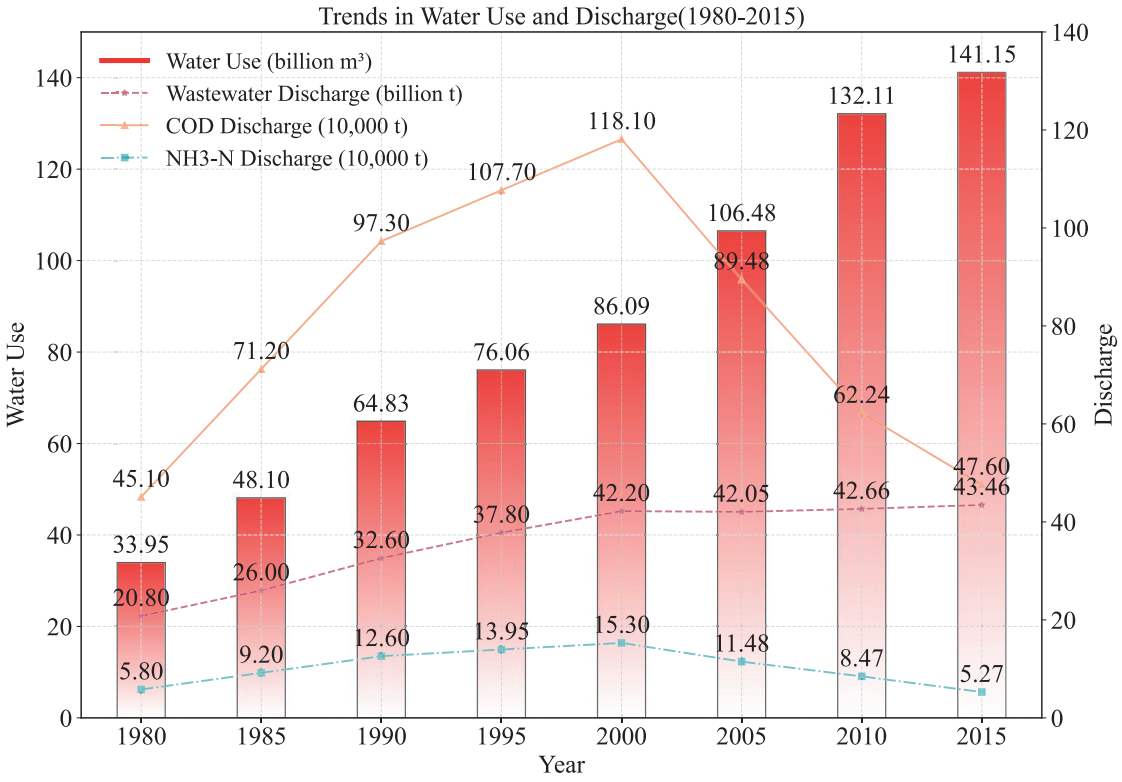

Figure 2. Water usage, wastewater discharge, and pollutant emissions in the Yellow River basin during 1980–2015. Water usage is plotted on left y axis; COD and NH_3-N are plotted on right y axis.

The red bars represent the total water usage per billion cubic meters (m^3). Over the 35-year period, water usage exhibits a marked increase, starting from 33.95 billion m^3 in 1980 and reaching a peak of 141.15 billion m^3 in 2015. This upward trend underscores the escalating demand for water resources driven by industrial growth, agricultural expansion, and urbanization. The purple dashed line with star markers illustrates the volume of wastewater discharged into the Yellow River basin, measured per billion tons. Wastewater discharge increased from 20.80 billion tons in 1980 to a peak of 43.46 billion tons in 2015. Notably, post-2000, the wastewater discharge fluctuated between 42 billion tons and 43 billion tons. While there is a slight increase from 42.20 billion tons in 2000 to 43.46 billion tons in 2015, the overall rate of increase in wastewater discharge is relatively small compared to the previous 20 years, during which it rose from 20.80 billion tons in 1980 to 42.20 billion tons in 2000. This slowdown in the pace indicates efforts to control and manage wastewater emissions through improved treatment facilities and regulatory measures.

The graph also tracks the discharge of two major pollutants: COD and NH_3-N, both critical indicators of water quality. The COD discharge is represented by the orange line with square markers; COD discharge shows a significant rise from 451,000 tons in 1980 to a peak of 1.181 million tons in 2000. Following this peak, there is a noticeable decline, with levels dropping to 476,000 tons by 2015. On the other hand, the NH_3-N discharge is indicated by the blue line with circular markers; NH_3-N discharge initially increased from 58,000 tons in 1980 to 153,000 tons in 2000. After reaching this peak, NH_3-N levels exhibited a steady decrease, reducing to 52,700 tons by 2015. The declines in both major pollutants signify the effectiveness of pollution control measures implemented over the years after 2000.

3.1.2. Classification of Overall Water Quality in the Yellow River Basin

Water quality is categorized into three classes to investigate the changes in overall water quality, which are Class I–III (good quality), Class IV–V (poor quality), and inferior Class V (very poor quality).

A radar chart is used to depict the river length ratio of different water quality classes from 1980 to 2020, with particular attention to key years (Figure 3). This chart provides an overview of the proportion of the river's length that falls into each water quality category over the years. Based on data from the surveillance program, more than 80% of the river segments monitored met Class III water quality standards in 1980. Therefore, the water quality of the Yellow River's mainstream was generally good at the time, except during the dry season in Lanzhou and Baotou, where some tributaries near large and medium-sized cities occasionally exceeded standards. By 1990 and 1995, the quality began to deteriorate, with an increase in segments classified as Class IV–V and inferior Class V. The year 2000 saw significant industrial development in the energy and chemical sectors, leading to increased water consumption and wastewater discharge. This period indicates a notable decline in water quality, with 32% of the water falling into inferior Class V. The year 2010 marked the lowest point in water quality, with approximately 16% of the water classified as inferior Class V, 25% as Class IV–V, and the remainder as Class I–III. During this period, 37.9% of the water at provincial boundaries was classified as inferior Class V, and 90.0% of main drinking water sources failed to meet standards. By the mid-2010s, the majority of the river length consistently fell into the Class I–III category. By 2020, there were improvements in water quality, with a significant reduction in segments classified as inferior Class V and Class IV–V.

A stacked bar graph illustrates the continuous changes in overall water quality from 2001 to 2022, depicted as section ratios (Figure 4). This figure illustrates the proportion of different water quality categories within specific sections of the river basin each year. Overall, the analysis using surveillance data from 2001 to 2022 indicates that the trend of water quality deterioration in the basin has been controlled in recent years, with overall water quality gradually improving. In 2001, the annual average proportion of water classified as inferior Class V quality in the basin was 56%, while only 12.2% of the water met Class

I to III standards. By 2022, the water quality had notably improved, with 87.4% meeting Class I to III standards, 10.3% falling into Class IV to V, and only 2.3% classified as inferior Class V. Compared to 2001, this represents a significant 75.2% increase in the proportion of water with Class I to III quality, and a notable 53.7% decrease in water classified as inferior Class V quality. The figure also shows that from 2001 to 2005, there were substantial fluctuations in water quality, with a considerable portion of the water classified as Class IV–V and inferior Class V. However, starting from 2006, there is a visible trend toward improvement, with the proportion of water in the good quality range (Class I–III) steadily increasing.

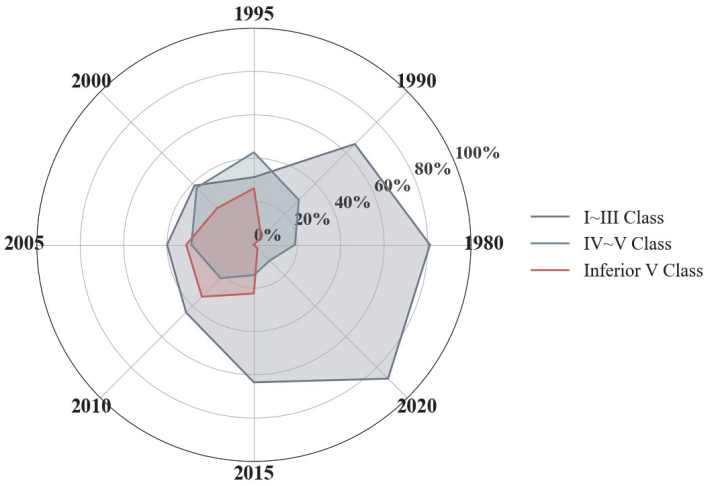

Figure 3. Changes in overall water quality in the Yellow River basin from 1980 to 2020.

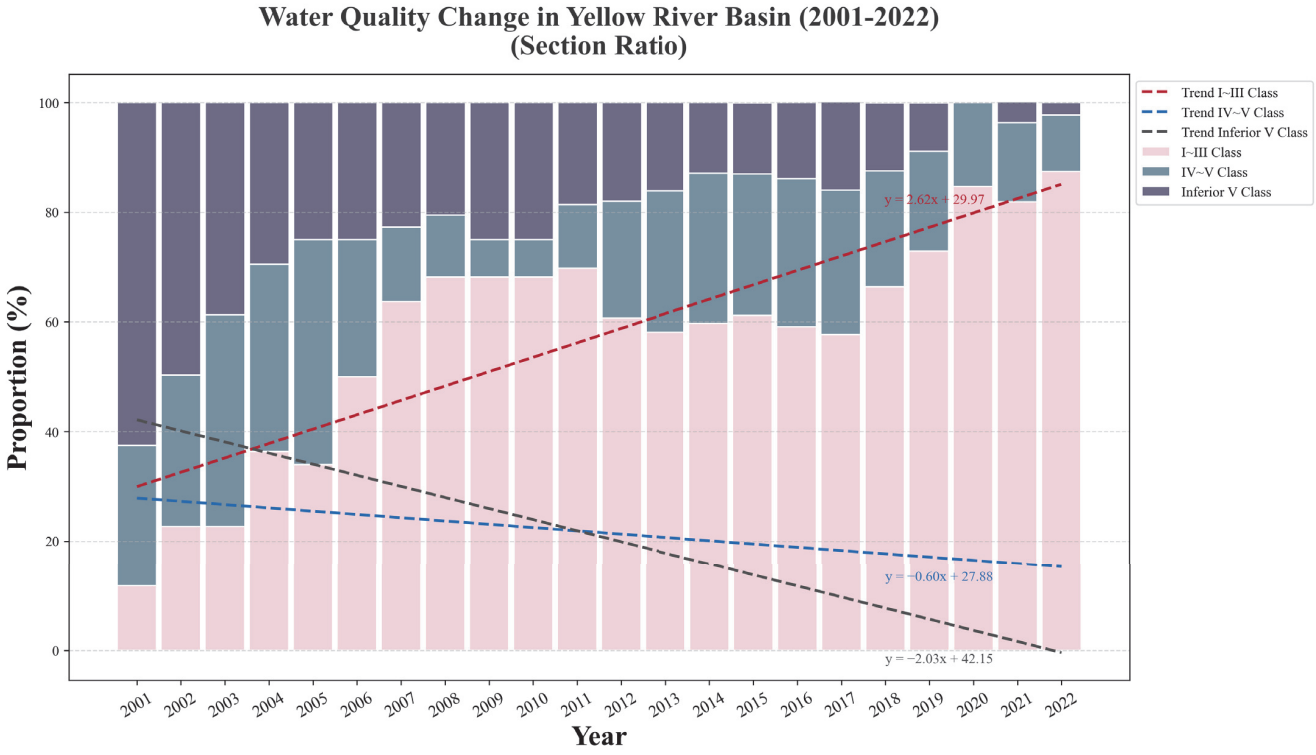

Figure 4. Changes in overall water quality in the Yellow River basin from 2001 to 2022.

3.2. Water Quality in the Yellow River Mainstream

3.2.1. Classification of Overall Water Quality in the Yellow River Mainstream

Figures 5 and 6 below provide insights into the water quality trends in the mainstream of the Yellow River from 2011 to 2022, highlighting key observations and patterns that reflect the mainstream's environmental status.

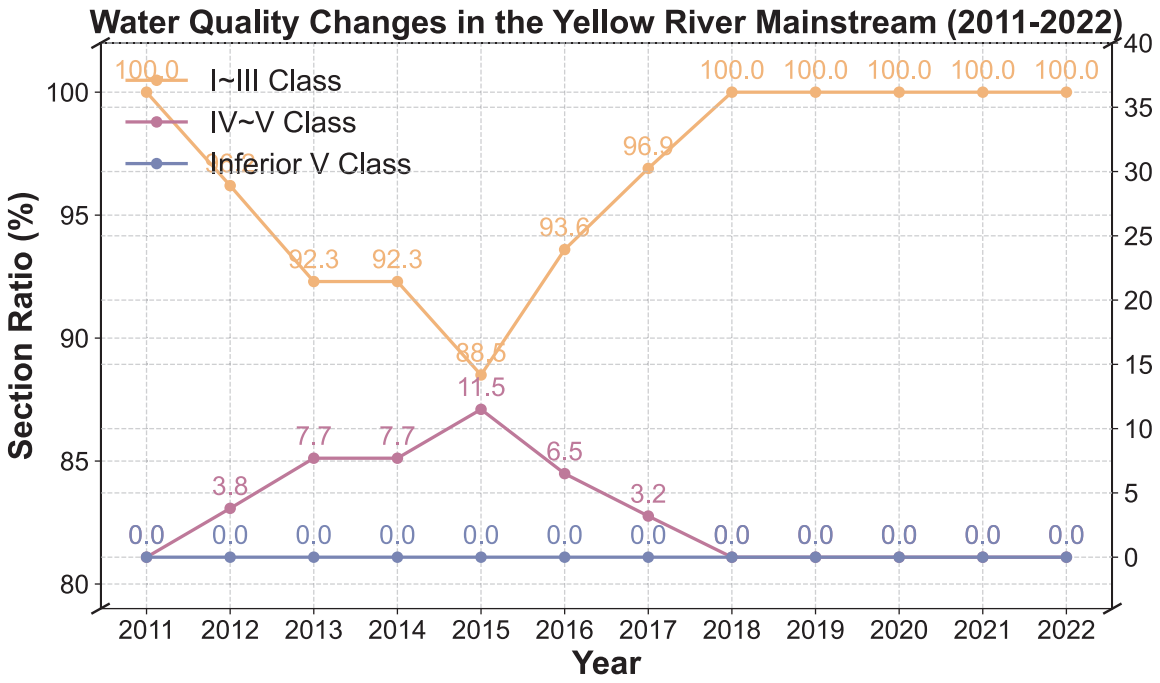

Figure 5. Changes in overall water quality in the Yellow River mainstream from 2011 to 2022.

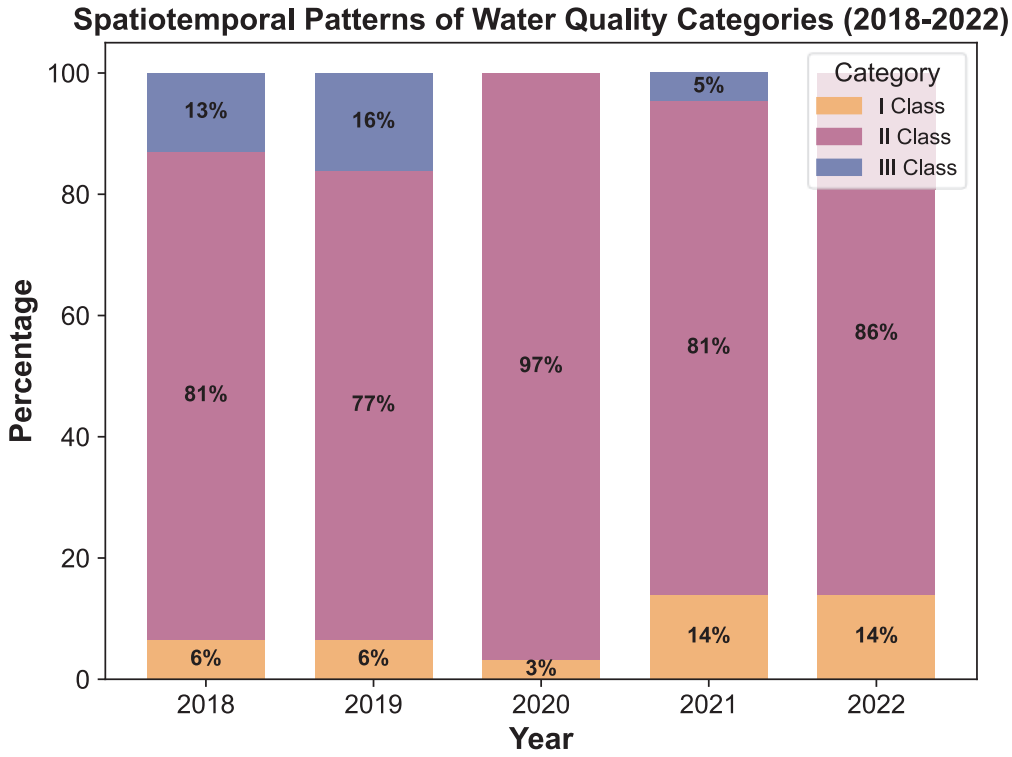

Figure 6. Classification of water quality in the Yellow River mainstream from 2018 to 2022.

The section ratio of various water quality classes over the years demonstrates a consistent trend of high water quality from 2011 to 2022 (Figure 5). Throughout this period, there was no instance of water being classified as inferior Class V quality in the mainstream. The mainstream generally maintained excellent water quality, with an average of 96.66% of the water classified as Class I to III and only 3.37% falling into Class IV to V. The year 2015 marked the lowest water quality, with 11.5% of the water in Class IV to V and 88.5% in Class I to III. Furthermore, the spatiotemporal distribution of water quality categories from 2018 to 2022 is visualized in Figure 6. Throughout this period, the mainstream consistently maintained Class I to III water quality, indicating a stable and positive trend. Notably, in both 2020 and 2022, the majority of the water quality was classified as Class II and above. In 2018, the distribution was 81% Class I, 13% Class II, and 6% Class III. By 2022, the quality had further improved, with 86% of the water in Class I, 14% in Class II, and none in Class III.

3.2.2. Pollutant Concentrations in the Yellow River Mainstream

A comparison of the concentrations of COD and NH_3-N in the mainstream of the Yellow River between the years 2000 and 2018 was conducted and concluded significant improvements in water quality over this period (Figure 7).

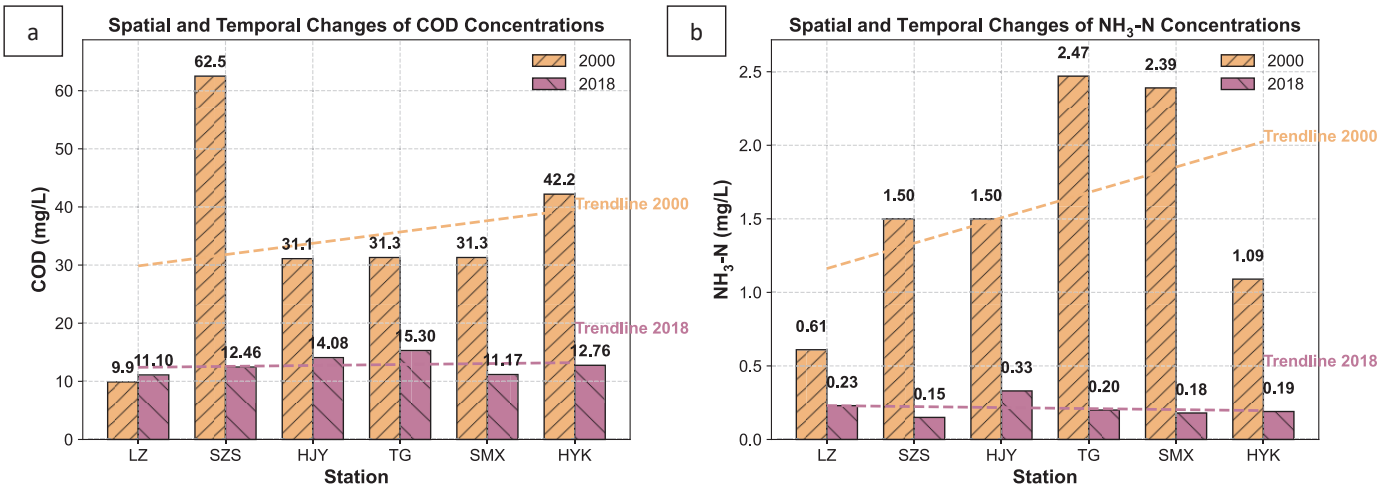

Figure 7. Changes in pollutant concentrations at the measured sites of the Yellow River mainstream in 2000 and 2018 with trendlines. (**a**) COD concentrations and (**b**) NH_3-N concentrations.

The results reveal a substantial decline in COD levels by 2018 compared to 2000 (Figure 7a). The average COD concentration across primary water bodies, including Lanzhou (LZ), Shizuishan (SZS), Huajiangying (HJY), Tongguan (TG), Sanmenxia (SMX), and Huayuankou (HYK), was 12.81 mg/L in 2018. This represents a reduction of 21.91 mg/L or 63.10% compared to the levels observed in 2000. For instance, Lanzhou saw a decrease from 62.5 mg/L in 2000 to 9.91 mg/L in 2018, while Huayuankou's COD concentration dropped from 42.2 mg/L to 12.76 mg/L. As for the changes in NH_3-N concentrations at the same measured sites (Figure 7b), the average NH_3-N concentration in 2018 was 1.59 mg/L, which is a decrease of 1.38 mg/L or 86.61% compared to 2000. Specific examples include Shizuishan, where NH_3-N levels dropped from 1.50 mg/L in 2000 to 0.15 mg/L in 2018, and Tongguan, which saw a reduction from 2.47 mg/L to 0.20 mg/L.

3.3. Water Quality of Major Tributaries in the Yellow River

3.3.1. Classification of Overall Water Quality in the Yellow River Tributaries

According to a contemporaneous comparative analysis from 2011 to 2022, the water quality of the Yellow River tributaries has improved significantly from moderate pollution to good condition. Changes in the overall water quality in the tributaries feeding into the

Yellow River were observed from 2011 to 2022 (Figure 8). On average, the proportion of water classified as Class I to III quality was 53.88%, while Class IV to V accounted for 28.32% and Class V comprised 17.77% of the total. Notably, in 2011, water quality was at its poorest, with approximately 62% of the water identified as Class V. However, by 2022, there was a remarkable improvement, with 85% of the water classified as Class I to III, 12.3% as Class IV to V, and only 2.7% as inferior Class V.

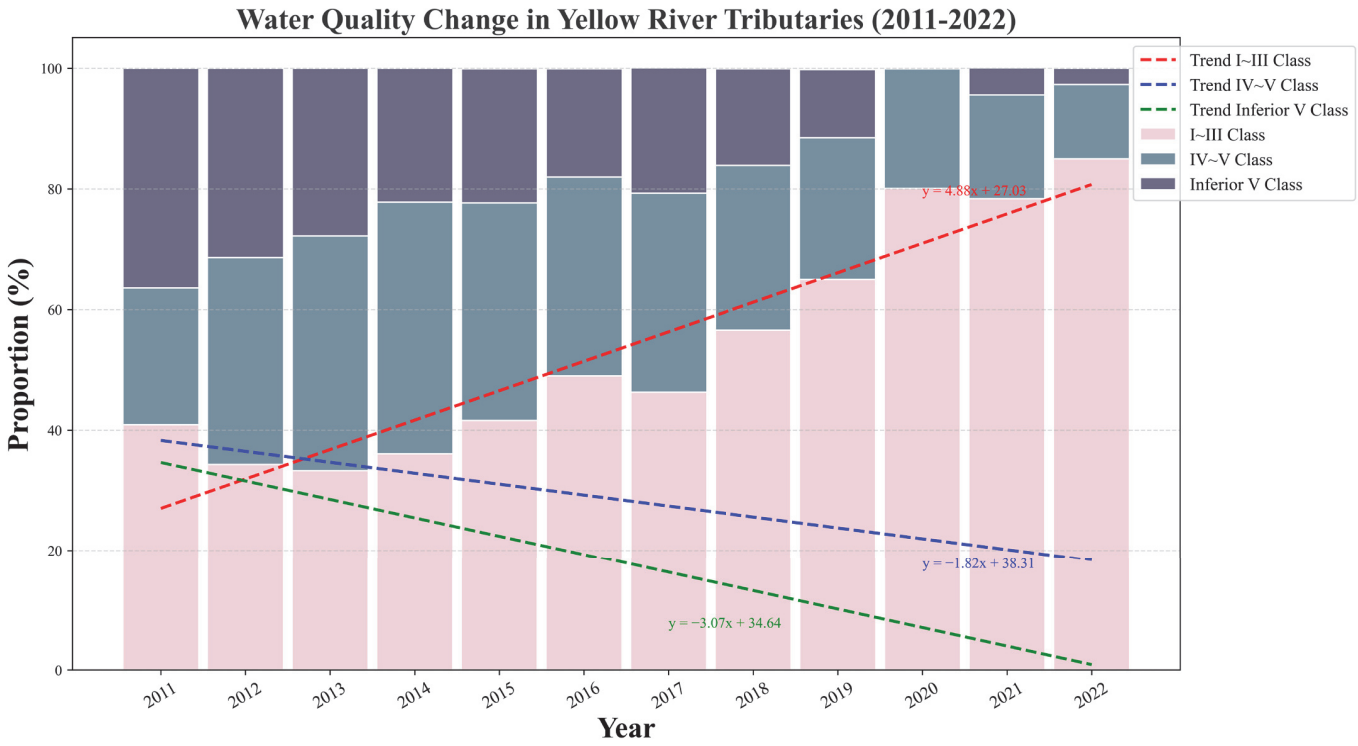

Figure 8. Changes in overall water quality in the Yellow River tributaries from 2011 to 2022.

3.3.2. Pollutant Concentrations in the Yellow River Tributaries

A comparison of the concentrations of major pollutants in specific segments of the Yellow River tributaries between 2000 and 2018 was also conducted, showing similarly significant decreases in pollution levels during this period as observed in the mainstream.

Changes in COD concentrations at various measured sites along the Yellow River tributaries are shown in Figure 9. The data reveal a substantial decline in COD levels by 2018 compared to 2000. For example, the COD concentration at the Fen River west division decreased by 92.60%, from 569.6 mg/L in 2000 to 42.17 mg/L in 2018. Similarly, at the Sushui River Puzhou site, COD levels dropped from 261.0 mg/L to 76.63 mg/L, and at the Wei River suspension bridge, from 53.0 mg/L to 18.63 mg/L. Figure 9b depicts the changes in NH_3-N concentrations at the same sites. The NH_3-N concentration at Sushui River Puzhou was notably reduced by 97.76%, from 237.26 mg/L in 2000 to 5.31 mg/L in 2018. At the Fen River west division, NH_3-N levels decreased from 16.32 mg/L to 0.90 mg/L, and at the Wei River suspension bridge, from 9.29 mg/L to 0.84 mg/L. Among the tributaries, the Huangshui site exhibited the least pollution in 2018, with COD levels dropping from 20.0 mg/L in 2000 to 10.42 mg/L and NH_3-N levels decreasing from 1.00 mg/L to 0.46 mg/L.

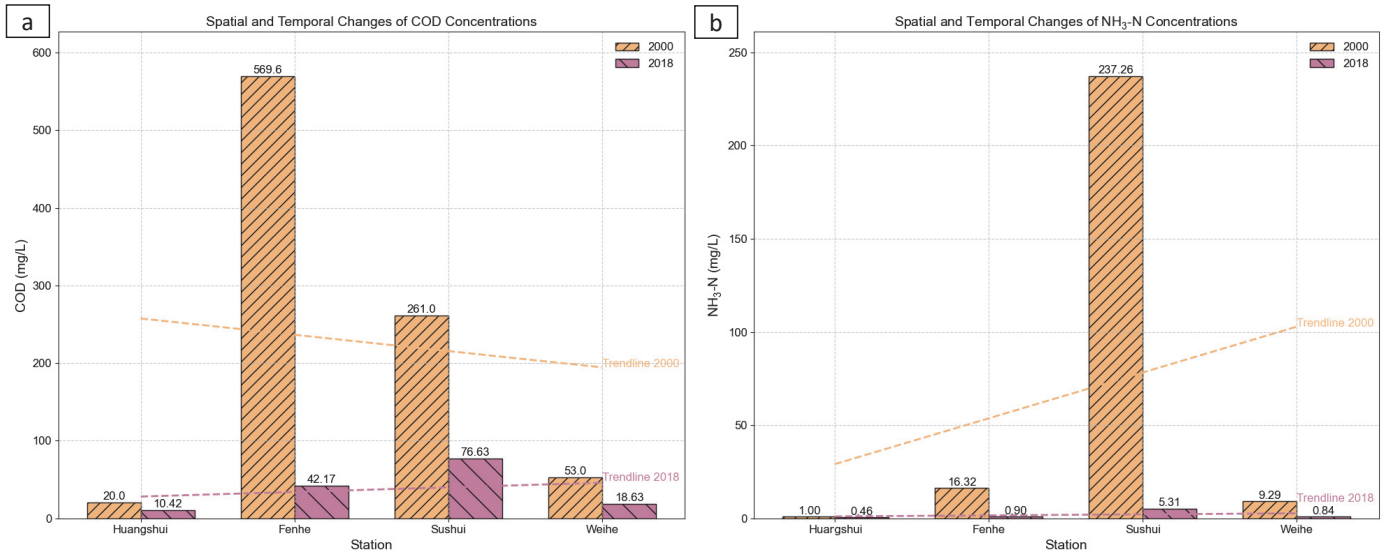

Figure 9. Changes in COD (**a**) and NH_3-N (**b**) concentrations at the measured sites of the Yellow River tributaries.

3.4. Variations in Water Quality in the Huayuankou Section

The time-dependent variations in primary pollutants' concentrations in the Huayuankou section of the Yellow River were analyzed to highlight daily, monthly, and annual fluctuations in COD, NH_3-N, and COD_{Mn} levels (Figure 10).

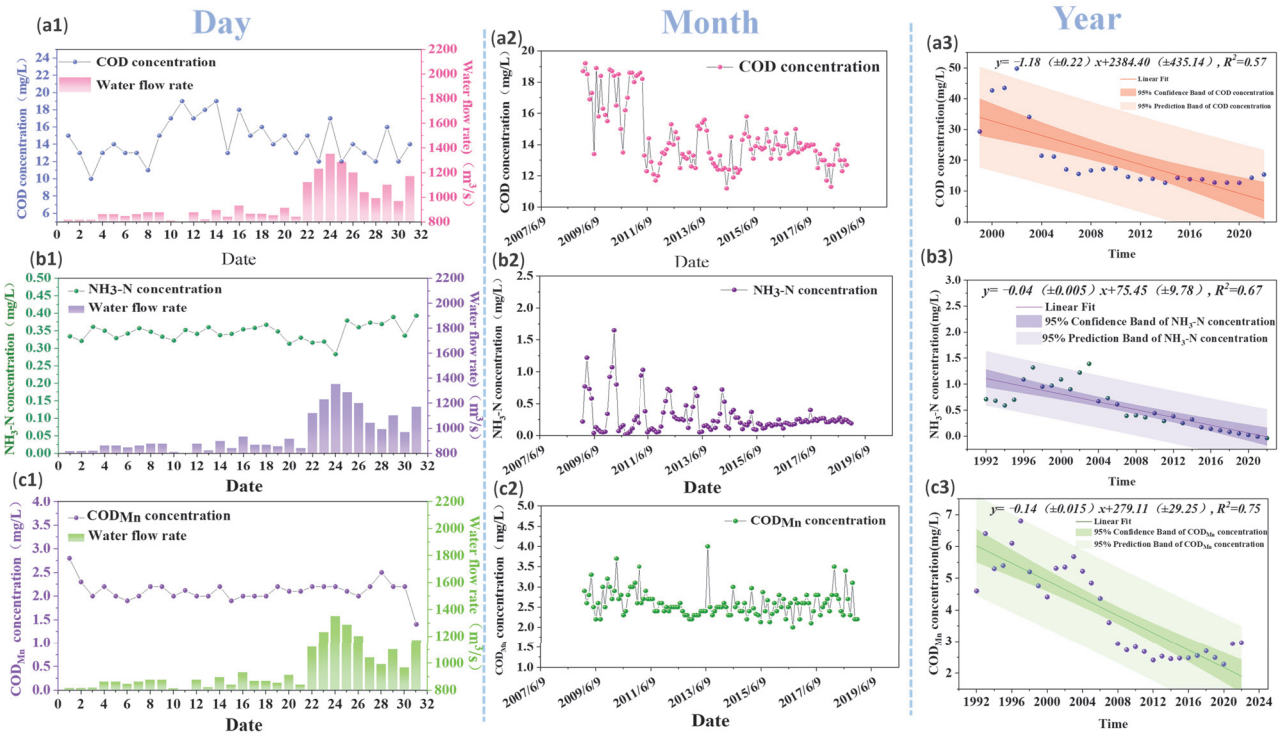

Figure 10. Time-dependent variation in primary pollutants' concentrations daily, monthly and yearly. Daily changes in concentrations and corresponding flow rates in the Huayuankou section for (**a1**) COD, (**b1**) NH_3-N, and (**c1**) COD_{Mn} along with their respective monthly (**a2**,**b2**,**c2**) and annual fluctuations (**a3**,**b3**,**c3**).

In 2020, from 1–31 March the average flow rate for COD was 947 m^3/s and the average water temperature was approximately 7.9 °C (Figure 10a1). COD concentrations ranged

from 10 to 19 mg/L, with an average of 14.45 mg/L. Throughout the month, the COD concentration was classified as Class II for 22 days and Class III for 9 days, with the highest frequency at 14.5 mg/L, indicating a near-normal distribution. Figure 10b1 illustrates the daily NH_3-N concentrations, which varied between 0.283 and 0.393 mg/L, averaging 0.346 mg/L. All NH_3-N measurements were within Class II standards for the entire month, following a normal distribution with the highest frequency at 0.34 mg/L. Figure 10c1 presents the daily COD_{Mn} concentrations, ranging from 1.4 to 2.8 mg/L, with an average of 2.11 mg/L. The COD_{Mn} concentration was classified as Class I for 18 days and Class II for 13 days, with the highest frequency at 2.2 mg/L.

The monthly water quality monitoring data from 2009 to 2018 in the Huayuankou section reveal significant intra-annual variations in pollutant concentrations. For example, in 2011, the COD concentration ranged from 12.7 to 18.6 mg/L, displaying notable seasonal patterns (Figure 10a2). During the wet season (July to October), the average COD concentration was 12.78 mg/L, while it increased to 15.43 mg/L in the dry season (November to February) and averaged 15.6 mg/L from March to June. After 2012, the COD concentrations remained relatively stable with less pronounced seasonal variations. Similarly, the NH_3-N concentration in 2010 fluctuated between 0.02 and 1.65 mg/L (Figure 10b2). The average NH_3-N concentration was 0.068 mg/L during the wet season, 0.585 mg/L during the dry season, and 0.663 mg/L from March to June. Notably, from 2009 to 2011, NH_3-N concentrations exceeded standard limits for several months, but improvements were observed post-2012, with fluctuations decreasing and stabilizing from 2015 onwards. In contrast, the CODMn concentrations exhibited more stable intra-annual variations compared to COD and NH_3-N levels (Figure 10c2). The peak fluctuation occurred in 2013, with concentrations ranging from 2.3 to 4 mg/L and an average of 2.53 mg/L. According to the national water quality standards (GB3838-2002), the water quality was classified as Class II.

The annual COD, NH_3-N, and COD_{Mn} levels in the Huayuankou section reveal a downward trend in the concentrations of all pollutants over this period from 1992 to 2022 (Figure 10a3,b3,c3). COD levels peaked at 49.8 mg/L in 2002, NH_3-N at 1.39 mg/L in 2003, and COD_{Mn} at 6.8 mg/L in 1997. Subsequently, the concentrations of these pollutants have decreased annually. In recent years, water quality has stabilized, with COD meeting Class I standards and NH_3-N and COD_{Mn} meeting Class II standards based on the national water quality standards (GB3838-2002).

4. Discussion

4.1. Water Quality in the Yellow River Basin, Mainstream, and Tributaries

The trends shown in Figure 2 underscore the critical role of targeted regulatory interventions and environmental campaigns in shifting the Yellow River basin from a state of severe pollution to improved water quality [2]. The dramatic reduction in Class IV–V water quality categories, particularly after 2015, can be attributed to the comprehensive 'Action Plan for Prevention and Control of Water Pollution' launched in 2015 [15]. This national agenda enforced stringent controls on industrial wastewater discharge, significantly upgraded urban sewage treatment facilities, and promoted eco-friendly agricultural practices. These measures were particularly impactful in the mainstream sections, where the majority of urban and industrial centers are located. Concurrently, the stabilization in wastewater and pollutant discharges underscores the effectiveness of regulatory policies and technological advancements in environmental protection [42]. Nevertheless, the presence of centralized return water and sewage in agricultural irrigation further complicates water quality management [43]. The results show a small portion of water bodies classified as Class V, indicating the need for sophisticated and adaptable pollution control strategies. Figure 2 ultimately highlights the effectiveness of current water management strategies that balance economic growth and water quality, although some areas still lack enforcement. Figures 3 and 4 further validate the success of pollution control initiatives, with a notable improvement in water quality categories from 2015 onward. The widespread adoption of advanced wastewater treatment technologies, driven by the 13th Five-Year Plan's

emphasis on environmental protection, played a crucial role in these advancements. In the mainstream, where population density and industrial activities are higher, these technologies were more effectively implemented, leading to consistently better water quality compared to the tributaries. In contrast, tributaries, often located in less urbanized regions, saw slower improvements due to challenges in infrastructure and enforcement. However, continuous monitoring and adaptive management are essential to maintain these improvements and address remaining Class V water.

A positive trend in the mainstream of the Yellow River from 2011 to 2022 is illustrated, with pollutant concentrations compared from 2000 to 2018 (Figures 5–7). This underscores the success in maintaining high water quality, with no Class V water after 2018. The sustained improvement highlights effective targeted interventions, stringent regulations, and advanced wastewater treatment. The decrease in both COD and NH_3-N levels demonstrates the impact of these measures. The high water quality standards are partly due to the relatively small number of sewage outlets in the mainstream, which are concentrated in large- and medium-sized cities with significant resource advantages. The consistent classification of the mainstream into higher water quality categories also reflects increased efforts to reduce pollution and efficiently manage water resources in key urban areas and resource-rich locations compared to the overall basin area.

Similarly, a positive trend in the Yellow River tributaries from 2011 to 2022 is also observed, along with a significant decrease in pollutant concentrations from 2000 to 2018 (Figures 8 and 9). This demonstrates the success of interventions and regulatory efforts in reducing pollution. These advancements again underscore the substantial impact of sustained environmental efforts on enhancing the health and quality of these critical water systems. However, regional economic development, the distribution of water systems, and variations in river potential have led to the majority of sewage outlets being located in tributaries, significantly impacting water pollution management [44]. Consequently, pollution in certain water bodies remains severe due to the accumulation of heavy contaminants [32,45]. This results in some waters being consistently classified above Class III, with a small proportion as Class V.

According to the latest report from 2022, water quality in some tributaries was categorized as Class IV or V, with 12.3% classified as Class IV and 2.7% as Class V. Although these percentages are small, they highlight the significant disparity in water quality improvements between the mainstream and its tributaries. While the mainstream consistently achieves high water quality, with 100% of the water classified as Class I–III and the majority as Class II, the tributaries lag behind. This disparity results from concentrated pollution control efforts and advanced wastewater treatment technologies in the mainstream, particularly in key urban and resource-rich areas. In contrast, tributaries face more severe pollution due to regional economic development, numerous sewage outlets, and the accumulation of heavy contaminants, leading to some waters being consistently classified above Class III. Addressing this gap requires focused and localized pollution control strategies in the tributaries.

In addition to addressing industrial and domestic pollutants, nutrient pollution, particularly from agricultural runoff, has been a significant concern in the Yellow River basin. Excessive nutrient input, especially nitrogen and phosphorus, has the potential to cause eutrophication, leading to algal blooms and subsequent oxygen depletion in water bodies. While the mainstream has generally maintained higher water quality standards, some tributaries and localized areas continue to face the risk of eutrophication due to the accumulation of nutrients. This risk is exacerbated by the sediment transport dynamics in the basin, where sediments can bind with these nutrients and facilitate their downstream movement. Effective management strategies must therefore not only focus on reducing traditional pollutants but also on controlling nutrient loads and preventing eutrophication, particularly in vulnerable tributaries.

4.2. Water Quality in the Huayuankou Section

The significant improvement in water quality in the Huayuankou section, as illustrated in Figure 10, reflects the cumulative impact of targeted interventions implemented over the years. Since 2000, the enforcement of the "Special Campaign for River Pollution Source Management" and the "Four Cleanups" initiative has effectively curtailed pollution across the Yellow River basin [15]. In addition to these broader initiatives, specific steps have been taken in the Huayuankou section and other key monitoring stations to control pollution. For instance, local governments have implemented enhanced regulations, such as stricter controls on discharge outlets and management of non-point source pollution. These efforts have been particularly rigorous in zones with higher pollution levels, leading to substantial improvements in water quality. The Huayuankou section, for example, saw targeted measures like increased monitoring, localized clean-up campaigns, and advanced wastewater treatment installations, which have been instrumental in reducing pollutant concentrations to meet national water quality standards. These extra steps, especially in critical zones, have contributed significantly to the overall success of pollution control in the Yellow River basin. Notably, the introduction of the "Water Pollution Prevention and Control Action Plan" in 2015 led to stricter regulations on industrial discharge and significant enhancements in urban wastewater treatment facilities.

Given the complex hydrological conditions in the Huayuankou section, these measures were enforced with particular rigor. Local governments undertook additional efforts to manage pollution sources, including strengthening the regulation of discharge outlets and increasing both internal and non-point source pollution control. The successful implementation of these measures, combined with heightened public awareness, has resulted in sustained improvements even in areas previously classified as poor water quality zones. Between 2000 and 2018, the chemical oxygen demand (COD) concentration at this section decreased from 42.2 mg/L to 12.76 mg/L, while ammonia nitrogen (NH_3-N) levels dropped from 1.50 mg/L to 0.15 mg/L. These data clearly demonstrate the significant impact of the implemented remediation measures.

Monthly data from 2009 to 2018 reveal significant seasonal variations, particularly in COD and NH_3-N levels, with higher pollutant concentrations during the dry season due to hydrological conditions [46]. The warming and drying trends have reduced water flow, thereby concentrating pollutants and exacerbating water quality issues during low-flow periods. The post-2012 stabilization of COD levels suggests effective pollution control and improved wastewater treatment. Long-term trends from 1992 to 2022 highlight a substantial reduction in pollutant concentrations. The early 2000s experienced the highest pollutant levels due to industrial and agricultural pressures but sustained environmental efforts have led to a marked improvement. The overall improvement in water quality in the Huayuankou section can be attributed to enhanced wastewater treatment, stringent regulatory policies, targeted interventions in pollution hotspots, and effective hydrological management. Despite these successes, challenges remain, such as the presence of centralized return water and sewage in agricultural irrigation, which complicates water quality management [43]. Continuous monitoring and adaptive management are essential to sustain these gains and address emerging issues. Further analysis of pollutant levels in conjunction with hydrological data will provide deeper insights into the effectiveness of various interventions and is critical for refining future management strategies to ensure the long-term sustainability of water resources in the Yellow River basin.

5. Conclusions

The Yellow River basin has experienced significant changes in water quality over the past four decades. Initially, water quality was good, but industrialization, agricultural intensification, and urban expansion in the 1980s and 1990s led to severe pollution. Key pollutants, including COD, NH_3-N, and COD_{Mn}, reached critical levels, resulting in widespread environmental degradation. Since 2000, effective pollution control measures and stringent regulations have significantly improved water quality. Enhanced water re-

source management and investments in wastewater treatment have led to notable improvements. Currently, COD levels meet Class I standards, while NH3-N and CODMn align with Class II standards according to national criteria.

Since 2000, stringent regulatory measures and enhanced water resource management have led to significant improvements across the basin. By 2022, COD levels in the mainstream met Class I standards, with average concentrations dropping by 63.1% from 34.8 mg/L in 2000 to 12.81 mg/L in 2018. NH_3-N concentrations also saw a drastic reduction of 86.61%, from an average of 2.96 mg/L in 2000 to 0.40 mg/L in 2018. These improvements underscore the effectiveness of the pollution control initiatives implemented over the past two decades.

However, improvements are not uniform across the basin. The mainstream of the Yellow River exhibits relatively good water quality, but many tributaries continue to suffer from severe pollution, with some classified as Class V. For instance, in 2022, 85% of the water in tributaries was classified as Class I to III, 12.3% as Class IV, and only 2.7% as Class V. In contrast, the mainstream demonstrated much better quality, with all water classified as Class I–III and notably, 86% reaching Class II and 14% reaching Class I. Nevertheless, the Huayuankou section, a critical monitoring point, has shown a marked decline in key pollution indicators over the past three decades, reflecting the positive impact of sustained pollution control measures. Seasonal and daily variations in water quality parameters like COD, NH_3-N, and COD_{Mn} often correlate with flow rates and temperature changes.

The Huayuankou section, a critical monitoring point, reflects these broader trends with a significant decline in key pollution indicators over the past three decades. The average COD concentration at Huayuankou dropped from 42.2 mg/L in 2000 to 12.76 mg/L in 2018, while NH_3-N levels reduced from 1.50 mg/L to 0.15 mg/L over the same period.

These findings emphasize the need for continuous and adaptive management strategies to sustain and further improve water quality in the Yellow River basin. While significant progress has been made, persistent pollution in several tributaries highlights the necessity for ongoing efforts and targeted actions. Enhanced regulatory frameworks, improved wastewater treatment technologies, and robust community engagement are essential to address these challenges. Localized strategies tailored to specific conditions within the basin can enhance the effectiveness of pollution control measures. Continuous research, monitoring, and adaptive management are crucial to ensure the long-term sustainability of the Yellow River basin's water environment, safeguarding it for future generations.

Supplementary Materials: The following supporting information can be downloaded at: https://www.mdpi.com/article/10.3390/w16172413/s1, Table S1. Environmental quality standard for surface water. Table S2. Test Result. Table S3. Testing Items, Methods, Instruments, and Detection Limits.

Author Contributions: Conceptualization, Z.Y., X.S. and L.Y.; methodology and visualization, Z.Y., X.S. and S.Y.; investigation, Z.Y., X.S. and Y.L.; writing—original draft preparation, Z.Y., X.S. and H.J.; writing—review and editing, L.Y. and S.Y. All authors have read and agreed to the published version of the manuscript.

Funding: This work was supported by the Outstanding Young Talents Science and Technology Foundation of Yellow River Conservancy Commission (Grant No. HQK-202320), the National Key Research and Development Program of China (Grant No. 2023YFC3206202), the Major Science and Technology Special Fund of Henan Province (Grant No. 201300311400), the Special Scientific Research Project of Yellow River Water Resources Protection Institute (Grant No. KYY- KYZX-2022-01), and the National Natural Science Foundation of China (Grant No. 51709126).

Data Availability Statement: The data presented in this study are available on request from the corresponding author. The data are not publicly available due to requirements of relevant regulatory agencies.

Conflicts of Interest: The authors declare no conflicts of interest.

References

1. Xia, J.; Jiang, Q.; Deng, S.; Zhou, M.; Cheng, Y.; Li, Z.; Wang, Z. Morphological characteristics and evolution processes of sharp bends in the Lower Yellow River. *Catena* **2022**, *210*, 105936. [CrossRef]
2. Chen, Y.P.; Fu, B.J.; Zhao, Y.; Wang, K.B.; Zhao, M.M.; Ma, J.F.; Wu, J.H.; Xu, C.; Liu, W.G.; Wang, H. Sustainable development in the Yellow River Basin: Issues and strategies. *J. Clean. Prod.* **2020**, *263*, 121223. [CrossRef]
3. Yin, L.; Feng, X.; Fu, B.; Wang, S.; Wang, X.; Chen, Y.; Tao, F.; Hu, J. A coupled human-natural system analysis of water yield in the Yellow River basin, China. *Sci. Total Environ.* **2021**, *762*, 143141. [CrossRef]
4. Wang, G.; Zhang, J.; Jin, J.; Weinberg, J.; Bao, Z.; Liu, C.; Liu, Y.; Yan, X.; Song, X.; Zhai, R. Impacts of climate change on water resources in the Yellow River basin and identification of global adaptation strategies. *Mitig. Adapt. Strateg. Glob. Change* **2017**, *22*, 67–83. [CrossRef]
5. Feng, Y.; Zhu, A. Spatiotemporal differentiation and driving patterns of water utilization intensity in Yellow River Basin of China: Comprehensive perspective on the water quantity and quality. *J. Clean. Prod.* **2022**, *369*, 133395. [CrossRef]
6. Chang, J.; Li, Y.; Yuan, M.; Wang, Y. Efficiency evaluation of hydropower station operation: A case study of Longyangxia station in the Yellow River, China. *Energy* **2017**, *135*, 23–31. [CrossRef]
7. Si, Y.; Li, X.; Yin, D.; Liu, R.; Wei, J.; Huang, Y.; Li, T.; Liu, J.; Gu, S.; Wang, G.; et al. Evaluating and optimizing the operation of the hydropower system in the Upper Yellow River: A general LINGO-based integrated framework. *PLoS ONE* **2018**, *13*, e0191483. [CrossRef] [PubMed]
8. Zhang, W.; Liang, W.; Gao, X.; Li, J.; Zhao, X. Trajectory in water scarcity and potential water savings benefits in the Yellow River basin. *J. Hydrol.* **2024**, *633*, 130998. [CrossRef]
9. Zhang, Y.; Zhao, Z.; Fu, B.; Ma, R.; Yang, Y.; Lü, Y.; Wu, X. Identifying ecological security patterns based on the supply, demand and sensitivity of ecosystem service: A case study in the Yellow River Basin, China. *J. Environ. Manag.* **2022**, *315*, 115158. [CrossRef]
10. Yu, S.-Y.; Li, W.-J.; Zhou, L.; Yu, X.; Zhang, Q.; Shen, Z. Human Disturbances Dominated the Unprecedentedly High Frequency of Yellow River Flood over the Last Millennium. *Sci. Adv.* **2023**, *9*, eadf8576. [CrossRef]
11. Quan, J.; Xu, Y.; Ma, T.; Wilson, J.P.; Zhao, N.; Ni, Y. Improving surface water quality of the Yellow River Basin due to anthropogenic changes. *Sci. Total Environ.* **2022**, *836*, 155607. [CrossRef] [PubMed]
12. Jiang, L.; Zuo, Q.; Ma, J.; Zhang, Z. Evaluation and prediction of the level of high-quality development: A case study of the Yellow River Basin, China. *Ecol. Indic.* **2021**, *129*, 107994. [CrossRef]
13. Zhang, M.; Wang, X.; Liu, C.; Lu, J.; Qin, Y.; Mo, Y.; Xiao, P.; Liu, Y. Identification of the heavy metal pollution sources in the rhizosphere soil of farmland irrigated by the Yellow River using PMF analysis combined with multiple analysis methods—Using Zhongwei city, Ningxia, as an example. *Environ. Sci. Pollut. Res.* **2020**, *27*, 16203–16214. [CrossRef] [PubMed]
14. Wu, N.; Liu, S.M.; Zhang, G.L.; Zhang, H.M. Anthropogenic impacts on nutrient variability in the lower Yellow River. *Sci. Total Environ.* **2021**, *755*, 142488. [CrossRef]
15. Ministry of Ecology and Environment of People's Republic of China, Action Plan for Prevention and Control of Water Pollution. Available online: https://english.mee.gov.cn/News_service/news_release/201504/t20150427_299595.shtml#:~:text=The%20action%20plan%20proposed%20that,level,%20the%20overexploitation%20of%20groundwater (accessed on 5 June 2024).
16. Zhou, Y.; Ma, J.; Zhang, Y.; Qin, B.; Jeppesen, E.; Shi, K.; Brookes, J.D.; Spencer, R.G.M.; Zhu, G.; Gao, G. Improving water quality in China: Environmental investment pays dividends. *Water Res.* **2017**, *118*, 152–159. [CrossRef]
17. Liu, S.; Qiu, Y.; Fu, R.; Liu, Y.; Suo, C. Identifying the water quality variation characteristics and their main driving factors from 2008 to 2020 in the Yellow River Basin, China. *Environ. Sci. Pollut. Res.* **2023**, *30*, 66753–66766. [CrossRef]
18. Sun, X.; Zhou, Z.; Wang, Y. Water resource carrying capacity and obstacle factors in the Yellow River basin based on the RBF neural network model. *Environ. Sci. Pollut. Res.* **2023**, *30*, 22743–22759. [CrossRef]
19. Liu, T.; Wang, F.; Michalski, G.; Xia, X.; Liu, S. Using 15N, 17O, and 18O to determine nitrate sources in the Yellow River, China. *Environ. Sci. Technol.* **2013**, *47*, 13412–13421. [CrossRef]
20. Li, B.; Feng, Q.; Wang, X.; Li, Z.; Wang, F.; Zhao, C.; Yu, T.; Chen, W. Formation of the upper reaches of the Yellow River: Provenance evidence from the strata of the Yellow River sedimentary basin. *Glob. Planet. Change* **2023**, *229*, 104224. [CrossRef]
21. Wu, Z.; Tian, G.; Xia, Q.; Hu, H.; Li, J. Connotation, calculation and influencing factors of the water-use rights benchmark price: A case study of agricultural water use in the Ningxia Yellow River irrigation area. *Agric. Water Manag.* **2023**, *283*, 108300. [CrossRef]
22. Xu, Z.; Liu, M.; Guan, G.; Guo, X. Emergency intervention modes for ice jam events in large-scale water diversion projects. *Hydrol. Res.* **2023**, *54*, 1134–1151. [CrossRef]
23. Wu, X.; Wei, Y.; Fu, B.; Wang, S.; Zhao, Y.; Moran, E.F. Evolution and Effects of the Social-Ecological System over a Millennium in China's Loess Plateau. 2020. Available online: https://www.science.org/doi/full/10.1126/sciadv.abc0276 (accessed on 8 June 2024).
24. Pan, B.; Hu, Z.; Wang, J.; Vandenberghe, J.; Hu, X.; Wen, Y.; Li, Q.; Cao, B. The approximate age of the planation surface and the incision of the Yellow River. *Palaeogeogr. Palaeoclimatol. Palaeoecol.* **2012**, *356–357*, 54–61. [CrossRef]
25. Kong, D.; Miao, C.; Li, J.; Zheng, H. Full-stream erosion in the lower Yellow River: Feasibility, sustainability and opportunity. *Sci. Total Environ.* **2022**, *807*, 150810. [CrossRef]

26. Zhou, Y.; Huang, H.Q.; Ran, L.; Shi, C.; Su, T. Hydrological controls on the evolution of the Yellow River Delta: An evaluation of the relationship since the Xiaolangdi Reservoir became fully operational. *Hydrol. Process.* **2018**, *32*, 3633–3649. [CrossRef]
27. He, H.; Yu, Q.; Zhou, J.; Tian, Y.Q.; Chen, R.F. Modelling complex flood flow evolution in the middle Yellow River basin, China. *J. Hydrol.* **2008**, *353*, 76–92. [CrossRef]
28. Gippel, C.; Jiang, X.; Zhang, D.; Cooling, M.; Kerr, G.; Close, P.; Jin, S.; Li, L.; Wang, Z.; Ma, Z.; et al. Environmental Flows Assessment for the Lower Yellow River. 2012. Available online: www.watercentre.org (accessed on 15 May 2024).
29. Liu, W.; Shi, C.; Zhou, Y. Trends and attribution of runoff changes in the upper and middle reaches of the Yellow River in China. *J. Hydro-Environ. Res.* **2021**, *37*, 57–66. [CrossRef]
30. Galler, J.J. Medium-and Long-Term Changes in Fluvial Discharge to the Sea: Medium-and Long-Term Changes in Fluvial Discharge to the Sea: The Yellow River Case Study the Yellow River Case Study. Master's Thesis, William & Mary, Williamsburg, VA, USA, 1999. [CrossRef]
31. Dai, Y.; Lu, F.; Ruan, B.; Song, X.; Du, Y.; Xu, Y. Decomposition of contribution to runoff changes and spatial differences of major tributaries in the middle reaches of the Yellow River based on the Budyko framework. *Hydrol. Res.* **2023**, *54*, 435–450. [CrossRef]
32. Zhao, M.M.; Wang, S.M.; Chen, Y.P.; Wu, J.H.; Xue, L.G.; Fan, T.T. Pollution status of the Yellow River tributaries in middle and lower reaches. *Sci. Total Environ.* **2020**, *722*, 137861. [CrossRef]
33. Wang, Z.C.; Zhang, S.X.; Mao, H.T.; Shen, J.W.; Guo, W.D. Analysis of Water and Sediment Characteristics of the Yellow River and Their Correlations. *Pol. J. Environ. Stud.* **2023**, *32*, 2909–2923. [CrossRef]
34. Jin, F.; Yang, W.; Fu, J.; Li, Z. Effects of vegetation and climate on the changes of soil erosion in the Loess Plateau of China. *Sci. Total Environ.* **2021**, *773*, 145514. [CrossRef]
35. Zhang, Y.; Chao, Y.; Fan, R.; Ren, F.; Qi, B.; Ji, K.; Xu, B. Spatial-temporal trends of rainfall erosivity and its implication for sustainable agriculture in the Wei River Basin of China. *Agric. Water Manag.* **2021**, *245*, 106557. [CrossRef]
36. Storozum, M.J.; Mo, D.; Wang, H.; Ren, X.; Zhang, Y.; Kidder, T.R. Anthropogenic origins of a late Holocene, basin-wide unconformity in the middle reaches of the Yellow River, the Luoyang Basin, Henan Province, China. *Quat. Res.* **2017**, *87*, 423–441. [CrossRef]
37. Lv, W.; Yang, H. Distribution of Phosphorus and Iron Species in the Sediments along the Path of Yellow River and Correlation of Contents of the Two Species. *Source: J. Coast. Res.* **2020**, *104*, 813–817. [CrossRef]
38. van Maren, D.S.; Yang, M.; Wang, Z.B. Predicting the Morphodynamic Response of Silt-Laden Rivers to Water and Sediment Release from Reservoirs: Lower Yellow River, China. *J. Hydraul. Eng.* **2011**, *137*, 90–99. [CrossRef]
39. Zhang, M.; Ping, J.; Mei, X.; Leng, W.; Li, H.; Zhao, J.; Liu, J. The trend of groundwater recharge in the secondary perched reaches of the Yellow River in the past 50 years. *Front. Environ. Sci.* **2023**, *11*, 1310181. [CrossRef]
40. China National Environmental Monitoring Centre, National Surface Water Quality Automatic Monitoring Real-Time Database. Available online: https://szzdjc.cnemc.cn:8070/GJZ/Business/Publish/Main.html (accessed on 1 April 2024).
41. *GB 3838-2002*; Environmental Quality Standards for Surface Water. Ministry of Ecology and Environment of People's Republic of China: Beijing, China, 2002.
42. Xu, Y.; Liu, S.; Wang, J. Impact of environmental regulation intensity on green innovation efficiency in the Yellow River Basin, China. *J. Clean. Prod.* **2022**, *373*, 133789. [CrossRef]
43. Lu, C.; Ji, W.; Hou, M.; Ma, T.; Mao, J. Evaluation of efficiency and resilience of agricultural water resources system in the Yellow River Basin, China. *Agric. Water Manag.* **2022**, *266*, 107605. [CrossRef]
44. Yu, J. Coordinated development of urban economy and total amount control of water environmental pollutants in the Yellow River basin. *Arab. J. Geosci.* **2021**, *14*, 658. [CrossRef]
45. Du, H.; Ji, X.; Chuai, X. Spatial Differentiation and Influencing Factors of Water Pollution-Intensive Industries in the Yellow River Basin, China. *Int. J. Environ. Res. Public Health* **2022**, *19*, 497. [CrossRef]
46. Liu, X.; Sheng, Y.; Liu, Q.; Li, Z. Suspended particulate matter affects the distribution and migration of heavy metals in the Yellow River. *Sci. Total Environ.* **2024**, *912*, 169537. [CrossRef]

water

MDPI

Article

Spatiotemporal Changes in the Quantity and Quality of Water in the Xiao Bei Mainstream of the Yellow River and Characteristics of Pollutant Fluxes

Zhenzhen Yu [1], Xiaojuan Sun [1,2], Li Yan [1,*], Yong Li [1], Huijiao Jin [1] and Shengde Yu [3]

[1] Yellow River Water Resources Protection Institute, Zhengzhou 450004, China; zzyuhydro@126.com (Z.Y.); sunxiaojuan@gs.zzu.edu.cn (X.S.); 2wi861015@163.com (Y.L.); 13980603356@163.com (H.J.)
[2] School of Water Conservancy and Transportation, Zhengzhou University, 100 Kexue Avenue, Zhengzhou 450001, China
[3] Ecohydrology Research Group, Department of Earth and Environmental Sciences, University of Waterloo, 200 University Avenue West, Waterloo, ON N2L 3G1, Canada; s228yu@uwaterloo.ca
* Correspondence: yanli_5677@163.com

Abstract: The Xiao Bei mainstream, located in the middle reaches of the Yellow River, plays a vital role in regulating the quality of river water. Our study leveraged 73 years of hydrological data (1951–2023) to investigate long-term runoff trends and seasonal variations in the Xiao Bei mainstream and its two key tributaries, the Wei and Fen Rivers. The results indicated a significant decline in runoff over time, with notable interannual fluctuations and an uneven distribution of runoff within the year. The Wei and Fen Rivers contributed 19.75% and 3.59% of the total runoff to the mainstream, respectively. Field monitoring was conducted at 11 locations along the investigated reach of Xiao Bei, assessing eight water quality parameters (temperature, pH, dissolved oxygen (DO), chemical oxygen demand (COD), ammonia nitrogen (NH_3-N), total phosphorus (TP), permanganate index (COD_{Mn}), and 5-day biochemical oxygen demand (BOD_5)). Our long-term results showed that the water quality of the Xiao Bei mainstream during the monitoring period was generally classified as Class III. Water quality parameters at the confluence points of the Wei and Fen Rivers with the Yellow River were higher compared with the mainstream. After these tributaries merged into the mainstream, local sections show increased concentrations, with the water quality parameters exhibiting spatial fluctuations. Considering the mass flux process of transmission of the quantity and quality of water, the annual NH_3-N inputs from the Fen and Wei Rivers to the Yellow River accounted for 11.5% and 67.1%, respectively, and TP inputs accounted for 6.8% and 66.18%. These findings underscore the critical pollutant load from tributaries, highlighting the urgent need for effective pollution management strategies targeting these tributaries to improve the overall water quality of the Yellow River. This study sheds light on the spatiotemporal changes in runoff, water quality, and pollutant flux in the Xiao Bei mainstream and its tributaries, providing valuable insights to enhance the protection and management of the Yellow River's water environment.

Keywords: runoff; environmental water quality; pollutant flux; spatiotemporal variations; Xiao Bei mainstream of the yellow river

1. Introduction

The Yellow River, as the second longest river in China, spans over 5400 km and flows through nine provinces [1]. It originates in the Bayangela Mountains in the west and terminates in the Bohai Gulf. The entire river is commonly divided into three reaches by the Toudaoguai and Huayuankou gauging stations, where the middle reach plays a significant role in the basin water's balances and availability for human use [2]. The middle reach has the most detrimental impact on water conditions, not only due to the inflow of the two largest tributaries, the Fen River and the Wei River. The mainstream also flows through the

Loess Plateau, which passes highly erodible soils into the main water body, contributing up to 90% of the its sediments [2,3]. As an important source of water for the Northwest and North China regions, the Yellow River supports food production in major agricultural areas [4], energy for power generation, and basic industrial sectors such as forestry, animal husbandry, and fisheries [5]. Specifically, about 15% of the irrigated agricultural land and 12% of the water supply for the Chinese population rely on the Yellow River [6]. Therefore, the Yellow River holds significant importance in national socioeconomic development.

Despite its importance, the Yellow River Basin faces water resource challenges, centred on water shortages and high pollutant levels [7,8]. From 2000 to 2016, the average runoff measured at Lanzhou, Sanmenxia, and Huayuankou hydrometric stations was reduced by 20.77%, 60.39%, and 59.48%, respectively [6]. Alongside the decreasing runoff trend, the pollutant load in the mainstream of the Yellow River has seen significant contributions from both discharge points and tributaries [1]. From the 1980s to 2017, the discharge of wastewater almost doubled from 21.7 to 44.94 million tons, while the average rate of water flow decreased continuously [9]. Most tributaries in the middle and lower reaches carry notable amounts of pollutants and contribute low-quality water to the mainstream [1,9]. Among these, the Jindi River in the lower reaches exhibits particularly poor water quality, with levels of total phosphorus (TP), total nitrogen (TN), biochemical oxygen demand (BOD_5), chemical oxygen demand (COD), total organic carbon (TOC), and coliform bacteria exceeding national standards by 155%, 1%, 97.5%, 35.5%, 114.2%, and 80%, respectively [9].

Anthropogenic activities, including excessive development of water resources and substantial industrial and agricultural discharge, have caused the accumulation of pollution levels, posing a serious threat to the ecological and socioeconomic stability of the region [8,10]. The construction of cascade dams can have significant impacts on the entire river basin, altering natural flow regimes, sediment transport, and nutrient dynamics [11–14]. Since 1976, the construction of cascade dams along the upper stretch of the Yellow River has notably transformed its original hydrological characteristics [15]. Specifically, the dams have reduced the maximum monthly difference in streamflow from 430 to 115 m^3/s, and decreased differences in the sand concentration from 0.52 to 0.39 kg/m^3 between 1977 and 2006 [16]. The Xiaolangdi Reservoir (XLDR) has significantly altered the hydrology and nutrient dynamics in the Yellow River, affecting nutrient levels upstream and downstream, with nutrient retention efficiencies of −1.4% for dissolved inorganic nitrogen (DIN), −11% for dissolved inorganic phosphorus (DIP), and −7% for dissolved silica (DSi) [17]. Furthermore, agriculture, industry, and urban residential areas account for 40%, 26%, and 16% of the reduced amount of water, respectively, with industrial wastewater, domestic wastewater, phosphorus, and nitrogen accounting for 66%, 21%, 8%, and 5% of the influence on water quality, respectively [6]. Combined with the effects of global warming, rising temperatures may further decrease the ability of natural water bodies to assimilate oxygen-demanding wastes [18,19]. Despite recent improvements in the Yellow River's water quality and ecological vulnerability, ongoing monitoring remains crucial [20–22].

Therefore, investigating runoff, water quality indicators, and pollutant dynamics in the Yellow River Basin is crucial for developing effective water management strategies. Understanding the spatiotemporal variations in these factors provides insights into the underlying causes of pollution and helps identify critical intervention points for improving the water quality. This knowledge is essential for ensuring the sustainable use of water resources, protecting ecosystem services, and ensuring compliance with water quality standards.

In light of these considerations, this study focused on the spatiotemporal changes in the quantity and quality of water in the Xiao Bei mainstream in the middle reach of the Yellow River. Three major investigations were included as follows. (1) The long-term variations in the average annual and intra-annual runoff at both the start and end of the Xiao Bei mainstream, as well as the Wei River and Fen River tributaries, were studied, spanning 73 years from 1951 to 2023. (2) The midstream section exhibited the highest concentrations of over-standard indexed pollutants for ammonia nitrogen, chemical oxygen demand (COD), and permanganate index (COD_{Mn}) [9]. According to the specified national indices

in the "Surface Water Environment Quality Standard" (GB 3838-2002) [23], these pollutants are key metrics for assessing river water's quality. Therefore, the study aimed to measure parameters including temperature, pH, dissolved oxygen (DO), COD, ammonia nitrogen (NH_3-N), total phosphorus (TP), COD_{Mn}, and 5-day biochemical oxygen demand (BOD_5) at 11 sampling points along the Xiao Bei mainstream during 28–30 August 2023. These test results allowed an analysis of the spatial trends along the Xiao Bei water body. (3) We examined the monthly changes in TP and NH_3-N fluxes in the Xiao Bei mainstream for 2021 to gain insights into intra-annual variations in the pollutant level. These data aimed to provide a comprehensive baseline to elucidate the patterns of water status and pollution in the Yellow River.

2. Materials and Methods

2.1. Study Area

The studied segment of the Yellow River, spanning from Longmen to Tongguan, lies in the middle reaches of the river, and this section extends over 132.5 km, constituting only 2.42% of the Yellow River's total length. It forms the lower part of the northern mainstream, known as the Xiao Bei mainstream, stretching from Tuoketuo in Inner Mongolia to Tongguan (Figure 1).

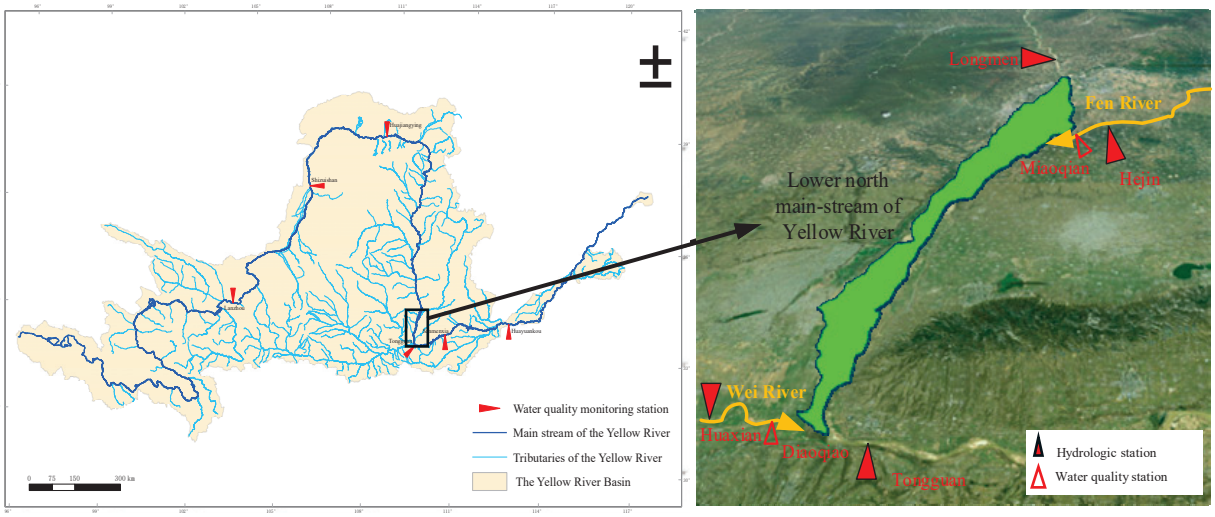

Figure 1. Yellow River (**left**) and map of the study area (**right**). The mainstream, tributaries, and basin area of the Yellow River are shown on the left. The investigated Xiao Bei mainstream, with the Wei River and Fen River tributaries and the proximal hydrologic and water quality stations are shown on the right.

The Xiao Bei mainstream is situated above the Xiaolangdi and Sanmenxia reservoirs and the entire lower Yellow River, lying below the outlet of the Yellow River's longest continuous gorge. This positioning gives it a critical role in connecting the upper and lower reaches, making it highly significant in the management and development of the Yellow River. This river section is characterized by its wide and shallow channel, numerous sandbars, and braided streams, exhibiting significant variability in its erosion and deposition patterns. The main channel frequently shifts, making it a typical wandering, sediment-laden river. The channel's width varies dramatically, from as wide as 18 km to as narrow as 3 km, resembling a dumbbell shape in plan view. Historically, there has been a saying, "Thirty years east of the river, thirty years west of the river", reflecting the river's unpredictable nature. All major management challenges of the Yellow River are concentrated in this Xiao Bei mainstream.

From the upper to the lower reaches, the left bank of the Xiao Bei mainstream receives inflows from tributaries such as the Fen River and Sushui River, while the right bank is

joined by the Zhuoshui, Xushui, Jinshui, and Wei Rivers. Among these, the Wei and Fen Rivers significantly impact the mainstream. The Wei River is the largest tributary of the Yellow River, entering the Yellow River at Tongguan County in Shaanxi Province, and is a major source of sediment. The Fen River, the second-largest tributary, flows within Shanxi Province and joins the Yellow River near Miaoqian Village in Wanrong County.

2.2. Runoff Data Collection

Our study collected data from various sources to conduct the analysis. The runoff data spanning 73 years of the Longmen and Tongguan hydrological stations were obtained from the *Hydrological Yearbook of the People's Republic of China from 1951 to 2020*, *Volume 4: Hydrological Data of the Yellow River Basin*. The runoff data from 2020 to 2023 were directly measured by our team. The concentrations of water quality parameters along the Xiao Bei mainstream were measured through field tests, with details provided in Section 2.3. Lastly, the monthly variations in the TP and NH3-N pollutant fluxes for 2021 were derived from the *Hydrological Yearbook of the People's Republic of China (2021)* and the concentration data were from the National Surface Water Quality Data Release System".

2.3. Water Sampling and Analysis

2.3.1. Sampling Sites and Procedures

Water samples were collected from the Xiao Bei tributary river section on 28–30 August 2023. Selection of the sampling points was guided by several key considerations to ensure comprehensive and representative monitoring of water quality. The goal was to use the fewest possible points to obtain sufficient environmental information while considering practical feasibility during sampling. Specific points included background sections, control sections, and estuary sections for watersheds or water systems. For administrative regions, the points included background sections for water sources or entry points for transboundary rivers. Selected points avoided stagnant water zones, return flow areas, and sewage outlets, preferring stable, straight river sections with a smooth flow and wide water surfaces. Monitoring points were aligned with the hydrological measurement sections to integrate monitoring of the water's quality and quantity. The layout also considered long-term monitoring needs, socioeconomic development, and current monitoring requirements. In synchronized watershed monitoring, the points were determined on the basis of watershed plans and pollution sources' compliance targets. According to these considerations, 11 sampling points were set up along a 237 km river section of the Xiao Bei mainstream for on-site monitoring of water quality, as shown in Table 1.

Table 1. Monitoring points of the Xiao Bei mainstream's water quality.

No.	Monitoring Point	Latitude and Longitude	Relative Distance
1	Longmen	110.60867786, 35.65471586	−37 km
2	Fen River entry to Yellow River, 0 km	110.46890259, 35.34281990	0 km
3	Fen River entry to Yellow River, downstream 2 km	110.45306683, 35.33249239	2 km
4	Fen River entry to Yellow River, downstream 5 km	110.44521332, 35.30496925	5 km
5	Fen River entry to Yellow River, downstream 20 km	110.37466049, 35.13514167	20 km
6	Fen River entry to Yellow River, downstream 50 km	110.32299042, 35.04194354	50 km
7	Fen River entry to Yellow River, downstream 100 km	110.27518272, 34.61943546	100 km
8	Wei River entry to Yellow River section, 0 km	110.28792858, 34.61049980	190 km
9	Wei River entry to Yellow River, downstream 1.5 km	110.30397892, 34.60940485	191.5 km
10	Wei River entry to Yellow River, downstream 4 km	110.33073664, 34.60912228	194 km
11	Wei River entry to Yellow River, downstream 10 km	110.41276932, 34.58863340	200 km

The sampling procedure ensured the collection of representative samples by avoiding disturbance of the sediment, positioning the sampling points accurately, and using GPS for precise location tracking. During sampling, careful documentation was maintained using the "Water Quality Sampling Record Form".

2.3.2. Sample Collection and Determination

Water samples were analyzed for parameters including temperature, pH, DO, COD, COD_{Mn}, BOD_5, NH_3-N, and TP. Samples were transported in a dedicated vehicle, protected from sunlight and physical damage, and the microbiological samples were transported in a cold, dark environment to reach the laboratory within 6 h. Each sample was tested three times to ensure accuracy, and the average value was taken as the result.

Water temperature was measured using a thermometer according to GB/T 13195-1991 The thermometer was inserted into the water at the desired depth, left for 5 min, and then read. DO was measured using an electrochemical probe as per HJ 506-2009, where oxygen permeated a selective membrane, creating a current proportional to the oxygen concentration. The pH was measured using a pH meter and electrodes according to HJ 1147-2020, with the calibration and measurement procedures involving standard buffer solutions. In the laboratory, COD was determined using the dichromate method (HJ 828-2017) by refluxing the sample with dichromate, cooling, and titrating. The permanganate index was measured according to GB 11892-89 by oxidizing the sample with permanganate in an acidic medium, reducing excess permanganate, and titrating with permanganate. BOD_5 was measured using the dilution and inoculation method (HJ 505-2009) by incubating the samples and measuring the dissolved oxygen before and after incubation. NH_3-N was measured using the colorimetric method of Nessler's reagent (HJ 535-2009) by preparing a standard series, treating the samples, and measuring the absorbance at 420 nm. TP was determined using the ammonium molybdate spectrophotometric method (GB/T 11893-1989) by digesting the samples, adding reagents, and measuring the absorbance at 700 nm.

2.3.3. Quality Assurance

The sampling process adhered to the guidelines provided in several key documents, including the *Environmental Quality Standards for Surface Water* (GB3838-2002), the *Environmental Water Quality Monitoring Quality Assurance Manual (Second Edition)*, the *Technical Guidelines for Water Quality Sampling* (HJ/T 494-2009), the *Technical Specifications for Environmental Quality Monitoring of Surface Water* (HJ/T 91.2-2022), and the *Technical Regulations for the Preservation and Management of Water Quality Sampling Samples* (HJ/T 493-2009).

Quality assurance and quality control for the laboratory analyses were performed following the standard methods outlined in the *Standard Methods for the Examination of Water and Wastewater of China* (HJ/T 91-2002). Blank samples were used at all monitoring stations to ensure the accuracy of the analyses. The samples were preserved and transported according to the specified guidelines to prevent contamination or degradation. The samples were also properly labeled and stored to maintain their integrity, including using specific preservatives and maintaining appropriate temperatures. The samples were transported using dedicated vehicles to prevent exposure to sunlight and to ensure that they reached the laboratory within the specified timeframe.

3. Results

3.1. Mainstream Section

3.1.1. Evolution of the Long-Term Runoff Series

According to 73 years of measured data from 1951 to 2023, the average annual runoff measured at the Longmen hydrological station, located in the initial section of the Xiao Bei mainstream, was 25.638 billion cubic meters, with a maximum of 53.729 billion cubic meters (1967) and a minimum of 13.019 billion cubic meters (1997). This represented a peak-to-trough ratio of 4.13. Significant interannual variability existed, with large fluctuations each year (Figure 2(a1)). Overall, there was a decreasing trend in runoff ($y = -0.0143x + 27.67$, $R^2 = 0.0529$, Figure 2(a1), where y represents the annual runoff in billion cubic meters and x represents the year.), with a sharp decline in 1986. The downward trend continued and remained at constantly low runoff volumes after 1986, which was evident in the comparison of the runoff with the average for each year (Figure 2(a2)). Except for a few positive deviations that mainly occurred around 2019, negative deviations from the average

dominant were observed in the latter half of the investigated years. From 1986 to 2023, runoff decreased by 33.8% compared with 1951–1985, with a more significant reduction reaching 48.9% during the flood season, primarily due to the construction of reservoir groups upstream, which mitigated flood-related runoff.

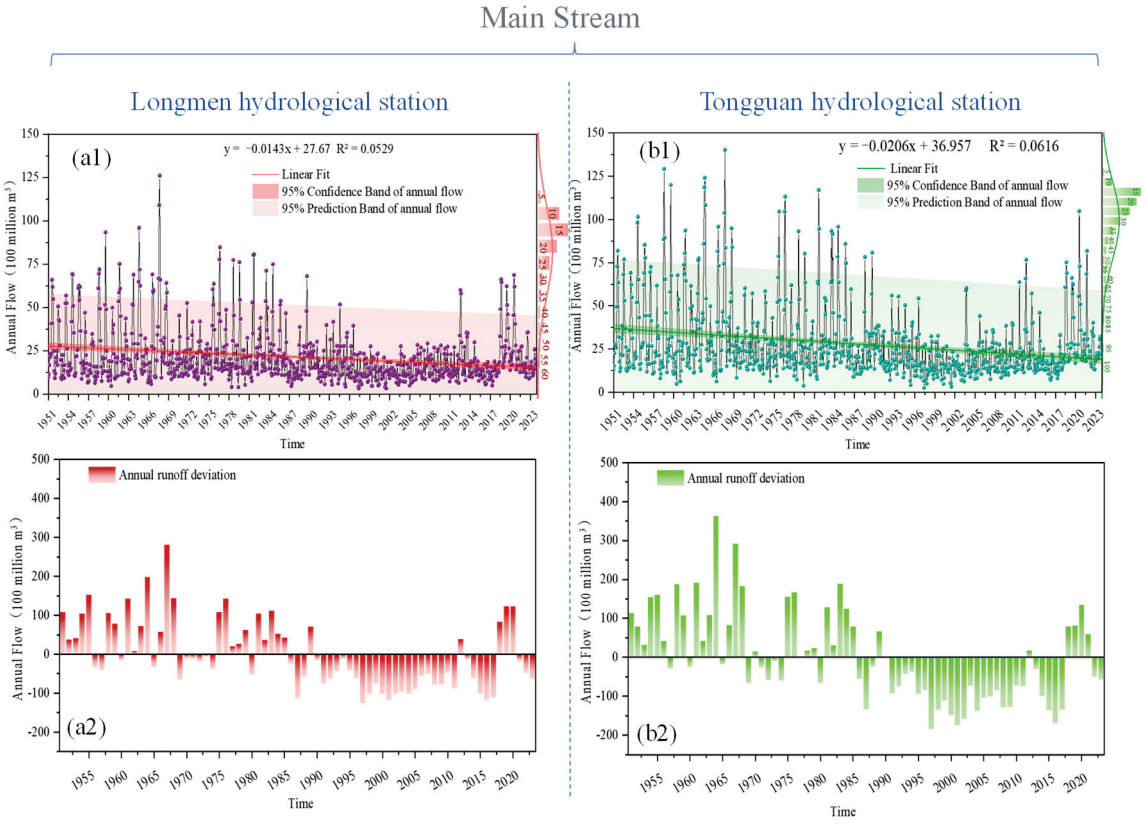

Figure 2. Trends and variations in monthly and annual runoff at Longmen and Tongguan hydrological stations from 1951 to 2023. (**a1**) Trend of monthly average runoff at Longmen hydrological station. (**a2**) Differences in runoff from the annual mean at Longmen hydrological station. (**b1**) Trend of monthly average runoff at Tongguan hydrological station. (**b2**) Differences in runoff from the annual mean at Tongguan hydrological station.

Based on the same series of annual statistics, the average annual runoff at the Tongguan hydrological station, located at the end of the Xiao Bei mainstream, was 33.448 billion cubic meters, with a maximum of 69.734 billion cubic meters (1964) and a minimum of 14.936 billion cubic meters (1997), demonstrating a difference of 4.67-fold. The runoff trend at the Tongguan section was similar to those at Longmen, also showing a decreasing trend ($y = -0.0206x + 36.957$, $R^2 = 0.0616$, Figure 2(b1), where y again represents the annual runoff in billion cubic meters and x represents the year). From 1986 to 2023, runoff decreased by 36% compared with 1951–1985, with a reduction of 48.3% during the flood season. Meanwhile, Tongguan's downstream station had overall higher runoff volumes than the upstream Longmen station from year to year, accompanied by greater variability.

The measured runoff at both the Longmen and Tongguan stations further decreased after 1995. This marked the beginning of a prolonged and extensive dry period for the Yellow River mainstream. From 1996 to 2011, the average runoff at Longmen and Tongguan was 17.055 billion cubic meters and 21.563 billion cubic meters, respectively. These figures were significantly lower than the long-term averages of 8.583 billion cubic meters for Longmen and 11.875 billion cubic meters for Tongguan.

Despite a prolonged period of low runoff, it was noteworthy that from 2018 to 2020, the Longmen hydrological station experienced a significant increase in runoff, surpassing the average levels and stabilizing at approximately 30 billion cubic meters. Similarly, the

Tongguan station observed a comparable rise in runoff from 2018 to 2021, with values ranging from 35 to 40 billion cubic meters.

3.1.2. Intra-Annual Variations in Runoff

The distribution of runoff within the year was uneven in the Xiao Bei mainstream, characterized by seasonal peaks and troughs. Figure 3 illustrates the distribution of the long-term average measured runoff for the Longmen (blue) and Tongguan (orange) stations over a period of 73 years. At Longmen, the highest monthly runoff occurred in August, reaching 3.9 billion cubic meters. In contrast, Tongguan experienced its peak runoff in September, with a value of 5.2 billion cubic meters. The lowest runoff was observed in January for both stations, with Longmen recording 1.2 billion cubic meters and Tongguan recording 1.4 billion cubic meters. The peak runoff months from July to October were particularly significant in both locations, accounting for 52% of the annual runoff at Longmen and 54% at Tongguan. This seasonal concentration highlighted the uneven distribution of runoff throughout the year. A notable spring flood occurred in March for both locations, driven by the melting of ice in the upper Yellow River. During this period, Longmen recorded a runoff of 2.2 billion cubic meters, while Tongguan recorded 2.4 billion cubic meters.

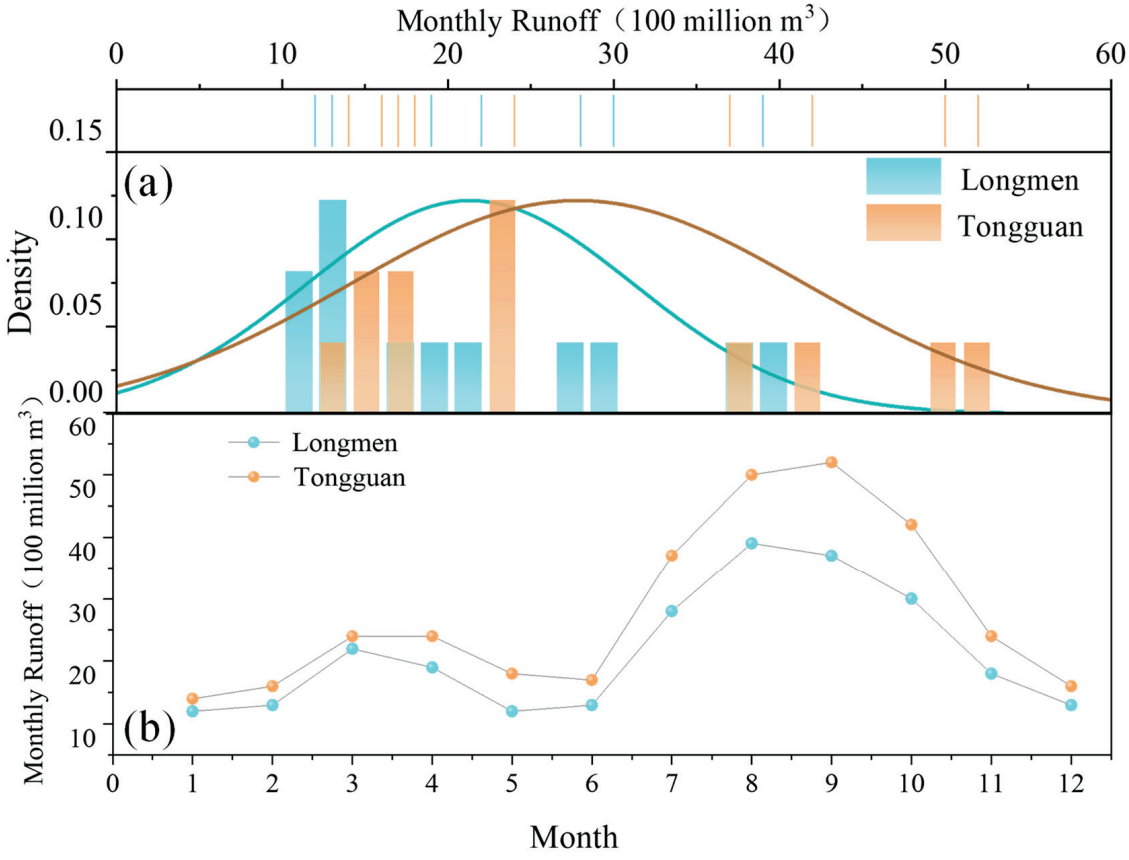

Figure 3. Intra-annual distribution of long-term average runoff for the Xiao Bei mainstream. (**a**) Graphs of the monthly distribution of density with histograms and rug plots for the Longmen (blue) and Tongguan (orange) stations over 73 years. The smooth curves represent the probability density functions of the runoff data, providing a continuous view of the data's distribution. The histograms illustrate the frequency of data points within specific intervals, while the rug plots show individual data points along the *x*-axis. (**b**) Line plot showing the measured intra-annual average runoff data for Longmen and Tongguan stations.

If we compare the data from two hydrological stations, the downstream Tongguan station witnessed higher average runoff each month, as demonstrated by the higher frequency

of high-value data in the distribution. The higher runoff at Tongguan station aligned with the annual evolutionary trend mentioned in the previous section.

3.2. Major Tributaries

3.2.1. Evolution of the Long-Term Runoff Series

The average annual runoff at the Huaxian hydrological station on the Wei River from 1951 to 2023 was 6.937 billion cubic meters, while at the Hejin hydrological station on the Fen River, it was 0.987 billion cubic meters. The peak-to-trough ratios for the annual runoff extremes at Huaxian and Hejin were 11.40 and 22.24, respectively, with coefficients of variation (Cv) of 0.53 and 0.81. The long-term data indicated an overall decreasing trend in runoff for both the Wei ($y = -0.0026x + 6.9588$, $R^2 = 0.0094$, Figure 4(a1)) and Fen Rivers ($y = -0.0012x + 1.3377$, $R^2 = 0.058$, Figure 4(b1)), where y represents the runoff and x is the time in years.

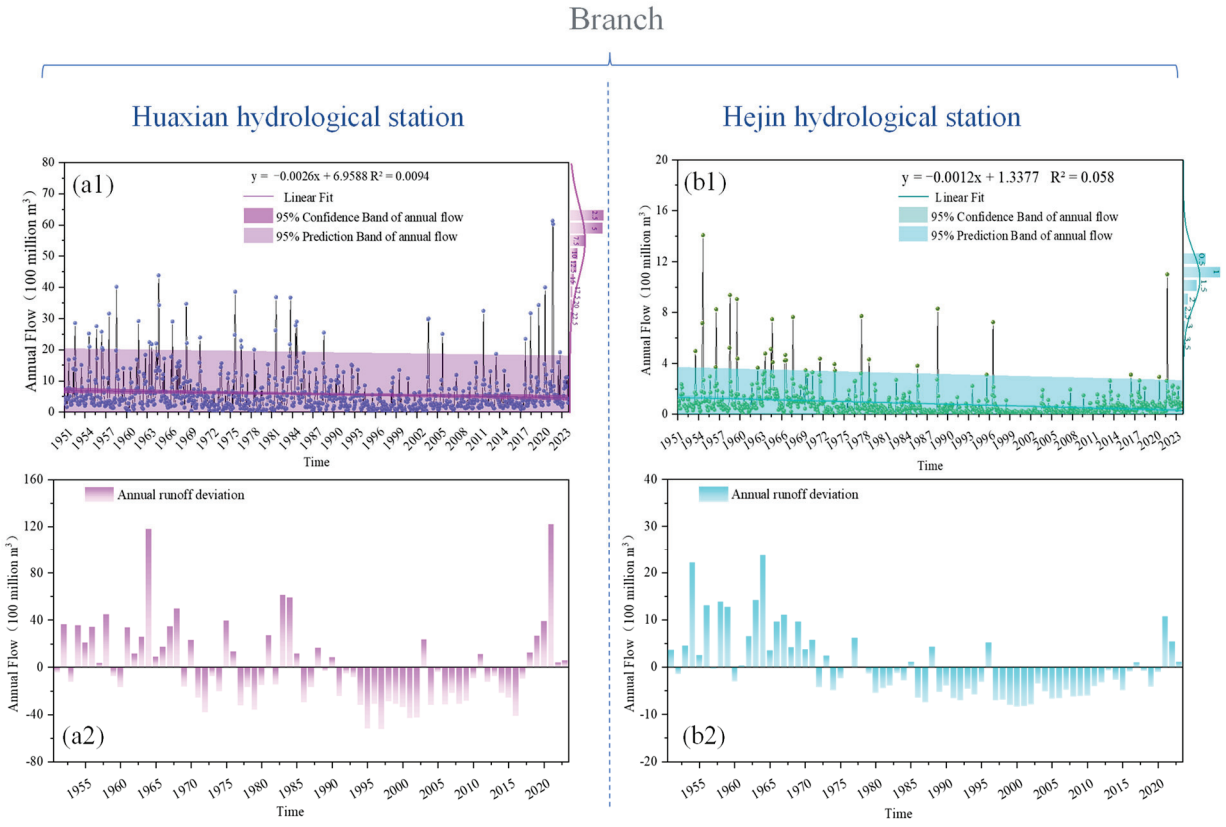

Figure 4. Trends and variations in monthly and annual runoff at Huaxian and Hejin hydrological stations from 1951 to 2023. (**a1**) Trend of monthly average runoff at Huaxian hydrological station. (**a2**) Differences in runoff from the annual mean at Huaxian hydrological station. (**b1**) Trend of monthly average runoff at Hejin hydrological station. (**b2**) Differences in runoff from the annual mean at Hejin hydrological station.

Both hydrological stations showed lower values in the second half of the measurement year and continued transitioning from positive to negative deviations in annual runoff (Figure 4(a2,b2)). A drastic increase in flow was also noted at the Huaxian hydrological station in 2018, peaking in 2021. The same low-to-high turnaround was observed at the Hejin station in similar years. However, the two tributaries exhibited significant differences in runoff, with the Wei River showing much higher values than the Fen River. This disparity was evident in the average values, maximum values, and overall distribution of runoff.

3.2.2. Intra-Annual Variations in Runoff

The intra-annual distribution of average monthly runoff over 73 years at Huaxian and Hejin is shown in Figure 5. In Figure 5a, the centered distribution below 2 billion cubic meters measured at Hejin station indicated relatively small intra-annual variations with low runoff in the Fen River. In contrast, the scattered distribution, ranging widely from around 2 to 13 billion cubic meters, suggested significant fluctuations and higher runoff volumes in the Wei River.

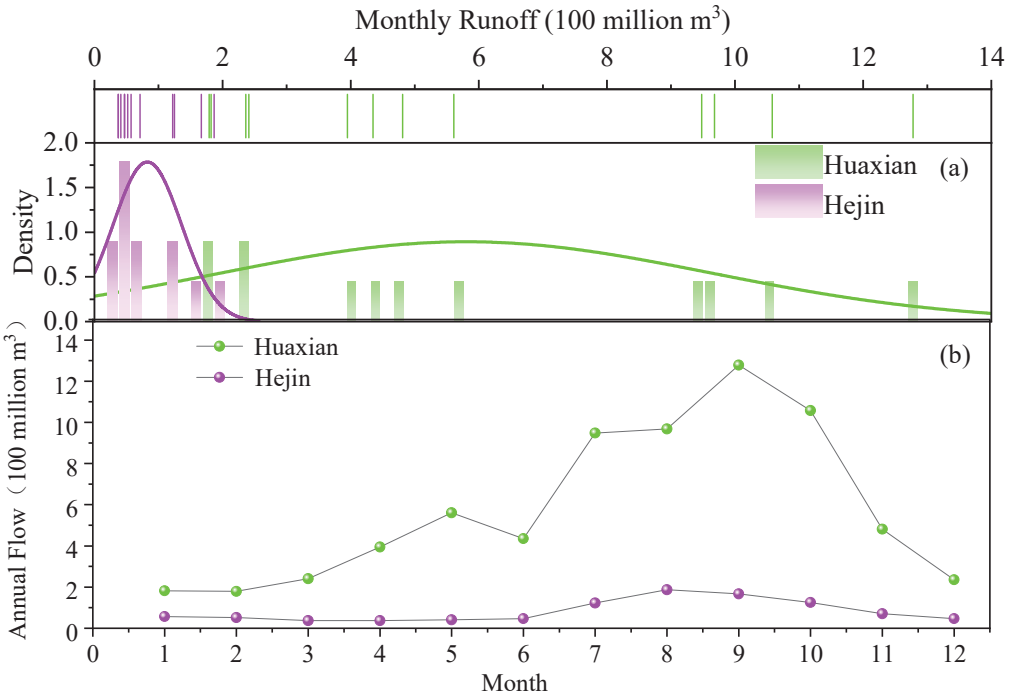

Figure 5. Intra-annual distribution of long-term average runoff from the Wei River (Huaxian hydrological station) and Fen River (Hejin hydrological station). (**a**) Graphs of the monthly distribution of density with histograms and rug plots for Huaxian (green) and Hejin (purple) stations over 73 years. The smooth curves represent the probability density functions of the runoff data, providing a continuous view of the data's distribution. The histograms illustrate the frequency of data points within specific intervals, while the rug plots show individual data points along the *x*-axis. (**b**) Line plot showing the measured intra-annual average runoff data for Huaxian and Hejin stations.

In Figure 5b, we can observe that the highest monthly runoff at Huaxian and Hejin occurred in September (1.278 billion cubic meters) and August (0.187 billion cubic meters), respectively; the lowest was in February (0.179 billion cubic meters at Huaxian) and March–April (0.037 billion cubic meters at Hejin). The surface runoff in the Wei and Fen Rivers was generated by rainfall, with the flood season (July to October) accounting for 61% of the annual runoff at both Huaxian and Hejin.

3.2.3. Intra-Annual Contribution Ratios of Tributaries' Runoff

The lower reaches of the Wei River transition from a meandering to a braided channel, with a gradient of 0.1–0.8‰. It is wide at the top and narrow at the bottom, with the river mouth having a width of approximately 0.2 km. Figure 6 provides a comparison of the average monthly runoff over the 73 years between the Yellow River mainstream and the Wei River and Fen River tributaries. The line plots showing the monthly contribution ratio of the tributaries to the mainstream are also included. Specifically, the monthly contribution ratio of the Wei River to the Yellow River mainstream's runoff ranged from 10.04% to 31.17%, averaging 19.75%. The runoff of the Fen River is relatively small compared with the Wei River, forming a wide and shallow river segment at the confluence with the Yellow River. The monthly contribution ratio of the Fen River to the Yellow River mainstream's

runoff ranged from 1.65% to 4.58%, averaging 3.59%. Considering the low runoff volumes of the Fen River discovered in the previous section, the contribution ratio to the mainstream was correspondingly smaller.

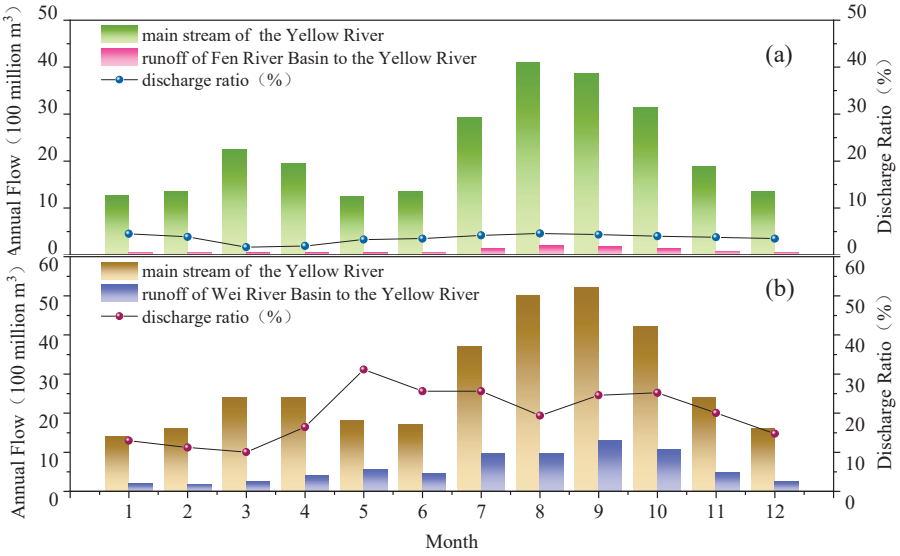

Figure 6. Comparison of average monthly runoff between the tributaries and mainstream of the Yellow River. (**a**) Contribution of the Fen River to the Yellow River (**b**) Contribution of the Wei River to the Yellow River.

3.3. Assessment of Water Quality

The concentration ranges of the water quality indicators at the monitoring point of the Xiao Bei mainstream were as follows and are shown in Figure 7: DO, 5.92–6.75 mg/L; COD, 13–24 mg/L; BOD_5, 2.7–4.6 mg/L; COD_{Mn}, 2.3–4.0 mg/L; NH_3-N, 0.16–0.67 mg/L; and TP, 0.05–0.12 mg/L.

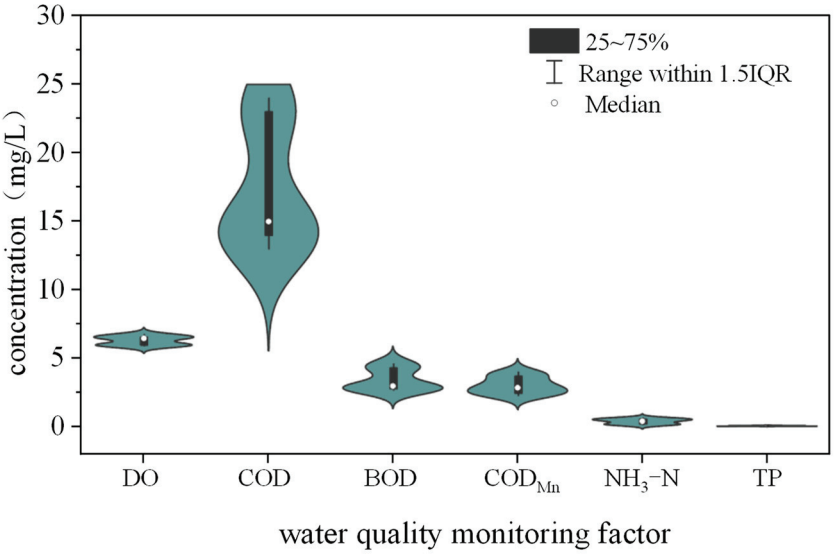

Figure 7. Characterization of the concentrations of factors for monitoring water quality in the Xiao Bei mainstream: Green area display the data distribution and dark area represents the inter quartile range, which spans from the 25th to the 75th percentile of the data.

The runoff volumes of the Wei River and the Fen River were relatively small, resulting in a low capacity for the assimilation of pollution. The Miaoqiao and Huaxian cross-sections represented the entrance from the upstream Fen River and downstream Wei River, reaching

the Yellow River at 0 km. The concentrations of pollutants at Miaoqian and Diaoqiao were relatively higher compared with the initial section of the Xiao Bei mainstream measured at Longmen. The comparison shown in Figure 8 revealed that the concentrations of COD, BOD_5, COD_{Mn}, NH_3-N, and TP at the Miaoqian section of the Fen River were 1.29 to 2.15 times higher than those at the Longmen section of the mainstream. Similarly, the concentrations of these same water quality factors at the Diaoqiao section of the Wei River were 1.57 to 2.08 times higher than those at the Longmen section of the mainstream.

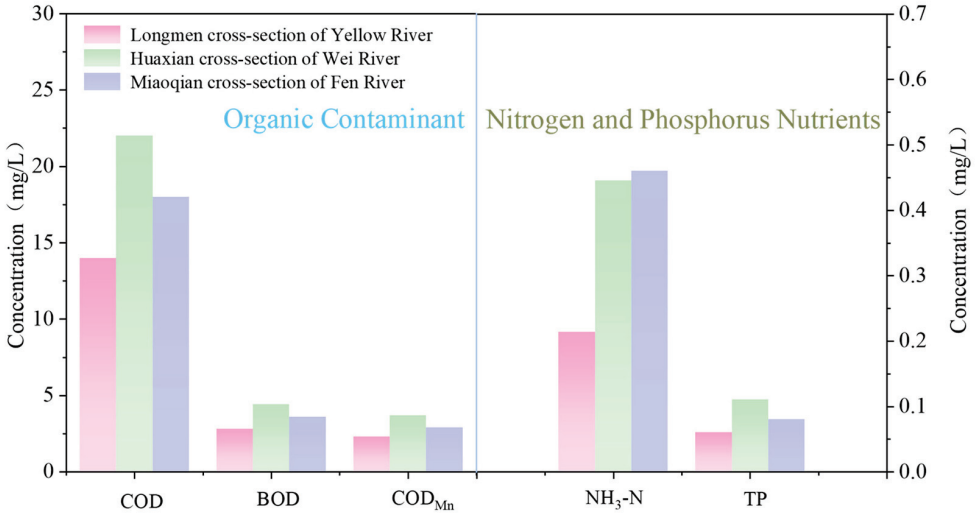

Figure 8. Comparison of water quality factors in the mainstream and tributaries of the Xiao Bei mainstream.

The results of monitoring from the 11 sampling points are shown in Figure 9, illustrating the spatial distribution characteristics of water quality parameters along the Xiao Bei mainstream. After the confluence of the Fen and Wei Rivers, varying impacts on the water quality of the mainstream were observed, either positive or negative. However, the water quality factors all increased at the final monitoring point compared with the initial point, after the confluence of the Wei River and Fen River.

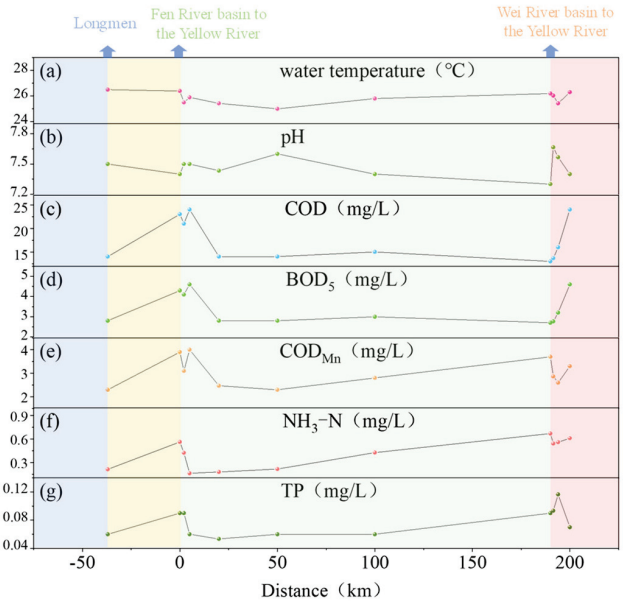

Figure 9. Changes in the monitored values of water quality factors over 11 sampling points along the studied reach. (**a**) Temperature, (**b**) pH, (**c**) chemical oxygen demand (COD), (**d**) ammonia nitrogen (NH_3-N), (**e**) total phosphorus (TP), (**f**) permanganate index (COD_{Mn}), (**g**) 5-day biochemical oxygen demand (BOD_5).

During the monitoring period, the average water temperature across the sections was 25.86 °C, with the highest (26.5 °C) at Longmen and the lowest (25 °C) at downstream from the Fen River's confluence. The distribution of water temperature was generally stable, with a slight decrease at the confluence points of the Fen and Wei Rivers, followed by an increase at the next monitoring point. The average pH was 7.5, ranging from 7.7 at 1.5 km downstream of the Wei River's confluence to 7.3 at the Wei River's confluence. The pH levels increased at the monitoring points after both confluences, with a relatively significant rise of 0.3, peaking after the Wei River's confluence.

Regarding other parameters, COD and BOD_5 exhibited similar trends along the measured section. Both parameters peaked at the monitoring points 5 km downstream from the Fen River's entry to the Yellow River mainstream and 10 km downstream from the Wei River's entry, with maximum concentrations of 24 and 4.6 mg/L, respectively. Initially, between the Longmen station and the Fen River's confluence, both parameters showed an upward trend. After the confluence with the Fen River, the concentrations initially decreased at the next monitoring point (2 km downstream from the Fen River's entry) before rising to their highest levels 5 km downstream. Subsequently, the concentrations declined and stabilized at around 15 mg/L for COD and 2.9 mg/L for BOD_5, observed at the observation point 20 km downstream from the Fen River's entry. The concentrations increased drastically and spiked again to their peak levels after the confluence with the Wei River. The average COD was 17 mg/L, with concentrations of 23 mg/L at the Fen River's confluence and 13 mg/L at the Wei River's confluence. The average BOD_5 was 3.4 mg/L, with concentrations of 4.3 mg/L at the Fen River's confluence and 2.8 mg/L at the Wei River's confluence. The trend of variation in COD_{Mn} was similar from the beginning to the monitoring point 50 km downstream from the Fen River's entry, after which, it gradually increased to 3.7 mg/L at the Wei River's confluence. Unlike COD and BOD_5, the concentration of COD_{Mn} decreased after the Wei River's confluence and rose again in the last measurement interval. The average COD_{Mn} was 3.0 mg/L, with concentrations of 3.9 mg/L at the Fen River's confluence and 3.7 mg/L at the Wei River's confluence. The concentration of NH_3-N decreased following the inflow from the Weihe River but rose again before the next monitoring point. In contrast, after the inflow from the Fen River, NH_3-N levels continued to decline, reaching their lowest value of 0.163 mg/L at a point 5 km downstream of the Fen River's entry into the Yellow River. This behavior was distinct from that of COD, BOD_5, and COD_{Mn}, for which the concentration reached the highest levels. Between the point 5 km downstream of the Fen River's entry and the Weihe River's inflow area, NH_3-N concentrations showed a rising trend. The average NH_3-N was 0.42 mg/L, with concentrations of 0.56 mg/L at the Fen River's confluence and 0.67 mg/L at the Wei River's confluence. The concentration of TP also declined first after the Fen River's confluence but dropped to the lowest at 0.053 mg/L at the point 20 km downstream from the Fen River's entry. The confluence of the Wei River witnessed an increase to 0.117 mg/L at the point 4 km downstream from the Wei River's entry, followed by an evident decrease within the last measured section. The average TP was 0.08 mg/L, with concentrations of 0.09 mg/L at the Fen River's confluence and 0.12 mg/L at the Wei River's confluence.

3.4. Changes in Pollutant Fluxes

Considering the overall transmission process of hydrological and water quality, the water quality and quantity fluxes constituted significant components of the total material flux of the river. In our study, the annual pollutant fluxes at the Longmen and Tongguan sections of the Yellow River mainstream and the confluence points of the Fen and Wei Rivers in 2021 were analyzed. Water quality fluxes were found to be positively correlated with runoff and pollutant concentrations at each cross-section. As shown in Figure 10, the annual NH_3-N and TP fluxes at the Longmen section of the Yellow River mainstream were 1749.54 t/a and 1802.86 t/a, respectively. With the inflow from the Fen and Wei Rivers,

the downstream Tongguan section recorded increased annual NH_3-N and TP fluxes of 8718.65 t/a and 3262.75 t/a.

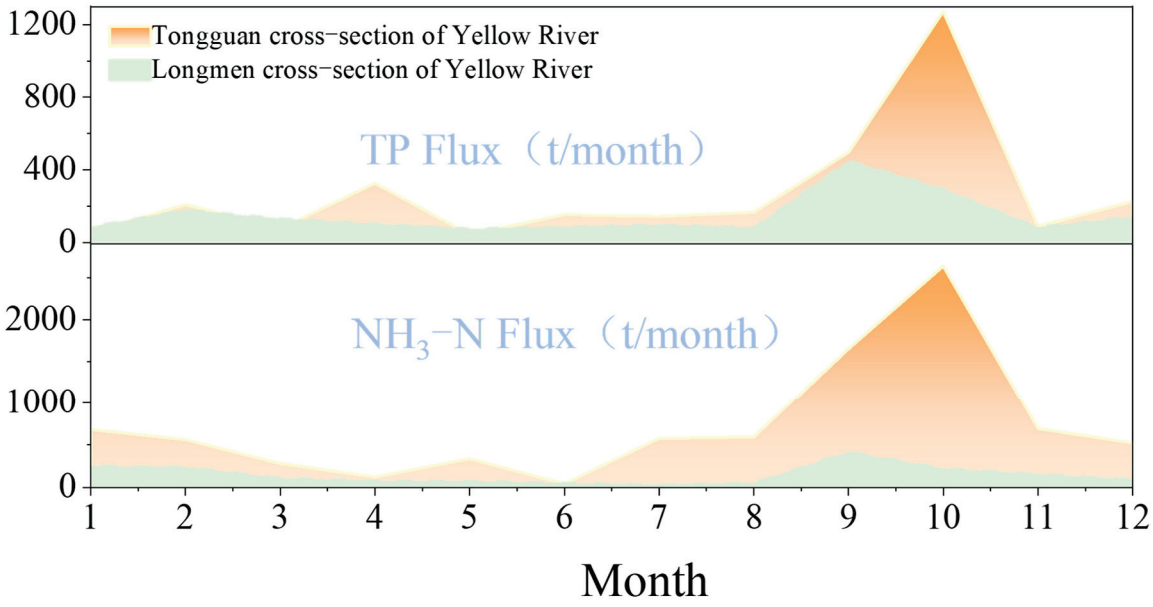

Figure 10. Monthly changes in TP and NH_3-N fluxes in the Xiao Bei mainstream in 2021.

In 2021, both total phosphorus (TP) and ammonia nitrogen (NH_3-N) exhibited similar patterns of monthly variation across all cross-sections. At the Longmen cross-section, TP and NH_3-N remained relatively stable throughout the spring and early summer. However, starting in August, there was a noticeable increase, peaking in September at 449.67 tons per month and 414.59 tons per month, respectively. At the Tongguan cross-section, TP experienced a minor peak in April and a major peak in October, reaching 1273.39 tons. The minor peak for NH_3-N was delayed by a month, occurring in May, with its major peak also occurring in October, reaching 2637.74 tons.

The Fen and Wei Rivers contributed significantly to the pollutant load of the mainstream. The NH_3-N and TP fluxes at the Fen River's Miao Qian section were 1004.95 t/a and 222.73 t/a, respectively, and at the Wei River's Diao Qiao section, they were 5847.25 t/a and 2159.13 t/a, respectively. With the Tongguan section of the Yellow River mainstream as a reference, the annual NH_3-N and TP inputs from the Fen River accounted for 11.5% and 6.8% of their totals in the Yellow River, while inputs from the Wei River accounted for 67.1% and 66.18%. The inflow of pollutants from the Fen and Wei Rivers increases the pollution risk of the mainstream.

4. Discussion

4.1. Temporal Variation in Runoff in the Xiao Bei Mainstream and Its Tributaries

The runoff in the entire mainstream and tributaries showed an overall decreasing trend, consistent with the results of many other studies [24,25]. The decline in the volume of runoff first became evident in 1986 (Figure 2). This observation also aligned with the findings of Wang et al., which identified 1985 as the turning point in the long-term reduction in runoff of the sections of Longmen–Tongguan [26]. The changes in runoff after the 1980s were identified to be dominated by human activities, which acted as the predominant influencing factor on the Yellow River's quality [26–29]. Despite the decreases, the results indicated a uniform increase in runoff for all investigated river reaches from approximately 2018 to 2020. This drastic climbing trend was also observed at the Lijin station [30]. The recent years' increase in water volume has been well-documented, with both government policy control and substantial investments playing a significant role in this achievement [31–33].

Upon comparison between the data measured from the mainstream hydrological stations and those from the tributaries, we observed that the runoff exhibited the trend of fluctuating high values followed by decreases. However, in contrast to the mainstream, which showed a turning point in 1986, the tributaries started their fluctuating decline much earlier, in around 1971 (Figure 4). This decline fluctuated and continued until stabilizing at lower values in 1986. Notably, there was a significant increase in runoff for all mainstreams and tributaries in around 2020.

The intra-annual variation in runoff based on the long-term monthly averages showed that the Fen River and Wei River tributaries followed the same pattern as those of the mainstream rivers. There was a slight increase in spring in around March to April and a peak during the summer months from July to October, thereby contributing seasonally to the Yellow River's volume of runoff. This consistent seasonal variation aligned with the previous studies of Zhang et al. in the Xiao Bei mainstream and corresponded with the regional climate pattern, where the winters are cold and dry with minimal rainfall, and summers are warm and wet, characterized by frequent storms in the middle reaches [34]. In wet seasons with more precipitation, water quality tends to be more degraded, posing potential health risks to residents that require our attention [35]. However, the contribution ratio exhibited different trends throughout the year compared with the runoff, as shown in Figure 6. The Fen River made its lowest contribution in March, followed by the second lowest in April. For the remaining months, its contribution ratio stabilized at approximately 5%. Similarly, the Wei River's contribution was minimal in March but peaked in May, despite the highest runoff occurring in September.

4.2. Factors of Water Quality and Pollutant Fluxes

Water quality was assessed using the single-factor evaluation method and classified against the national water quality standard GB3838-2002. By comparing each parameter's concentration with the target standard level, the category of water quality was determined on the basis of the worst-performing factor. According to the water quality parameters measured at Tongguan, the specific measurements were as follows: DO, 6.75 mg/L, Class II; COD, 13 mg/L, Class I; BOD_5, 2.7 mg/L, Class I; NH_3-N, 0.671 mg/L, Class III; TP, 0.09 mg/L, Class II; and COD_{Mn}, 3.7 mg/L, Class II. On the basis of these parameters, the overall water quality in the Xiao Bei reach during the monitoring period was classified as Class III.

The confluence of the Wei and Fen Rivers with the mainstream significantly impacted the overall water quality of the Yellow River (Figure 9). According to the 2017 Report on the State of the Ecology and Environment in China, the water quality of these tributaries was classified as intermediately polluted [36]. In our study, the concentrations of the targeted water quality parameters increased following the merging of these tributaries. However, these parameters exhibited different responses, depending on the specific tributary. To gain a comprehensive understanding, further investigation into the water quality of the tributaries themselves is necessary. Figure 10 illustrates the increased total pollutant flux from upstream to downstream, indicating that the tributaries are likely to be the primary sources of pollutants. This suggested that focusing management efforts on these tributaries could be highly effective. Additionally, the seasonal patterns of fluctuation in the pollutants aligned with those of the overall runoff. Other studies have shown that the middle reaches of the Yellow River are influenced by multiple sources and can be significantly impacted by the variations observed in tributaries during the high-flow season, while manure and sewage waste are the largest contributors to the Yellow River Basin during the low-flow season [37]. The mean concentrations of total phosphorus were higher in the rainy season than in the dry season, underscoring the importance of incorporating the influence of seasonality to pollutant fluxes when developing water management strategies [38].

4.3. Agricultural Impacts and Policy Measures on Pollutant Loads in the Yellow River Basin

Agricultural activities in the Yellow River Basin, especially along the Xiao Bei mainstream, significantly affect water quality. Although overall pollutant emissions have decreased, the proportion of COD and NH_3-N from agricultural sources has risen, largely due to extensive irrigation. Pollutants such as nitrogen and phosphorus from irrigated areas, particularly in the Fen–Wei Plain, flow into tributaries such as the Weihe and Fenhe Rivers, exacerbating pollution in the Xiao Bei mainstream.

4.3.1. Effectiveness of Policy on Pollutant Loads

While national policies aim to reduce fertilizer and pesticide use, regional differences in enforcement limit their impact. Ecological drainage systems and water management reforms remain uneven across provinces, contributing to inconsistent progress in reducing pollutants. The Yellow River Basin has a long history of agricultural activities and is one of China's major agricultural regions, contributing about one-third of the country's total grain production. Based on data from two national pollution source surveys, a temporal analysis of agricultural non-point source pollution in the Yellow River Basin indicates that, compared with 2006, the total pollutant emissions in 2017 had significantly decreased. However, the proportion of COD and NH_3-N pollution from agricultural sources rose to 56% and 83%, respectively. In the Fen–Wei Plain, excess nitrogen from agricultural production increased from 1.12 million tons in 2006 to 1.37 million tons in 2014. Irrigated areas in the Yellow River Basin are typically equipped with comprehensive irrigation and drainage systems. Agricultural return flows, carrying nitrogen and phosphorus pollutants, enter natural downstream water bodies through drainage systems, impacting water quality. These pollutants are carried via the Weihe and Fenhe rivers, contributing to sustained increases in total nitrogen and phosphorus concentrations in the Xiao Bei mainstream.

4.3.2. Soil Salinization and Water Quality

Soil salinization in northern China exacerbates the degradation of water quality, particularly in regions such as the Yellow River Basin, where irrigation return flows are prevalent [6,39]. As these flows carry salts from agricultural lands into natural water bodies, the salinity of both surface and groundwater increases significantly. For example, in the Yellow River Delta, salt accumulation in the soil can reach up to 1.99–3.77 g/kg, resulting in high cation concentrations that further degrade the quality of soil and water [40]. The increased salinity poses a direct threat to freshwater ecosystems, complicating agricultural production and raising the costs of water treatment. In the Xiao Bei mainstream, this salinization results in worsened water conditions, requiring more extensive filtration processes and increasing the costs of treating potable water. Effective soil management practices, such as using superabsorbent polymers for improving the soil's structure, are necessary to mitigate these impacts. The introduction of these technologies can reduce nutrient losses and adapt crops to saline soils, creating a more sustainable environment in the long term.

4.3.3. Dams and Water Quality

Dams, particularly the cascade dams constructed along the Yellow River, have significantly altered the river's natural flow regime [15,41]. These dams trap vast amounts of sediments, especially in areas such as the Loess Plateau, where the Yellow River naturally carries a large sediment load, far exceeding that of other major rivers, such as the Yangtze River [42]. The retention of both sediment and water alters the nutrient dynamics and reduces the river's capacity to naturally dilute pollutants [11,43–46]. This phenomenon is particularly notable in downstream sections, where pollutants accumulate in the Xiao Bei mainstream, increasing contaminant concentrations. The reduced flow not only traps harmful nutrients and chemical pollutants but also decreases the self-purification ability of the river, exacerbating water quality issues in densely populated areas.

5. Conclusions

This study revealed the spatiotemporal variations in runoff, the water's environmental quality, and the characteristics of pollutant flux of the Xiao Bei mainstream and its tributaries in the middle reach of the Yellow River. It provided baseline data and analyzed trends to strengthen the understanding of the patterns and evolution of the rivers' water quality, thus supporting and providing insights into the protection of the Yellow River's water environment. Our findings have important implications for sustainable water management strategies, particularly in addressing the challenges posed by decreasing runoff and increasing pollutant loads from tributaries. The main findings from this study are summarized as follows.

(1) According to 73 years of long-term measured data (1951–2023), the runoff of the Xiao Bei mainstream exhibited significant interannual variability and an uneven intra-annual distribution, with a clear decreasing trend. After 1986, the runoff dropped sharply, with a 36% reduction at the Tongguan section and a 48.3% reduction during the flood season compared with 1951–1985. The sharp decline in runoff after 1986 coincided with major hydrological interventions such as the construction of dams and increased water withdrawals for agriculture and industry. This reduction in water flow not only affected the river's capacity to naturally dilute pollutants but also has implications for maintaining ecological flows, exacerbating the region's water scarcity issues.

(2) The long-term data indicated a decreasing trend in the runoff of the Wei and Fen River tributaries as well. The annual contribution ratios of the Wei and Fen Rivers' runoff to the Yellow River mainstream were 19.75% (ranging from 10.04% to 31.17% monthly) and 3.59% (ranging from 1.65% to 4.58% monthly), respectively. The decreasing contributions of the tributaries are indicative of broader hydrological shifts in the region, which are likely influenced by changing precipitation patterns, land use changes, and water management policies. The significant contribution of the Wei River compared with the Fen River emphasizes the need for targeted management interventions in specific sub-basins.

(3) On-site monitoring of eight water quality parameters at 11 locations showed that the water quality of the Xiao Bei mainstream during the monitoring period (August) was classified as Class III overall. The concentrations of the water quality parameters at the confluence points of the Wei and Fen Rivers with the Yellow River were higher than those in the mainstream, with certain spatial fluctuations observed along the mainstream after the tributaries merged.

(4) Water quality fluxes were positively correlated with runoff and pollutant concentrations at each cross-section. The Fen and Wei Rivers contributed significantly to the pollutant load of the mainstream, with annual NH_3-N and TP inputs from the Fen River accounting for 11.5% and 6.8% of the totals in 2021, respectively, and inputs from the Wei River accounting for 67.1% and 66.18%. The inflow of pollutants from the Fen and Wei Rivers increased the pollution risk of the mainstream.

In conclusion, the present study analyzed the long-term quality and quantity of water in the Xiao Bei Basin. It examined the contribution and impact of tributaries on the mainstream in terms of the volume and quality of water. The findings suggested that the reduction in runoff and the significant pollutant inputs from tributaries are the primary reasons for the situation of severe water pollution in the Xiao Bei mainstream of the Yellow River. These insights offer scientific evidence for developing effective management strategies for the water environment, emphasizing the role of tributaries as a crucial element in the overall management plan.

Author Contributions: Conceptualization, Z.Y., X.S. and L.Y.; methodology, Z.Y., X.S. and S.Y.; investigation, Z.Y., X.S. and Y.L.; writing—original draft preparation, Z.Y., X.S. and H.J.; writing—review and editing, L.Y. and S.Y. All authors have read and agreed to the published version of the manuscript.

Funding: This work was supported by the Outstanding Young Talents Science and Technology Foundation of Yellow River Conservancy Commission (Grant No. HQK-202320), the National Key

Research and Development Program of China (Grant No. 2023YFC3206202), the Major Science and Technology Special Fund of Henan Province (Grant No. 201300311400), the Special Scientific Research Project of Yellow River Water Resources Protection Institute (Grant No. KYY-KYZX-2022-01), and the National Natural Science Foundation of China (Grant No. 51709126).

Data Availability Statement: The data presented in this study are available on request from the corresponding author. The data are not publicly available due to confidentiality and government regulations.

Conflicts of Interest: The authors declare no conflicts of interest.

References

1. Xie, F.; Yu, M.; Yuan, Q.; Meng, Y.; Qie, Y.; Shang, Z.; Luan, F.; Zhang, D. Spatial Distribution, Pollution Assessment, and Source Identification of Heavy Metals in the Yellow River. *J. Hazard Mater.* **2022**, *436*, 129309. [CrossRef] [PubMed]
2. Zhu, Z. International Water Resources Association The Yellow River Basin: Water Accounting, Water Accounts, and Current Issues. *Water Int.* **2004**, *29*, 2–10. [CrossRef]
3. Wang, S.; Fu, B.; Liang, W.; Liu, Y.; Wang, Y. Driving Forces of Changes in the Water and Sediment Relationship in the Yellow River. *Sci. Total Environ.* **2017**, *576*, 453–461. [CrossRef] [PubMed]
4. Wei, J.; Lei, Y.; Yao, H.; Ge, J.; Wu, S.; Liu, L. Estimation and Influencing Factors of Agricultural Water Efficiency in the Yellow River Basin, China. *J. Clean Prod.* **2021**, *308*, 127249. [CrossRef]
5. Zhang, X.; Yu, W.; Zhang, T.; Shen, D. The Influencing Factors of Water Uses in the Yellow River Basin: A Physical, Production-Based, and Consumption-Based Water Footprint Analysis by the Random Forest Model. *Water* **2023**, *15*, 170. [CrossRef]
6. Chen, Y.-P.; Fu, B.-J.; Zhao, Y.; Wang, K.-B.; Zhao, M.M.; Ma, J.-F.; Wu, J.H.; Xu, C.; Liu, W.-G.; Wang, H. Sustainable Development in the Yellow River Basin: Issues and Strategies. *J. Clean Prod.* **2020**, *263*, 121223. [CrossRef]
7. Shen, Y.; Guo, Y.; Guo, Y.; Wu, L.; Shen, Y. Evaluating Water Resources Sustainability of Water-Scarcity Basin from a Scope of WEF-Nexus Decomposition: The Case of Yellow River Basin. In *Environment, Development and Sustainability*; Springer: Berlin/Heidelberg, Germany, 2024. [CrossRef]
8. Feng, K.; Siu, Y.L.; Guan, D.; Hubacek, K. Assessing Regional Virtual Water Flows and Water Footprints in the Yellow River Basin, China: A Consumption Based Approach. *Appl. Geogr.* **2012**, *32*, 691–701. [CrossRef]
9. Zhao, M.M.; Wang, S.-M.; Chen, Y.-P.; Wu, J.-H.; Xue, L.-G.; Fan, T.T. Pollution Status of the Yellow River Tributaries in Middle and Lower Reaches. *Sci. Total Environ.* **2020**, *722*, 137861. [CrossRef]
10. Wu, S.; Hu, Y.H.; Zuo, D. Discussion on Parameter Choice for Managing Water Quality of the Drinking Water Source. *Procedia Environ. Sci.* **2011**, *11*, 1465–1468.
11. Maavara, T.; Chen, Q.; Van Meter, K.; Brown, L.E.; Zhang, J.; Ni, J.; Zarfl, C. River Dam Impacts on Biogeochemical Cycling. *Nat. Rev. Earth Environ.* **2020**, *1*, 103–116. [CrossRef]
12. Wang, W.; Li, S.L.; Zhong, J.; Wang, L.; Yang, H.; Xiao, H.; Liu, C.Q. CO_2 emissions from Karst Cascade Hydropower Reservoirs: Mechanisms and Reservoir Effect. *Environ. Res. Lett.* **2021**, *16*, 044013. [CrossRef]
13. Xu, Y.; Yu, S.; Liu, D.; Ma, J.; Chuo, M. The Impact of the Three Gorges Reservoir Operations on Hydraulic Characteristics in the Backwater Region: A Comprehensive 2D Modeling Study. *Water* **2024**, *16*, 2045. [CrossRef]
14. Shi, W.; Wang, W.; Yu, S.; Liang, L.; Zhong, J.; Yi, Y.; Li, S.L. Influences of Hydrodynamics on Dissolved Inorganic Carbon in Deep Subtropical Reservoir: Insights from Hydrodynamic Model and Carbon Isotope Analysis. *Water Res.* **2024**, *250*, 121058. [CrossRef] [PubMed]
15. Jin, W.; Chang, J.; Wang, Y.; Bai, T. Long-Term Water-Sediment Multi-Objectives Regulation of Cascade Reservoirs: A Case Study in the Upper Yellow River, China. *J. Hydrol.* **2019**, *577*, 123978. [CrossRef]
16. Ouyang, W.; Hao, F.; Song, K.; Zhang, X. Cascade Dam-Induced Hydrological Disturbance and Environmental Impact in the Upper Stream of the Yellow River. *Water Resour. Manag.* **2011**, *25*, 913–927. [CrossRef]
17. Mu, J.; Zhang, H.; Liu, S.M.; Wu, N.; Song, G.; Ding, S.; Zhang, X. Nutrient Dynamics in the Yellow River—A Case Study of Different Reservoir Regulation Operations. *J. Hydrol.* **2024**, *629*, 130563. [CrossRef]
18. Chapra, S.C.; Camacho, L.A.; McBride, G.B. Impact of Global Warming on Dissolved Oxygen and Bod Assimilative Capacity of the World's Rivers: Modeling Analysis. *Water* **2021**, *13*, 2408. [CrossRef]
19. Wang, Y.; Tan, D.; Han, L.; Li, D. Review of climate change in the Yellow River Basin. *J. Desert Res.* **2021**, *41*, 235.
20. Liu, S.; Qiu, Y.; Fu, R.; Liu, Y.; Suo, C. Identifying the Water Quality Variation Characteristics and Their Main Driving Factors from 2008 to 2020 in the Yellow River Basin, China. *Environ. Sci. Pollut. Res.* **2023**, *30*, 66753–66766. [CrossRef]
21. Sun, X.; Zhou, Z.; Wang, Y. Water Resource Carrying Capacity and Obstacle Factors in the Yellow River Basin Based on the RBF Neural Network Model. *Environ. Sci. Pollut. Res.* **2023**, *30*, 22743–22759. [CrossRef]
22. Wang, X.; Duan, L.; Zhang, T.; Cheng, W.; Jia, Q.; Li, J.; Li, M. Ecological Vulnerability of China's Yellow River Basin: Evaluation and Socioeconomic Driving Factors. *Environ. Sci. Pollut. Res. Int.* **2023**, *30*, 115915–115928. [CrossRef] [PubMed]
23. *GB 3838-2002*; Environmental Quality Standard for Surface Water. Ministry of Ecology and Environment: Beijing, China, 2002. Available online: https://english.mee.gov.cn/standards_reports/standards/water_environment/quality_standard/200710/t20071024_111792.htm (accessed on 7 September 2024).

24. Wang, H.; Sun, F. Variability of Annual Sediment Load and Runoff in the Yellow River for the Last 100 Years (1919–2018). *Sci. Total Environ.* **2021**, *758*, 143715. [CrossRef] [PubMed]
25. Shi, C.; Zhou, Y.; Fan, X.; Shao, W. A Study on the Annual Runoff Change and Its Relationship with Water and Soil Conservation Practices and Climate Change in the Middle Yellow River Basin. *Catena* **2013**, *100*, 31–41. [CrossRef]
26. Wang, S.; Yan, M.; Yan, Y.; Shi, C.; He, L. Contributions of Climate Change and Human Activities to the Changes in Runoff Increment in Different Sections of the Yellow River. *Quat. Int.* **2012**, *282*, 66–77. [CrossRef]
27. Jiang, L.; Zuo, Q.; Ma, J.; Zhang, Z. Evaluation and Prediction of the Level of High-Quality Development: A Case Study of the Yellow River Basin, China. *Ecol. Indic.* **2021**, *129*, 107994. [CrossRef]
28. Wang, B.; Wang, H.; Jiao, X.; Huang, L.; Chen, H.; Guo, W. Runoff Change in the Yellow River Basin of China from 1960 to 2020 and Its Driving Factors. *J. Arid. Land* **2024**, *16*, 168–194. [CrossRef]
29. Xu, J.; Jiang, X.; Sun, H.; Xu, H.; Zhong, X.; Liu, B.; Li, L. Driving Forces of Nature and Human Activities on Water and Sediment Changes in the Middle Reaches of the Yellow River in the Past 100 Years. *J. Soils Sediments* **2021**, *21*, 2450–2464. [CrossRef]
30. Qin, H.; Shi, H.; Gai, Y.; Qiao, S.; Li, Q. Sensitivity Analysis of Runoff and Wind with Respect to Yellow River Estuary Salinity Plume Based on FVCOM. *Water* **2023**, *15*, 1378. [CrossRef]
31. Zhou, Y.; Ma, J.; Zhang, Y.; Qin, B.; Jeppesen, E.; Shi, K.; Brookes, J.D.; Spencer, R.G.M.; Zhu, G.; Gao, G. Improving Water Quality in China: Environmental Investment Pays Dividends. *Water Res.* **2017**, *118*, 152–159. [CrossRef]
32. Ministry of Ecology and Environment the People's Republic of China. *Action Plan for Prevention and Control of Water Pollution Printed and Distributed*; Ministry of Ecology and Environment the People's Republic of China: Beijing, China, 2015.
33. Wang, Y.; Zhao, W.; Wang, S.; Feng, X.; Liu, Y. Yellow River Water Rebalanced by Human Regulation. *Sci. Rep.* **2019**, *9*, 9707. [CrossRef]
34. Zhang, Q.; Jin, Z.; Zhang, F.; Xiao, J. Seasonal Variation in River Water Chemistry of the Middle Reaches of the Yellow River and Its Controlling Factors. *J. Geochem. Explor.* **2015**, *156*, 101–113. [CrossRef]
35. Zhao, M.M.; Chen, Y.; Xue, L.; Fan, T.T.; Emaneghemi, B. Greater Health Risk in Wet Season than in Dry Season in the Yellow River of the Lanzhou Region. *Sci. Total Environ.* **2018**, *644*, 873–883. [CrossRef] [PubMed]
36. Ministry of Ecology and Environment the People's Republic of China. *2017 Report on the State of the Ecology and Environment in China*; Ministry of Ecology and Environment the People's Republic of China: Beijing, China, 2018.
37. Yue, F.J.; Li, S.L.; Liu, C.Q.; Zhao, Z.Q.; Ding, H. Tracing Nitrate Sources with Dual Isotopes and Long Term Monitoring of Nitrogen Species in the Yellow River, China. *Sci. Rep.* **2017**, *7*, 8537. [CrossRef]
38. Hu, N.; Sheng, Y.; Li, C.; Li, Z.; Liu, Q. The Reactivity of Dissolved and Suspended Particulate Phosphorus Pools Decreases with Distance Downstream in the Yellow River. *Commun. Earth Environ.* **2023**, *4*, 294. [CrossRef]
39. Chen, G.; Wei, Z.; Liu, H. Study on Soil Desalination Process of Saline-Alkaline Grassland along the Yellow River in Western Inner Mongolia under Subsurface Drainage. *Sustainability* **2022**, *14*, 14494. [CrossRef]
40. Zhang, Y.; Yang, P.; Liu, J.; Zhang, X.; Zhao, Y.; Zhang, Q.; Li, L. Sustainable Agricultural Water Management in the Yellow River Basin, China. *Agric. Water Manag.* **2023**, *288*, 108473. [CrossRef]
41. Cai, X.; Rosegrant, M.W. Optional Water Development Strategies for the Yellow River Basin: Balancing Agricultural and Ecological Water Demands. *Water Resour. Res.* **2004**, *40*. [CrossRef]
42. Wang, S.; Fu, B.; Piao, S.; Lü, Y.; Ciais, P.; Feng, X.; Wang, Y. Reduced Sediment Transport in the Yellow River Due to Anthropogenic Changes. *Nat. Geosci.* **2016**, *9*, 38–41. [CrossRef]
43. Yu, S. Modeling Phosphorus Cycling in a Seasonally Stratified Reservoir (Fanshawe Reservoir, ON, Canada). Master Thesis, University of Waterloo, Waterloo, ON, Canada, 2020. Available online: http://hdl.handle.net/10012/16346 (accessed on 7 September 2024).
44. Scott Winton, R.; Calamita, E.; Wehrli, B. Reviews and Syntheses: Dams, Water Quality and Tropical Reservoir Stratification. *Biogeosciences* **2019**, *16*, 1657–1671. [CrossRef]
45. Maavara, T.; Parsons, C.T.; Ridenour, C.; Stojanovic, S.; Dürr, H.H.; Powley, H.R.; Van Cappellen, P. Global Phosphorus Retention by River Damming. *Proc. Natl. Acad. Sci. USA* **2015**, *112*, 15603–15608. [CrossRef]
46. Kao, N.; Mohamed, M.; Sorichetti, R.J.; Niederkorn, A.; Van Cappellen, P.; Parsons, C.T. Phosphorus Retention and Transformation in a Dammed Reservoir of the Thames River, Ontario: Impacts on Phosphorus Load and Speciation. *J. Great Lakes Res.* **2022**, *48*, 84–96. [CrossRef]

water

MDPI

Article

Soil Erosion Dynamics and Driving Force Identification in the Yiluo River Basin Under Multiple Future Scenarios

Jun Hou [1,2], Jianwei Wang [2,*], Xiaofeng Chen [3], Yong Hu [3] and Guoqiang Dong [3]

[1] School of Resources and Environment, Anqing Normal University, Anqing 246133, China; 172309@aqnu.edu.cn
[2] Henan Key Laboratory of Ecological Environment Protection and Restoration of Yellow River Basin, Yellow River Institute of Hydraulic Research, Zhengzhou 450003, China
[3] Anhui and Huaihe River Institute of Hydraulic Research, Hefei 230088, China; chxf508@163.com (X.C.); huyong@ahwrri.org.cn (Y.H.); dgqiwhr@163.com (G.D.)
* Correspondence: wangjw0603@163.com

Abstract: Our study focused on identifying the evolution of soil erosion and its key drivers under multiple future scenarios in the Yiluo River Basin. Integrating the Universal Soil Loss Equation (USLE), future land use and vegetation cover simulation methods, and the Geodetector model, we analyzed historical soil erosion trends (2000–2020), projected future soil erosion risks under multiple Shared Socioeconomic Pathways (SSPs), and quantified the interactive effects of key driving factors. The results showed that soil erosion within the basin exhibited moderate intensity. Over the past 20 years, soil erosion decreased by 28.78%, with 76.29% of the area experiencing reduced erosion intensity. Future projections indicated an overall declining trend in soil erosion, showing reductions of 4.93–35.95% compared to baseline levels. However, heterogeneous patterns emerged across various scenarios, with the highest risk observed under SSP585. Land use type was identified as the core driving factor behind soil erosion (explanatory capacity q-value > 5%). Under diverse future climate scenarios, interactions between land use type and precipitation and temperature exhibited high sensitivity, highlighting the critical regulatory role of climate change in regulating erosion processes. This research provides a scientific foundation for the precise prevention and adaptive management of soil erosion in the Loess Plateau region.

Keywords: Universal Soil Loss Equation; Future Land Use Simulation; soil erosion; Geodetector; Shared Socioeconomic Pathways

1. Introduction

The Loess Plateau ranks among the regions globally experiencing the most severe soil erosion [1,2]. The Yellow River discharges approximately 1.6 billion tons of sediment annually, shaping vast downstream alluvial plains while threatening the comprehensive high-standard growth of the basin [3,4]. As a primary right-bank tributary of the middle Yellow River, the Yiluo River Basin forms a crucial ecological corridor bridging the Loess Plateau's hilly regions and downstream plains [5,6]. However, situated in a transitional zone from semi-humid to semi-arid climates characterized by active geological structures and loose surface cover, coupled with the prolonged high-intensity exploitation of water–land resources and intense demographic pressure, the basin has become a hotspot for severe soil erosion within the Yellow River Basin [7,8]. Against escalating universal climate variation, intensifying extreme weather occurrences, and rapid regional socioeconomic transformation, projecting future soil erosion risks under multiple scenarios and identifying

their key driving factors are critically imperative. These endeavors hold irreplaceable strategic significance and represent an urgent practical necessity for promoting the high-standard advancement of the Yellow River Basin [9–11].

Empirical–physical models, epitomized by the USLE and its derivatives, have been extensively applied for watershed/regional-scale soil erosion quantification. Their widespread adoption stems from their clear structure, accessible input parameters, and effective multisource spatial data integration [12–14]. Studies across typical Loess Plateau watersheds have indicated significantly declining erosion intensities in recent decades, primarily driven by integrated ecological conservation strategies, such as the Grain-for-Green Program, terracing, and check-dam systems [15–17]. Soil erosion emerges from complex natural–socioeconomic interactions [18]. Natural drivers (rainfall, topography, soil erodibility, vegetation cover) establish soil erosion potential [19]. Human activities, such as land use changes, farming practices, conservation engineering, and urbanization processes, accelerate or mitigate erosion by altering surface conditions and hydrology [20,21]. Methodologies have evolved from qualitative descriptions to quantitative attribution using Geodetector, Structural Equation Modeling, and machine learning [22,23]. Such investigations have revealed regional divergent dominant drivers and complex nonlinear interactions exhibiting enhancement/suppression effects [24]. For instance, the improvement of vegetation coverage on the Loess Plateau is identified as the most crucial inhibitory factor for weakened soil erosion, while short-duration heavy rainfall events and the existence of sloping farmland constitute key risk factors [25,26].

Integrating future climate scenarios data with future land use/vegetation prediction methods constitutes a critical approach for exploring future soil erosion risks [27,28]. Such studies typically employ future climate models, land use/vegetation evolution simulations, and physically based erosion models to conduct multiscenario, multitemporal projections of soil erosion risks [29,30]. These projections are essential for anticipating priorities, challenges, and adaptive strategies under various development pathways [31,32]. However, fundamental questions persist regarding how the key drivers of soil erosion and their underlying mechanisms will evolve under future climate scenarios. These critical knowledge gaps remain underexplored in current research, representing scientific bottlenecks for achieving precise soil erosion prevention and adaptive watershed management.

Our study systematically integrates long-term remote sensing imagery, high-resolution geospatial data, and future climate scenarios datasets. Utilizing Geographic Information System (GIS) technology and numerical simulation methods, we establish a comprehensive research framework to analyze soil erosion dynamics and identify driving forces in the Yiluo River Basin under multiple future scenarios. The research comprises the following: (1) the spatiotemporal dynamics of soil erosion intensity; (2) future soil erosion projections; and (3) the identification of soil erosion driving factors. Our objectives are to reveal the soil erosion evolution patterns and future risks in the basin and quantitatively identify the key driving factors along with their interaction mechanisms.

2. Data and Methods

2.1. Study Area

The Yiluo River, a primary right-bank tributary of the middle Yellow River, originates from the confluence of the Yi River and Luo River near Yanshi City, Henan Province. It ultimately flows into the Yellow River at Gongyi City, draining a total basin area of approximately 18,800 km^2 (Figure 1). The upper reaches are characterized by mid-low mountains with steep slopes, serving as the primary water conservation zone. The middle reaches transition into loess hills and intermountain basins with gradually gentler terrain. The lower reaches enter the flat and open Huang-Huai-Hai Plain. Situated in

a climatic transition zone from semi-humid to semi-arid, the basin experiences a yearly mean temperature of 12.6 °C and a yearly mean precipitation of 680 mm. Rainfall is predominantly concentrated during the flood-prone season, making the area susceptible to flooding disasters. The watershed encompasses six prefecture-level cities, including Zhengzhou, Luoyang, Sanmenxia, Shangluo, Xi'an, and Weinan. Among these, Luoyang City occupies the largest area, accounting for approximately 59.45% of the total basin. Cultivated land is the predominant land use category, covering approximately 46% of the total basin area, making it an important area for grain and economic crop production. With its distinctive location, complex topography, significant water resource endowments, and profound cultural heritage, the Yiluo River Basin represents a strategically crucial area for implementing ecological conservation and high-quality development initiatives within the Yellow River Basin.

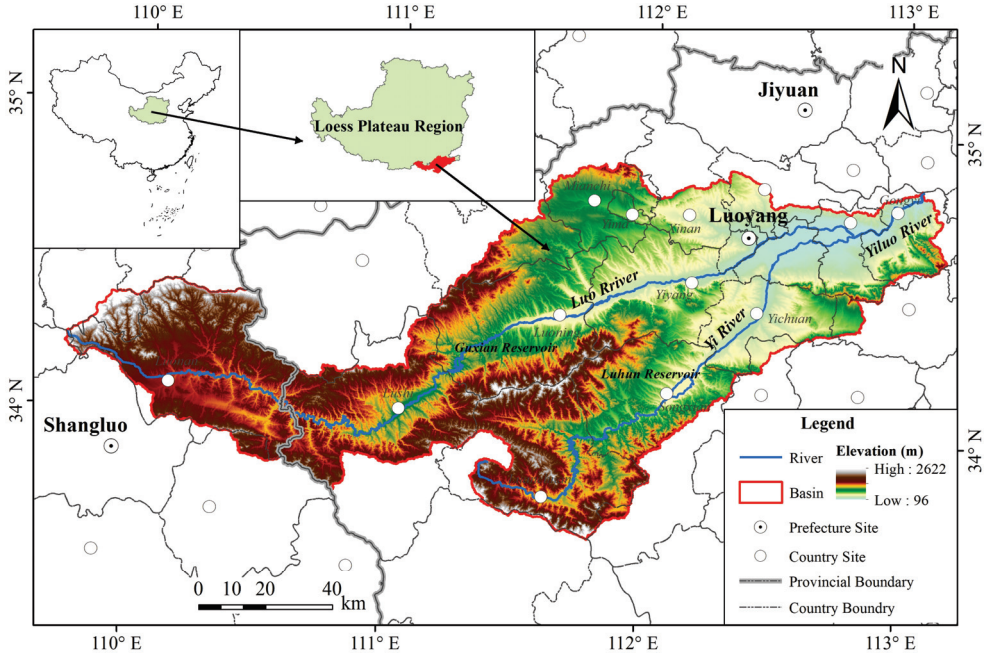

Figure 1. The geographical location, topography, and major cities of the Yiluo River Basin.

2.2. Data

The data utilized in this study comprise meteorological, topographic, land use, soil, and vegetation data, and a future climate model dataset, with detailed information presented in Table 1.

Table 1. The data types, years, sources, and descriptions used in the study.

Types	Years	Sources	Descriptions
Precipitation Temperature	1961–2020	http://data.cma.cn/ (accessed on 1 June 2025)	Daily data
DEM	2000	http://www.gscloud.cn/ (accessed on 1 June 2025)	90 m resolution
Land use	2000, 2010, 2020	http://www.ncdc.ac.cn (accessed on 1 1 June 2025)	30 m resolution
EVI	2001–2020	https://lpdaac.usgs.gov/ (accessed on 1 June 2025)	250 m resolution
Soil depth	2018	http://globalchange.bnu.edu.cn/research/cdtb.jsp (accessed on 1 June 2025)	100 m resolution
Soil type	2009	http://www.geodata.cn/ (accessed on 1 June 2025)	1000 m resolution
Soil erosion	2001–2020	Sediment Bulletin of the Yellow River	-
Future precipitation Future temperature	2021–2050	https://aims2.llnl.gov/search/cmip6/ (accessed on 1 June 2025)	1000 m resolution

2.3. Methods

2.3.1. Soil Erosion Model

Soil erosion was calculated via the Universal Soil Loss Equation (USLE), expressed as

$$A = R \times K \times LS \times C \times P \tag{1}$$

where A denotes the soil loss amount ($t/(hm^2 \cdot a)$); R refers to precipitation erosivity ($MJ \cdot mm/(hm^2 \cdot h \cdot a)$); K indicates soil erodibility ($t \cdot h/(MJ \cdot mm)$); LS represents the topographic; and C and P are the dimensionless vegetation management and conservation practice, respectively, each ranging from 0 to 1. All factors were spatially resampled to a uniform resolution of 500 × 500 m. The computational methods for each factor are detailed below:

(1) Rainfall Erosivity (R)

The R-factor was computed utilizing monthly and yearly precipitation data. It quantifies the erosive potential of rainfall, where higher R values indicate a greater capacity to induce soil erosion. The calculation formula is

$$R = \sum_{i=1}^{12} \left(1.735 \times 10^{1.5 \times lg \frac{P_i^2}{P} - 0.8088} \right) \tag{2}$$

where i represents the month index; P_i indicates monthly precipitation (mm); and P denotes yearly precipitation (mm).

(2) Soil Erodibility (K)

The K-factor was calculated using the Erosion Productivity Impact Calculator (EPIC) model [33]. It quantifies a specific soil type's susceptibility to rainfall erosion, where higher K values indicate greater erodibility. The calculation formula is

$$\begin{aligned} K = &\left[0.2 + 0.3e^{-0.0256 S_a \left(1 - \frac{S_i}{100}\right)} \right] \times \left(\frac{S_i}{C_l + S_i} \right)^{0.3} \times \\ &\left[1 - \frac{0.25C}{C + e^{(3.72 - 2.95C)}} \right] \times \left[1 - \frac{0.7 S_n}{S_n + e^{(-5.51 + 22.9 S_n)}} \right] \end{aligned} \tag{3}$$

$$S_n = 1 - \frac{S_a}{100} \tag{4}$$

where S_a denotes the sand content (0.1–2.0 mm); S_i indicates the silt content (0.002–0.1 mm); C_l represents the clay content (<0.002 mm); and C refers to the organic carbon content (%).

(3) Slope Length and Steepness (LS)

The LS-factor quantifies the integrated effect of topography on soil erosion [34]. The calculation formulas are

$$S = \begin{cases} 10.80 \times sin\theta + 0.03, \ \theta < 5^\circ \\ 16.80 \times sin\theta - 0.50, \ 5^\circ \le \theta < 10^\circ \\ 21.91 \times sin\theta - 0.96, \ \theta \ge 10^\circ \end{cases} \tag{5}$$

$$L = \left(\frac{\lambda}{22.13} \right)^m \tag{6}$$

$$\lambda = l \times cos\theta \tag{7}$$

where θ indicates the slope angle (°); λ represents the horizontal slope length (m); l refers to the flow path length (m); and m is the variable slope exponent: If $\theta < 1^\circ$, $m = 0.2$; if $1^\circ \le \theta < 3^\circ$, $m = 0.3$; if $3^\circ \le \theta < 5^\circ$, $m = 0.4$; and if $\theta \ge 5^\circ$, $m = 0.5$.

(4) Vegetation Management (*C*)

The *C*-factor reflects the protective effect of crops or vegetation on soil, where higher *C* values indicate greater effectiveness in preventing soil erosion [35]. The calculation formulas are

$$f_c = \frac{EVI - EVI_{min}}{EVI_{max} - EVI_{min}} \tag{8}$$

$$C = \begin{cases} 1, & f_c = 0 \\ 0.6508 - 0.3436lg_c, & 0 < f_c < 78.3\% \\ 0, & f_c \geq 78.3\% \end{cases} \tag{9}$$

where f_c is fractional vegetation cover (%); and EVI represents the Enhanced Vegetation Index.

(5) Conservation Practice (*P*)

The P-factor represents the effectiveness of specific engineering measures for soil and water conservation. A lower *p* value signifies the better performance of conservation practices. Drawing on previous studies [36,37], the P-factor was assigned a value of 0.31 for farmland, 0.16 for grassland, and 0.05 for forestland. For water bodies, construction land, and bare land, where conservation measures are generally not implemented, the values are set at 1.

(6) Soil Erosion Intensity Classification

The classification of soil erosion intensity followed China's national standard, Standard for Classification and Grading of Soil Erosion (SL 190-2007), promulgated by the Ministry of Water Resources [38], with detailed information presented in Table 2.

Table 2. Classification of Soil Erosion Intensity.

Level	Slight	Light	Moderate	Strong	Severe	Violent
Soil erosion modulus t/(hm^2·a)	<5	5~25	25~50	50~80	80~150	>150

2.3.2. Future Projection Methodology

Future projections took 2020 as the baseline year, with short-term planning to 2030 and the long-term outlook to 2050. In line with the future climate dataset, land use projections employed the Future Land Use Simulation (FLUS) model. The Enhanced Vegetation Index (EVI) was simulated via bivariate linear regression. All simulations results underwent rigorous calibration and validation, yielding satisfactory outcomes confirming their suitability for subsequent analysis. Future soil erosion was quantified by jointly inputting climate scenarios, projected land use, and vegetation cover data into the USLE model.

(1) Future climate data

Future climate data incorporate four emission scenarios: SSP126 (Sustainable Development), SSP245 (Moderate Development), SSP370 (Regional Development), and SSP585 (Conventional Development). The future climate model data underwent downscaling using bilinear interpolation, with bias correction via the linear scaling method [39]. The calculation formulas are

$$Tem_f = CMIP_f + (CMIP_h - CMA_h) \tag{10}$$

$$Pre_f = \frac{CMA_h}{CMIP_h} \times CMIP_f \tag{11}$$

where Tem_f and Pre_f denote bias-corrected future temperature and precipitation data, respectively; $CMIP_f$ and $CMIP_h$ represent future and historical climate model data from CMIP6, respectively; and CMA_h indicates historical observational climate data from the China Meteorological Administration Data Center.

(2) Future Land Use Simulation

Future land use was projected by the FLUS model [40,41]. Accessible driving factors were selected, including topographic factors (DEM, slope, aspect), socioeconomic factors (population, GDP), and meteorological factors (precipitation, temperature). All data were unified to a spatial resolution of 500 × 500 m. The simulation workflow is illustrated in Figure 2.

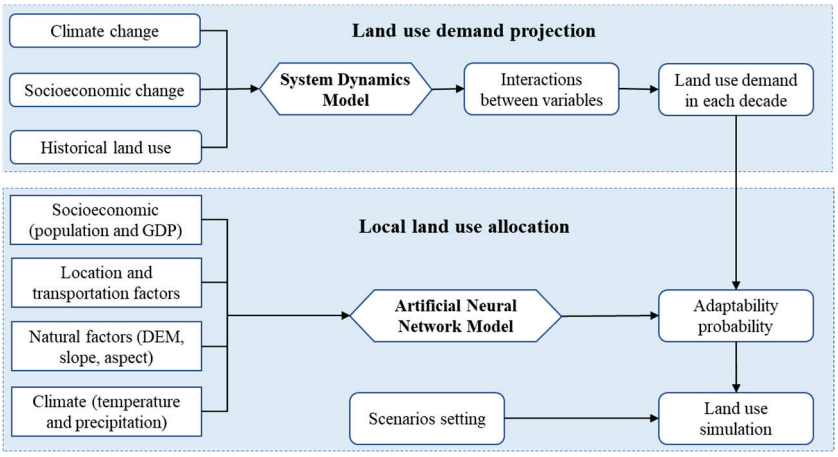

Figure 2. Workflow of the FLUS model.

(3) Future EVI Simulation

The EVI was simulated using a bivariate linear regression model [42], with the EVI as the dependent variable and concurrent precipitation and temperature as independent variables. The calculation formula is

$$EVI_f = a \cdot PRE + b \cdot TEM + c \quad (12)$$

where EVI_f refers to the projected EVI value, PRE and TEM represent the annual mean precipitation and temperature, a and b are the regression coefficients, and c is a constant term.

2.3.3. Geodetector Model

The Geodetector method was applied to identify the key drivers of soil erosion, utilizing its single-factor and interaction detection modules [43,44]. The single-factor detection module quantified the explanatory capacity of a given driver X on the spatial heterogeneity of variable Y. The interaction detector evaluated how paired driving factors jointly influence variable Y, specifically evaluating whether the combined effect of driver 1 and driver 2 will enhance or diminish their explanatory power for Y, or whether they operate independently. A larger q-statistic signifies the greater explanatory capacity of variable X in relation to Y, while a smaller value suggests a weaker influence.

The following driving factors were chosen to analyze their impact on soil erosion: land use type (X1), vegetation coverage (X2), temperature (X3), precipitation concentration (X4), annual precipitation (X5), heavy rainfall days (X6), elevation (X7), slope (X8), and soil depth (X9). The data processing of driving factors is detailed in Table 3.

Table 3. Data Processing of Driving Factors.

Driving Factors	Code Name	Method/Data Source	Descriptions
Land use	X1	See Table 1	Land use categories
Vegetation coverage	X2	Mean value method	Annual mean vegetation coverage
Temperature	X3	Mean value method	Annual mean temperature
Precipitation concentration	X4	Precipitation concentration index (PCI)	Intra-annual precipitation distribution
Annual precipitation	X5	Mean value method	Annual precipitation
Heavy rainfall days	X6	Daily precipitation > 25 mm	Annual heavy rainfall days
Elevation	X7	See Table 1	Topographic elevation
Slope	X8	Derived from DEM	Terrain steepness
Soil depth	X9	See Table 1	Soil layer thickness

3. Results

3.1. Spatiotemporal Dynamics of Soil Erosion Intensity

Based on the USLE, soil erosion in the Yiluo River Basin was modeled from 2000 to 2020. The simulation outcomes were consistent with the soil erosion intensity reported in the Yellow River Sediment Bulletin, indicating that the model performed well in simulating soil erosion and can be used for subsequent calculations. The multiyear average erosion modulus was 37.49 $t/(hm^2 \cdot a)$, classified as moderate erosion intensity. Areas of relatively strong erosion intensity were largely concentrated in the middle and upper reaches, while the lower reaches experienced slight- and light-level erosion (Figure 3a–c). Regarding the various land use categories, cultivated land exhibited the highest soil erosion modulus, reaching 64.77 $t/(hm^2 \cdot a)$, followed by grassland (42.38 $t/(hm^2 \cdot a)$) and forestland (27.57 $t/(hm^2 \cdot a)$) (Figure 3d). Water bodies and construction land showed negligible erosion. Over the past two decades, the soil erosion modulus showed a fluctuating decreasing trend, with a reduction of 28.78%, of which forestland and grassland experienced reductions of 43.8% and 18.8%, respectively (Figure 4). Specifically, the areas with slight- and light-level erosion continuously increased by 3.75% and 13.14%, respectively, while moderate, - strong-, and severe-level erosion zones continuously decreased by 5.75%, 6.20%, and 3.03%, respectively, with violent-level soil erosion showing a fluctuating decrease of 1.91%.

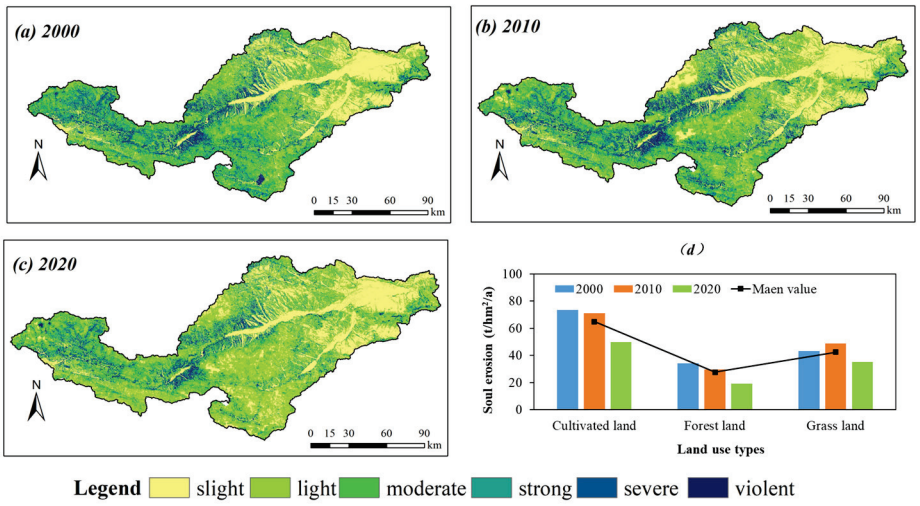

Figure 3. Spatiotemporal Pattern of Soil Erosion Intensity in the Yiluo River Basin from 2000 to 2020. (**d**) Soil Erosion in different land use types from 2000-2020. The terms "slight, light, moderate, strong, severe, violent" in the legend represent soil erosion intensities.

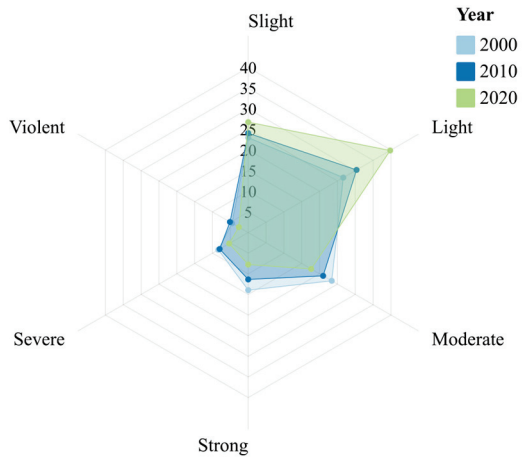

Figure 4. Percentage Composition of Soil Erosion Intensity in the Yiluo River Basin from 2000 to 2020.

Spatially, changes in soil erosion in the Yiluo River Basin exhibited pronounced heterogeneity (Figure 5a–c). From 2000 to 2020, 76.29% of the area showed declining trends, while 23.71% exhibited increasing trends. The regions with increasing soil erosion were largely concentrated in the lower reaches of the basin. Specifically, 51.82% of the area experienced a decreasing trend, and 48.18% showed an increasing trend in the first decade (2000–2010), while the proportion with a decreasing trend accounted for 76.52%, and the area exhibited an upward trend comprising 23.44% in the latter decade (2010–2020). We further quantified the land-use-specific spatial distributions of soil erosion trends (Figure 5d). From 2000 to 2020, declining erosion occurred across 65.74% of cultivated land, 94.66% of forestland, and 68.92% of grassland. Specifically, decreasing trends covered 37.11% of cultivated land, 72.41% of forestland, and 31.39% of grassland in the first decade, while these proportions rose to 73.01% (cultivated land), 79.47% (forestland), and 63.31% (grassland) in the latter decade.

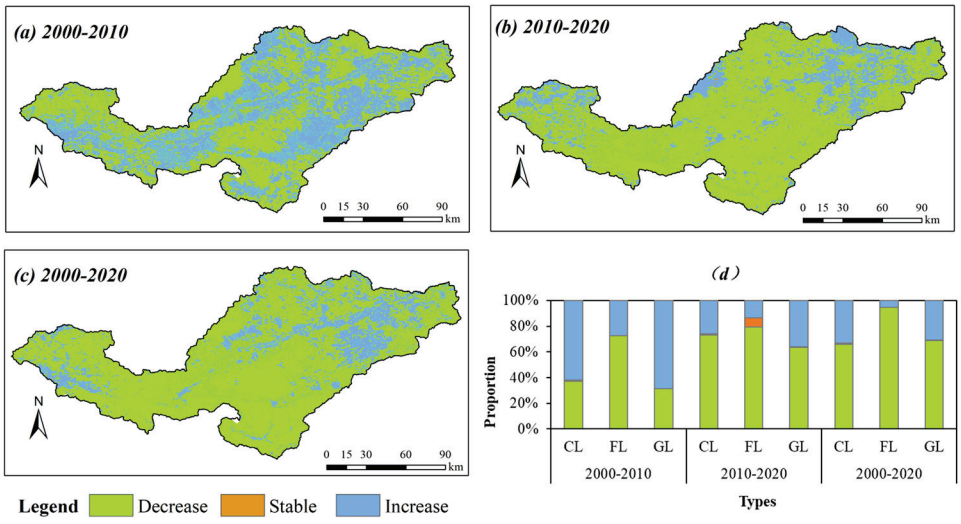

Figure 5. Spatiotemporal Changes in the Soil Erosion Modulus of the Yiluo River Basin from 2000 to 2020. (**d**) Changes of the Soil Erosion for different land use types from 2000 to 2010. The terms "decrease, stable, increase" in the legend represent the change trend of soil erosion intensity.

3.2. Future Projections of Soil Erosion

Based on the bias correction future climate model data and the simulated future land use and vegetation cover data, the USLE model was applied to simulate the spatial patterns of future soil erosion in the Yiluo River Basin for the years 2030 (Figure 6a–d)

and 2050 (Figure 7a–d) under the SSP126, SSP245, SSP370, and SSP585 scenarios. The results indicated that in the short term (2030), the soil erosion modulus was the highest under the SSP370 scenario and the lowest under the SSP126 scenario, ranging from 18.8 to 26.44 t/(hm^2·a) across different SSPs (Figure 8). Compared to the baseline year, the soil erosion modulus decreased by 9.94% to 35.95%. In the long term (2050), the soil erosion modulus was the highest under the SSP585 scenario and the lowest under the SSP370 scenario, ranging from 21.85 to 27.91 t/(hm^2·a) across different SSPs (Figure 8). Compared to the baseline year, the soil erosion modulus decreased by 4.93% to 25.58%. In terms of different SSP scenarios, the soil erosion modulus showed an increasing trend under the SSP126 and SSP585 scenarios, with increases of 20.97% and 21.28% in the long term versus the short term, respectively, while the soil erosion modulus exhibited a decreasing trend under the SSP245 and SSP370 scenarios, with decreases of 1.27% and 17.36% in the long term versus the short term, respectively.

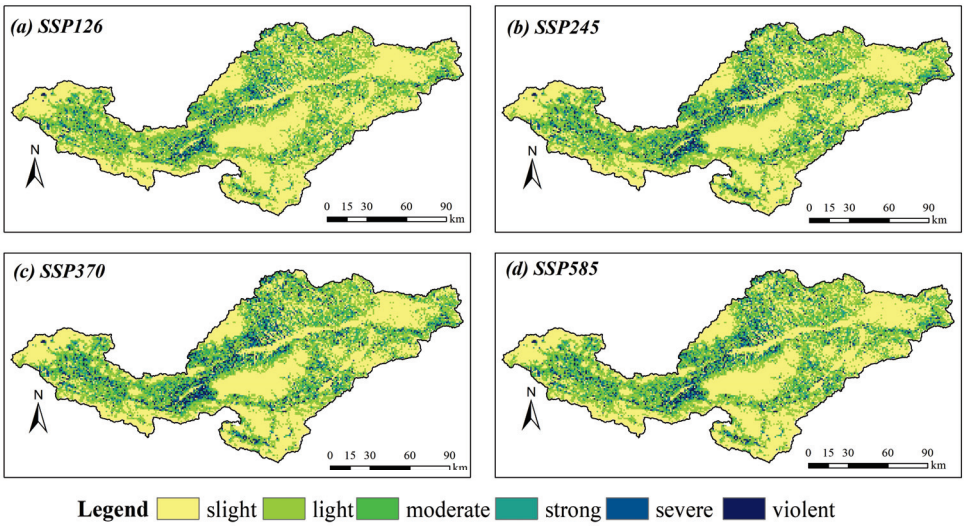

Figure 6. Soil Erosion Intensity Under Different SSP Scenarios in 2030. The terms "slight, light, moderate, strong, severe, violent" in the legend represent soil erosion intensity.

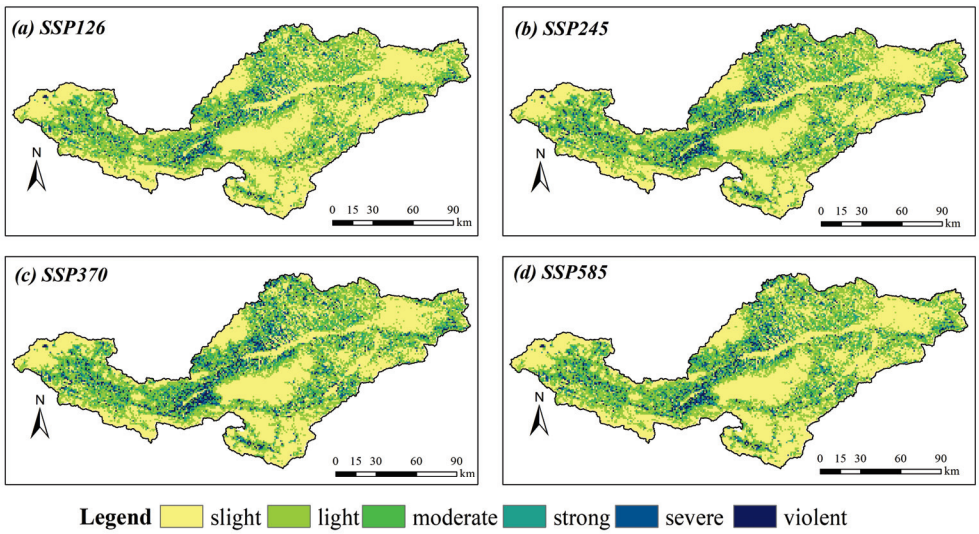

Figure 7. Soil Erosion Intensity Under Different SSP Scenarios in 2050. The terms "slight, light, moderate, strong, severe, violent" in the legend represent soil erosion intensity.

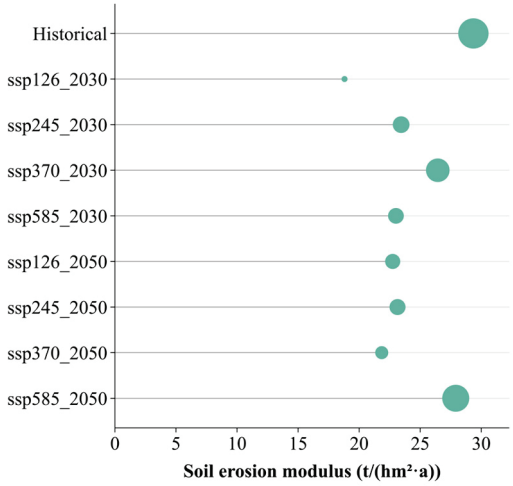

Figure 8. Soil erosion modulus in the Yiluo River Basin from 2020 to 2050.

3.3. Driving Factor Identification of Soil Erosion

Utilizing the Geodetector model, we analyzed the influences of various factors on soil erosion in the Yiluo River Basin. The single-factor detection findings (Figure 9) revealed that the q-values of various driving factors on soil erosion ranged from 0.45 to 5.31% (2020), 0.19 to 5.57% (2030), and 0.15 to 6.13% (2050). Among these factors, the land use type dominated with q-values exceeding 5%, followed by vegetation coverage, soil depth, elevation, temperature, and PCI, with q-values ranging from 1 to 4%, while other factors contributed minimally, with q-values below 1%. Notably, PCI and temperature, as major driving factors, exhibited significant fluctuations across different periods. Specifically, in the short term (2030), the q-values for PCI were minimized under SSP126 and maximized under SSP370, while the q-values of temperature peaked under SSP126 and troughed under SSP370. Compared to the baseline, the q-values for PCI ranged from −59.86% to 15.92%, and for temperature, from 74.76% to 115.67%. In the long term (2050), the q-values for both PCI and temperature were the lowest under the SSP585 scenario and highest under the SSP126 scenario, PCI change relative to the baseline ranged from −61.77% to −1.79%, while temperature changes ranged from −0.05% to 44.2%.

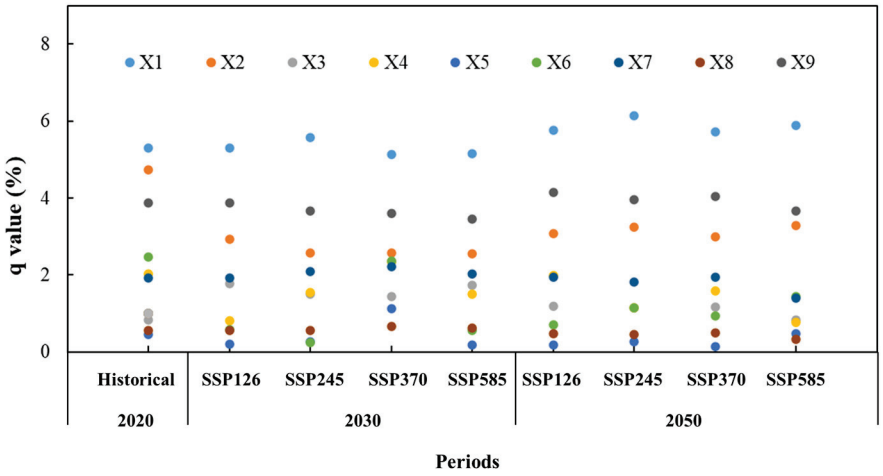

Figure 9. The q-values of each driving factor.

The interaction detection results (Figure 10) indicated that pairwise interactions among the driving factors significantly enhanced their effects on soil erosion, far exceeding the effects of individual factors. Specifically, the interaction between land use type and elevation exerted the strongest effect, followed by the interactions of land use type and PCI, soil

depth, and temperature, all presenting a nonlinear enhancement. The q-values for these interactions in the baseline year were quantified at 26.81%, 24.29%, 23.62%, and 18.06%, respectively (Figure 10a). Compared to the baseline year, the interactions involving land use type with elevation and soil depth showed relatively minor changes in both the short term (2030) and long term (2050). Conversely, the interactions of land use type and PCI and temperature exhibited more noticeable fluctuations. In the short term (2030), the land use type and PCI interaction was smallest under the SSP126 scenario and largest under the SSP245 scenario. The land use type and temperature interaction was largest under the SSP126 scenario and SSP370 scenario (Figure 10b–e). Compared to the baseline year, these interactions changed by −31.43% to 0.72% and 44.32% to 51.07%, respectively. In the long term (2050), the land use type and PCI interaction was smallest under the SSP370 scenario and largest under the SSP245 scenario. The land use type and temperature interaction was largest under the SSP245 scenario and smallest under the SSP585 scenario (Figure 10f–i). Compared to the baseline year, these interactions changed by −23.91% to 9.18% and 46.01% to 59.15%, respectively.

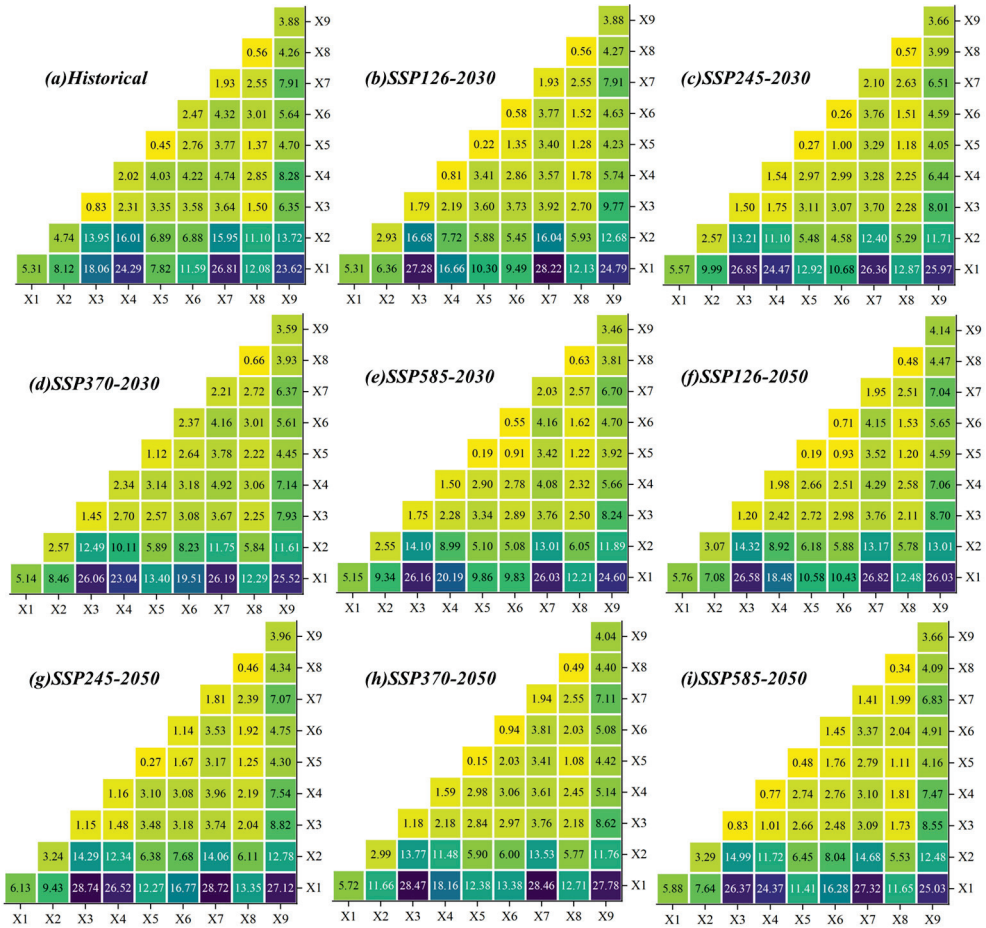

Figure 10. Interactive detection values (%) among different driving factors.

4. Discussion

4.1. Influence of Climatic Factors on Soil Erosion

Studies have shown that precipitation and temperature were the primary driving forces behind the dynamic changes in soil erosion in the Yiluo River Basin, consistent with existing studies [45–47]. Climate factors profoundly govern erosion dynamics through their direct provision of erosive energy (precipitation) and indirect modification of the erosion environment (temperature). Statistical analyses have revealed that the multiyear

average precipitation was 680.88 mm (Figure 11a). The precipitation within the basin exhibited a trend of "slight decrease in total amount but increased extremity", with an increasing frequency of short-duration, high-intensity rainstorm events. Such rainfall events possess a far greater capacity to detach and transport surface soil compared to general precipitation, easily triggering severe gully and slope erosion [48,49]. Compared to the baseline period, the annual average precipitation increased by 9.11% to 11.62%. Altered rainfall patterns under climate change may further amplify soil erosion risks. Additionally, the annual average temperature under different SSP scenarios increased by 4.36% to 7.74% compared to the baseline (Figure 11b). Although temperature is not directly incorporated in USLE calculations, it indirectly modulates erosion by influencing vegetation phenology and growth (affecting the C-factor). The impact of temperature presents dual effects: extended growing seasons and enhanced vegetation NPP may mitigate rainfall erosivity through improved ground cover, partially offsetting the negative impacts of extreme rainfall. Conversely, in semi-arid regions, the warming–drying trend exacerbates soil moisture deficits, suppresses vegetation recovery, and may even cause degradation, ultimately weakening surface erosion resistance [50,51]. Notably, climate factors exhibited strong spatial heterogeneity in erosion impacts, primarily resulting from the synergistic amplification between inherent climatic spatial variability and complex interactions with topographic features and land use/cover patterns.

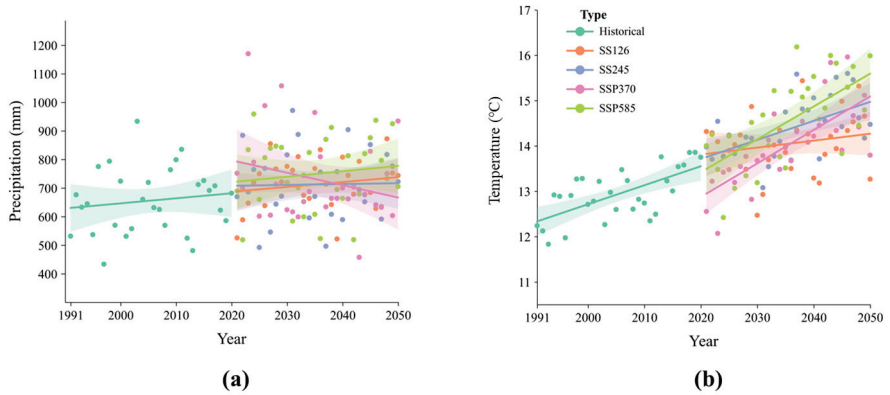

Figure 11. Interannual variations in precipitation (**a**) and temperature (**b**) of the Yiluo River Basin from 1991 to 2050. The shaded area is the 95% confidence interval.

4.2. Impacts of Land Use Factors on Soil Erosion

Land use and vegetation cover changes profoundly reshape surface coverage (affecting the C-factor) and conservation practices (influencing the P-factor), constituting the primary anthropogenic pathway for erosion regulation [51]. Our research identified that land use type exhibited the strongest explanatory power for soil erosion in the Yiluo River Basin, with q-values greater than 5% across the baseline year, the short term (2030), and the long term (2050). Furthermore, the interaction between land use and other factors enhanced its influence on soil erosion [52]. Land use change analyses indicated a 1.28% expansion in forested areas over the past two decades (Figure 12). This increase was attributable to post-2000 ecological restoration initiatives, particularly the Grain-for-Green Program and protected area conservation measures. Coupled with the heightened public awareness of forest protection and reduced deforestation [53,54], forested areas have increased by 1.28%. Increased forest and grassland coverage has reduced soil erosion by 43.8% and 18.8%, respectively. Future multiscenario simulations further confirmed the consistent patterns. Cultivated land area is projected to decrease by 3.39% to 8.92% versus the baseline, while forestland is expected to increase by 0.69% to 1.48%. Consequently, soil erosion is projected to decrease by 9.94% to 35.95% (2030) and by 4.93% to 25.58% (2050) versus the

current year. Notably, the spatial heterogeneity in vegetation coverage (C-factor) directly governs erosion risk patterns [55,56]. Upper basin regions exhibited favorable natural conditions with stable forest cover (low C-values) and minimal erosion. Reforested areas predominantly cluster in the central-northern loess hilly region, spatially coinciding with significant erosion reduction zones. Critically, built-up land has expanded by 85.53% over 20 years and is projected to increase by 16.7–43.42% in future scenarios. Urbanization encroaches on prime cropland and forests, while surface impermeabilization concentrates runoff, potentially exacerbating downstream erosion risks [57,58].

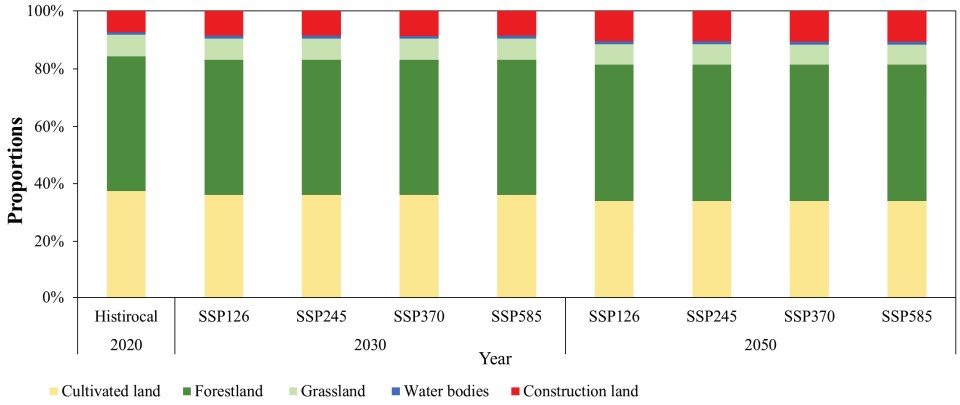

Figure 12. Land use changes in the Yiluo River Basin from 2020 to 2050.

4.3. Impacts of Topography and Soil Depth Factors on Soil Erosion

Topography (LS-factor) and soil properties (K-factor) constitute the fundamental environmental background for erosion dynamics. Topography fundamentally controls the spatial pattern of erosion dynamics and the intensity of erosion processes by influencing precipitation redistribution, runoff convergence pathways, flow scouring capacity, and gravitational potential energy [52,59]. Simultaneously, topography exerts a magnifying effect on precipitation erosion [9,22]. In the upper reaches of the watershed, steep terrain significantly accelerated surface runoff convergence, enhanced its scouring capacity, and increased erosion risk. In the downstream plains, despite minimal changes in precipitation, flat topography (extremely low LS-factor values) and intensive agricultural management substantially reduced the actual erosive power of precipitation. The widespread loess-derived cinnamon soils in the watershed, characterized by loose structure, low clay content, and high silt–sand ratio, are highly susceptible to dispersion and transport by runoff [26,60]. Particularly in the Loess Plateau regions of the middle Luo River, the deep loess layers (reaching tens or even hundreds of meters) provide an exceptionally abundant material source for erosion. Moreover, land use in this area is predominantly cropland, where tillage loosens the soil, further exacerbating topsoil loss, especially on sloping farmland.

4.4. Limitations and Uncertainties

Our study implemented the USLE model to calculate soil erosion. Daily precipitation data were used to determine the rainfall erosivity factor (R), the EPIC method to compute the soil erodibility factor (K), the EVI to estimate the cover management factor (C), high-resolution DEM to generate the slope length and steepness factor (LS), and high-precision land use data to indirectly estimate the support practice factor (P). Nevertheless, non-negligible uncertainties persist, primarily stemming from model structure, parameter acquisition, and data limitations. A key limitation regarding model validation, the lack of monitoring data generally necessitates comparisons with regional empirical data or known studies and cross-validation between different model simulations. For projecting future erosion responses under climate scenarios, we used the FLUS model to predict future land

use based on future climate model data and a multiple linear regression model to simulate future EVIs. These projections are highly dependent on the reliability of the selected climate models and the accuracy of downscaling methods, resulting in considerable uncertainty. In future research, field observation experiments should be integrated to strengthen in situ measurements of key parameters (K, C, P) and improve model parameterization and simulation validation.

5. Conclusions

Based on the USLE model, our study systematically revealed the spatiotemporal evolution of soil erosion in the Yiluo River Basin from 2000 to 2020. By coupling the USLE model with future land use and vegetation cover simulation models, we projected future erosion risks under multiple scenarios from 2030 to 2050. Additionally, the Geodetector model was employed to quantitatively identify the key driving factors of soil erosion under different future scenarios. Our work addressed the research gaps regarding how the key driving factors and mechanisms of soil erosion in the Loess Plateau region would evolve under future climate scenarios. The key conclusions are as follows:

(1) Soil erosion showed a decreasing trend from 2000 to 2020 in the study area. The multiyear average erosion modulus was 37.49 $t/(hm^2 \cdot a)$ (moderate intensity). Total erosion decreased by 28.78% over 20 years, with 76.29% of the area showing reduced intensity, primarily attributed to the Grain-for-Green Program and protected area conservation.

(2) Future soil erosion showed a decreasing trend but scenario-dependent heterogeneity. It will decrease by 9.94–35.95% (2030) and 4.93–25.58% (2050) versus the baseline. Erosion will increase under SSP126 and SSP585 but decrease under SSP245 and SSP370, highlighting the heterogeneity of soil erosion under different development pathways.

(3) Factor interactions amplify their impacts on soil erosion. Land use type dominated as the core driver ($q > 5\%$). Under different future climate scenarios, interactions between land use and PCI/temperature exhibited heightened sensitivity and significant fluctuations, emphasizing the critical regulatory role of future climate change on soil erosion.

(4) Limitations and prospects. While this study coupled the USLE model with future land use and vegetation cover simulation models to effectively reveal the evolution characteristics and key driving factors of soil erosion under different scenarios, uncertainties in parameters and future data remain. Future research will integrate field observations to strengthen the in situ measurements of key parameters (K, C, P), optimize parameterization, and enhance the reliability of model simulation validation.

Author Contributions: Conceptualization, J.H. and J.W.; writing—original draft preparation, J.H.; writing—review and editing, J.H. and X.C.; supervision, Y.H. and G.D.; funding acquisition, J.H. and X.C. All authors have read and agreed to the published version of the manuscript.

Funding: This research was supported by the Open Research Fund of Henan Key Laboratory of Ecological Environment Protection and Restoration of Yellow River Basin (LYBEPR202401), the National Science Fund for Young Scholars (52409002), the Anhui Provincial Natural Science Foundation (2208085US16), and the Key Project of Natural Science Research of Anhui Provincial Education Department (2024AH051101).

Data Availability Statement: Any additional information required to reanalyze the data reported in this paper is available from J.H.

Conflicts of Interest: The authors declare no competing interests.

Abbreviations

The following abbreviations are used in this manuscript:

SSPs	Shared Socioeconomic Pathways
USLE	Universal Soil Loss Equation
EVI	Enhanced Vegetation Index
PCI	Precipitation Concentration index
FLUS	Future Land Use Simulation

References

1. Li, P.; Chen, J.; Zhao, G.; Holden, J.; Liu, B.; Chan, F.; Hu, J.; Wu, P.; Mu, X. Determining the drivers and rates of soil erosion on the Loess Plateau since 1901. *Sci. Total Environ.* **2022**, *823*, 153674. [CrossRef]
2. Tian, P.; Tian, X.; Geng, R.; Zhao, G.; Yang, L.; Mu, X.; Gao, P.; Sun, W.; Liu, Y. Response of soil erosion to vegetation restoration and terracing on the Loess Plateau. *Catena* **2023**, *227*, 107103. [CrossRef]
3. Liu, X.; Wang, P.; Dang, S. Variations in water and sediment of the Yellow River: Historical perspectives, current status, and future outlook. *J. Hydraul. Eng.* **2024**, *55*, 1135–1145. [CrossRef]
4. Zhang, W.; Liu, J.; Liu, S.; Yang, S.; Huang, E.; Ren, S.; Gong, L. Multi-effect synergistic induction of unsaturated MnO(x) on sandy sediment for enhanced manganese adsorption and byproduct resource recovery in solar evaporation. *J. Hazard. Mater.* **2025**, *487*, 137165. [CrossRef] [PubMed]
5. Hou, J.; Qin, T.; Yan, D.; Feng, J.; Liu, S.; Zhang, X.; Li, C. Evaluation of water-land resources regulation potential in the Yiluo River Basin, China. *Ecol. Indic.* **2023**, *153*, 110410. [CrossRef]
6. Xu, S.; Qin, T.; Lu, J.; Liu, S.; Hou, J.; Feng, J.; Li, W.; Liu, H.; Abebe, S. Identification of driving mechanisms of actual evapotranspiration in the Yiluo River Basin based on structural equation modeling. *Ecol. Process.* **2024**, *13*, 69. [CrossRef]
7. Zheng, F.L. Effect of vegetation changes on soil erosion on the Loess Plateau. *Pedosphere* **2006**, *16*, 420–427. [CrossRef]
8. Bai, R.; Wang, X.; Li, J.; Yang, F.; Shangguan, Z.; Deng, L. The impact of vegetation reconstruction on soil erosion in the Loess plateau. *J. Environ. Manag.* **2024**, *363*, 121382. [CrossRef]
9. Guo, X.; Shao, Q. Spatial pattern of soil erosion drivers and the contribution rate of human activities on the Loess Plateau from 2000 to 2015: A boundary line from northeast to southwest. *Remote Sens.* **2019**, *11*, 2429. [CrossRef]
10. Li, Z.; Fang, H. Impacts of climate change on water erosion: A review. *Earth-Sci. Rev.* **2016**, *163*, 94–117. [CrossRef]
11. Chen, Y.; Fu, B.; Zhao, Y.; Wang, K.; Zhao, M.; Ma, J.; Wu, J.; Xu, C.; Liu, W.; Wang, H. Sustainable development in the Yellow River Basin: Issues and strategies. *J. Clean. Prod.* **2020**, *263*, 121223. [CrossRef]
12. Gao, G.; Liang, Y.; Liu, J.; Dunkerley, D.; Fu, B. A modified RUSLE model to simulate soil erosion under different ecological restoration types in the loess hilly area. *Int. Soil Water Conserv. Res.* **2024**, *12*, 258–266. [CrossRef]
13. Senanayake, S.; Pradhan, B.; Alamri, A.; Park, H. A new application of deep neural network (LSTM) and RUSLE models in soil erosion prediction. *Sci. Total Environ.* **2022**, *845*, 157220. [CrossRef]
14. Alewell, C.; Borrelli, P.; Meusburger, K.; Panagos, P. Using the USLE: Chances, challenges and limitations of soil erosion modelling. *Int. Soil Water Conserv. Res.* **2019**, *7*, 203–225. [CrossRef]
15. Yu, Y.; Zhao, W.; Martinez-Murillo, J.F.; Pereira, P. Loess Plateau: From degradation to restoration. *Sci. Total Environ.* **2020**, *738*, 140206. [CrossRef] [PubMed]
16. Li, E.; Mu, X.; Zhao, G.; Sun, W. Effects of check dams on runoff and sediment load in a semi-arid river basin of the Yellow River. *Stoch. Environ. Res. Risk Assess.* **2017**, *31*, 1791–1803. [CrossRef]
17. Wang, J.; Zhao, W.; Wang, G.; Yang, S.; Pereira, P. Effects of long-term afforestation and natural grassland recovery on soil properties and quality in Loess Plateau (China). *Sci. Total Environ.* **2021**, *770*, 144833. [CrossRef] [PubMed]
18. Li, Z.; Zhang, Y.; Zhu, Q.; Yang, S.; Li, H.; Ma, H. A gully erosion assessment model for the Chinese Loess Plateau based on changes in gully length and area. *Catena* **2017**, *148*, 195–203. [CrossRef]
19. Ran, Q.; Chen, X.; Hong, Y.; Ye, S.; Gao, J. Impacts of terracing on hydrological processes: A case study from the Loess Plateau of China. *J. Hydrol.* **2020**, *588*, 125045. [CrossRef]
20. Haidong, G.; Mengdie, W.; Xinjing, H. Check dams in the Yellow River basin: Sediment reduction efficiency and future development. *Land. Degrad. Dev.* **2024**, *35*, 4042–4054. [CrossRef]
21. Yang, R.; Yang, S.; Chen, L.; Yang, Z.; Xu, L.; Zhang, X.; Liu, G.; Zhang, X.; Jiao, C.; Bai, R.; et al. Effect of vegetation restoration on soil erosion control and soil carbon and nitrogen dynamics: A meta-analysis. *Soil Tillage Res.* **2023**, *230*, 105705. [CrossRef]
22. Gao, J.; Shi, C.; Yang, J.; Yue, H.; Liu, Y.; Chen, B. Analysis of spatiotemporal heterogeneity and influencing factors of soil erosion in a typical erosion zone of the southern red soil region, China. *Ecol. Indic.* **2023**, *154*, 110590. [CrossRef]

23. Cao, Y.; Hua, L.; Tang, Q.; Lin Liu, L.; Cai, C. Evaluation of monthly-scale soil erosion spatio-temporal dynamics and identification of their driving factors in Northeast China. *Ecol. Indic.* **2023**, *150*, 110187. [CrossRef]
24. Sahour, H.; Gholami, V.; Vazifedan, M.; Saeedi, S. Machine learning applications for water-induced soil erosion modeling and mapping. *Soil Tillage Res.* **2021**, *211*, 105032. [CrossRef]
25. Wang, K.; Zhou, J.; Tan, M.L.; Lu, P.; Xue, Z.; Liu, M.; Wang, X. Impacts of vegetation restoration on soil erosion in the Yellow River Basin, China. *Catena* **2024**, *234*, 107547. [CrossRef]
26. Liu, Y.F.; Liu, Y.; Shi, Z.H.; López-Vicente, M.; Wu, G. Effectiveness of re-vegetated forest and grassland on soil erosion control in the semi-arid Loess Plateau. *Catena* **2020**, *195*, 104787. [CrossRef]
27. Panagos, P.; Borrelli, P.; Matthews, F.; Leonidas Liakos, L.; Bezak, N.; Diodato, N.; Ballabio, C. Global rainfall erosivity projections for 2050 and 2070. *J. Hydrol.* **2022**, *610*, 127865. [CrossRef]
28. Zhang, H.; Meng, C.; Wang, Y.; Wang, Y.; Li, M. Comprehensive evaluation of the effects of climate change and land use and land cover change variables on runoff and sediment discharge. *Sci. Total Environ.* **2020**, *702*, 134401. [CrossRef]
29. Kumar, N.; Singh, S.K.; Dubey, A.K.; Ray, R.L.; Mustak, S.; Rawat, K.S. Prediction of soil erosion risk using earth observation data under recent emission scenarios of CMIP6. *Geocarto Int.* **2022**, *37*, 7041–7064. [CrossRef]
30. Wang, H.; Wu, L.; Yue, Y.; Jin, Y.; Zhang, B. Impacts of climate and land use change on terrestrial carbon storage: A multi-scenario case study in the Yellow River Basin (1992–2050). *Sci. Total Environ.* **2024**, *930*, 172557. [CrossRef]
31. Wang, S.; Fu, B.; Piao, S.; Lü, Y.; Ciais, P.; Feng, X.; Wang, Y. Reduced sediment transport in the Yellow River due to anthropogenic changes. *Nat. Geosci.* **2016**, *9*, 38–41. [CrossRef]
32. Eekhout, J.P.C.; de Vente, J. Global impact of climate change on soil erosion and potential for adaptation through soil conservation. *Earth-Sci. Rev.* **2022**, *226*, 103921. [CrossRef]
33. Xu, J.; Chen, J.; Liu, Y.; Fan, F. Identification of the geographical factors influencing the relationships between ecosystem services in the Belt and Road region from 2010 to 2030. *J. Clean. Prod.* **2020**, *275*, 124153. [CrossRef]
34. Fu, S.; Liu, B.; Zhou, G.; Sun, Z.; Zhu, X. Calculation tool of topographic factors. *Sci. Soil Water Conserv.* **2015**, *13*, 105–110. [CrossRef]
35. Cai, C.; Ding, A.; Shi, Z.; Huang, L.; Zhang, G. Study of Applying USLE and Geographical Information System IDRISI to Predict Soil Erosion in Small Watershed. *J. Soil Water Conserv.* **2000**, *14*, 19–24. [CrossRef]
36. Yan, R.; Zhang, X.; Li, G.; Chen, H. Soil Erosion and Sediment Yield Assessment Based on RUSLE in Beiluo River on the Loess Plateau, China. *J. Soil Water Conserv.* **2017**, *31*, 32–37. [CrossRef]
37. Wu, C.; Wang, S. Sensitivity evaluation of soil erosion in Lanzhou section of the Yellow River Basin. *Sci. Technol. Eng.* **2021**, *21*, 12390–12397.
38. *SL 190-2007*; Standard for Classification and Grading of Soil Erosion. Ministry of Water Resources of the People's Republic of China: Beijing, China, 2008.
39. Zhang, Q.; Zhu, B.; Yang, J.H.; Ma, P.; Liu, X.; Lu, G.; Wang, Y.; Yu, H.; Liu, W.; Wang, D. New characteristics about the climate humidification trend in Northwest China. *Chin. Sci. Bull.* **2021**, *66*, 3757–3771. [CrossRef]
40. Liu, X.; Liang, X.; Li, X.; Xu, X.; Ou, J.; Chen, Y.; Li, S.; Wang, S.; Pei, F. A future land use simulation model (FLUS) for simulating multiple land use scenarios by coupling human and natural effects. *Landsc. Urban. Plan.* **2017**, *168*, 94–116. [CrossRef]
41. Liang, X.; Liu, X.; Li, X.; Chen, Y.; Tian, H.; Yao, Y. Delineating multi-scenario urban growth boundaries with a CA-based FLUS model and morphological method. *Landsc. Urban. Plan.* **2018**, *177*, 47–63. [CrossRef]
42. Zhou, Z.; Ding, Y.; Shi, H.; Cai, H.; Fu, Q.; Liu, S.; Li, T. Analysis and prediction of vegetation dynamic changes in China: Past, present and future. *Ecol. Indic.* **2020**, *117*, 106642. [CrossRef]
43. Wang, J.; Xu, C. Geodetector: Principle and prospective. *Acta Geogr. Sin.* **2017**, *72*, 116–134. [CrossRef]
44. Hou, J.; Yan, D.; Qin, T.; Liu, S.; Yan, S.; Li, J.; Abebe, S.; Cao, X. Evolution and attribution of water yield coefficient in the Yiluo river basin. *Front. Environ. Sci.* **2022**, *10*, 1067318. [CrossRef]
45. Liu, S.; Huang, S.; Xie, Y.; Leng, G.; Huang, Q.; Wang, L.; Xue, Q. Spatial-temporal changes of rainfall erosivity in the loess plateau, China: Changing patterns, causes and implications. *Catena* **2018**, *166*, 279–289. [CrossRef]
46. Fowler, H.J.; Lenderink, G.; Prein, A.F.; Westr, S.; Allan, R.P.; Ban, N.; Barbero, R.; Berg, P.; Blenkinsop, S.; Hong, X.D.; et al. Anthropogenic intensification of short-duration rainfall extremes. *Nat. Rev. Earth Environ.* **2021**, *2*, 107–122. [CrossRef]
47. Ayat, H.; Evans, J.P.; Sherwood, S.C.; Soderholm, J. Intensification of subhourly heavy rainfall. *Science* **2022**, *378*, 655–659. [CrossRef] [PubMed]
48. Zhao, L.; Fang, Q.; Hou, R.; Wu, F. Effect of rainfall intensity and duration on soil erosion on slopes with different microrelief patterns. *Geoderma* **2021**, *396*, 115085. [CrossRef]
49. Chen, Y.; Wei, T.; Li, J.; Xin, Y.; Ding, M. Future changes in global rainfall erosivity: Insights from the precipitation changes. *J. Hydrol.* **2024**, *638*, 131435. [CrossRef]
50. Guo, W.; Liu, M.; Zhang, Q.; Deng, Y.; Chu, Z.; Qin, H.; Li, Y.; Liu, Y.; Zhang, H.; Zhang, W.; et al. Warming-Induced Vegetation Greening May Aggravate Soil Mercury Levels Worldwide. *Environ. Sci. Technol.* **2024**, *58*, 15078–15089. [CrossRef]

51. Jin, X.Y.; Jin, H.J.; Iwahana, G.; Marchenko, S.S.; Luo, D.; Li, X.; Liang, S. Impacts of climate-induced permafrost degradation on vegetation: A review. *Adv. Clim. Change Res.* **2021**, *12*, 29–47. [CrossRef]
52. Zhao, J.; Wang, Z.; Dong, Y.; Yang, Z.; Govers, G. How soil erosion and runoff are related to land use, topography and annual precipitation: Insights from a meta-analysis of erosion plots in China. *Sci. Total Environ.* **2022**, *802*, 149665. [CrossRef] [PubMed]
53. Shi, P.; Li, P.; Li, Z.; Sun, J.; Wang, D.; Min, Z. Effects of grass vegetation coverage and position on runoff and sediment yields on the slope of Loess Plateau, China. *Agric. Water Manag.* **2022**, *259*, 107231. [CrossRef]
54. Hou, J.; Qin, T.; Liu, S.; Wang, J.; Dong, B.; Yan, S.; Nie, H. Analysis and Prediction of Ecosystem Service Values Based on Land Use/Cover Change in the Yiluo River Basin. *Sustainability* **2021**, *13*, 6432. [CrossRef]
55. Chen, J.; Xiao, H.; Li, Z.; Liu, J.; Wang, D.; Wang, L.; Tang, C. Threshold effects of vegetation coverage on soil erosion control in small watersheds of the red soil hilly region in China. *Ecol. Eng.* **2019**, *132*, 109–114. [CrossRef]
56. Zhang, X.; Song, J.; Wang, Y.; Sun, H.; Li, Q. Threshold effects of vegetation coverage on runoff and soil loss in the Loess Plateau of China: A meta-analysis. *Geoderma* **2022**, *412*, 115720. [CrossRef]
57. Whitney, J.W.; Glancy, P.A.; Buckingham, S.E.; Ehrenber, A.C. Effects of rapid urbanization on streamflow, erosion, and sedimentation in a desert stream in the American Southwest. *Anthropocene* **2015**, *10*, 29–42. [CrossRef]
58. Russell, K.L.; Vietz, G.J.; Fletcher, T.D. Global sediment yields from urban and urbanizing watersheds. *Earth-Sci. Rev.* **2017**, *168*, 73–80. [CrossRef]
59. Heckmann, T.; Cavalli, M.; Cerdan, O.; Foerster, S.; Javaux, M.; Lode, E.; Smetanov, A.; Vericat, D.; Brardinoni, F. Indices of sediment connectivity: Opportunities, challenges and limitations. *Earth-Sci. Rev.* **2018**, *187*, 77–108. [CrossRef]
60. Dong, L.; Li, J.; Zhang, Y.; Bing, M.; Liu, Y.; Wu, J.; Hai, X.; Li, A.; Wang, K.; Wu, P.; et al. Effects of vegetation restoration types on soil nutrients and soil erodibility regulated by slope positions on the Loess Plateau. *J. Environ. Manag.* **2022**, *302*, 113985. [CrossRef]

water

MDPI

Article

Coordination Analysis and Driving Factors of "Water-Land-Energy-Carbon" Coupling in Nine Provinces of the Yellow River Basin

Daiwei Zhang [1,2,3,4,*], Ming Jing [1,2,3,4], Buhui Chang [1,2,3,4], Weiwei Chen [1,2,3,4], Ziming Li [1,2,3,4], Shuai Zhang [1,2,3,4] and Ting Li [1,2,3,4]

[1] Yellow River Institute of Hydraulic Research, YRCC, Zhengzhou 450003, China; jingming1023@163.com (M.J.); changbuhui@163.com (B.C.); chenwei0217@126.com (W.C.); lzm7512523@163.com (Z.L.); zhangqshuai@163.com (S.Z.); desertskies@126.com (T.L.)
[2] Yellow River Laboratory, Zhengzhou 450003, China
[3] Henan Engineering Research Center of Rural Water Environment Improvement, Zhengzhou 450003, China
[4] Henan Key Laboratory of YB Ecological Protection and Restoration, Zhengzhou 450003, China
* Correspondence: zhangdaiwei1994@163.com

Abstract: As an important ecological barrier and economic belt in China, the sustainable development of the Yellow River Basin (YRB) is of great significance to national ecological security and regional economic balance. Based on the coupled and coordinated development analysis of the water–soil–energy–carbon (W-L-E-C) system in the provinces of the Yellow River Basin from 2002 to 2022, this study systematically analyzed the interaction relationship among the various factors through WLECNI index assessment, factor identification, and driving factor exploration. Thus, it fully reveals the spatiotemporal evolution law of regional coordinated development and its internal driving mechanism. It is found that the coordinated development of the W-L-E-C system in different provinces of the Yellow River Basin presents significant spatiotemporal differentiation, and its evolution process is influenced by multiple factors. It is found that the coordination of the YRB presents a significant spatial difference, and Inner Mongolia and Shaanxi, as high coordination areas, have achieved significant improvement in coordination, through ecological restoration and clean energy replacement, arable land intensification, and industrial water-saving technology, respectively. Shandong, Henan, and Shanxi in the middle coordination zone have made some achievements in industrial greening and water-saving technology promotion, but they are still restricted by industrial carbon emissions and land resource pressure. The Ningxia and Gansu regions with low coordination are slow to improve their coordination due to water resource overload and inefficient energy utilization. Barrier factor analysis shows that the water resources utilization rate (W4), impervious area (L4), energy consumption per unit GDP (E1), and carbon emissions from energy consumption (C3) are the core factors restricting coordination. Among them, the water quality compliance rate (W5) of Shanxi and Henan is very low, and the impervious area (L4) of Shandong is a prominent problem. The interaction analysis of the driving factors showed that there were significant interactions between water resource use and ecological protection (W-E), land resource and energy use (L-E), and carbon emissions and ecosystem (C-E). Inner Mongolia, Shaanxi, and Shandong achieved coordinated improvement through "scenic energy + ecological restoration", cultivated land protection, and industrial greening. Shanxi, Henan, and Ningxia are constrained by the "W-L-E-C" complex obstacles. In the future, the Yellow River Basin should implement the following zoning control strategy: for the areas with high coordination, it should focus on consolidating the synergistic advantages of ecological protection and energy development; water-saving technology and energy consumption reduction measures should be promoted in the middle coordination area.

In the low coordination area, efforts should be made to solve the problem of resource overload, and the current situation of low resource utilization efficiency should be improved by improving the utilization rate of recycled water and applying photovoltaic sand control technology. This differentiated governance plan will effectively enhance the level of coordinated development across the basin. The research results provide a decision-making framework of "zoning regulation, system optimization and dynamic monitoring" for the sustainable development of the YRB, and provide a scientific basis for achieving high-quality development of the basin.

Keywords: Yellow River Basin; W-L-E-C; coupling coordination; factor analyze; interactive analysis

1. Introduction

In the context of globalization, the health and sustainable development of watershed ecosystems has become a hot topic of global concern [1,2]. As the second largest river in China, the YRB, with its unique geographical location, rich natural resources, and profound cultural heritage, has become an important support for national ecological security, water resources management, agricultural production, and regional economic development. However, with climate change, the intensification of human activities, and the increasing pressure on resources and environment, the YRB is facing unprecedented challenges, especially given the complex relationship between the water–soy–energy–carbon system, which needs to be analyzed further [3].

The "W-L-E-C" system is an interdependent and complex system, in which the distribution and utilization of water resources, the maintenance and improvement of soil quality, the balance and regulation of the carbon cycle, and the stability and restoration of the ecosystem constitute the cornerstone of the sustainable development of the basin [4–6]. The coupling coordination between water, soil, energy, and carbon directly affects the ecological security, water resource security, food security, and economic security of the YRB. Therefore, it is of great significance to carry out the coordination analysis of "W-L-E-C" coupling and the research on driving factors in the nine provinces of the YRB to reveal the internal mechanism of the basin ecosystem, optimize resource allocation, and formulate scientific and reasonable basin management policies.

In recent years, scholars at home and abroad have carried out extensive research on the "W-L-E-C" coupling system, and have achieved a series of important results. However, most of the existing studies focus on the interaction between a single element or two elements, and there is a lack of systematic analysis of the multi-element coupling relationship of "W-L-E-C". In addition, the research on the coordination level of "W-L-E-C" coupling and its driving factors in the nine provinces of the YRB is still insufficient. The use of Wu et al.'s (2024) [7] simulation framework based on SPCR is proposed. A non-dominated sorting genetic algorithm (NSGA-II) and entropy weight-based approximate ideal sorting method (TOPSIS) were used to optimize the land use structure with the aim of minimizing net carbon, nitrogen, and phosphorus emissions. Li et al. (2023) [8] proposed the conceptual model DSWUNWUSWSNWSA ("Driving force—water for social development—water for natural development—social water resources situation—natural water resources situation—improvement") and established the water cycle health evaluation system of the Central Plain urban agglomeration.

This study takes nine provinces in the YRB as the research object, constructs the evaluation index system of "W-L-E-C" coupling coordination, and uses the coupling coordination

degree model and spatial autocorrelation analysis to analyze the spatiotemporal evolution characteristics of the "W-L-E-C" coupling coordination level in nine provinces in the YRB, as well as to explore its driving factors. The novelty of this study is reflected in the construction of the W-L-E-C multi-system coupling analysis framework for the first time, breaking through the limitations of traditional single-factor research, and revealing more complex rules of the sustainable development of watershed by integrating the interaction mechanism of the four systems. Based on 20 years of time series data from 2002 to 2022, this study innovatively adopted the WLECNI index quantitative assessment to systematically analyze the spatiotemporal evolution characteristics of the coordination degree in the Yellow River Basin, found the dynamic process from "low level equilibrium" to "regional differentiation", and proposed the scientific classification criteria for the high–medium–low coordination area for the first time. In terms of methodology, the study not only identified the common factors, such as energy consumption per unit GDP, but also revealed the regional-specific problem of the extremely low rate of water quality compliance in Shanxi Province, and found the nonlinear interaction relationship between the systems through driving interaction analysis. The governance paradigm of "zoning regulation" proposed at the application level has important innovative value, such as designing a collaborative model of "landscape energy + ecological restoration" for high coordination areas, customizing precise solutions such as photovoltaic sand control for low coordination areas, and forming a complete decision-making loop of "assessment—diagnosis—governance—monitoring". These multidimensional innovations not only promote the theoretical development of human–land system coupling in the basin, but also provide operational scientific tools for differentiated governance, and have important guiding significance for the realization of ecological protection and high-quality development in the Yellow River Basin. The research results can provide a scientific basis and decision-making reference for ecological protection and high-quality development in the YRB.

This study aims to achieve the following deep scientific and policy objectives, and is not limited to specific analytical methods: First of all, the research is committed to establishing a new assessment framework for watershed sustainable development, through the construction of the W-L-E-C multi-system coupling model, breaking through the limitations of traditional research on a single environmental factor, and developing a quantifiable WLECNI index as a standardized measurement tool for the cross-regional coordination degree. Secondly, the study aims to reveal the spatiotemporal evolution of the W-L-E-C coordination degree in the provinces of the Yellow River Basin during 2002–2022, identify key transition thresholds (such as the critical point at which energy structure adjustment begins to improve the coordination degree), and provide a basis for phased policy formulation. Thirdly, the research systematically diagnoses the bottleneck factors and collaborative opportunities of basin development, not only locating specific obstacle factors (such as water resources overload in Ningxia and high-carbon industries in Shanxi), but also analyzing the cross-system leverage points (such as how land use policies can simultaneously alleviate water resources pressure and reduce carbon emissions).

2. Materials and Methods

2.1. Overview of the Study Area and Date Source

2.1.1. Overview of the Study Area

The YRB is the second-longest river in China, flowing through nine provinces and regions of Qinghai, Sichuan, Gansu, Ningxia, Inner Mongolia, Shanxi, Shaanxi, Henan, and Shandong, with a total length of about 5464 km and a watershed area of about 795,000 square kilometers [7,9]. The topography of the basin is high in the west and low in the east, spanning the three major geomorphic units of the Qinghai–Tibet Plateau,

the Loess Plateau, and the North China Plain. The climate types are diverse, from the upper reaches of the high cold climate to the lower reaches of the temperate monsoon climate, and the precipitation distribution is uneven [10]. The YRB water resources have limited time and space distribution, the upstream water resources utilization rate is low, but the relatively abundant middle water loss and soil erosion is serious, and there is a contradiction between the supply and demand of downstream water sharp. There are various types of land resources, but the problems of soil erosion and land degradation are prominent in the Loess Plateau, while the downstream plain area is rich in cultivated land resources but faces the threat of salinization. In addition, the YRB is rich in energy resources, especially large reserves of coal, oil, and natural gas, but the development and utilization of energy has also brought ecological and environmental problems such as air pollution, water consumption, and carbon emission increase [11].

The economic development level of the nine provinces and regions in the YRB is significantly different, with the economy of the upper reaches being relatively backward, and the economy of the middle and lower reaches being more developed. The basin is densely populated, and the system of agriculture, industry, and service industry is relatively complete; however, the industrial structure still needs to be optimized and upgraded. In recent years, with the rise of ecological protection and high-quality development in the YRB as a national strategy, regional coordinated development has ushered in important opportunities. However, problems such as water shortage, soil erosion, energy consumption increase, and carbon emission pressure are interwoven, forming a complex "W-L-E-C" coupling system. Studying the regional water–soil–carbon coupling coordination and its driving factors in ecological protection, as well as its ability to promote the YRB development, is of great significance. The overview of the research area is shown in Figure 1.

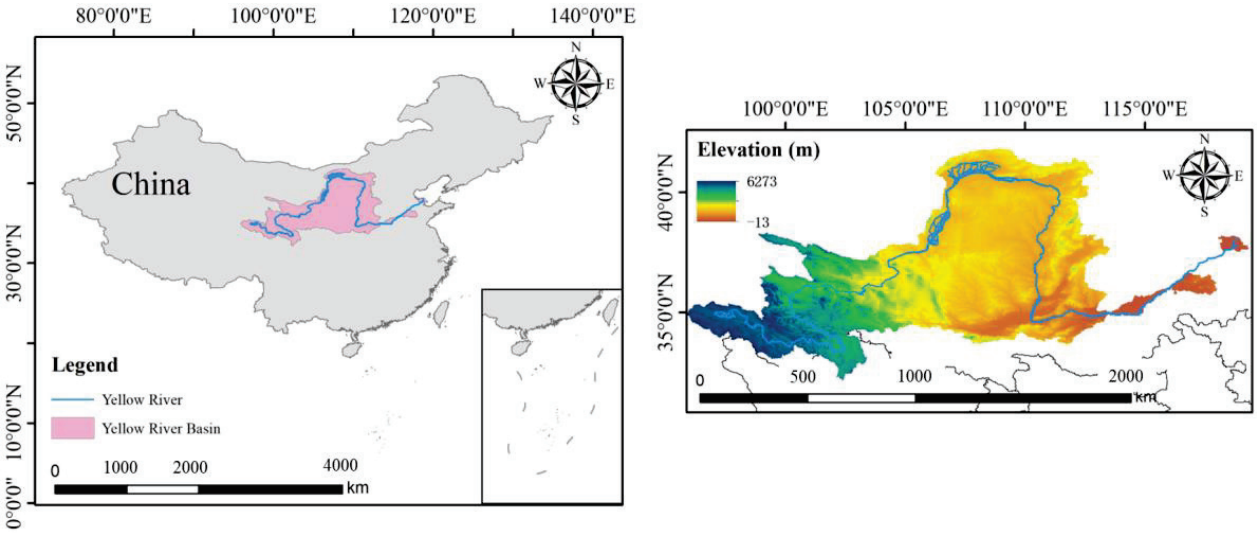

Figure 1. Research overview map.

2.1.2. Date Source

The original data of nine provinces and regions from the four evaluation years were obtained by sorting and analyzing relevant data from the China Statistical Yearbook, the National Bureau of Statistics, the water resources Bulletin, the China Ecological Environment Bulletin, and the Statistical yearbook.

2.2. Multidimensional Evaluation Model

2.2.1. Evaluation Index System Construction

In this study, the evaluation index system of W-L-E-C coupling-coordinated development is constructed using the systematic method. Firstly, the interaction mechanism between the four subsystems is analyzed deeply, and the theoretical model of the coupling coordination degree is established. In the index screening stage, the five principles of scientific, systematic, operable, regional, and dynamic are strictly followed. Through a literature analysis, expert consultation, and field research, 20 core indicators are selected from the 4 systems of water resources, land resources, energy and carbon emissions, and, finally, a quantitative evaluation model, wherein the coupling degree function and coordination degree function are constructed. The system innovatively realizes the organic integration of the four systems, which can not only independently evaluate the development status of each subsystem, but can also comprehensively analyze the interaction between the systems. The research team further conducts empirical tests based on the provincial panel data from 2002 to 2022, and continuously optimizes the indicator setting through sensitivity analysis to ensure that the indicator system has both theoretical rigor and practical guidance value. It provides a systematic and scientific evaluation tool for the decision-making of the sustainable development of the river basin.

The establishment of the evaluation index system of "W-L-E-C" coupling-coordinated development is the key to studying the harmonious relationship between resource utilization and the ecological environment in the nine provinces of the YRB. Based on scientific, systematic, operational, and regional principles, the system covers the following four subsystems: water resources, land resources, and energy and carbon emissions; furthermore, it selects specific indicators such as water resources per capita, gross production per unit of cultivated land in the primary industry, water consumption per unit of energy, and carbon dioxide emissions per capita. This index system can not only evaluate the spatiotemporal evolution characteristics of the "W-L-E-C" system in the nine provinces of the YRB, but it can also identify key driving factors, providing a scientific basis and practical guidance for regional ecological protection and high-quality development [12–16]. The evaluation index system is shown in Figure 2.

2.2.2. Index Weight Determination

In this paper, the AHP method is used to calculate the subjective weight, while the CRITIC weight method is used to calculate the objective weight, and on this basis, the minimum information entropy principle is introduced to form a combination weight calculation method based on the minimum information entropy principle.

On the basis of a single weight calculation method, this paper introduces the combination weight based on minimum information entropy. The principle of minimum information entropy can use subjective and objective weights to obtain the optimal combination weight value, which minimizes the deviation between subjective and objective weights and makes the obtained combination weight value more scientific [8,17,18]. The weight calculation results are shown in Figure 3, and the calculation formula is as follows:

$$w_{ei} = \frac{[w_{Ei} \times w_{Ai}]^{0.5}}{\sum_{i=1}^{m} [w_{Ei} \times w_{Ai}]^{0.5}}$$

where w_{ei} is the comprehensive weight; w_{Ei} is the objective weight determined using the entropy method; w_{Ai} is the subjective weight determined by the analytic hierarchy process; and m is the number of indicators.

Target layer	Criterion layer	Index layer	Index unit	Stats
Evaluation index system of "Water-Land-Energy-Carbon" bond relationship index (WLCENI)	$WLCENI_W$	Water Consumption per capita (W1)	m^3/person	-
		Water resources per capita (W2)	m^3/person	+
		Ecological water consumption ratio (W3)	%	+
		Utilization rate of Water Resources (W4)	%	+
		Water quality compliance rate (W5)	%	+
	$WLCENI_L$	Sown area (L1)	km^2	+
		Water Area (L2)	km^2	+
		Cultivated land area (L3)	km^2	+
		Impervious area (L4)	km^2	+
		Gross product per unit of cultivated land of primary industry (L5)	million CNY/km^2	+
	$WLCENI_C$	Energy consumption per unit GDP (E1)	tec/10, 000 yuan	-
		Energy Consumption per capita (E2)	tce/person	-
		Energy Quality Productivity (E3)	kg/tec	-
		Energy consumption per unit of water (E4)	tec/m^3	-
		Water consumption per unit of energy production (E5)	m^3/tec	-
	$WLCENI_E$	Ecosystem carbon uptake (C1)	t	+
		Carbon emissions from food Production (C2)	t	-
		Carbon emissions from energy consumption (C3)	t	-
		Ecosystem carbon absorption rate (C4)	t	+
		CO_2 emissions per capita (C5)	t	-

Figure 2. Evaluation index system of "W-L-E-C" system coupling-coordinated development.

2.2.3. "W-L-E-C" System Coupling-Coordinated Development Index

In this paper, the "W-L-E-C" bond index (WLECNI) is proposed based on the existing research results.

Reflecting the coupling and coordinated development level of the "W-L-E-C" system, the formula is as follows:

$$L_i^+ = (X_i - X_{\min})/(X_{\max} - X_{\min})$$

$$L_i^- = (X_{\max} - X_i)/(X_{\max} - X_{\min})$$

$$WLECNI = \sum_{i=1}^{n} w_i L_i / \sum_{i=1}^{n} w_i$$

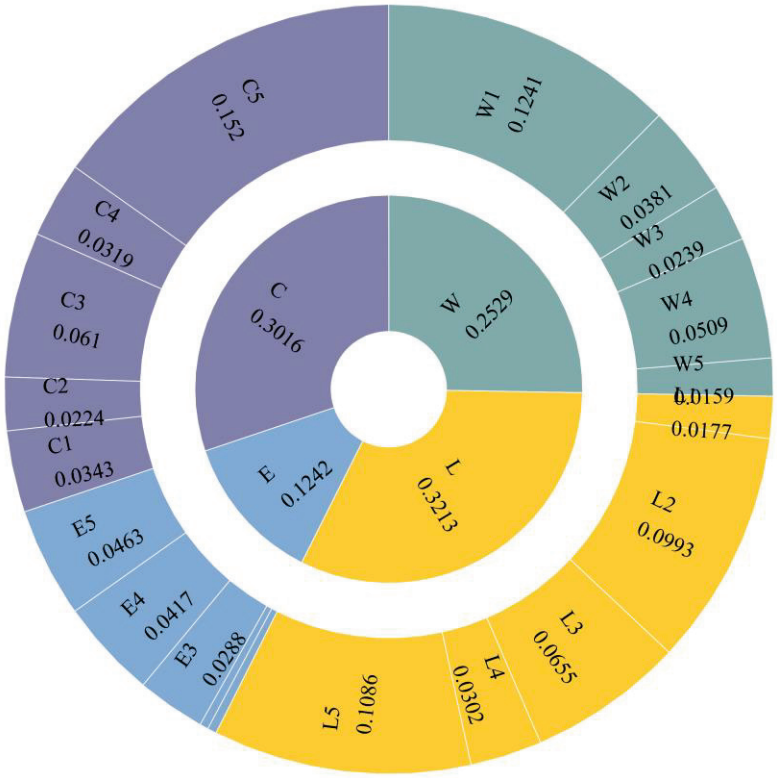

Figure 3. Weight chart of evaluation indicators.

2.3. Driving Factor Analysis

2.3.1. Factor Analysis

In this paper, the "W-L-E-C" bond index (WLECNI) is proposed based on the existing research results. In this study, the obstacle degree model is introduced to analyze the factors of the indicators in the evaluation system, to determine the main factors affecting the coordinated development of the system coupling, and then to formulate more targeted improvement measures [19–21]. The specific steps are as follows:

(1) Calculate the contribution degree of the j-th evaluation index F_j as follows:

$$F_j = w_i^* \times w_i$$

where w_i^* is the weight value of the criterion layer corresponding to the indicator.

(2) Calculate deviation I_j as follows:

$$I_j = 1 - x_{ij}$$

(3) Calculate the obstacle degree of each evaluation index P_j as follows:

$$P_j = \frac{F_j I_j}{\sum_{j=1}^{n} F_j I_j}$$

2.3.2. Single Subsystem Indicator Results

The geographic detector model is a statistical method to detect spatial heterogeneity and reveal its driving factors, consisting of four detectors—factor detection, interaction detection, risk detection, and ecological detection—the first two components of which are used in this study. The core idea of factor detection is to determine whether the explained variable plays a decisive role by comparing whether the explained variable and the unexplained variable have similar spatial distributions [22,23]. In the geographical detector,

the analysis of factor interaction effects quantifies the explanatory power of individual factors and their combinations on the dependent variable using the q statistic. The q-value represents the degree to which a single factor or factor interaction explains the spatial heterogeneity of the dependent variable, ranging from [0,1], with higher values indicating stronger explanatory power. The detection of interaction effects is determined by comparing the q-values of individual factors to the combined q-values of two factors. Specifically, it can be categorized into the following five scenarios: non-linear weakening (interaction q-value is less than the sum of individual q-values), single linear weakening (interaction q-value is less than the maximum individual q-value), bilinear enhancement (interaction q-value is greater than the maximum individual q-value), independence (interaction q-value equals the sum of individual q-values), and non-linear enhancement (interaction q-value is greater than the sum of individual q-values). If the interaction q-value is significantly higher than the individual q-values, it indicates that the combined effect of the two factors has a stronger influence on the dependent variable. The layer in the geographical detector refers to the process of discretizing continuous variables (e.g., using equal intervals, quantiles, or natural breaks) or reclassifying categorical variables, aiming to minimize within-stratum variation and maximize between-stratum variation. The calculation process is as follows:

$$q = 1 - \sum_{h=1}^{L} \frac{N_h \sigma_h^2}{N \sigma^2}$$

where $q \in [0,1]$ is the explanatory power of the driving factor of the system coordination level, wherein the larger the value of q, the stronger the explanatory power of the driving factor; $h = 1, \ldots, L$ is the stratification of variables or factors; N_h and N are the number of units in the layer and the whole area; and σ_h^2 and σ^2 are the variance of the layer and global values.

3. Results and Discussion

3.1. Analysis of Coordinated Development of "W-L-E-C" Coupling System

We adopted a multidimensional method to ensure the reliability of the conclusions. First, provincial-level data (2002–2022) from authoritative institutions such as the National Bureau of Statistics and the Ministry of Water Resources were adopted, key indicators were calibrated strictly in accordance with IPCC guidelines, and discrepancy data (difference rate < 5%) were revised through local environmental bulletins. In terms of model verification, the comparative test of the entropy weight method and analytic hierarchy process shows that the influence of a WLECNI index weight adjustment on provincial ranking is less than 10%, and the coupling coordination degree results are highly consistent with the Tapio decoupling analysis.

3.1.1. Single Subsystem Indicator Results

The results of single subsystem indicators are shown in Figure 4. From 2002 to 2022, the four indicators of water (W), soil (L), energy (E), and carbon (C) in nine provinces showed significant spatiotemporal differentiation. From the perspective of time, water resource utilization efficiency (W) has generally improved, and the average annual growth rate of the W-value in all provinces is between 3.8% and 8.2%. Take Sichuan Province as an example, wherein its W-value increased from 0.158 in 2002 to 0.326 in 2022, an increase of 106%, reflecting the remarkable effect of water-saving irrigation technology promotion and water resource management policies. The growth rate of the W-value in western regions such as Qinghai and Gansu (6.5% per annum) is higher than that in eastern provinces (4.2% per annum), which may be closely related to the inclined ecological protection poli-

cies and the improvement of marginal benefits of water-saving technologies in arid regions. The overall land use intensity (L) remained high, but the regional fluctuation was obvious, described as follows: the L-value of Qinghai Province led for a long time, reaching 0.499 in 2022 (the highest in China), which was closely related to the strict land planning of the Sanjiangyuan Ecological Protection Area; furthermore, the L-value of Shandong Province increased from 0.399 in 2002 to 0.475 in 2022, indicating that agricultural modernization and urbanization have a significant driving effect on land-intensive use.

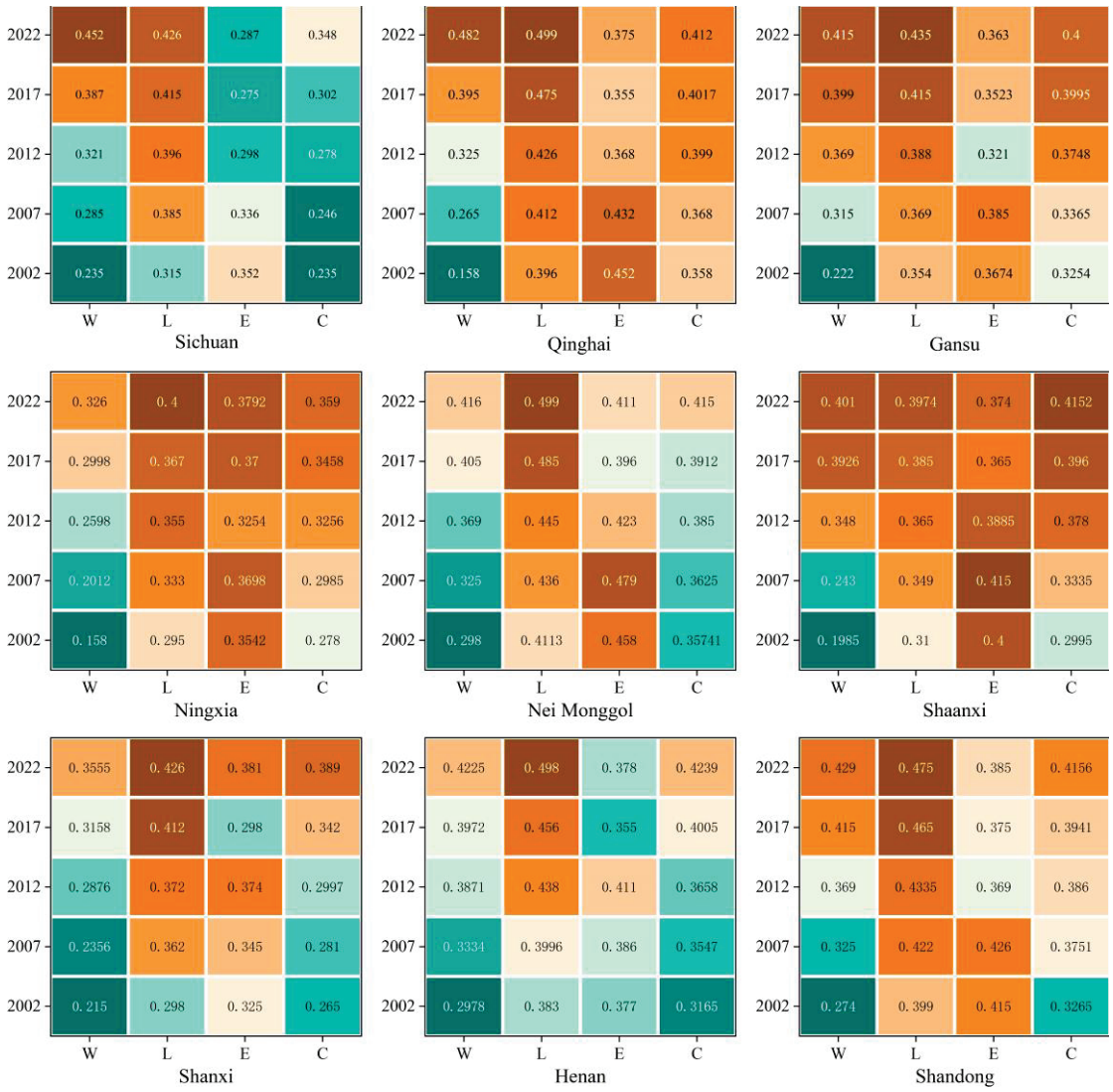

Figure 4. Single-index evaluation results of nine provinces in the YRB.

Energy consumption efficiency (E) presents a spatial pattern of "rising in the west and falling in the east". The E-value of western provinces such as Ningxia and Gansu continued to rise, and Ningxia's E-value increased by 10.7% (from 0.3542 to 0.3792) from 2002 to 2022, which may benefit from the expansion of new energy installed capacities, such as photovoltaic and wind power. In the eastern industrial provinces, such as Shandong and Henan, the E-value fell slightly due to the decline in traditional energy dependence, and the decline in Shandong Province reached 9.6%. Carbon emission intensity (C) generally showed a "slowing growth" characteristic, and the average annual increase of the C-value in most provinces dropped to less than 2% after 2017. In Inner Mongolia, for example, its C-value rose from 0.3165 in 2002 to 0.4239 in 2022, but the increase narrowed to 1.8% in 2017–2022, indicating that the constraint effect of the "dual carbon" policy on high-carbon

industries is beginning to emerge. It is worth noting that the C-value of central and western provinces, such as Shaanxi, increased by only 5% in 2022 compared to 2017, indicating the gradual penetration of emission reduction policies in energy-intensive regions.

From the perspective of spatial dimension, the regional differences of the four indexes are significant. In western China (Qinghai, Gansu, and Ningxia), the absolute value of water use efficiency (W) was low (mean value of 0.381 in 2022), but the growth rate was higher than that of the whole country, highlighting the marginal benefit of water-saving technology in arid areas. The land use intensity (L) in Qinghai has exceeded 0.48 for five consecutive years, ranking first in China, due to the support of ecological protection policies. The central provinces (Shaanxi, Shanxi, and Henan) are under pressure from the energy transition, with Shanxi's E-value rising from 0.345 in 2007 to 0.381 in 2022; however, its coal consumption still accounts for more than 60%, resulting in a high-carbon emission intensity (C) (C-value of 0.389 in 2022). The eastern provinces (Shandong and Inner Mongolia) showed the characteristics of "high L-C", which are as follows: the L-value of Shandong reached 0.475 (2022), reflecting the balance strategy between cultivated land protection and urban expansion; furthermore, due to the concentration of coal and chemical industries, Inner Mongolia's C-value (0.4239) is the highest in the country, being 8.9% higher than the second, Ningxia. The driving mechanism of regional differences can be summarized into the following three categories: policy intervention, resource endowment, and technology penetration. For example, after the "dual carbon" goal was proposed in 2017, the growth rate of the C-value in high-carbon provinces (Inner Mongolia and Ningxia) slowed down significantly (an average annual decline of 1.2–1.5 percentage points). Additionally, the advantages of new energy resources in western provinces promote the increase of E-value. For example, the installed capacity of wind power in Gansu accounts for more than 30%. In eastern provinces, optimizing land management through digital technologies (such as the "smart agriculture" pilot in Shandong) has supported the continued L-value growth.

The interaction between the indicators showed the coexistence of "water-energy synergy" and "carbon-energy contradiction". In western China, there is a significant positive correlation between water resource utilization efficiency (W) and energy consumption efficiency (E) ($R^2 = 0.72$), indicating that the collaborative development model of hydropower and new energy has achieved initial results. For example, the "water-light complementarity" project in Longyang Gorge, Qinghai Province has reduced energy consumption per unit GDP by 12%. However, in energy-intensive provinces (Inner Mongolia, Shanxi), carbon intensity (C) is negatively correlated with energy efficiency (E) ($R^2 = 0.65$), reflecting that traditional energy dependence is still the bottleneck of emission reduction. After 2017, the policy-driven effect became prominent, as the growth rate of carbon emissions in all provinces generally declined, but the improvement rate of water resources and land use efficiency accelerated (W- and L-values in 2022 increased by 14.3% and 7.6% on average compared to 2017), indicating the adjustment of resource management priorities under the "ecological priority" policy framework. Future regional development needs differentiated policies; for example, the western region should increase the proportion of renewable energy through the integration of landscape and water storage; Central China needs to explore the coupling model of coal power and carbon capture technology (CCUS); and the eastern part of the country can pilot a carbon emission trading market to force industrial low-carbon transformation through economic means.

To summarize, the spatiotemporal evolution of water, soil, energy, and carbon indicators in various provinces in China is driven by multiple factors, such as policies, resources, and technologies. It is thus suggested to establish a resource–energy–carbon emission accounting system of regional linkage to identify the potential of cross-provincial collab-

orative emission reduction, to increase investment in water-saving technology and new energy infrastructure for ecologically fragile areas in western China. Furthermore, in the central and eastern industrial agglomeration areas, carbon quota constraints and green technology innovation subsidies will be strengthened. Follow-up studies can be combined with high-resolution remote sensing data and policy text analysis to further quantify the contribution of policy interventions to the evolution of indicators.

3.1.2. WLECNI Index Results

Based on the WLECNI index time series data of "W-L-E-C" system coupling and coordinated development in the provinces of the YRB from 2002 to 2022, the horizontal differentiation, dynamic evolution characteristics, and regional differences of coordination were systematically analyzed. The WLECNI result is shown in Figure 5. As can be seen in the figure, the coordination of the YRB presents significant spatial–temporal differentiation. The high coordination areas (0.4–0.6) were represented by Inner Mongolia and Shaanxi. The WLECNI index of Inner Mongolia increased steadily from 0.372 (2002) to 0.442 (2022), with an average annual growth rate of 1.7%, benefiting from the synergistic effect of grassland ecological restoration and clean energy replacement. Shaanxi increased from 0.290 (2002) to 0.550 (2022), with an average annual growth rate of 3.4%, and significantly alleviated the pressure on resources and the environment through the intensification of cultivated land and industrial water-saving technology, becoming a benchmark for the improvement of coordination in the middle reaches. The middle coordination zone (0.2–0.4) includes Shandong, Henan, and Shanxi. Shandong increased from 0.348 (2002) to 0.434 (2022), with an average annual growth rate of 1.1%, and the promotion of green industry and water-saving technology has achieved remarkable results. Henan (0.441) and Shanxi (0.391) experienced slower growth due to the pressure of industrial carbon emissions and land resources. The low coordination areas (<0.4) were represented by Ningxia and Gansu. Although Ningxia (0.366) and Gansu (0.410) showed an increasing trend, their coordination remained low for a long time due to the constraints of water resource overload and inefficient energy utilization. Qinghai (0.453) has better coordination than the other upstream provinces due to having a higher ecological protection input.

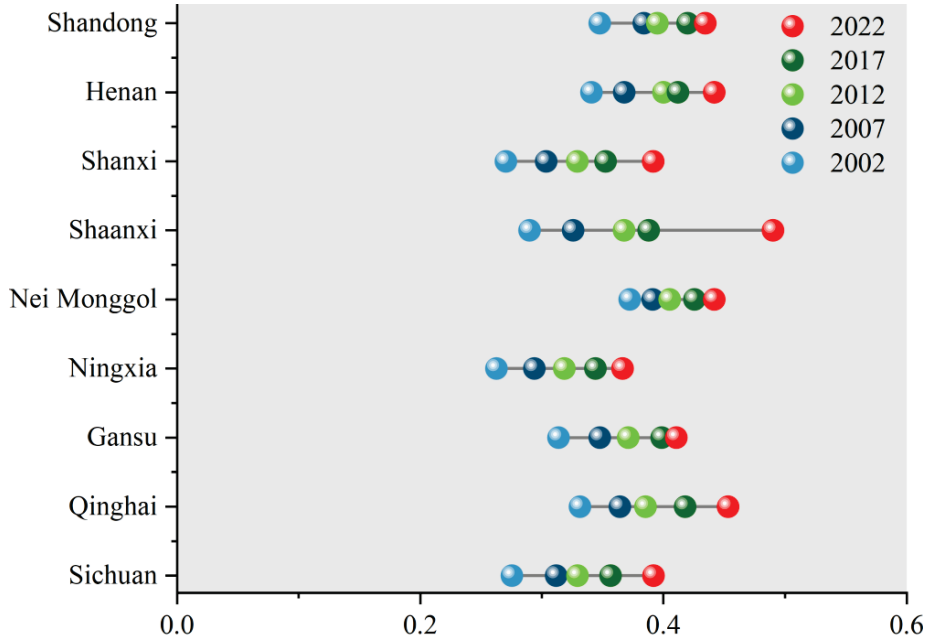

Figure 5. Spatiotemporal evolution of WLECNI in nine provinces.

Regional difference analysis showed that Inner Mongolia, Shaanxi, and Shandong achieved significant improvement in coordination through the "scenic energy + ecological restoration" model, cultivated land protection policy, and industrial greening, while Shanxi and Henan, restricted by industrial carbon emissions and land resource pressure, had lower growth than the average river basin. Due to the superposition of water resources' development intensity and desertification, Ningxia's coordination is weak. Future policies should be implemented in different areas. For example, the high coordination area should consolidate the advantages of eco-energy coordination and explore cross-provincial carbon sink trading mechanism. In the middle coordination area, the application of water-saving and consumption-reducing technology is strengthened to reduce the system vulnerability. Finally, low coordination areas have priority in solving the problem of resource overload and inefficient utilization, and they promote the utilization of renewable water and photovoltaic sand control technology.

3.2. Analysis of the Factors of Coordinated Development of "W-L-E-C" System Coupling

The results of the factor analysis for 2022 are shown in Figure 6. The per capita water consumption (W1) of all provinces in the figure is generally high, especially for Shanxi (0.1980) and Ningxia (0.1830), reflecting that extensive water use patterns are still dominant. There were significant regional differences in W5, and the values of Shanxi (0.0020) and Henan (0.0025) were very low, indicating that the superposition of industrial pollution and agricultural non-point source pollution led to the failure of water quality management. In Inner Mongolia (0.0980), water quality barriers were relatively light due to the high investment in ecological restoration. The low water resource utilization rate (W4) in Gansu (0.0315) and Qinghai (0.0125) is directly related to the lack of local water resources endowment, and the risk of over-exploitation should be vigilant.

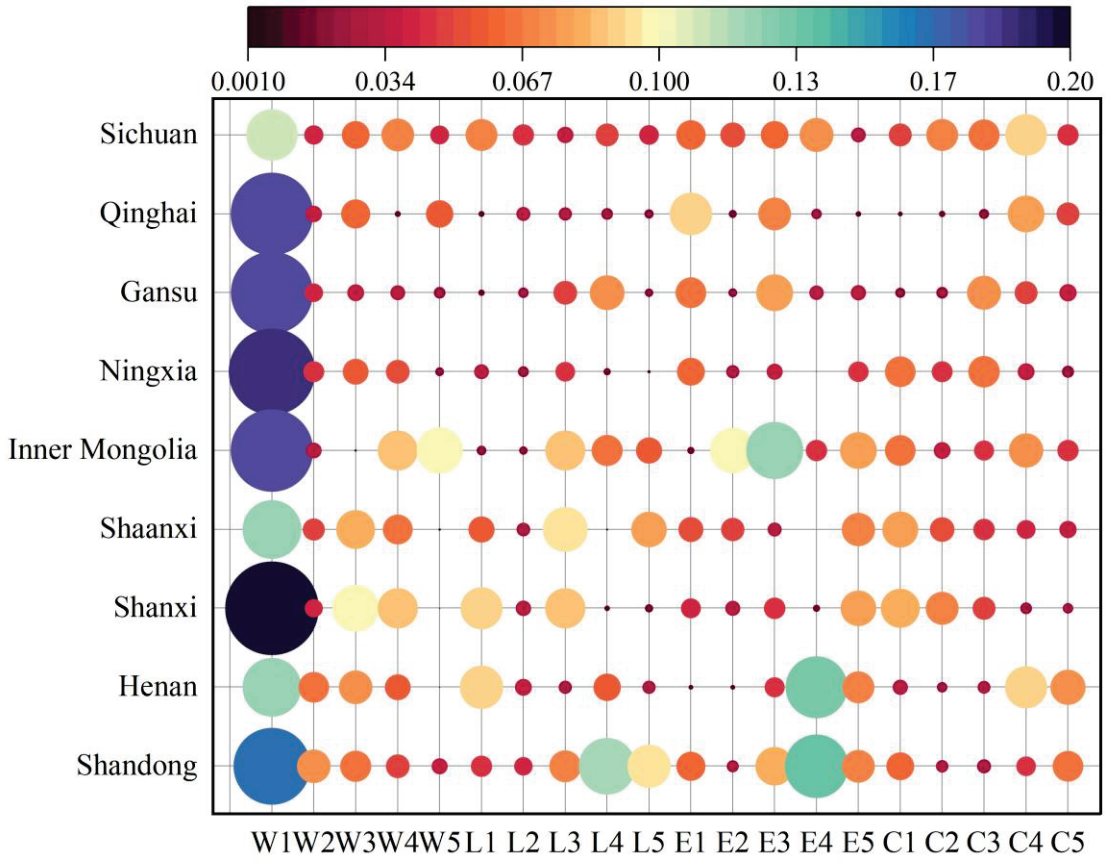

Figure 6. Factor analysis results for 2022.

The obstacle of the cultivated land area (L3) was higher in Shaanxi (0.0950) and Inner Mongolia (0.0850), and the urbanization and ecological farmland return policy aggravated the loss of cultivated land. The barrier of the impervious area (L4) reached its peak in Shandong (0.1200), indicating that rapid urbanization led to prominent surface hardening problems. In energy utilization, the energy consumption per unit GDP (E1) in Inner Mongolia (0.0150) is significantly lower than that in other provinces, thanks to the optimization of energy structure and the promotion of energy efficiency technology. Furthermore, the high unit water consumption of Shanxi (0.0420) and Henan (0.0100) (E4, 0.1310 and 0.1340, respectively) exposed the lag of industrial water-saving technology, forming a "water-energy" two-way restriction.

Energy consumption carbon emission (C3) was high in Gansu (0.0664) and Ningxia (0.0752), which is closely related to the coal-dependent industrial structure. The carbon uptake (C1, C4) of the ecosystem was weak in Shanxi (C1 = 0.0826) and Henan (C4 = 0.0887), and the degradation of the ecological carbon sink function intensified the pressure of carbon neutrality. The per capita carbon dioxide emissions (C5) were higher in Henan (0.0742) and Shandong (0.0647), highlighting the urgent task of reducing emissions in densely populated areas.

In the upper reaches of the YRB (Qinghai and Gansu), the complex barriers of low water resource utilization (W1 and W4) and low energy quality and productivity (E3 $\geq$ 0.078) should be solved first. The middle reaches (Shaanxi, Shanxi) should focus on the coordination of cultivated land protection (L3) and industrial emission reduction (C3, C4), while the downstream section (Henan, Shandong) needs to contain impervious expansion (L4) and a high-carbon lock-in effect (C5). It is suggested to strengthen the W-E collaboration through a cross-provincial ecological compensation mechanism, promote water-saving and consumption reduction technologies (such as reclaimed water utilization W5, photovoltaic sand control L2), and to establish a linkage system of the carbon emission quota and carbon sink trading, to systematically reduce the intensity of factors and promote the high-quality development of the basin.

3.3. Interactive Detection and Analysis of "W-L-E-C" System Driving Factors

The interactive detection results among the impact factors in the nine provinces of the YRB are shown in Figure 7. Based on the interaction intensity data of the "W-L-E-C" system from 2002 to 2022, this study reveals the dynamic evolution characteristics and internal mechanism of the system. The data are presented in the following triangular matrix, covering the strength of the X1 to X8 factors themselves, and their interaction strength. The analysis shows that the system presents a significant trend of network strengthening, which is as follows: the average interaction strength increases from 0.35 (2002) to 0.58 (2022), and the core nodes of X5, X7, and X8 drive the network density. Among them, the strength of X5 jumped from 0.56 to 1 (2022), and the interaction strength with X4, X6, and X7 exceeded 0.9, becoming the core hub of the system. The interaction strength of X7 with X6 and X8 reaches saturation values of 1 and 0.89 (2022), respectively, highlighting its information relay function. At the same time, the system complexity increases, the vulnerability risk becomes prominent, and the highly dependent feature of the core node may cause cascading failures.

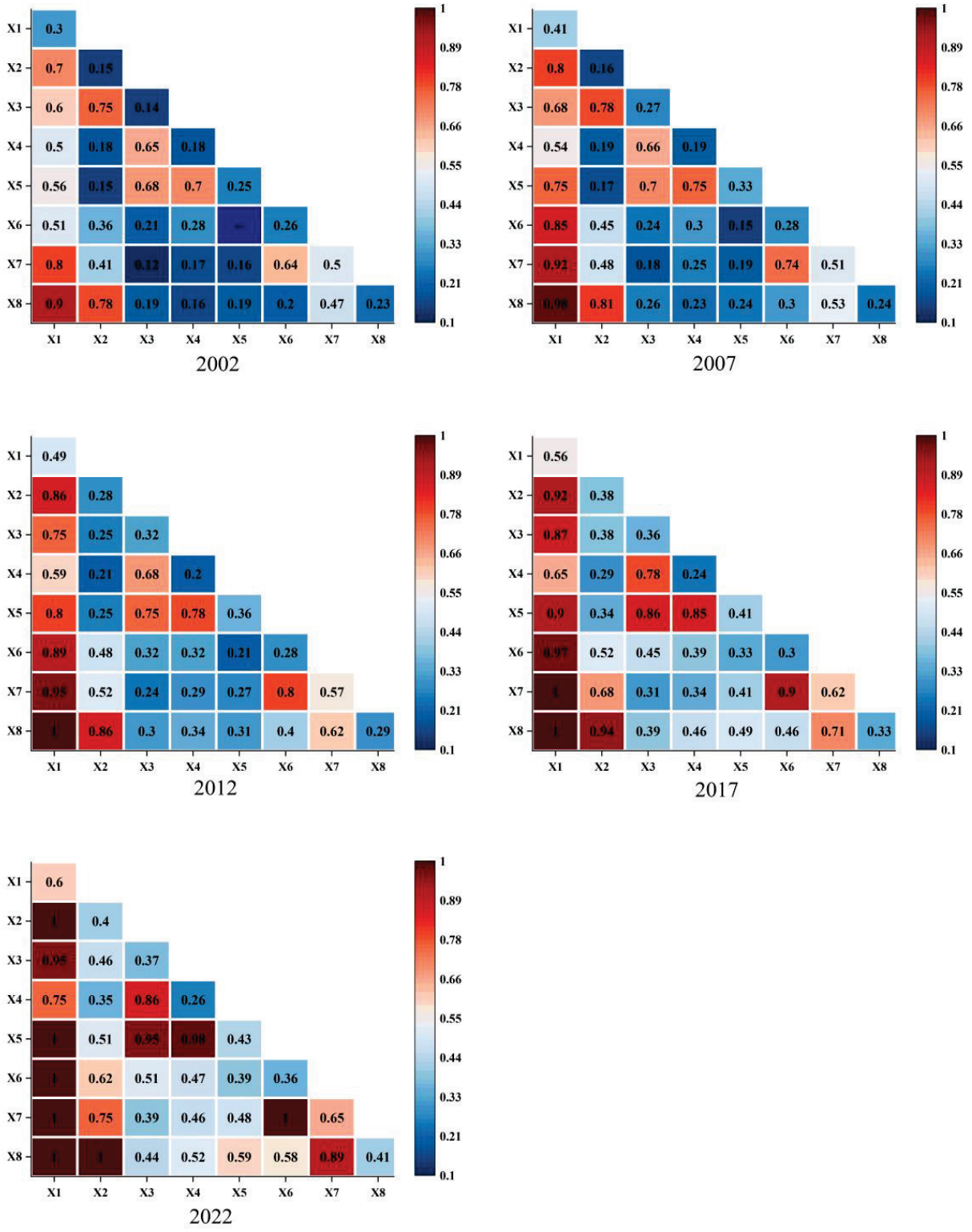

Figure 7. Interactive detection results of influencing factors in nine provinces of the YRB.

The phased evolution characteristics show that 2012 was a key turning point, as the interaction intensity of X3 and X1 suddenly increased to 0.87 (45% increase over the previous period), while the growth rate of the interaction intensity of most factors slowed down, which is presumed to be related to an external intervention or system adaptive adjustment. Anomalies such as a sharp drop in X2's own strength in 2017 (0.69 vs. 0.92 previously) and fluctuations in the X3–X2 interaction strength (0.75 → 0.38 → 0.46) require validation of data reliability or exploration of perturbation mechanisms. It is

thus suggested to focus on the dynamic behavior of X5 and X7, whose intensity saturation phenomenon may reach the system threshold, and the mechanism analysis should be carried out in combination with driving factors such as policy and technology. Future studies can quantify the impact of network topology changes on system stability through heat map modeling and robust simulation, and they can provide a theoretical basis for complex system optimization.

4. Conclusions

This study draws the following conclusions: The coupling coordination of the "W-L-E-C" system in the YRB presents significant spatial differentiation and temporal dynamic changes. Inner Mongolia and Shaanxi have become the benchmark of the high coordination zone through ecological restoration, clean energy replacement, and cultivated land intensification, while Ningxia and Gansu have been in the low coordination zone for a long time due to water resource overload and inefficient energy utilization. Barrier factor analysis shows that the water resources' utilization rate (W4), impervious area (L4), energy consumption per unit GDP (E1), and carbon emissions from energy consumption (C3) are the core factors restricting coordination. Among them, the water quality compliance rate (W5) of Shanxi and Henan is very low, and the impervious area (L4) of Shandong is a prominent problem. The interaction analysis of the driving factors revealed a significant interaction between water resource utilization and ecological protection (W-E), land resource and energy use (L-E), and carbon emissions and the ecosystem (C-E). Inner Mongolia, Shaanxi, and Shandong achieved coordinated improvement through "scenic energy + ecological restoration", cultivated land protection, and industrial greening. Shanxi, Henan, and Ningxia are constrained by the "W-L-E-C" complex obstacles.

In the future, the YRB needs to implement a zoning regulation strategy in order for the high-coordination area to consolidate the advantages of ecological energy coordination, for the middle coordination area to strengthen the application of water-saving and consumption reduction technology, and for the low coordination area to solve the problem of resource overload and inefficient use of renewable water utilization and photovoltaic sand control technology, in order to achieve high-quality development of the whole basin. This study provides a scientific basis and policy suggestions for the sustainable development of the YRB.

Author Contributions: Conceptualization and writing—review and editing, S.Z. and B.C.; writing—original draft preparation, M.J. and T.L.; software, Z.L. and D.Z.; supervision and project administration, W.C. and Z.L. All authors have read and agreed to the published version of the manuscript.

Funding: This study was financially supported by the National Natural Science Foundation of China (52409058).

Data Availability Statement: The original contributions presented in the study are included in the article; further inquiries can be directed to the corresponding author.

Conflicts of Interest: The authors declare no conflicts of interest.

References

1. Han, Y.; Li, J.; Zhao, M.; Guo, H.; Wang, C.; Huang, H.; Cao, R. Analysis of rainfall abundance and drought occurrence and probability of flood and drought occurrence in Yellow River Basin based on Copula function family. *J. Hydrol. Reg. Stud.* **2025**, *58*, 102242. [CrossRef]
2. Li, S.; Xiang, N.; Shu, C.; Xu, F. Unveiling the industrial synergy optimization pathways in Beijing-Tianjin-Hebei urban agglomeration based on water-energy-carbon nexus. *J. Environ. Manag.* **2025**, *376*, 124528. [CrossRef] [PubMed]
3. Yin, L.; Li, H.; Liu, D.; Zhang, L.; Wang, C.; Li, M.; Faiz, M.A.; Li, T.; Cui, S. Interpretation and Comprehensive Evaluation of Regional Water–Land–Energy Coupling System Carrying Capacity. *Sustainability* **2025**, *17*, 1669. [CrossRef]

4. Zhou, H.; Liu, J.; Gao, C.; Li, W.; Ou, S.; Zhou, Y.; Luan, Q. Copula-based joint impact assessment of rainfall and tidal level on flood risk in tidal-influenced plain river network areas, Taihu Lake Basin. *J. Hydrol.* **2025**, *653*, 132785. [CrossRef]
5. Wakchaure, G.; Minhas, P.; Biswas, A.; Meena, K.K.; Pradhan, A.; Gawhale, B.; Choudhary, R.; Kumar, S.; Fagodiya, R.K.; Reddy, K.S.; et al. Assessment of gains in productivity and water-energy-carbon nexus with tillage, trash retention and fertigation practices in drip irrigated sugarcane. *Renew. Sustain. Energy Rev.* **2025**, *211*, 115294. [CrossRef]
6. Xu, W.; Wang, H.; Zhao, X.; Zhao, D.; Ding, X.; Yin, Y.; Liu, Y. Study on Evaluation and Dynamic Early Warning of Urban Water Resources Security. *Water* **2025**, *17*, 242. [CrossRef]
7. Wu, L.; He, Y.; Tan, Q.; Zheng, Y. Land-use simulation for synergistic pollution and carbon reduction: Scenario analysis and policy implications. *J. Environ. Manag.* **2024**, *356*, 120603. [CrossRef]
8. Li, J.; Zhao, M.; Han, Y.; Wei, J. Assessment on water cycle health in the Central Plains Urban cluster based on the DSWU NWU SWS NWS A—WCHI model. *Ecol. Indic.* **2023**, *157*, 111236. [CrossRef]
9. Wu, Z.; Fan, Y.; Zhang, S.; Qian, X.; Wang, G. Dynamic assessment of water resources carrying capacity under human impacts on the water cycle: A finer perspective at the spatiotemporal scale of basin. *J. Clean. Prod.* **2025**, *486*, 144602. [CrossRef]
10. Lyu, H.; Qiao, J.; Fang, G.; Liang, W.; Tang, Z.; Lv, F.; Zhang, Q.; Qiu, Z.; Huang, G. Variations in Water Stress and Its Driving Factors in the Yellow River Basin. *Land* **2024**, *14*, 53. [CrossRef]
11. Ma, D.; Duan, S.; Zhang, X.; Xu, B.; Xu, Y. Spatiotemporal Dynamic Assessment of Water Resources Carrying Capacity and Identification of Obstacle Factors in Yunnan Province Based on Grey Water Footprint Theory. *Water* **2024**, *16*, 3651. [CrossRef]
12. Sobkowiak, L.; Wrzesiński, D. Impacts of Climate Change on Water Resources: Assessment and Modeling—First Edition. *Water* **2024**, *16*, 3578. [CrossRef]
13. Kang, Y.; He, S.; Ni, T.; Wang, J.; Liu, L. Analysis of water–energy–carbon coupling and influencing factors in food production. *J. Water Clim. Change* **2024**, *15*, 5939–5956. [CrossRef]
14. Hadipour, M.; Pourebrahim, S.; Heidari, H.; Nikooy, F.; Ahmed, A.N.; Ern, C.J. Evaluation of water resource balance in the Urmia Lake Basin: Integrating carrying capacity and water footprint model for sustainable management. *Ecol. Indic.* **2024**, *166*, 112464. [CrossRef]
15. Du, L.; Niu, Z.; Zhang, R.; Zhang, J.; Jia, L.; Wang, L. Evaluation of water resource carrying potential and barrier factors in Gansu Province based on game theory combined weighting and improved TOPSIS model. *Ecol. Indic.* **2024**, *166*, 112438. [CrossRef]
16. Yu, L.; Peng, K.; Huang, Y.; Peng, K.; Huang, Y.; Chen, F.; Chen, S.; Xia, Y.; Huang, X.; Ni, X.; et al. Application of a water-energy-carbon coupling index to evaluate the long-term operational stability of the anaerobic-anoxic-oxic-membrane bioreactor (A2/O-MBR) process under the influence of rainstorms. *Water Res.* **2024**, *255*, 121489. [CrossRef]
17. Feng, Y.; Wang, J.; Ren, X.; Zhu, A.; Xia, K.; Zhang, H.; Wang, H. Impact of water utilization changes on the water-land-energy-carbon nexus in watersheds: A case study of Yellow River Basin, China. *J. Clean. Prod.* **2024**, *443*, 141148. [CrossRef]
18. Li, J.; Zhao, M.; Han, Y.; Wei, J. Analysis of water resource ecological optimization and obstacles based on the water resources-socio-economic-ecological environment model framework—A case study of the core area of the Central Plains urban agglomeration. *Front. Ecol. Evol.* **2023**, *11*, 1263601. [CrossRef]
19. Jiang, W.; Zhang, Z.; Wen, J.; Yin, L.; Song, B. Spatio-temporal variation and influencing factors of industrial carbon emission effect in China based on water-land-energy-carbon nexus. *Ecol. Indic.* **2023**, *152*, 110307. [CrossRef]
20. Zhao, M.; Li, J.; Zhang, Y.; Han, Y.; Wei, J. Water cycle health assessment based on combined weight and hook trapezoid fuzzy TOPSIS model: A case study of nine provinces in the Yellow River basin, China. *Ecol. Indic.* **2023**, *147*, 109977. [CrossRef]
21. Yao, X.; Chen, W.; Song, C.; Gao, S. Sustainability and efficiency of water-land-energy-food nexus based on emergy-ecological footprint and data envelopment analysis: Case of an important agriculture and ecological region in Northeast China. *J. Clean. Prod.* **2022**, *379*, 134854. [CrossRef]
22. Lyu, K.; Tian, J.; Zheng, J.; Zhang, C.; Yu, L. Evaluation of Water–Carbon–Ecological Footprint and Its Spatial–Temporal Changes in the North China Plain. *Land* **2024**, *13*, 1327. [CrossRef]
23. Jin, K.; Zhang, S.; Yang, Y.; Chen, X.; Wang, S.; Li, T.; Wang, Y. Evaluation of water-carbon-ecological footprints and its spatial–temporal pattern in the central plains urban agglomeration. *Ecol. Indic.* **2023**, *155*, 110982. [CrossRef]

MDPI AG
Grosspeteranlage 5
4052 Basel
Switzerland
Tel.: +41 61 683 77 34

Water Editorial Office
E-mail: water@mdpi.com
www.mdpi.com/journal/water

Academic Open
Access Publishing

mdpi.com

ISBN 978-3-7258-5990-0